This dissertation has been 65-9565
microfilmed exactly as received

LOTT, Jerry Lee, 1935-
THE SELECTIVE OXIDATION OF METHANE
AT HIGH PRESSURES.

The University of Oklahoma, Ph.D., 1965
Engineering, chemical

University Microfilms, Inc., Ann Arbor, Michigan

Downloaded from SHAREOK. Persistent Handle URL: https://hdl.handle.net/11244/1866

Copyright by

JERRY LEE LOTT

1965

THE UNIVERSITY OF OKLAHOMA

GRADUATE COLLEGE

THE SELECTIVE OXIDATION OF METHANE AT HIGH PRESSURES

A DISSERTATION

SUBMITTED TO THE GRADUATE FACULTY

in partial fulfillment of the requirements for the

degree of

DOCTOR OF PHILOSOPHY

BY

JERRY LEE LOTT

Norman, Oklahoma

1965

THE SELECTIVE OXIDATION OF METHANE AT HIGH PRESSURES

APPROVED BY

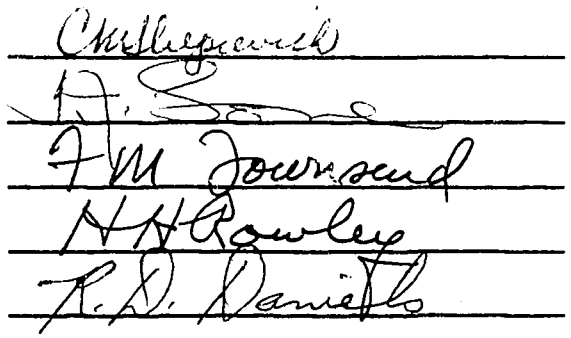

DISSERTATION COMMITTEE

ABSTRACT

The partial oxidation of methane was studied in two high pressure reaction systems; one designed for a pressure of 25,000 psi at 1000°F and the other designed for a pressure of 200,000 psi at 800°F. The methane-oxygen ratio of the feed mixture varied between 10:1 and 11.6:1. Reactor pressure was varied from 2000 to 200,000 psi and the initial temperature was varied between 476 and 640°F. A combination of chromatography and volumetric methods was used to analyze the products.

In the oxidation of methane pressure has a strong influence on the product distribution. In general an increase in pressure increases the yield of methyl alcohol and other oxygenated organic liquid products. At a given pressure the maximum yield of methyl alcohol occurs at an initial temperature corresponding to a relatively short residence time. The cool flame phenomenon was observed at high pressures for the first time. The nature and surface condition of the vessel affect the kinetics of the oxidation process as well as the product distribution.

The most plausible mechanism for the partial oxidation of methane at high pressures is by a chain mechanism

with degenerate branching. In this proposed mechanism the rate of formation of formaldehyde must be considered since the speed at which it occurs at extreme pressures is most likely commensurate with the rate-controlling step.

It has been demonstrated that high pressure equipment can be fabricated for studying chemical reactions in fluid systems of at least 500 cubic centimeters at pressures up to 200,000 psi and temperatures up to 800°F.

ACKNOWLEDGEMENTS

The author is particularly indebted to his committee chairman, Dr. C. M. Sliepcevich, for his interest, inspiration, and guidance throughout the author's graduate work, and to the other members of his committee, Dr. F. M. Townsend, Dr. T. J. Love, Dr. R. D. Daniels, and Dr. H. H. Rowley.

My sincerest appreciation is extended to my colleague, Dr. O. A. Pipkin, for his interest and helpful suggestions during this investigation.

I wish to thank Mr. E. L. Johnson who assisted in the installation of the equipment and in the analytical work. Dr. S. E. Babb, Jr. and Mr. G. J. Scott of the Physics Department and Mr. F. Maginnis of the Research Instrument Company gave many helpful suggestions.

The writer is grateful to Autoclave Engineers, Inc., for the financial support for the high pressure equipment and, in particular, to Mr. W. W. Robertson of this company for his assistance in the design of the 200,000 psi reaction system. The courteous service of the Vanadium-Alloys Steel Company is appreciated.

Financial support was received from a NDEA fellowship. The major sponsor of this project has been the National

Science Foundation. The author thanks Continental Oil Company for their advice on the analytical problems and for supplying the chromatograph columns without charge. Continental Oil Company and the University of Michigan provided some of the high pressure equipment used in this investigation.

Jerry Lee Lott

TABLE OF CONTENTS

Page

LIST OF TABLES ix

LIST OF ILLUSTRATIONS x

Chapter

I. INTRODUCTION 1

II. THEORETICAL CONSIDERATIONS 4

Basic Principles of Chemical Chain Reactions
Theoretical Development of the Mechanism for Methane Oxidation at Low Pressures
Theoretical Aspects of the Mechanism for Methane Oxidation at High Pressures

III. REVIEW OF PREVIOUS WORK. 32

Experimental Work
Reaction Mechanism and Kinetics
Range of Pressures

IV. DESIGN CONSIDERATIONS FOR HIGH PRESSURE EQUIPMENT 59

Principles for the Design and Construction of High Pressure Equipment
Reactor Design
Compression Cylinder Design
Intensifier Design
Auxiliary High Pressure Equipment

V. DESCRIPTION OF EXPERIMENTAL EQUIPMENT. 89

Feed Preparation and Storage System
25,000 psi Reaction System
200,000 psi Reaction System
Product Section
Auxiliaries

Page

VI. EXPERIMENTAL PROCEDURE 120

Preliminary Procedures
Run Procedure
Difficulties Encountered

VII. ANALYTICAL PROCEDURE AND EQUIPMENT 132

Description of Chromatograph Equipment
Operation and Calibration of the Chromatograph
Volumetric Analysis

VIII. DISCUSSION OF RESULTS. 142

IX. CONCLUSIONS. 183

NOMENCLATURE. 185

LITERATURE CITED. 188

APPENDICES

A. CHROMATOGRAPH CALIBRATION. 194

B. VOLUMETRIC ANALYSIS. 209

C. MANGANIN PRESSURE CELL AND RECORDER CALIBRATIONS. 213

D. SUMMARY OF EXPERIMENTAL DATA 215

E. SAMPLE CALCULATIONS. 221

LIST OF TABLES

Table		Page
1.	The Variation of the Maximum Rate of Oxidation with Concentrations of the Methane and Oxygen at Different Temperatures	57
2.	Summary of Data for Figure 2	73
3.	Summary of Data for Figure 5	83
4.	Summary of Data for Figure 7	86
5.	Summary of Experimental Results at High Pressures	176
6.	Chromatograph Calibration Data for Carbon Monoxide, Oxygen, and Methane	196
7.	Chromatograph Calibration Data for Carbon Dioxide	201
8.	Chromatograph Calibration Data for Methanol	204
9.	Chromatograph Calibration Data for Methyl Formate	207
10.	Influence of Methanol, Formic Acid, and Methyl Formate on Formaldehyde Determination	212
11.	Reproducibility of Formic Acid Determination by Neutralization	212
12.	Summary of Experimental Results at Elevated Pressures	216
13.	Summary of Analytical Results	218

LIST OF ILLUSTRATIONS

Figure		Page
1.	Details of 200,000 psi Reactor.	68
2.	Shear Stress Distribution for Reactor	72
3.	Details of Electrode Assembly	74
4.	Details of 200,000 psi Compression Cylinder . . .	76
5.	Shear Stress Distribution for Compression Cylinder.	82
6.	Details of Intensifier Assembly	84
7.	Shear Stress Distribution for Intensifier Assembly.	87
8.	Process Flow Diagram of Feed System	91
9.	Details of 25,000 psi Compression Cylinder. . . .	96
10.	Equipment Inside the High Pressure Cell	97
11.	25,000 psi Reaction System.	98
12.	Process Flow Diagram of 25,000 psi Reaction System.	99
13.	Details of 25,000 psi Reactor	101
14.	Process Flow Diagram of 200,000 psi Reaction System.	106
15.	200,000 psi Compression Cylinder.	108
16.	200,000 psi Equipment Inside the High Pressure Cell	110
17.	200,000 psi Reactor	112
18.	Internal Heater and High Pressure Fittings. . . .	114

Figure Page

19. Chromatograph 133

20. Effect of Temperature on Residence Time 146

21. Observed Temperature Boundary Between Slow Oxidation Reactions and Instantaneous Reactions at High Pressures 148

22. Effect of Temperature on Methanol Yield (Data of Newitt and Haffner) 149

23. Effect of Temperature on Yield (5400 psi) 150

24. Effect of Temperature on Total Oxygenated Liquid Product Yield (5400 psi) 151

25. Effect of Temperature on Carbon Monoxide/ Carbon Dioxide Ratio (5400 psi) 152

26. Effect of Temperature on Yield (7000 psi) 153

27. Effect of Temperature on Total Oxygenated Liquid Product Yield (7000 psi) 154

28. Effect of Temperature on Carbon Monoxide/ Carbon Dioxide Ratio (7000 psi) 155

29. Effect of Residence Time on Methanol Yield (7000 psi) 156

30. Effect of Residence Time on Total Oxygenated Liquid Product Yield (7000 psi) 157

31. Effect of Residence Time on Carbon Monoxide/ Carbon Dioxide Ratio (7000 psi) 158

32. Effect of Temperature on Yield (10,000 psi) . . . 159

33. Effect of Temperature on Total Oxygenated Liquid Product Yield (10,000 psi) 160

34. Effect of Temperature on Carbon Monoxide/ Carbon Dioxide Ratio (10,000 psi) 161

35. Effect of Temperature on Yield (15,000 psi) . . . 162

36. Effect of Temperature on Total Oxygenated Liquid Product Yield (15,000 psi) 163

Figure Page

37. Effect of Temperature on Carbon Monoxide/ Carbon Dioxide Ratio (15,000 psi) 164

38. Effect of Residence Time on Yield (50,000 psi). . 165

39. Effect of Residence Time on Carbon Monoxide/ Carbon Dioxide Ratio (50,000 psi) 166

40. Methanol Yield Temperature Dependence at Various Pressures 171

41. Total Oxygenated Liquid Product Yield Temperature Dependence at Various Pressures. 172

42. Effect of Residence Time on Methanol Yield at Various Pressures. 173

43. Effect of Residence Time on Total Oxygenated Liquid Product Yield at Various Pressures 174

44. Effect of Pressure on the Maximum Oxygenated Liquid Product Yield. 175

45. Cool Flame Phenomenon: Temperature-Time Curve (Run JLL-254) 179

46. Cool Flame Phenomenon: Pressure-Time Curve (Run JLL-254) 179

47. Hot Flame Temperature-Time Curve (Run JLL-201). . 180

48. Hot Flame Pressure-Time Curve (Run JLL-201) . . . 180

49. Chromatograph Calibration for Oxygen. 199

50. Chromatograph Calibration for Carbon Monoxide . . 200

51. Chromatograph Calibration for Carbon Dioxide. . . 202

52. Chromatograph Calibration for Methanol. 206

53. Chromatograph Calibration for Methyl Formate. . . 208

54. Calibration of Manganin Pressure Cell and Recorder. 214

THE SELECTIVE OXIDATION OF METHANE AT HIGH PRESSURES

CHAPTER I

INTRODUCTION

The partial oxidation of hydrocarbons has a very important role in the utilization of petroleum stock since the incomplete oxidation leads to the derivation of many intermediate products in heavy organic synthesis. For many years the partial oxidation of methane has been the object of numerous investigations in an attempt to elucidate the reaction mechanism of methane oxidation and to aid in elucidating the reaction mechanism of hydrocarbon oxidation in general. The majority of oxidation studies on methane have been carried out at atmospheric or subatmospheric pressures whereas only a limited number of investigations have been carried out at elevated pressures.

Pressure is an important control variable in chemical reactions since pressure shifts the reaction equilibrium and affects the reaction rate. The effect of pressure on the reaction product distribution is the primary interest of this study.

With the accumulation of technological information and the availability of ultra-high strength steel alloys, reaction systems to study the effect of pressure on chemical reactions at higher pressure levels can now be constructed. It is not uncommon to find complete units which can attain pressures in the vicinity of 100,000 psi and small scale equipment is now available which can attain pressures up to 200,000 psi (81).

The primary objectives of this investigation were: (1) to develop experimental equipment for studying chemical reactions in fluid systems of about 500 cc volume at pressures up to 200,000 psi and temperatures up to 800°F and (2) to demonstrate the utility of this equipment by conducting a comprehensive study on the partial oxidation of methane at high pressures.

Anticipating that the fabrication time for such a system would be at least a year it was decided that preliminary exploration of the reaction at elevated pressures would be profitable. Originally this temporary system was to be used for developing techniques and operating procedures for controlling the rate of reaction; however sufficient time was available before delivery of the 200,000 psi system to obtain data on the partial oxidation of methane.

Data on the partial oxidation of methane carried out in the intermediate pressure apparatus were obtained at pressures ranging from 2000 to 15,000 psi and temperatures

ranging from 550 to 645°F. Limited data on the partial oxidation of methane carried out in the 200,000 psi system were obtained at pressures ranging from 15,000 to 200,000 psi and temperatures ranging from 476 to 517°F

CHAPTER II

THEORETICAL CONSIDERATIONS

Gas-phase oxidation of hydrocarbons belongs to the general class of chain reactions with degenerate branching. This chapter is devoted to a summary of the current state of the theory relating to the various reaction mechanisms which have been proposed. In the first section the principles of chain reaction theory are briefly reviewed and in the second section Semenov's theoretical development of the mechanism for methane oxidation at low pressures is presented. The theoretical aspects of the mechanism for methane oxidation at high pressures is discussed in the third section.

Basic Principles of Chemical Chain Reactions

The failure to explain the experimental data of many chemical reactions with a mechanism represented by a direct reaction between molecules was the basis for the formulation of chain theory for chemical reactions. Semenov (64) has stated that in every chemical reaction uni- or bimolecular reactions and a chain process are occurring simultaneously; therefore the mechanism is determined by

the relative rates of the competitive reactions. For a chemical reaction in which the rate of the chain process is predominate over the direct reaction rate, all chain reactions that are possible from the standpoint of structure are taking place. Since the rates of these chain processes are quite different, one particular chain process usually predominates and determines the experimentally observed rate and the composition of the intermediate and final products. Under different conditions, particularly at different temperatures, the controlling chain process may yield to another chain process which may alter the final products. In such cases there is a transition region in which both chain processes may occur with essentially equal rates and, as a result, a large variety of products are possible.

The essence of chain theory is the existence of active centers (free radicals and atoms) which are responsible for the mechanism of the chain process. The high chemical activity of these active centers is responsible for the development of the chain process since the free radical is capable of reacting with molecules accompanied by low energies of activation. The small activated energy associated with such reactions is attributed to the free electron of the free radical acting on the electrons forming the bonds in the molecule. The continuation or propagation of the chain process is based on the indestructibility of

the free radical during the reaction of a free radical with a molecule, i.e., the formation of a new radical for each reaction between a free radical and a molecule.

With the above concepts the initiation step which involves the formation or generation of free radicals from molecules is the only step which requires a significant energy consumption. Even though a high energy consumption is required for the initiation step, the comparable ease of the chain propagation step often enables the chain reaction to proceed rather than the direct reaction of molecules.

Termination of the chain usually involves one of the following: (1) quadratic breaking which is the recombination in the gas-phase of two free radicals to form a molecule, (2) the adsorption of the free radical on the wall of the reaction vessel with subsequent recombination, and (3) reaction of the free radical with an impurity to form a less-active free radical which eventually leads to recombination. The last two types of chain termination are denoted as linear breaking.

In the following discussion and mathematical treatment the terminology and nomenclature are essentially those presented by Shtern (65).

Before reviewing the kinetics of chain reactions there are several definitions and terms which should be discussed. The chain length, denoted by γ, is defined as

the number of chain steps occurring between the initiation step and the termination step or the number of elementary reactions stimulated by an active center. The symbols used to denote the probability of chain breaking and the probability of chain branching are β and δ, respectively. The kinetic coefficients are defined as the product of the specific rate constant and the concentration of the molecule taking part in the reaction. In the case when only free radicals take part in the reaction, i.e., no molecules take part in the reaction, the kinetic coefficient and the specific rate constant are identical.

The reaction rate of any chain reaction is approximately equal to the rate of chain propagation since the rate of chain initiation is negligible in comparison with the rate of chain propagation; stated mathematically

$$W = an \tag{2-1}$$

where W is the rate of reaction, a is the kinetic coefficient of the chain propagation step, and n is the concentration of active centers.

The concentration of the active centers is determined by solving the appropriate differential equation for the rate of change of the concentration of active centers with the condition that the concentration at the start of the reaction ($t = 0$) is zero ($n = 0$). For an unbranched chain reaction the rate is

$$W = \frac{aW_o}{g} (1 - e^{-gt}) \qquad (2\text{-}2)$$

where a and g are the kinetic coefficients of propagation and termination, respectively, and t is time.

Inspection of Equation (2-2) shows that, after the transient portion of the rate (e^{-gt}) becomes negligible in comparison with unity, the rate of reaction and the concentration of active centers n remain constant. So long as the decrease in the concentration of the initial reactants does not affect the chain propagation step, the above will hold.

Chain reactions have the property of producing new chains by branching. Chain branching is the result of a free radical and a molecule reacting to give three monovalent radicals or one monovalent and one divalent radical instead of only one free radical. The original chain propagation is continued by one of the radicals and new chains may be started by the other radicals. Since the branching step continues the chain and also generates new chains, the branching step opposes chain breaking.

In the course of a branched reaction there are three possibilities: (1) the probability of chain termination is greater than the probability of branching ($\beta > \delta$), (2) the probabilities of chain breaking and chain branching are equal ($\beta = \delta$), and (3) the probability of chain termination is less than the probability of chain branching ($\beta < \delta$).

The first possibility in a branched reaction ($\beta > \delta$) leads to the following expression for the rate:

$$W = \frac{aW_o}{g - f}\{1 - e^{-(g-f)t}\} \qquad (2\text{-}3)$$

where f is the kinetic coefficient of chain branching. Since the kinetic coefficient of breaking is greater than the kinetic coefficient of branching, i.e., $g > f$, this type of branched reaction exhibits the same properties as the unbranched chain reaction.

In the particular case when $\beta = \delta$ (or $g = f$) the rate of reaction becomes

$$W = aW_o t \qquad (2\text{-}4)$$

It is obvious that this type of branched reaction is nonstationary since the reaction rate and the concentration of active centers increase linearly with time. Although these branched reactions include both a termination step and a branching step, the reaction, once started, cannot be stopped until the consumption of initial reactants affects the chain process.

The rate of reaction for the case when $\beta < \delta$ (or $g < f$) is

$$W = \frac{aW_o}{f - g}\{e^{(f-g)t} - 1\} \qquad (2\text{-}5)$$

For relatively large values of t, Equation (2-5) reduces to

$$W = Ae^{\varphi t} \qquad (2\text{-}6)$$

where

$$A = \frac{aW_o}{f - g} \quad \text{and} \quad \varphi = f - g$$

This type of branched reaction ($\beta < \delta$) proceeds as if the termination step were nonexistent; therefore the reaction is auto-accelerating with respect to time.

It should be pointed out that in the preceding discussion on chain reactions it has been assumed that only one active center has participated in the reaction. For the majority of chain reactions more than one free radical is responsible for the chain process. Therefore, in the development of an expression for the overall rate of reaction, it is necessary to set up as many differential equations as there are active centers:

$$\frac{dn_i}{dt} = f(n_1, n_2, \ldots, n_i) \qquad (2\text{-}7)$$

In principle the system of differential equations can be solved; however, by using the method of quasi-stationary concentrations the determination of the concentrations of the free radicals is simpler. This method is based on the hypothesis that throughout the whole chain process the concentrations of the free radicals are considerably less than those of the reactants since the lifetime of these radicals is extremely short compared with the duration of the reaction. The assumption is made that the active centers are at steady state, or

$$\frac{dn_i}{dt} = o \qquad (2\text{-}8)$$

As a result of this approximation the concentration of the free radicals can be determined in terms of the reactants and the constants for the elementary radical reactions.

In the majority of cases the free radical responsible for a branching process reacts considerably slower than the other radicals participating in the chain reaction. The activation energy for this branching step is usually greater than the activation energy associated with the propagation step; therefore the concentration of the radical responsible for branching is considerably greater than the concentrations of the other radicals. Since the radical responsible for branching cannot be considered as steady, a modification of the method of quasi-steady states must be used. For this case it can be assumed, without a considerable loss in accuracy, that the remaining free radicals are at steady state, i.e., $dn_i/dt = o$. With this assumption only the differential equation for the non-stationary free radical remains.

The existence of another class of chain reactions was recognized in the early 1930's and designated as chain reactions with degenerate branching. This type of chain process exhibits the same self-acceleration that branched reactions exhibit in chain ignition; however the acceleration is many times slower. The same law for acceleration

applies to these reactions, i.e.,

$$W = Ae^{\varphi t} \qquad (2\text{-}6)$$

The time required for the rate to increase e times in degenerate branching reactions may be minutes or hours whereas the time required in chain ignition may be a fraction of a second.

The basis of the mechanism for reactions with degenerate branching is that intermediate molecular products are responsible for the branching step. These intermediate molecular products, formed in the chain propagation step, can form primary free radicals with greater ease than the original reactants. The rate of formation of primary radicals from these intermediates then determines the characteristic time for self-acceleration.

Theoretical Development of the Mechanism for Methane Oxidation at Low Pressure

The mechanism of the gas-phase oxidation of methane at low pressures appears to be well established with only a few obscurities still remaining to be answered. This section is devoted to the theoretical development of the mechanism of methane oxidation as presented by Semenov (64) and is included to illustrate some of the theoretical aspects of the kinetics of chain reactions.

After considering all the available data on the oxidation of methane at low pressures (one atmosphere or

less), Semenov proposed the following mechanism:

0) $CH_4 + O_2 \rightarrow \dot{C}H_3 + H\dot{O}_2$

1) $\dot{C}H_3 + O_2 \rightarrow HCHO + \dot{O}H$

2) $\dot{O}H + CH_4 \rightarrow H_2O + \dot{C}H_3$

2') $\dot{O}H + HCHO \rightarrow H_2O + H\dot{C}O$

3) $HCHO + O_2 \rightarrow H\dot{C}O + H\dot{O}_2$

4) $H\dot{C}O + O_2 \rightarrow CO + H\dot{O}_2$

5) $H\dot{O}_2 + CH_4 \rightarrow H_2O_2 + \dot{C}H_3$

5') $H\dot{O}_2 + HCHO \rightarrow H_2O_2 + H\dot{C}O$

6) $\dot{O}H \xrightarrow{\text{wall}}$ chain breaking

7) $HCHO \xrightarrow{\text{wall}}$ chain breaking

The initiation step is the reaction between methane and oxygen to give $\dot{C}H_3$ and $H\dot{O}_2$ radicals. The activation energy for this initiation step is 55 kcal/mole. At the beginning of the reaction when little formaldehyde is present, the rate of reaction is

$$W_{CH_4} = k_o [CH_4][O_2] \qquad (2\text{-}8)$$

where k_o is the specific rate constant. Using a pre-exponential term or frequency factor equal to 10^{-10} in the Arrhenius equation, the rate of initiation is

$$W_{CH_4} \approx 10^{-10}\ e^{-55000/RT}\ [CH_4][O_2] \qquad (2\text{-}9)$$

Formaldehyde, the main intermediate product, is the intermediate product responsible for the degenerate branching step. Theoretical analysis (64, Chapter VII) has shown that the degenerate branching step is

$$HCHO + O_2 \rightarrow \dot{HO}_2 + \dot{HCO} \qquad (2\text{-}10)$$

The activation energy for this step is 32 kcal/mole and since the reverse reaction is a recombination of radicals with a low activation barrier, the activation energy of this reaction must be close to its endothermicity. Therefore, additional free radicals are produced with greater ease in the degenerate branching step than in the initiation step.

As formaldehyde accumulates, radical initiation also occurs by step 3 at a rate

$$W_{HCHO} = k_3\ [HCHO][O_2] \qquad (2\text{-}11)$$

where k_3 is the specific rate constant. Using a pre-exponential term or frequency factor equal to 10^{-10}, the rate becomes

$$W_{HCHO} \approx 10^{-10}\ e^{-32000/RT}\ [HCHO][O_2] \qquad (2\text{-}12)$$

The ratio of the rates of the degenerate branching step and the initiation step becomes

$$R = \frac{k_3\ [HCHO][O_2]}{k_o\ [CH_4]\ [O_2]} \approx e^{23000/RT}\ \frac{[HCHO]}{[CH_4]} \qquad (2\text{-}13)$$

As a result the reaction proceeds immeasurably small at first, and as the formaldehyde accumulates the rate accelerates progressively. The time required for the accumulation of the formaldehyde to a certain concentration constitutes the observed induction period.

Chain propagation is the result of the following reactions:

$$1)\quad \dot{C}H_3 + O_2 \rightarrow CH_3O\dot{O}$$

$$1')\quad CH_3O\dot{O} \rightarrow HCHO + \dot{O}H \qquad (2\text{-}14)$$

$$2)\quad \dot{O}H + CH_4 \rightarrow \dot{C}H_3 + H_2O$$

From experimental data the rate of step 1, above, is

$$W_1 \approx 10^{-13}[O_2][\dot{C}H_3] = a_1[\dot{C}H_3] \qquad (2\text{-}15)$$

where a_1 is the kinetic coefficient. Apparently no activation energy is required for this reaction. In a stoichiometric mixture at 700°K and 235 mm mercury the kinetic coefficient a_1 is estimated to be 2.2×10^5 sec^{-1}.

From experimental data the rate of step 2 is

$$W_2 = 10^{-10}\, e^{-8500/RT}\, [CH_4][\dot{O}H] = a_2[\dot{O}H] \qquad (2\text{-}16)$$

At the same conditions as above a_2 is estimated to be 2.2×10^5 sec^{-1}.

Before the alkylperoxide radical $CH_3O\dot{O}$ can decompose into a formaldehyde molecule and a hydroxyl radical, $\dot{O}H$, it

first must isomerize.

$$CH_3O\dot{O} \rightarrow \dot{C}H_2\text{-}O\text{-}OH \qquad (2\text{-}17)$$

Apparently this reaction requires a large activation energy which is estimated at 20 kcal/mole. Then

$$W_1' = 10^{13}\, e^{-20000/RT}\, [CH_3O\dot{O}] = a_1'[CH_3O\dot{O}] \qquad (2\text{-}18)$$

At 700°K a_1' is equal to 6.3×10^6 sec^{-1}. Since a_1' is approximately 30 times larger than a_1 and a_2, the formation of formaldehyde may be represented in a single step, i.e.,

$$\dot{C}H_3 + O_2 \rightarrow HCHO + \dot{O}H$$

Chain termination is the result of the adsorption of hydroxyl radicals by the wall of the reactor with subsequent recombination and the heterogeneous oxidation of formaldehyde on the wall of the reactor. Since a_1 and a_2 are approximately equal, the concentrations of the methyl and hydroxyl radicals should be the same order of magnitude. It is known that the wall capture of hydroxyl radicals is greater than the wall capture of hydrogen atoms and that the wall capture of hydrogen atoms is probably greater than the wall capture of methyl radicals. The latter is based on the experimental results of cracking reactions. It can also be shown (64) that inclusion of a step for wall destruction of $H\dot{O}_2$ radicals does not alter the results obtained by omitting this step. Thus, the conclusion is reached that only the hydroxyl

radical and formaldehyde need to be considered in the chain breaking mechanism.

In addition to the omission of chain breaking reactions discussed above, the following reactions have also been omitted in the proposed mechanism: (1) reaction between formyl radicals, $\dot{HCO}$, and methane, (2) reaction between formyl radicals, $\dot{HCO}$, and formaldehyde, and (3) reaction between methyl radicals, $\dot{CH}_3$, and formaldehyde. Since the reaction between formyl radicals and methane is endothermic and the reaction between formyl radicals and oxygen is exothermic, the former can be neglected. Since the methane concentration is approximately 400 times greater than the concentration of formaldehyde, then the reaction between formyl radicals, $\dot{HCO}$, and formaldehyde can also be neglected. The reaction between methyl radicals and formaldehyde can be neglected on the basis that the reaction between methyl radicals and oxygen is approximately 40 times faster than the omitted reaction.

In the early stages of the oxidation process, the reactions of formaldehyde with free radicals can be neglected, but the degenerate branching step must be included. Even in the early stages when the formaldehyde concentration is low the generation of primary radicals by the branching step far exceeds that of the reaction between methane and oxygen.

The system of differential equations for the rate of change of radical concentrations in the early stages of

the reactions listed on page 13 is, when neglecting steps 2' and 5':

$$\frac{d[\dot{C}H_3]}{dt} = W_o + a_2[\dot{O}H] + a_5[H\dot{O}_2] - a_1[\dot{C}H_3]$$

$$\frac{d[\dot{O}H]}{dt} = a_1[\dot{C}H_3] - a_2[\dot{O}H] - a_6[\dot{O}H]$$

$$= a_1[\dot{C}H_3] - (a_2 + a_6)\,[\dot{O}H] \qquad (2\text{-}19)$$

$$\frac{d[H\dot{C}O]}{dt} = a_3[HCHO] - a_4[H\dot{C}O]$$

$$\frac{d[H\dot{O}_2]}{dt} = W_o + a_3[HCHO] - a_5[H\dot{O}_2] + a_4[H\dot{C}O]$$

$$\frac{d[HCHO]}{dt} = a_1\,[\dot{C}H_3] - a_3[HCHO] - a_7[HCHO]$$

Since the formaldhyde concentration determines the radical concentrations, the remaining radicals are assumed to be at steady state. Thus

$$\frac{d[\dot{C}H_3]}{dt} = \frac{d[\dot{O}H]}{dt} = \frac{d[H\dot{C}O]}{dt} = \frac{d[H\dot{O}_2]}{dt} = 0 \qquad (2\text{-}20)$$

Combining the set, Equation (2-19), and Equation (2-20),

$$[\dot{O}H] = \frac{2(W_o + a_3[HCHO])}{a_6} \qquad (2\text{-}21)$$

and

$$[H\dot{O}_2] = \frac{W_o}{a_5} \qquad (2\text{-}22)$$

Then:

$$\frac{d[HCHO]}{dt} = 2W_o\left(\frac{a_2}{a_6} + 1\right) + 2a_3[HCHO]\left(\frac{a_2}{a_6} - \frac{1}{2}\right) - a_7[HCHO] \tag{2-23}$$

Simplification of Equation (2-23) can be accomplished by observing that the ratio a_2/a_6 is the chain length γ which is estimated to be approximately 100. Neglecting both 1 and 1/2 in Equation (2-23), the rate of change of formaldehyde concentration becomes

$$\frac{d[HCHO]}{dt} = 2W_o \frac{a_2}{a_6} + \left(2a_3 \frac{a_2}{a_6} - a_7\right)[HCHO] \tag{2-24}$$

The solution of this differential equation with the condition that the formaldehyde concentration is zero at the start of the reaction is

$$[HCHO] = \frac{2W_o(a_2/a_6)}{\varphi}\left(e^{\varphi t} - 1\right) \tag{2-25}$$

where

$$\varphi = 2a_3 \frac{a_2}{a_6} - a_7 \tag{2-26}$$

Referring to Equations (2-16) and (2-21) the rate of methane oxidation for this scheme is

$$-\frac{d[CH_4]}{dt} = a_2[\dot{O}H] = a_2 \frac{2(W_o + a_3[HCHO])}{a_6} \tag{2-27}$$

or, with Equation (2-25),

$$-\frac{d[CH_4]}{dt} = 2W_o \frac{a_2}{a_6}\left[1 + \frac{2a_3a_2/a_6}{\varphi}\left(e^{\varphi t} - 1\right)\right] \tag{2-28}$$

The term φ in Equations (2-25) and (2-28) is a function of pressure since the term a_3a_2/a_6 is at least proportional to the square of the pressure whereas the term a_7 is only slightly affected by pressure. Thus, the term φ may be either positive or negative. If φ is positive, then Equation (2-28) applies; if φ is negative then

$$-\frac{d[CH_4]}{dt} = 2W_o \frac{a_2}{a_6}\{1 + 2a_3 \frac{a_2}{a_6}(1 - e^{-\varphi t})\} \qquad (2\text{-}29)$$

where

$$\varphi = \left|2a_3 \frac{a_2}{a_6} - a_7\right|$$

The critical pressure and critical diameter for the slowly accelerating reaction are determined by the condition that $\varphi = 0$, or

$$2a_3 \frac{a_2}{a_6} = a_7 \qquad (2\text{-}30)$$

since the product a_2a_3 is proportional to the square of the pressure and a_6 and a_7 are inversely proportional to the diameter of the reactor.

At pressures considerably greater than the critical pressure the heterogeneous oxidation of formaldehyde can be neglected, i.e., a_7 in Equation (2-26) = 0. Therefore, Equation (2-28) simplifies to

$$-\frac{d[CH_4]}{dt} = 2W_o \gamma e^{\varphi t} \qquad (2\text{-}31)$$

where

$$\gamma = a_2/a_6$$

The reaction rate determined from Equation (2-31) applies only during the early stages of the oxidation, viz., up to approximately 10 per cent conversion. For higher conversions the reactions between formaldehyde and free radicals must be included. The appropriate kinetic equations for the active centers will now include steps 2', and 5', listed on page 13. The formaldehyde concentration is rate controlling both during the initial and all subsequent stages of oxidation. Therefore, at these high conversions, all the free radical concentrations can be assumed to have attained steady state. The rate equations for high conversions, corresponding to the set, Equation (2-19), which was restricted to the initial stages of oxidation, will differ by the fact that Step 2' and 5' are included. Thus,

$$\frac{d[HCHO]}{dt} = a_1[\dot{C}H_3] - a_3[HCHO] - a_7[HCHO] - a_5'[H\dot{O}_2] - a_2'[\dot{O}H]$$

$$\frac{d[\dot{C}H_3]}{dt} = W_o + a_2[\dot{O}H] + a_5[H\dot{O}_2] - a_1[\dot{C}H_3] = 0$$

$$\frac{d[H\dot{C}O]}{dt} = a_3[HCHO] - a_4[H\dot{C}O] + a_2'[\dot{O}H] + a_5'[H\dot{O}_2] = 0$$

$$\frac{d[H\dot{O}_2]}{dt} = W_o + a_3[HCHO] - a_5[H\dot{O}_2] - a_5'[H\dot{O}_2] + a_4[H\dot{C}O] = 0$$

$$\frac{d[\dot{O}H]}{dt} = a_1[\dot{C}H_3] - a_2[\dot{O}H] - a_6[\dot{O}H] - a_2'[\dot{O}H] = 0$$

These 5 equations when combined yield

$$\frac{d[HCHO]}{dt} = (a_2 + a_6)\left\{\frac{2W_o + 2a_3[HCHO]}{a_6}\right\} - a_3[HCHO] - a_7[HCHO]$$

$$- \frac{a_5'}{a_5}\{2W_o + 2a_3[HCHO]\} - \frac{a_5'a_2'}{a_5a_6}\{2W_o + 2a_3[HCHO]\} + \frac{a_5'}{a_5}W_o$$

According to Semenov $a_2 >> a_6$ and $W_o << a_3[HCHO]$. Further, since $a_2' = k_2'[HCHO]$ and $a_5' = k_5'[HCHO]$, the preceding equation then reduces to

$$\frac{d[HCHO]}{dt} = \left(\frac{2a_2a_3}{a_6}[HCHO] - a_3[HCHO] - a_7[HCHO]\right)$$

$$- \frac{2a_3k_5'}{a_5}[HCHO]^2 - \frac{2k_2'k_5'a_3}{a_5a_6}[HCHO]^3 \qquad (2\text{-}32)$$

When the pressure is far in excess of the critical pressure, the term $a_7[HCHO]$ can be neglected. Also, since the term $a_3[HCHO]$ is about 200 times smaller than the first term in the parenthesis of Equation (2-32), the term $a_3[HCHO]$ can also be neglected. With these assumptions and substitution of the product of the specific rate constant and molecular product concentration for some of the kinetic coefficients, Equation (2-32) becomes

$$\frac{d[HCHO]}{dt} = \frac{2a_2a_3}{a_6}[HCHO]\left\{1 - \frac{k_5'a_6[HCHO]}{k_5a_2[CH_4]}\left(1 + \frac{k_2'a_2}{k_2a_6}\frac{[HCHO]}{[CH_4]}\right)\right\} \qquad (2\text{-}33)$$

If it is assumed that the steric factors for the specific rate constants k_2' and k_2 are equal and the steric factors for the specific rate constant k_5' and k_5 are also

equal, then the ratios k_2'/k_2 and k_5'/k_5 can be determined by the differences in activation energies. The differences in the activation energies for k_2 and k_2' and k_5 and k_5' are estimated to be 6 kcal/mole and 11 kcal/mole, respectively. At 700°K

$$k_2'/k_2 = e^{6000/RT} \approx 70$$

and

$$k_5'/k_5 = e^{11000/RT} \approx 2.5 \times 10^3$$

Then

$$\frac{d[HCHO]}{dt} = \frac{2a_2a_3}{a_6}[HCHO]\{1 - 25\alpha\ (1 + 7000\alpha)\} \qquad (2\text{-}34)$$

where

$$\alpha = \frac{[HCHO]}{[CH_4]} \text{ and } a_2/a_6 = \gamma \approx 100$$

With dimensionless time $\tau = ta_6/2a_2a_3$, Equation (2-34) becomes

$$\frac{1}{[HCHO]}\frac{d[HCHO]}{d\tau} = 1 - 25\alpha(1 + 7000\alpha) = 1 - f(\alpha) \qquad (2\text{-}35)$$

If various values of α are assumed, the right hand side of Equation (2-35) can be determined and the results plotted. At α = 0.234 per cent of the methane content the righthand side of the equation is zero and

$$\frac{d[HCHO]}{dt} = 0$$

After the attainment of steady state the formaldehyde concentration does not change. The experimental value for α at 700°K is 0.51 per cent of the methane content of the mixture.

Substituting the products of the specific rate constant and the concentration of the molecular substance for the remaining kinetic coefficients, and neglecting unity in front of $k_2'a_2[HCHO]/k_2a_6[CH_4]$, Equation (2-33) reduces to

$$\frac{d[HCHO]}{dt} = \frac{2k_2k_3}{a_6}[CH_4][O_2][HCHO]\left(1 - \frac{k_2'k_5'}{k_2k_5}\frac{[HCHO]^2}{[CH_4]^2}\right) \qquad (2\text{-}36)$$

When the formaldehyde concentration reaches a maximum, Equation (2-36) becomes

$$[HCHO]_{max} = \sqrt{\frac{k_5k_2}{k_5'k_2'}}[CH_4] \qquad (2\text{-}37)$$

$$= e^{-8500/RT}[CH_4]$$

which agrees reasonably well with the experimental results of Karmilova, Yenikolopyan, and Nalbandyan (29). These investigators found that the maximum formaldehyde concentration followed the law:

$$[HCHO]_{max} \propto e^{-10000/RT}$$

The rate of methane oxidation at conversions greater than 10 per cent is (similar to derivation of Equation 2-32):

$$-\frac{d[CH_4]}{dt} = a_2[\dot{O}H] + a_5[H\dot{O}_2]$$

or

$$-\frac{d[CH_4]}{dt} = \{k_2'[HCHO] + a_2\}\ 2\ \left\{\frac{W_o + a_3[HCHO]}{a_6}\right\}$$

$$+ W_o + 2a_3[HCHO] \qquad (2\text{-}38)$$

Since $W_o << a_3[HCHO]$ and $1 << a_2/a_6$, and noting that $a_3 = k_3[O_2]$, the above expression reduces to

$$-\frac{d[CH_4]}{dt} = \frac{2}{a_6}\{k_2[CH_4] + k_2'[HCHO]\}\{k_3[HCHO][O_2]\} \qquad (2\text{-}39)$$

When the formaldehyde concentration reaches a maximum as given by Equation (2-37), the overall reaction rate also reaches a maximum which is

$$-\frac{d[CH_4]}{dt} = \frac{2}{a_6}\left\{k_2 + k_2'\left(\frac{k_2k_5}{k_2'k_5'}\right)^{\frac{1}{2}}\right\}\left\{k_3\left(\frac{k_2k_5}{k_2'k_5'}\right)^{\frac{1}{2}}[O_2][CH_4]^2\right\} \qquad (2\text{-}40)$$

Since the ratios of k_2'/k_2 and k_5'/k_5 have been approximated and the term $k_2'\left(\frac{k_2k_5}{k_2'k_5'}\right)^{\frac{1}{2}}$ is approximately six times smaller than the term k_2, a rough approximation of the overall reaction rate is

$$-\frac{d[CH_4]}{dt} = \frac{2k_2k_3}{a_6}\left(\frac{k_2k_5}{k_2'k_5'}\right)^{\frac{1}{2}}[CH_4]^2[O_2] \qquad (2\text{-}41)$$

A relationship of this type was found by Norrish (48).

Theoretical Aspects of the Mechanism for Methane Oxidation at High Pressures

The mechanism generally accepted for the oxidation of methane at low pressures does not adequately represent the oxidation process at high pressures. The experimental fact that an increase in pressure increases the quantity of methanol formed and decreases the yield of formaldehyde can not be explained by the kinetic mechanism presented in the

previous section. The purpose of this section is to discuss a possible mechanism for the oxidation of methane at high pressures.

The oxidation process at high pressures is also a chain reaction with degenerate branching. Formation of $\dot{C}H_3$ radicals and $H\dot{O}_2$ radicals from the molecular reaction between methane and oxygen initiates the chain process. Degenerate branching is attributed to the reaction between formaldehyde and oxygen to form $H\dot{C}O$ and $H\dot{O}_2$ radicals.

Semenov has shown for the low pressure mechanism that formaldehyde formation can be represented as a single reaction, i.e.,

$$\dot{C}H_3 + O_2 \rightarrow HCHO + H\dot{O}$$

The rate of isomerization and decomposition of the peroxide radical $CH_3\dot{O}O$ is sufficiently fast to allow such a representation. However, at the conditions encountered at higher pressures a reaction between the peroxide radical and methane may compete strongly with the decomposition and greatly affect the product distribution. This reaction forms a methyl radical and methylhydroperoxide which decomposes into methoxy and hydroxyl radicals. Methyl alcohol is formed by a reaction between the methoxy radical and methane.

In the liquid phase oxidation of hydrocarbons, it has been shown experimentally that the alkylhydroperoxide is the first stable intermediate product. The formation of alcohols and other oxygen-containing compounds are due to

the further transformation of the alkylhydroperoxide (76). Gray (21) has shown that the stability of the methoxy radical toward decomposition is sufficient at the temperatures of gas-phase oxidation of hydrocarbons to allow reaction with the initial hydrocarbon. The experimental work of Nalbandyan and Kleimenov (43) indicates that at least 90 per cent of the formaldehyde comes from the peroxide radical and not from the peroxide.

Incorporation of the above ideas into a chain process suggests the following mechanism for the high pressure oxidation of methane:

$$
\begin{aligned}
&0)\quad CH_4 + O_2 \rightarrow \dot{C}H_3 + H\dot{O}_2 \\
&1)\quad \dot{C}H_3 + O_2 \rightarrow CH_3O\dot{O} \\
&2)\quad CH_3O\dot{O} + CH_4 \rightarrow \dot{C}H_3OOH + \dot{C}H_3 \\
&3)\quad \dot{C}H_3OOH \rightarrow CH_3\dot{O} + \dot{O}H \\
&4)\quad CH_3\dot{O} + CH_4 \rightarrow CH_3OH + \dot{C}H_3 \qquad (2\text{-}42) \\
&5)\quad CH_3O\dot{O} \rightarrow HCHO + \dot{O}H \\
&6)\quad \dot{O}H + CH_4 \rightarrow H_2O + \dot{C}H_3 \\
&7)\quad \dot{O}H + HCHO \rightarrow H_2O + H\dot{C}O \\
&8)\quad HCHO + O_2 \rightarrow H\dot{C}O + H\dot{O}_2 \\
&9)\quad H\dot{C}O + O_2 \rightarrow H\dot{O}_2 + CO \\
&10)\quad H\dot{O} \xrightarrow{\text{wall}} \text{chain breaking}
\end{aligned}
$$

11) $CH_3O\dot{O} \xrightarrow{\text{wall}}$ chain breaking

The following reactions have not been included: (1) the reaction between formyl radicals and methane, (2) the reaction between formyl radicals and formaldehyde, (3) the reaction between methyl radicals and formaldehyde, and (4) the chain breaking reactions involving the adsorption of $\dot{C}H_3$ and $H\dot{O}_2$ radicals by the wall of the vessel with subsequent recombination and the heterogeneous oxidation of formaldehyde. The two reactions involving the participation of formyl radicals, methane, and formaldehyde are neglected on the basis that these reactions are endothermic, whereas the reaction between formyl radicals and oxygen is exothermic. The rate of the reaction between methyl radicals and oxygen is approximately 40 times greater than the rate of reaction between methyl radicals and formaldehyde (64); therefore the latter reaction is neglected. Omission of chain breaking steps involving $\dot{C}H_3$ and $H\dot{O}_2$ radicals is justified by the fact that the probability of wall capture of these radicals is less than the probability of wall capture of the hydroxy and peroxide radicals (64). Chain breaking by the heterogeneous oxidation of formaldehyde only applies at pressures close to the critical pressure of the reaction.

Some interesting points are brought out if the rates of steps 1 through 6 and 8 are compared. It should be pointed out that the estimations of these rates are extremely rough since rate data for these reactions at high pressure are

not available. The assumption is also made that the radical concentrations are approximately equal; therefore the kinetic coefficients can be used in the comparisons. At low pressures the usual range for the activation energy of a reaction between radicals and molecules is 7 to 10 kcal/mole and the pre-exponential term, or frequency factor, varies between 10^{-11} and 10^{-13} (64, 65). In the estimations which follow, the concentrations of methane and oxygen are determined for a $10CH_4 + O_2$ mixture at 2000 psi and 640°F.

If it is assumed that the rate of reaction 1 is equal to the rate at low pressures (25, 26), i.e.,

$$W_1 = 10^{-13}[O_2][\dot{C}H_3] = a_1[\dot{C}H_3] \qquad (2\text{-}43)$$

then a_1 is equal to 6.02×10^{7} sec^{-1}.

Assuming that the activation energy required for step 2 is 10 kcal/mole and the frequency factor is 10^{-11}, the rate is

$$W_2 = 10^{-11}\, e^{-10000/RT}[CH_4][\dot{C}H_3] = a_2[\dot{C}H_3] \qquad (2\text{-}44)$$

and a_2 is equal to 5.9×10^{-6} sec^{-1}.

According to Semenov (64) the activation energy for the decomposition of an alkylhydroperoxide lies between 31 and 35 kcal/mole. Assuming that the activation energy is 32 kcal/mole and the frequency factor is 10^{13}, the rate for step 3 is

$$W_3 = 10^{13}\, e^{-32000/RT}[\dot{C}H_3OOH] \qquad (2\text{-}45)$$

Since the concentration of methylhydroperoxide is unknown, the rate can be expressed only as a function of the peroxide concentration.

$$W_3 = 18.8\ [\dot{C}H_3OOH] \qquad (2\text{-}46)$$

Since steps 2, 4, and 6 are reactions between a radical and a molecule, and if the same values for the activation energy and frequency factor are used, a_4 and a_6 are also equal to $5.9 \times 10^6\ sec^{-1}$.

Semenov (64) has estimated the activation energy for the isomerization of peroxide radicals to be approximately 20 kcal/mole. If the frequency factor is assumed to be 10^{13}, then

$$W_5 = 10^{13}\ e^{-20000/RT}[\dot{C}H_3OO] = a_5[\dot{C}H_3OO] \qquad (2\text{-}47)$$

and a_5 is equal to $8.56 \times 10^5\ sec^{-1}$.

According to Semenov (64) the rate of reaction for step 8 is

$$W_8 = 10^{-10}\ e^{-32000/RT}\ [HCHO][O_2] \qquad (2\text{-}48)$$

or

$$W_8 = 0.308\ [HCHO] \qquad (2\text{-}49)$$

Comparing the reaction rates of steps 1, 2, and 5, it is observed that the slowest step is that of the isomerization and decomposition of the peroxide radical. If this assumption is valid, then the formation of formaldehyde cannot be represented in a single step. It is also interesting

to note that, for an equivalent branching rate, the concentration of formaldehyde is approximately 60 times greater than that of the peroxide. A similar observation was pointed out by Shtern (65) in his discussion on the oxidation of heavier hydrocarbons.

The possibility thus arises that perhaps the rate of decomposition of the peroxide, CH_3OOH, is fast enough to consider that methyl alcohol is formed in a termolecular reaction.

$$CH_3O\dot{O} + 2CH_4 \rightarrow 2CH_3OH + \dot{C}H_3 \qquad (2\text{-}50)$$

Jost, et al., (28) also suggested such a reaction for the oxidation of heavier hydrocarbons, but experimental verification of this termolecular reaction has not been attempted.

CHAPTER III

REVIEW OF PREVIOUS WORK

The homogeneous gas-phase oxidation of methane and paraffinic hydrocarbons with molecular oxygen can be divided into two basic regions: (1) the slow oxidation region which covers a temperature range between 200 and 600°C and (2) the region of explosive oxidation of the hydrocarbon in flames. The discussion in this chapter is limited to the gas-phase, slow oxidation of methane by free oxygen.

Prior to the end of the nineteenth century all experimental work was conducted at explosive conditions (65). In 1874 Armstrong (2), after observing the inconsistencies of the proposed mechanism for oxidation of hydrocarbons, proposed that the intermediate stages of this process could be represented by the formation of an unstable hydroxylated molecule. These unstable hydroxylated molecules were subsequently broken-down at the high temperatures of the combustion process into oxygen-containing products. Armstrong pointed out that in order to explain the combustion of hydrocarbons, studies at more favorable conditions for the determination of the actual mechanism of combustion must be carried-out. As a result, by the end of the nineteenth

century more attention was being given to studies of the slow oxidation, rather than the explosive reactions, of hydrocarbons.

Since these initial investigations on the slow oxidation of hydrocarbons, an ever increasing amount of work has been devoted to the elucidation of the mechanism for hydrocarbon oxidation. For a thorough treatment of the development of the research on hydrocarbon oxidation in the gas-phase the reader is referred to the monograph by Shtern (65). Shtern has conveniently divided the development into three periods. The first period covers the period between the late 1890's to the end of the 1920's and deals primarily with the identification of stable intermediate and end products arising in the reacting mixture throughout the course of the reaction. The second period, which covers the period from the end of the 1920's to the middle of the 1930's, deals primarily with the formulation and examination of the kinetic mechanism of hydrocarbon oxidation in terms of the chain theory which was rapidly developing in this period. The third period, which covers the period from the middle of the 1930's to the early 1960's, deals primarily with the investigation of the oxidation process. By this time the precise chemical definition of the kinetic mechanism had been established as being of a chain nature involving degenerate branching.

Experimental Work

After Bone and Lean (9), Bone and Cain (7) and Smithells and Ingle (68) had definitely established that the

products in the explosive combustion of hydrocarbons occurring in a deficiency of oxygen were carbon monoxide and hydrogen, Bone and his coworkers began a series of studies on the slow oxidation of hydrocarbons. In 1902 Bone and Wheeler (10) reported the first results on the slow oxidation of methane under static conditions. Bone and Wheeler (11) subsequently studied the slow oxidation of methane using a closed system in which the reacting mixture could be continuously circulated over a heated surface. The first study was conducted at initial temperatures of 300-400°C and at pressures of the order of 2 atmospheres. The initial temperatures of the second study were varied between 400 and 500°C and the pressure was varied between 400 and 600 mm mercury. A reaction mixture containing two volumes of methane and one volume of oxygen was used throughout. In the first study carbon monoxide, carbon dioxide, and water were formed; however, in the second study, in addition to the above products, formaldehyde and formic acid were also detected in the products. Free carbon and free hydrogen were not found in the reaction products during either study.

In 1932 Bone and Allum (6) published the results of a comprehensive investigation on the slow combustion of methane. Throughout these studies the authors were successful in conducting carbon, hydrogen, and oxygen balances throughout the course of the oxidation. The reactivity of various compositions of the initial mixture of methane and oxygen

were studied at various initial temperatures and pressures. The products of the oxidation reaction were reported to be carbon monoxide, carbon dioxide, water, and formaldehyde. The influence of "foreign" vapors on the duration of the induction period and the reaction period was also studied. The "foreign" vapors added to the reaction mixture in small concentrations included water, methyl alcohol, formaldehyde, nitrogen dioxide, and iodine. Addition of these "foreign" vapors eliminated the induction period and shortened the reaction time with the exception of water vapor, which shortened the induction period as well as the reaction period. Later, Bone and Gardner (8) found that the addition of iodine vapor increased rather than decreased the induction period and the reaction period.

Bone and Gardner (8) studied the kinetics of methane oxidation with respect to pressure increase and with respect to the accumulation of formaldehyde. They noted that the attainment of a maximum concentration of formaldehyde occurred almost simultaneously with the end of the induction period. In addition the time of attainment of maximum formaldehyde concentration coincided with the time of maximum rate as determined by the pressure increase. Furthermore, the reaction rate and formaldehyde concentration remained essentially constant to the end of the reaction. The addition of formaldehyde to the initial mixture reduced or eliminated the induction period. These facts led the authors to the conclusion

that formaldehyde was the active intermediate product which determined the kinetics and chemical nature of the reaction.

Newitt and Haffner (45) were the first to study the oxidation of methane at elevated pressures. The reaction mixture employed in this study had the composition $2CH_4 + O_2 +$ (6 to 6.5)X, where X represents either excess methane, nitrogen, carbon dioxide, or steam. The initial temperature was varied from 335 to 400°C while the pressure was varied from 10 to 150 atmospheres. The products of the oxidation of methane at elevated pressures were reported to be carbon monoxide, carbon dioxide, water, formaldehyde, methyl alcohol, and traces of formic acid. The results of this work showed that: (1) methyl alcohol was formed at elevated pressures, (2) there was an optimum temperature at a particular pressure for optimum production of methyl alcohol and formaldehyde, (3) increasing the pressure increased the quantity of methanol and formaldehyde as well as the ratio of methanol to formaldehyde, (4) the addition of a diluent other than excess methane increased the induction period, and (5) both methyl alcohol and formaldehyde appeared in the early stages of the oxidation.

Two years later Newitt and Szego (46) reported the results of their study on the oxidation of methane in a flow system operated at elevated pressures. Mixtures of $90CH_4 + 3O_2 + 7N_2$ and $90CH_4 + 5O_2 + 5N_2$ were used in this study. The results of their work indicated that an increase in oxygen

concentration while maintaining approximately the same temperature, pressure, and contact time decreased the yield of methyl alcohol and formaldehyde. Decreasing the residence time at constant temperature and pressure increased the yield of alcohol and formaldehyde.

All of the methane oxidation studies cited above were conducted by Bone or one of his students. However, there were several other investigators who also contributed to the accumulation of experimental data necessary for the elucidation of the mechanism. In 1928 Pease and Cheseboro (58) observed for the first time that the reaction rate in a glass tube packed with broken glass was less than the reaction rate observed in an empty glass tube. The same phenomenon was also observed by Fort and Hinshelwood (18) in 1930. These authors found that the reaction rate was proportional to the third or even the fourth power of the vessel diameter. It was thus established that an increase in the surface-volume ratio decreased the reaction rate. An effect of this type is characteristic of a reaction that proceeds by a chain mechanism, wherein the packed tube serves as a more efficient chain-terminator.

In the same year that Newitt and Szego published the results of their work on methane oxidation at elevated pressures, the results of two other studies conducted at elevated pressure were reported. Wiezevich and Frolich (80) and Paris (52) confirmed the results already obtained; however,

the former reported a larger quantity of formic acid in the liquid products than the other investigators had reported.

Shtern (65) has pointed out that Bone and his school made a significant contribution to the mechanism formulation although Bone did not use it to extend his own theory. In these investigations Bone and his co-workers were the first to attempt to derive a composition balance not only in terms of the end products of the oxidation but also in terms of the stable products formed during the course of the reaction. The significance of the composition balance during the course of the reaction lies in the fact that it allows drawing accurate conclusions regarding the real mechanism of the oxidation process.

In addition to the above contribution by Bone and his followers, their experimental investigations are of great value for another reason. During these studies a start was made to determine how the pressure changes during the course of the reaction and how temperature, pressure, nature and treatment of the surface, change in the surface-volume ratio, addition of inert gases and chemically active additives affect the reaction.

Shtern also points out that Newitt and his co-workers (45, 46) obtained "important factual material of undoubted significance for the detailed understanding of the mechanism of hydrocarbon oxidation" because only a limited number of gas-phase hydrocarbon oxidation studies has been made at elevated pressures.

Norrish and Foord (48) continued the investigation of methane oxidation under static conditions at subatmospheric pressure. The steady maximum rate was represented by the expression

$$W_{max} = k[CH_4]^2 [O_2]P$$

where P is the total pressure. The magnitude of k depends upon the catalytic activity of the surface of the vessel. Confirmation of previous data regarding the shape of the pressure rise with respect to time, the effect of vessel diameter, addition of various "foreign" vapors, and the effect of pressure was obtained. These authors formulated a mechanism based upon the experimental data available and the chain theory with degenerate branching introduced by Semenov (63). Norrish and Foord were among the first investigators to use the method of quasi-stationary states in hydrocarbon oxidation in an attempt to verify experimental data and the proposed mechanism (65).

Norrish and Reagh (51) conducted a special study of the effect of the diameter of the reaction vessel on the oxidation of methane and other hydrocarbons. For all hydrocarbons studied it was found that only with a diameter less than 12-16 mm did the diameter affect the reaction rate. It was determined that, in vessels having a diameter less than 5 mm, reaction was not detected even after 24 hours.

In 1946 Patry and Monceaux (53) reported their results on the oxidation of methane at atmospheric pressure and

temperatures up to 800°C. Formaldehyde was the only oxygenated organic compound identified and the yield was always low.

Even with the abundance of experimental data available on the oxidation of methane and heavier paraffinic hydrocarbons, there were still many unanswered questions. The actual role of the formaldehyde, the identification of the intermediate product responsible for degenerate branching, the explanations for discrepancies in the activation energies, and the variations of the maximum reaction rate with respect to the pressure rise were not known. In an attempt to answer some of these questions additional studies were made by the investigators of hydrocarbon oxidation in the late 1940's.

A study to determine the role of formaldehyde in methane oxidation was conducted by Norrish and Harding (49). In this study formaldehyde was added to the reaction mixture in an amount greater than the maximum concentration attained in the straight oxidation of methane (without addition of formaldehyde). The induction period was eliminated and the maximum reaction rate was initially accelerated. The rate rapidly decreased to that rate corresponding to a system without additives (formaldehyde) and then remained unchanged throughout the remaining portion of the reaction. Vanpée and Grard (75) later showed that, if the added formaldehyde corresponded to the maximum concentration attained during the reaction without additives, the induction period was eliminated. However, the reaction rate corresponded to that

attained in a reaction without additives. Norrish and Patnaik (50) confirmed the hypothesis that the concentration of formaldehyde was linked to the reaction rate by subjecting a methane-oxygen mixture, contained in a quartz vessel at 485°C, to ultraviolet light with a wave length between 2400 and 3800 Å.

Hoare and Walsh (23, 24) carried out experiments on methane oxidation which can be divided into two groups according to the temperature. The first group, studied at temperatures around 500°C, indicated that the nature and surface condition has an effect on the reaction rate, on the orders of the reaction, and on its activation energy. The second group, studied at temperatures between 650 and 750°C, confirmed that the role of carbon monoxide in the process of methane oxidation was linked with its own oxidation. Egerton, Minkoff, and Salooja (16), while studying the effect of the surface on the course of methane oxidation, noted that the rate of reaction was considerably lowered by exposing the surface of the reaction vessel (pyrex, soda glass, packed beds, and coated vessels) to air between experiments. They also reported that increasing the surface to volume ratio did not change the rate, activation energy, or reaction order. In addition to formaldehyde, hydrogen peroxide was detected in the liquid products.

Karmilova, Yenikolopyan, and Nalbandyan (29, 30) obtained kinetic curves with respect to pressure increase,

consumption of methane and oxygen, and accumulation of carbon monoxide, carbon dioxide, water, formaldehyde, and hydrogen peroxide for the oxidation of methane in a quartz vessel at subatmospheric pressure. The variation of the maximum concentration of formaldehyde with temperature followed the law

$$[HCHO]_{max} \propto e^{-10000/RT}$$

In 1959 Magee, (38) after studying the kinetics of methane oxidation at 815°F, stated that the results indicated a need for revising the previous, slow oxidation mechanisms for methane.

The only additional research on the oxidation of methane at elevated pressures since 1934 was done by Furman (19) and Furman, Shestakova, and Radle-Desyatnik (20). Confirmation of the results reported by Newitt and Szego (46) was obtained. It was concluded by these authors that at elevated pressures, the oxidation of methane (paraffins) proceeds according to a chain mechanism.

In 1955 Vanpée reported the occurrence of peaks in the pressure rise curves during methane oxidation ($2CH_4 + O_2$) under static conditions at a temperature of 500°C and a pressure of 800 mm mercury. The cool flame phenomenon had been observed earlier for other hydrocarbons (see, for example, Aivazov and Neiman (1) or Knox and Norrish (33); however, this study was the first time that methane oxidation had yielded the phenomenon.

Reaction Mechanism and Kinetics

The earliest theory on the mechanism of methane oxidation proposed that carbon and water were the initial products of the reaction or that hydrogen burned rather than carbon. In 1861 Kersten (31) proposed that carbon monoxide and hydrogen were the primary products and, although carbon may be produced throughout the course of the reaction, it oxidized to carbon monoxide before the hydrogen reacted. Late in the nineteenth century Bone (7, 9) and Smithells and Ingle (68) showed experimentally that carbon monoxide and hydrogen were formed in the explosive combustion of hydrocarbon occurring in a deficiency of oxygen. These reliable experimental results apparently answered the question concerning the mechanism of the hydrocarbon oxidation and the preferential combination of the oxygen with the carbon of the ruptured hydrocarbon.

However, late in the nineteenth century there was evidence that this viewpoint was in error since it was possible to react oxygen with a hydrocarbon without rupture of the carbon skeleton. In 1874 Armstrong (2), after observing the inconsistency of the proposed mechanism, proposed that the intermediate stages of the combustion of hydrocarbons could be represented by the formation of an unstable, hydroxylated molecule by the introduction of an oxygen into the hydrocarbon molecule. These hydroxylated molecules were then decomposed at the high temperatures.

In 1903 Armstrong (3) suggested that the oxygen acts as molecular oxygen and combines with the methane molecule to form hydroxyl compounds. He further proposed that water takes part in the reaction and that hydrogen peroxide is formed; however he could never substantiate his theory with experimental data.

In the same year Bone (11) formulated the hydroxylation theory for the mechanism of hydrocarbon oxidation. After the accumulation of additional data (12) Bone postulated that the slow oxidation of methane (and paraffinic hydrocarbons in general) can be represented as a series of successive hydroxylating and thermal decomposition steps. By this scheme methyl alcohol is the first stable intermediate product formed. In successive stages formaldehyde, formic acid, and carbonic acid are formed. He theorized that methanol was formed by the introduction of an oxygen atom between separated hydrogen and carbon atoms in a methane molecule. Thus, for the oxidation of methane the hydroxylation theory can be illustrated in the following manner.

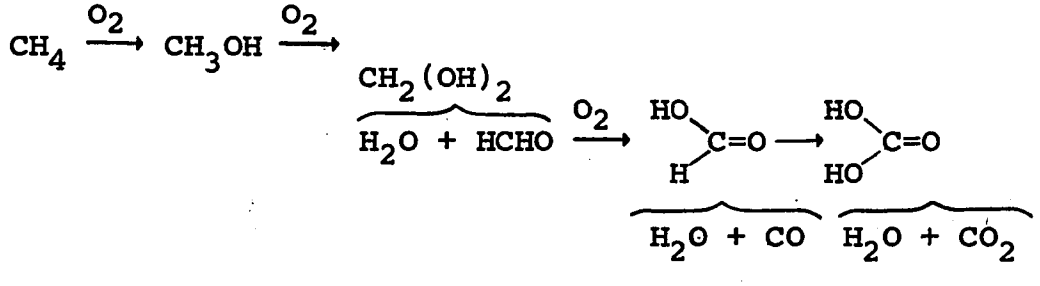

It was quickly pointed out by opponents of the mechanism that methanol had not been discovered in the

products of the oxidation process. Also, since formaldehyde and formic acid, which were found in the products, were less stable to oxidation than methanol, then the first stable intermediate product could not be methanol. In spite of this criticism Bone remained convinced that the hydroxylation theory was correct. For the next thirty years Bone and his followers carried out numerous studies in an attempt to isolate methanol and hence verify the theory.

The first discovery of alcohol in the products was reported in 1932 when Newitt and Haffner (45) published their results on methane oxidation studies at elevated pressures. Similar results were obtained for the oxidation of ethane (12). Finally in 1936 Newitt and Gardner (44) established the formation of alcohol at atmospheric pressures. Norrish and Foord (48) criticized the results of this study on the basis that the nature of the experimental procedure required to obtain the methyl alcohol indicated a catalytic reaction. Hence, the results had no bearing on the origin of the formaldehyde in the homogeneous gas-phase oxidation of methane.

Now that alcohols had been found in the products of the oxidation of hydrocarbons Bone felt that he had solved the basic problem and that the main objection to his theory had been overruled. However, by the middle thirties when alcohols were found in the products, new ideas on the reaction mechanism were being developed and once again the hydroxylation theory was no longer acceptable.

The peroxidation scheme for the oxidation of hydrocarbons derived its origin from general peroxide theory of oxidizing reactions, which was simultaneously and independently formulated by Bach (4) and Engler (17) in 1897. The basic principle of this scheme is that a peroxide is formed in the first stage of the oxidation by the direct addition of the oxygen to the substance undergoing oxidation. In the 1920's investigators concerned with the combustion process in the internal combustion engine applied the peroxidation theory to hydrocarbon oxidation in the gas phase. In 1926 Callender (13) introduced his theory that engine "knocking" was the result of the explosion of the organic peroxides formed during the preflame, slow oxidation process. Four fundamental investigations devoted to the objective of verifying the formation of such peroxides were conducted by Callender (13), Mardles (40), and Mondain-Monval and Quanquin (41, 42). Peroxides were detected in these investigations in a qualitative manner and only in very minute quantities. It should be pointed out that in only one of these studies (41) was methane used and the peroxide test was negative. The nature of the peroxides was not determined. Proponents of the hydroxylation scheme doubted that these peroxides were alkyl peroxides.

Two other mechanisms for hydrocarbon oxidation were proposed before the development of the mechanisms based upon chain reaction theory. The first of these mechanisms was

introduced by Edgar and his co-workers (59). The basic hypothesis was that aldehydes are the first products of the oxidation reaction and the transformation of the hydrocarbon is a step-by-step degradation of aldehydes. In 1927, the second mechanism was introduced by Lewis (35) who postulated that the first step in the oxidation of paraffinic hydrocarbons is the splitting-off of a hydrogen molecule with the formation of an unsaturated hydrocarbon, i.e., the oxidation is initiated by the dehydrogenation of the paraffinic hydrocarbon. The further oxidation of the unsaturated hydrocarbon thus formed a wide variety of oxygenated products.

The four schemes, hydroxylation, peroxidation, aldehyde degradation, and dehydrogenation, proposed before the development of chain reaction theory were based upon the assumption that the complete oxidation process could be described or represented in step-by-step reactions between molecules of the initial fuel and the products formed and molecules of oxygen. The primary disagreement among these schemes involved the first intermediate product formed in the process. Two of the schemes (hydroxylation and aldehyde degradation) set forth a step-by-step sequence of the complete transformation of the hydrocarbon molecule (through stable intermediate products) to the end products (oxides of carbon and water). The schemes of peroxidation and dehydrogenation were concerned only with the establishment of the first stable product of the oxidation process.

Between 1934 and 1937 six mechanisms based upon radical chain theory were introduced. Semenov (63) introduced the first radical-chain mechanism for the oxidation of methane. On the basis that the first stable reaction product was formaldehyde and not a peroxide, Semenov proposed a chain reaction which developed by di-radicals:

$$\ddot{O} + CH_4 \longrightarrow \ddot{C}H_2 + H_2O$$

$$\ddot{C}H_2 + O_2 \longrightarrow HCHO + \ddot{O}$$

For the further oxidation of formaldehyde, overall equations were presented instead of chain mechanisms. The chain breaking step was assumed to be the destruction of the oxygen di-radical at the wall. In Semenov's scheme the chain carriers are the methylene radical and the oxygen atom. Although the introduction of di-radicals as the chain carriers was a novelty, there had been previous experimental evidence of their occurrence (61).

Two years passed before Norrish and Foord (48) presented another radical-chain scheme for methane oxidation. The chain mechanism was represented in the following way.

$$CH_4 + O_2 \longrightarrow HCHO + H_2O$$

$$HCHO + O_2 \longrightarrow \ddot{O} + HCOOH$$

$$\ddot{O} + CH_4 \longrightarrow \ddot{C}H_2 + H_2O$$

$$\ddot{C}H_2 + O_2 \longrightarrow HCHO + \ddot{O}$$

$H_2O + CO$ — Branching

Chain Initiation

Basic Chain

$$HCHO \xrightarrow{\text{oxidation}} CO + H_2O$$

$$HCHO + \ddot{O} \longrightarrow X$$

$$\ddot{O} \xrightarrow{\text{wall}} 1/2\ O_2$$

$$\ddot{O} + CH_4 + M \longrightarrow CH_3OH + M.$$

Basically, the scheme is the same as Semenov's scheme; however, the following points are new: (1) chain initiation in which methane and oxygen react to formaldehyde, which subsequently oxidizes to formic acid and an oxygen atom; (2) an attempt to explain the main path for the further oxidation of formaldehyde to a certain product X which yields carbon monoxide and an oxygen atom, and (3) an explanation for the formation of methyl alcohol by the collision of an oxygen atom, a methane molecule, and a third molecule M.

Experimentally the maximum reaction rate as determined by the pressure rise curve was represented by

$$W_{max} = \frac{dp}{dt} = k[CH_4]^2\ [O_2]P$$

where P is the total pressure and the magnitude of k depends upon the catalytic activity of the vessel surface. Applying the method of quasi-stationary states to the proposed mechanism, Norrish and Foord found that the maximum rate of methane consumption was

$$-\frac{d\ CH_4}{dt} = \frac{k_2k_3\ [CH_4]^2\ [O_2]\ Pd}{k_6k_7S}$$

where the k's are the rate constants for the various reactions proposed, d is the vessel diameter, and S is the surface

activity per unit area. Although excellent agreement between the experimental results and theoretical considerations was obtained, it should be pointed out that confirmation of the scheme cannot be considered as decisive. The fact that there are several other similar mechanisms, which will also agree with the experimental results, prohibit one from reaching the conclusion that the results cannot be questioned.

In addition to the above mechanisms applying chain-radical theory to methane oxidation, several other mechanisms for the oxidation of higher paraffinic hydrocarbons were introduced. Since these schemes contained relevant information leading to the generally accepted mechanism for methane oxidation, they are briefly discussed in the next paragraph.

In 1935 Pease (55, 56, 57) proposed a monoradical mechanism which considered the monovalent propyl radical $\dot{C}_3H_7$ and the methoxy radical $CH_3\dot{O}$ as the chain-initiating free radicals in the oxidation of propane. In the same year Ubbelohde (72) introduced another radical-chain scheme for the low temperature oxidation of paraffinic hydrocarbons. This mechanism proposed that the peroxide radical $RCH_2O\dot{O}$ was formed by the combination of an alkyl radical and an oxygen atom. The $RCH_2O\dot{O}$ then combined with the initial hydrocarbon molecule to form the alkylhydroperoxide RCH_2OOH. The incorporation of the peroxide concepts in the form of a chain mechanism was thus introduced into the literature for the first time for hydrocarbon oxidation. Jost, Muffling, and

Rohrmann (28) followed the Ubbelohde proposal with an analogous radical-chain scheme (independently formulated) which also considered the formation of alkylhydroperoxides; however a means for the formation of alcohols was included. The alcohols were formed by a reaction between the peroxide radical and the initial hydrocarbon to produce an alkoxy radical, which in turn reacted with the initial hydrocarbon. The last oxidation scheme during this period of development was introduced by Lewis and von Elbe (36) in 1937. This mono-radical mechanism considered the hydroxy radical, $\dot{O}H$, as the chain-initiating radical.

It is interesting to note, as Shtern (65) has pointed out, that the fundamental ideas proposed in the non-chain mechanisms of aldehyde degradation, peroxidation, and hydroxylation have been reflected in the corresponding radical-chain mechanisms. Semenov, Norrish, Pease, and Lewis and von Elbe considered aldehyde as the first intermediate product, and Jost, et al., considered both the alkylhydroperoxide and alcohol as the first intermediate product.

Additional data on the oxidation of hydrocarbon led Norrish (47) to revise his earlier di-radical chain scheme. Norrish now believed that the first and only intermediate product of methane oxidation was formaldehyde. The chain initiation step included the formation of formaldehyde from a reaction between methane and molecular oxygen, a reaction between formaldehyde and molecular oxygen to give a divalent

oxygen atom, and the formation of methyl radicals and hydroxy radicals from the reaction between a methane molecule and a divalent oxygen atom. The chain was propagated by the reaction of a methane molecule with a hydroxy radical to give a methyl radical and water, and the reaction between a methyl radical and molecular oxygen to give formaldehyde and a hydroxy radical. The chain was terminated by the destruction of the hydroxy radical at the wall, and methyl alcohol formation was attributed to a termolecular reaction between methane, a divalent oxygen atom, and a third molecule. Again, by the method of quasi-stationary states, the proposed mechanism agreed with the experimental data.

Yenikolopyan (83) presented a scheme which he accepted as being typical of the oxidation of saturated hydrocarbons. For the case of the oxidation of methane, the mechanism reduces to the following:

$$CH_4 + O_2 \longrightarrow \dot{C}H_3 + H\dot{O}_2$$

$$\dot{C}H_3 + O_2 \longrightarrow CH_3O\dot{O}$$

$$CH_3O\dot{O} + CH_4 \longrightarrow CH_3OOH + \dot{C}H_3$$

$$CH_3O\dot{O} \longrightarrow HCHO + H\dot{O}$$

$$H\dot{O} + CH_4 \longrightarrow H_2O + \dot{C}H_3$$

$$H\dot{O} + HCHO \longrightarrow H_2O + H\dot{C}O$$

$$H\dot{C}O + O_2 \longrightarrow H\dot{O} + CO_2$$

$$CH_3OOH \longrightarrow CH_3\dot{O} + OH$$

$$HCHO + O_2 \longrightarrow H\dot{C}O + H\dot{O}_2$$

$$CH_3O\dot{O} \xrightarrow{\text{wall}} \text{chain breaking}$$

$$2CH_3O\dot{O} \longrightarrow \text{chain breaking}$$

$$\dot{C}H_3 \xrightarrow{\text{wall}} \text{chain breaking}$$

Using this scheme and taking into account the competition between the parallel and consecutive reactions as the temperature changed, Yenikolopyan was able to explain partially the change of order of the reaction with respect to the methane and oxygen concentrations.

In 1958 Semenov (64) introduced his second radical-chain mechanism for the oxidation of methane at low pressures. This monoradical mechanism is generally accepted today as the scheme best explaining the experimental facts. For this reason Semenov's scheme has also been included in Chapter II.

The reaction is initiated by a reaction between the methane molecule and the oxygen molecule to form the two monoradicals $\dot{C}H_3$ and $H\dot{O}_2$. The methyl radical, formed by a reaction between a hydroxy radical and methane, is responsible for chain propagation. Degenerated branching occurs by a molecular reaction between formaldehyde and oxygen to give the monoradicals $H\dot{C}O$ and $H\dot{O}_2$. Chain termination is accomplished by the wall destruction of the hydroxy radical.

Using the method of quasi-stationary concentrations the maximum concentration of formaldehyde for this mechanism varies with temperature according to the law:

$$[HCHO]_{max} = e^{-8500/RT} [CH_4]$$

which agrees well with experimental work (29, 30). For the theoretical maximum rate of methane consumption, it was found that

$$-\frac{d[CH_4]}{dt} \propto [CH_4]^2 [O_2]$$

which also agrees with the experimental results reported by various authors. In addition the theoretical energy of activation was estimated by Semenov to be approximately 46 kcal/mole which agrees with the experimental value of 40-46 kcal/mole reported by Karmilova, Yenikolopyan, and Nalbandyan (29, 30).

It is interesting to note that only in the radical-chain mechanisms proposed by Norrish was an attempt made to explain the formation of methyl alcohol during the oxidation of methane. Earlier Bone (5) had proposed a non-chain mechanism for high pressure oxidation of methane which proceeded through the monoxide $CH_4(O_2)$ to yield methyl alcohol by reacting with methane.

With the accumulation of experimental data on the slow oxidation of methane, appreciable differences in the time of attainment of the maximum reaction rate as determined by the

slope of the pressure rise-time curves were noted. Curves of different forms were reported. The variations of the shape ranged from almost completely symmetrical curves, in which the maximum rate occurred when approximately 50 per cent of the total pressure rise was reached, to curves in which the maximum rate occurred at the beginning of the pressure increase and thereafter remained essentially constant. Curves of the first type were reported by Fort and Hinshelwood (18) and curves of the second type were observed by Bone and Gardner (8). Bone and Allum (6), and Slotin and Style (67), reported an intermediate type curve in which the maximum reaction rate occurred when approximately 15-30 per cent of the total pressure increase was reached. Hoare (22) attributes the curve variations to different experimental techniques in obtaining reproducible results.

According to the most recent mechanisms on methane oxidation, the maximum reaction rate varies with the concentration of methane and oxygen in the following manner:

$$W_{max} \propto [CH_4]^m [O_2]^n$$

At low temperatures (up to 500°C) and at essentially atmospheric pressure the order of the reaction ($m \approx 2$ and $n \approx 1$) agrees well with experimental data. With an increase in temperature the order of the reaction with respect to methane decreases, but the order increases with respect to oxygen. Thus a difference between the order of reaction predicted from the

proposed mechanisms and the experimental data is observed. Yenikolopyan (83) has been able to explain partially the change in order of the reaction in his treatment of the parallel and consecutive reactions occurring by his mechanism. Table 1 is presented to illustrate the change of order of the reaction with respect to the methane and oxygen concentrations as the temperature changes.

In addition to the above discrepancy between the mechanisms and experimental data regarding the reaction order, different values for the total activation energy of methane oxidation have also been reported. Vanpée (74) reported a value of 93 kcal/mole for the temperature range 377-422°C; Bone and Allum (6) reported a value of about 90 kcal/mole for the temperature range 423-477°C; and Fort and Hinshelwood (18) reported a value of 62 kcal/mole for the temperature range 447-487°C. Karmilova, Yenikolopyan, and Nalbandyan (29, 30) estimated the activation energy from the variation of the natural logarithm of the maximum rate with the reciprocal of the absolute temperature. The maximum rate was determined by several methods: (1) according to pressure increase, (2) consumption of oxygen, (3) consumption of methane, (4) accumulation of carbon monoxide, and (5) accumulation of water. The reported activation energy by the different methods varied between 41.5 and 43.0 ±1 kcal/mole.

In 1955 Hoare and Walsh (23, 24), in their investigation of the surface effect on the oxidation of methane,

TABLE 1

THE VARIATION OF THE MAXIMUM RATE OF OXIDATION WITH CONCENTRATIONS OF METHANE AND OXYGEN AT DIFFERENT TEMPERATURES*

Temp. °C	Vessel Description	Order of Reaction With Respect to Methane, m	Order of Reaction With Respect to Oxygen, n	Reference
376	Pyrex	2.3	0.5	74
416	Pyrex	2.0	0.5	73
467	Clean Vessel	1.6	1.0	18
480	Clean Vessel	2.0	1.0	48
500	Quartz, treated by heating	2.4	1.0-1.6	23
570	--	1.4	2.4	74
617	--	0.11	2.5	74
650	Quartz, treated by heating	0-0.7	2.3-2.7	24
666	--	-0.14	3.8	74
750	--	-0.4→+0.4	2-2.4	24

*Taken from Shtern (65).

reported values of the energy of activation which varied between 43 and 76 kcal/mole. It was concluded that the activation energy was a function of both the temperature and the mixture composition. Thus the expression generally accepted for the maximum rate

$$W_{max} = k[CH_4]^m [O_2]^n p^t e^{-E_A/RT}$$

did not satisfy the actual kinetic law determining the course of the reaction. These authors also detected a considerable variation in the kinetic laws of the reaction with respect to the nature and surface condition of the reaction vessel.

Range of Pressure

Only a limited number of investigations on the effect of pressure on the homogeneous, gas-phase oxidation of methane have been made. In fact it can be stated that only a limited number of studies have been reported in the literature concerning the effect of pressure on the homogenous, gas-phase oxidation of paraffinic hydrocarbons. Since the initial investigation by Newitt and Haffner (45), only the elevated pressure studies of Newitt and Szego (46), Wiezevich and Frolich (80), Paris (52), and Furman and co-workers (19, 20) have been reported in the literature on methane oxidation.

Prior to the present investigation the maximum pressure employed in a comprehensive investigation of methane oxidation was 4500 psi (20). The present work covers a pressure range from 2000 psi to 200,000 psi. The maximum pressure used in this investigation exceeds the maximum pressure used in any study on chemical reactions reported in the literature. The highest reported pressure preceeding this study was 120,000 psi (78).

CHAPTER IV

DESIGN CONSIDERATIONS FOR HIGH PRESSURE EQUIPMENT

The extreme operating conditions encountered in this investigation made it necessary to use multi-wall or compound vessels. This chapter presents the design principles used in the construction of such equipment.

Principles for the Design and Construction of High Pressure Equipment

The elastic stress distribution in a uniformly thick cylinder is determined by the Lamé relationships (34):

$$\sigma_t = \frac{P_i - P_o K^2 + (r_o/r)^2 (P_i - P_o)}{K^2 - 1} \tag{4-1}$$

$$\sigma_r = \frac{P_o K^2 - P_i + (r_o/r)^2 (P_i - P_o)}{K^2 - 1} \tag{4-2}$$

and

$$\sigma_z = \frac{P_i - K^2 P_o}{K^2 - 1} \tag{4-3}$$

where

σ_t = tangential stress

σ_r = radial stress

σ_z = longitudinal stress

r_i = internal radius

r_o = external radius

r = any radius within the cylinder wall

P_i = internal pressure

P_o = external pressure

K = diameter ratio, $2r_o/2r_i$

Inspection of Equations (4-1), (4-2), and (4-3) reveals that the tangential and radial stresses have their maximum absolute value at the inner surface and that the tangential stress at the bore is always numerically greater than the internal pressure. However, the radial stress is limited in value to the applied pressure. The Lamé equations are applicable so long as the wall material of the vessel is not stressed beyond the range of elastic bheavior.

Since the Lamé equations are not design equations, some criterion must be specified to set the limit of elastic action. According to the theory of maximum energy of distortion of von Mises, the value of the strain energy of distortion at the limit of elastic action for a particular metal is a constant and is related to the three dimensional stresses as follows:

$$(\sigma_t - \sigma_r)^2 + (\sigma_r - \sigma_z)^2 + (\sigma_z - \sigma_t)^2 = 2\sigma_y^2 = \text{a constant} \tag{4-4}$$

where σ_y is the yield strength of the material in simple tension.

The maximum shear stress at any radius within the cylinder wall is equal to one-half the algebraic difference between the maximum and minimum principal stresses (71, p. 15). For the Lamé distribution the longitudinal stress is exactly the average of the radial and tangential stress at any given radius. Therefore, the maximum shear stress is

$$\tau = \tfrac{1}{2}(\sigma_t - \sigma_r) \tag{4-5}$$

Observing that $\sigma_z = \tfrac{1}{2}(\sigma_t + \sigma_r)$ and upon substituting Equation (4-5) into Equation (4-4), one obtains

$$\tau = \tau_y = \sigma_y/\sqrt{3} \tag{4-6}$$

where τ_y is the shear yield stress. This expression implies that the breakdown of elastic behavior is reached when the maximum shear stress attains a value equal to $1/\sqrt{3}$ times the yield stress in simple tension.

In the construction of compound (multi-wall) vessels the inner cylinders are prestressed by shrinking the outer cylinder over the inner cylinder. If all the cylinders are of the same material, the completed vessel is designed so that when only internal pressure is applied at a constant temperature, each component of the vessel has the same shear stress distribution, which is the lowest possible. Since both the tangential and radial stresses have their maximum magnitude at the inner surface, the maximum shear stress also has its greatest value at the inner surface. Manning's

development for this case (39) shows that the maximum shear stress at the inner radius of a vessel made of m geometrically similar cylinders is

$$\tau_{max} = \frac{P_i K^{2/m}}{m(K^{2/m} - 1)} \tag{4-7}$$

The maximum allowable pressure for elastic action is determined by setting the maximum shear stress, τ_{max}, in each cylinder equal to the shear yield strength, τ_y. Rearranging Equation (4-7), combining with Equation (4-6), and setting $P_i = P_{max}$, $\tau_{max} = \tau_y$,

$$P_{max} = \frac{m\tau_y(K^{2/m} - 1)}{K^{2/m}} = \frac{m\sigma_y(K^{2/m} - 1)}{\sqrt{3}\, K^{2/m}} \tag{4-8}$$

In addition Manning has shown that the interference or shrinkage per unit of radial length, δ_r, required for the optimum shear stress distribution is

$$\delta_r = \frac{2P_i}{m\, E} \tag{4-9}$$

where E is Young's modulus.

With this interference the residual shear stress in the completed vessel was shown by Manning to be

$$\tau_{R_n} = \frac{b_n^2}{r^2}(P_i - P_o)\left\{\frac{1}{m(K^{2/m} - 1)} - \frac{K^{2(1 - n/m)}}{K^2 - 1}\right\} \tag{4-10}$$

where τ_{R_n} is the residual shear stress in the nth cylinder and b_n is the outer radius of the nth cylinder. It is obvious

from this equation that the maximum value of the residual shear stress occurs at the bore of the vessel.

In the design and construction of high pressure equipment, thermal stresses as well as pressure stresses should be considered. Whalley and Morris (79) have developed relationships for the diameter ratio, interference between cylinders, and shear stress distribution for a cylindrical vessel of similar material subjected to pressure and to steady-state thermal gradients. They have shown that all components of a compound vessel subjected to pressure and to steady-state thermal gradients have the same diameter ratio. The interference between each component, determined from the dimensions before assembly, is

$$\delta_r = \frac{2\{(P_i - P_o) - \tfrac{1}{2}\beta\}}{m\,E} \tag{4-11}$$

with

$$\beta = \frac{\alpha\, E(T_i - T_o)}{(1 - \nu)} \tag{4-12}$$

where α is the thermal coefficient of expansion, ν is Poisson's ratio, and T_i and T_o are the internal and external wall temperatures, respectively.

Whalley and Morris have also shown that the maximum shear stress within each component of the vessel is at the inner surface and equal to

$$\tau_{max} = \frac{(P_i - P_o)K^{2/m}}{m(K^{2/m} - 1)} - \tfrac{1}{2}\beta\left\{\frac{K^{2/m}}{m(K^{2/m} - 1)} - \frac{1}{2\ln K}\right\} \tag{4-13}$$

The maximum allowable operating pressure within elastic limits of a compound cylinder is determined by setting the maximum shear stress, τ_{max}, equal to the shear yield strength, τ_y. Rearranging Equation (4-13), replacing $(P_i - P_o)$ by P_{max}, and combining with Equation (4-6),

$$P_{max} = \frac{m\tau_y(K^{2/m} - 1)}{K^{2/m}} + \tfrac{1}{2}\beta\left\{\frac{K^{2/m}}{m(K^{2/m} - 1)} - \frac{1}{2 \ln K}\right\}$$

$$= \frac{m\sigma_y(K^{2/m} - 1)}{\sqrt{3}\, K^{2/m}} + \tfrac{1}{2}\beta\left\{\frac{K^{2/m}}{m(K^{2/m} - 1)} - \frac{1}{2 \ln K}\right\} \qquad (4\text{-}14)$$

It is obvious from Equations (4-12) and (4-14) that the maximum allowable internal pressure is increased if the temperature of the inner surface is greater than the temperature of the outer surface, i.e., if β is positive. On the other hand, if the temperature of the inner surface is less than the temperature of the outer surface, then the maximum allowable internal pressure is decreased.

In the preceding discussion it has been implied that in the construction of compound pressure vessels there is no limit to the applied internal pressure so long as the diameter ratio K and the number of components m are increased. From a theoretical viewpoint, both the maximum shear stress and the residual shear stress have their maximum intensity (opposite in sign) at the bore of the vessel. Also the algebraic difference of the working stress and the residual

stress is equal to the shear stress in an equivalent monoblock cylinder. Consequently, neither can have a value greater than one-half of the shear stress of the equivalent monoblock cylinder. Accordingly, as shown by Manning (39), the maximum pressure which can be applied without exceeding the limit of elastic action is

$$P_{max} = \frac{2\sigma_y(K^2 - 1)}{\sqrt{3}\,K^2} \qquad (4\text{-}15)$$

This criterion in the design of compound vessels must be used if the material of the vessel is to remain in the region of elastic action. From a practical viewpoint the cost of shrink-fitting the geometrically similar cylinders restricts the number of concentric cylinders used in the vessel. Furthermore the actual temperature difference which can be employed to achieve the shrink-fit limits the maximum resulting residual stress.

The preceding discussion has been restricted to the elastic deformation of the cylinder wall. It has been pointed out that the maximum allowable pressure has a limit based on theoretical (elastic limit) and practical (cost) grounds. However, it is possible to increase the maximum internal pressure by causing inelastic deformation of the inner layers of the cylinder. Any increase in the internal pressure above the elastic-breakdown pressure causes inelastic deformation which starts at the inner wall. As the internal pressure is

increased the region of inelastic strains moves outward through the wall. The internal pressure required to cause inelastic action to reach the outer wall of the cylinder is the overstrain pressure. For a cylinder which yields at constant stress, it can be shown (14) that the overstrain pressure is

$$P_{os} = \frac{2\sigma_y}{\sqrt{3}} \ln K \qquad (4\text{-}16)$$

The application of a pressure greater than the elastic-breakdown pressure and less than the overstrain pressure, P_{os}, deforms the inner layers of the cylinder inelastically and consequently raises the residual stresses, which in turn permits an increase in allowable working pressure. This technique is known as autofrettage. In an autofrettaged vessel the maximum pressure which can be tolerated without increasing the inelastic strains beyond that caused by the initial application of pressure is

$$P_{max} = \frac{\sigma_y}{\sqrt{3}} \left\{ \frac{r_o^2 - r_e^2}{r_o^2} + 2 \ln \frac{r_e}{r_i} \right\} \qquad (4\text{-}17)$$

where r_e is the radius at the outer edge of the region of inelastic strains (14).

Up to this point the factors to be considered in the selection of metals to be used in the construction of high pressure equipment have not been discussed. It has been implied that metals with the required mechanical properties

are available. Since a discussion on the factors influencing the selection of metals is outside the scope of this manuscript, the reader is referred to other sources (14).

Reactor Design

The reactor, designed for 200,000 psi and 800°F, was a duplex vessel (shrink-fit construction) made from 18 per cent nickel maraging steel obtained from Vanadium-Alloys Steel Company, Latrobe, Pennsylvania. This nickel steel (Vascomax 250 CVM) is a consumable electrode, vacuum-melted alloy which is aged at approximately 900°F for about 3 hours. The excellent mechanical properties of this steel make it well suited for this application. Details of the reactor are shown in Figure 1.

In the design of compound vessels the number of geometrically similar cylinders and the diameter ratio must be determined. The cost of shrink-fitting generally limits the number of components to 2 or 3. In this case a duplex vessel was selected. For a working pressure of 200,000 psi at 800°F, for m equal to 2, and for a yield strength for the maraging steel of 211,000 psi at 800°F (77), the minimum diameter ratio can be determined from Equation (4-8).

$$K = \frac{(2)(211,000)}{\{(2)(211,000) - (\sqrt{3})(200,000)\}} = 5.6$$

For the final design a diameter ratio of 6 was used.

To take advantage of thermal stresses, according to Equation (4-14), internal heating was employed so that

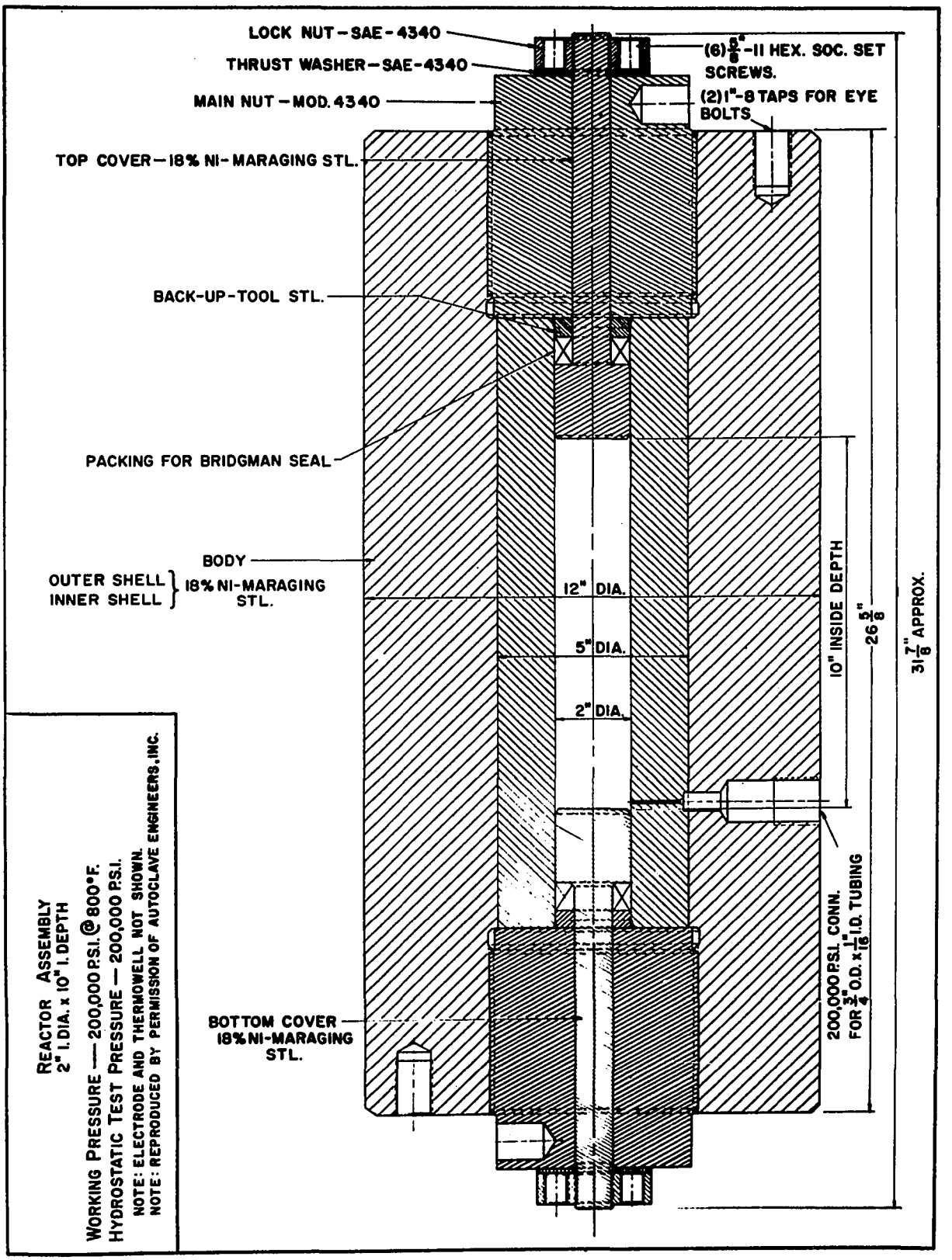

Figure 1. Details of 200,000 psi Reactor

the reactor would operate with a higher temperature at the inner wall than the outer wall. Before Equation (4-14) can be used to determine the maximum pressure in this case, it is necessary to know the temperature drop across the vessel wall. Since the actual temperature drop is not known, only a qualitative statement regarding the effect of the thermal stresses on the maximum pressure can be made. Inspection of Equation (4-14) shows that the thermal stresses introduced by the thermal gradient permit an increase in the operating pressure. So long as the inside wall temperature of the reactor is greater than the outside wall temperature, Equation (4-8) gives a conservative value for the pressure.

To insure that the design pressure of 200,000 psi is acceptable, Equation (4-15) for a monoblock cylinder must be used. Thus, for $K = 6$, $\sigma_y = 211{,}000$,

$$P_{max} = \frac{2(211)(10^3)(35)}{(\sqrt{3})(36)} = 237{,}000 \text{ psi}$$

which is greater than 200,000 psi. Therefore, from a theoretical viewpoint, it can be concluded that the material of the vessel will remain within the limits of elastic action.

From the practical viewpoint the interference and the temperature difference required in the shrink-fit process must be compatible with the material of construction. At room temperature the modulus of elasticity of Vascomax 250 CVM is 26.5×10^6 psi (77); therefore the required shrinkage per unit of radial length from Equation (4-9) is

$$\delta_r = \frac{(2)(200,000)}{(2)(26.5 \times 10^6)} = 0.0075 \text{ in/in}$$

For a 2.5 inch outer radius of the inner cylinder the total radial shrinkage is 2.5 x 0.0075 or 0.0188 inches. Therefore the difference between the outside diameter of the inner cylinder and the inside diameter of the outer cylinder is 0.0376 inches before assembly. Assuming that a clearance of at least 0.010 inches is required for assembly, the temperature difference required for the shrink-fit is

$$\Delta T = \frac{(0.0376 + 0.010)}{(5)(5.6 \times 10^{-6})} = 1700°F$$

Since the maraging steel is aged at 900°F, this temperature cannot be exceeded during shrink-fitting. If it is assumed that the inner cylinder is cooled to -100°F for shrink-fitting then the diametral interference is, for a diameter of 5.0 inches,

$$(\delta_r \times d) = (5)(5.6 \times 10^{-6})(1000) - 0.01$$
$$= 0.018 \text{ inches}$$

For an outside diameter of the inner cylinder of 5.000 inches, the bore diameter of the outer cylinder should be machined to 4.982 inches.

Because of the incompatibility of the 1700°F calculated above for optimum, maximum shear stress distribution with the maximum permissible operating temperature of 900°F, the only alternative for obtaining the required residual

compressive stress at the inner bore is to use a combination of shrink-fit and autofrettage. For autofrettage the depth of inelastic strain from Equation (4-17), for P_{max} = 200,000 psi, is given by

$$r_e \approx 1.23 \text{ inches}$$

In most cases, either autofrettage or shrink-fit is used, but not both. In this case, in order to achieve the highest possible working pressure, both techniques had to be used.

The resulting maximum shear stress distribution for the reactor under full load at 800°F is shown in Figure 2 and Table 2.

Additional factors considered in the design of this reactor were the type of closure, the location of the gas inlet (and outlet), and the method of introducing thermocouples and electrical leads for the internal furnace. Full Bridgman closures were selected to seal both ends of the reactor since this closure is extremely reliable.

Only one electrode (electrical lead) was required for power input to the internal furnace since the reactor can be used for the ground connection. The electrode, introduced through one of the reactor end plugs, was sealed with an unsupported area type seal which allowed electrical insulation between the electrode and reactor. A detailed drawing of the electrode assembly is presented in Figure 3.

Introduction of thermocouples was accomplished by placing a thermowell in one of the end-plugs. The thermowell

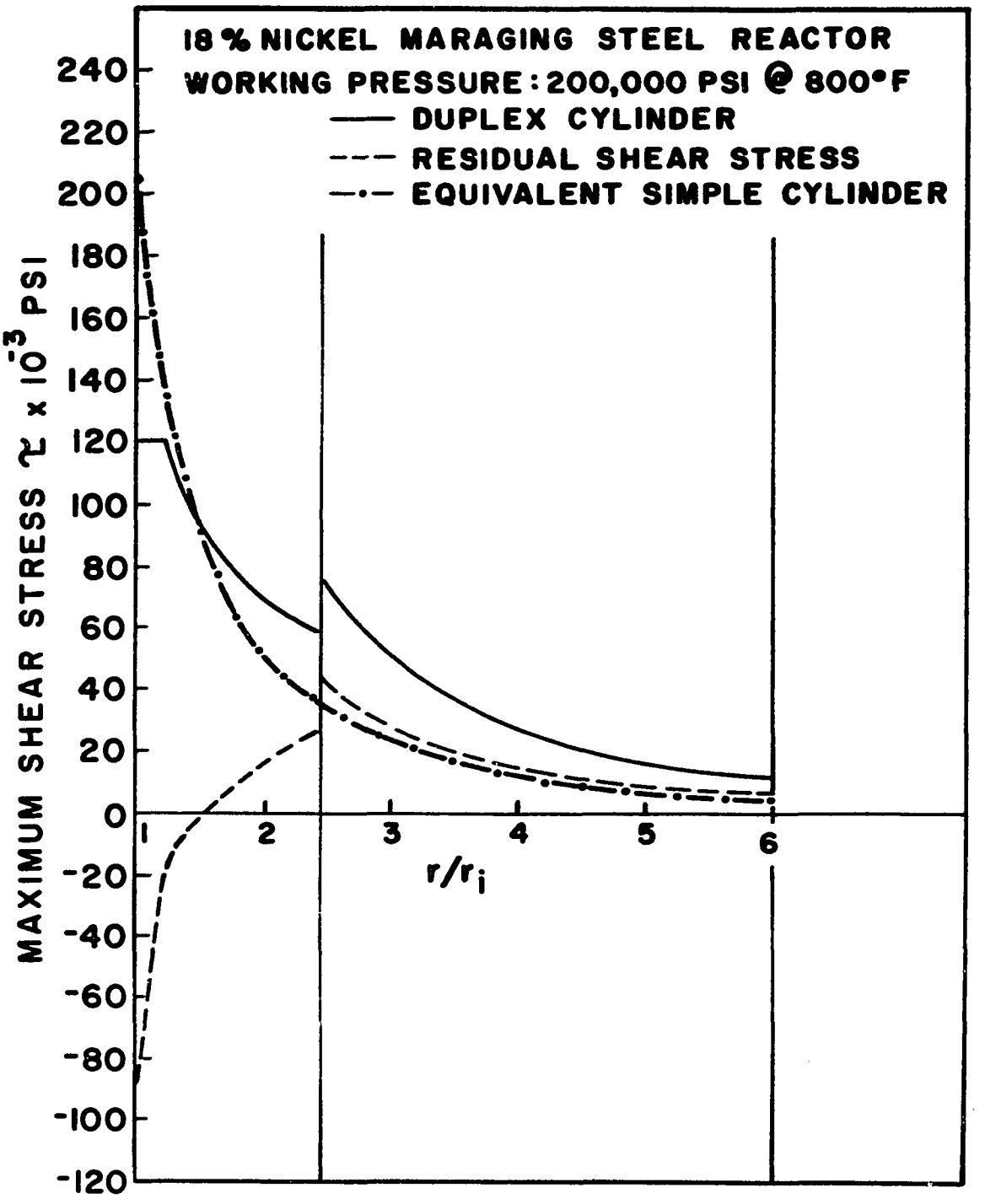

Figure 2. Shear Stress Distribution for Reactor

TABLE 2

SUMMARY OF DATA FOR FIGURE 2

r/r_i	$\tau \times 10^{-3}$	$\tau_e \times 10^{-3}$	$\tau_{R_n} \times 10^{-3}$
	Inner Cylinder		
1.00	121.80	205.70	-83.90
1.20	121.80	145.70	-23.90
1.25	118.80	131.90	-13.10
1.30	110.50	118.85	- 8.35
1.50	94.00	96.50	- 2.50
2.00	69.50	51.40	+18.10
2.45	59.08	31.45	+27.63
	Outer Cylinder		
2.45	76.58	31.45	+45.13
3.00	50.26	22.80	+27.46
4.00	28.52	12.90	+15.62
6.00	12.68	5.70	+ 6.98

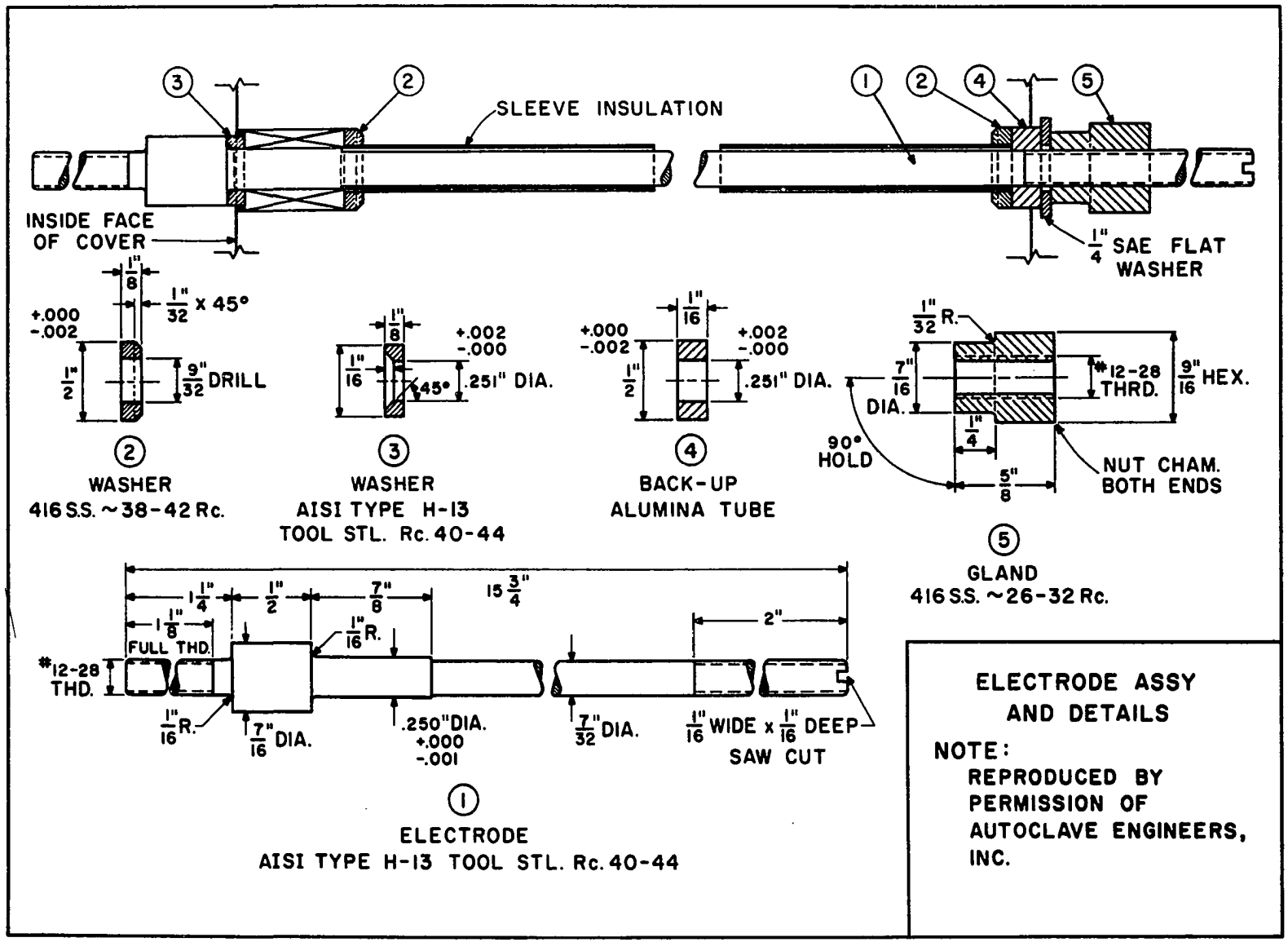

Figure 3. Details of Electrode Assembly

was constructed from standard high pressure tubing, 5/16-inch o.d. by 1/16-inch i.d. One end of the tubing was sealed by welding, and the other end was connected to the end plug with a single cone connection.

Since both end plugs were used for the electrode and thermowell, the opening for the gas inlet (or outlet) was placed in the reactor wall. A double cone joint was used to connect the reactor to the high pressure tubing.

The preliminary design of the reactor was done by the author, but the final design and fabrication was done by Autoclave Engineers, Inc.

Compression Cylinder Design

The compression cylinder, designed for a working pressure of 200,000 psi at 300°F, was a triplex vessel (shrink-fit construction) fabricated from modified 4340 gun-steel. A free piston was located in the compression cylinder to separate the pressure transmitting fluid and the reaction mixture. The purpose of the free piston was to minimize the contamination of the reaction mixture with the pressurizing fluid and to eliminate the loss of the reaction mixture by the increased solubility of the gas in the hydraulic fluid at high pressures. Details of the compression cylinder are provided in Figure 4.

For economical reasons a triplex design was selected for this compression cylinder. The minimum diameter ratio can be determined from Equation (4-8) for a working pressure

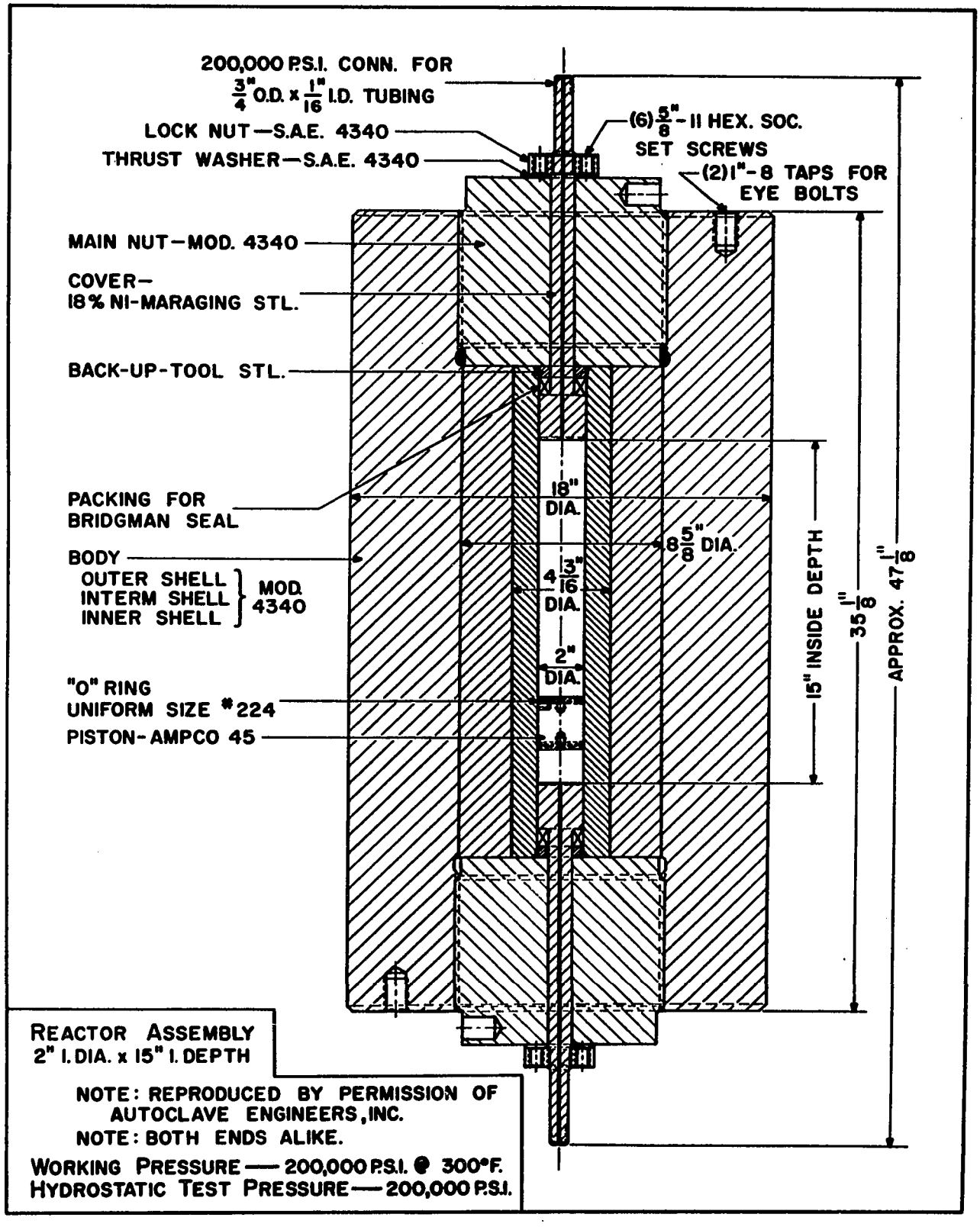

Figure 4. Details of 200,000 psi Compression Cylinder

of 200,000 psi, for m equal to 3, and a yield strength of 150,000 psi for the modified 4340 gun steel.

$$K = \left\{ \frac{(2)(150,000)}{(2)(150,000) - (\sqrt{3})(200,000)} \right\}^{3/2} = 7.95$$

In the final design a diameter ratio of 9 was used.

To insure that the shrink-fit operation does not cause reverse yielding, Equation (4-15) is used. Thus, for $K = 9$ and $\sigma_y = 150,000$,

$$P_{max} = \frac{(2)(150)(10^3)(80)}{(\sqrt{3})(81)} = 171,000 \text{ psi}$$

The result of this calculation brings out the fact that the required residual stresses cannot be obtained in the shrink-fit operation before reverse yielding occurs. Since the maximum magnitude of the residual shear stresses obtained by shrink-fitting is obtained in the inner cylinder, the minimum yield strength of this cylinder should be increased.

The minimum yield strength for the inner cylinder can be determined from Equation (4-15). Thus, for $K = 9$, and $P_{max} = 200,000$,

$$\sigma_y = \frac{(\sqrt{3})(81)(200,000)}{2(81 - 1)} = 175,000 \text{ psi}$$

With the inner cylinder made from a steel having a minimum yield strength of 175,000 psi and the middle and outer cylinders made from a steel having a minimum yield strength of 150,000 psi, the required residual shear stresses

can be obtained in the shrink-fit process. However, in this case the shrinkage cannot be determined by Equation (4-9).

It can be shown (39) that the diametral interference between the middle and outer cylinders for this case is

$$(\delta_r \times d)_3 = \frac{4P_3' \, r_{o,2} \left(\frac{r_{o,2}^2}{r_i^2}\right)\left(\frac{r_o^2}{r_i^2} - 1\right)}{E\left(\frac{r_{o,2}^2}{r_i^2} - 1\right)\left(\frac{r_o^2}{r_i^2} - \frac{r_{o,2}^2}{r_i^2}\right)} \tag{4-18}$$

where P_3' is the residual contact pressure between the middle and outer cylinder, E is the modulus of elasticity, and r_i, $r_{o,2}$, and r_o are respectively the inside radius of the vessel, the outside radius of the middle cylinder, and the outside radius of the vessel.

Similarly the diametral interference between the inner and middle cylinders is

$$(\delta_r \times d)_2 = \frac{4P_2' \, r_{o,1} \left(\frac{r_{o,1}^2}{r_i^2}\right)\left(\frac{r_{o,2}^2}{r_i^2} - 1\right)}{E\left(\frac{r_{o,1}^2}{r_i^2} - 1\right)\left(\frac{r_{o,2}^2}{r_i^2} - \frac{r_{o,1}^2}{r_i^2}\right)} \tag{4-19}$$

where P_2' is the residual contact pressure between the inner and middle cylinders, E is the modulus of elasticity, and r_i, $r_{o,1}$, and $r_{o,2}$ are the inside radius of the vessel, the

outside radius of the inner cylinder, and the outside radius of the middle cylinder, respectively.

All terms in Equation (4-18) and (4-19) are known except the contact pressures P_2' and P_3'. These quantities are calculated from the pressure drop across the cylinder wall, when the reactor is loaded at the maximum operating pressure. The pressure drop across the middle cylinder, ΔP_2, is given by

$$\Delta P_2 = \sigma_{r,2} + P_2' + \sigma_{r,2}' - \Delta P_3 \qquad (4\text{-}20)$$

where

$$\sigma_{r,2} = \frac{P_i\left\{\left(\frac{r_o}{r_{o,1}}\right)^2 - 1\right\}}{K^2 - 1}$$

$$\sigma_{r,2}' = \frac{P_3'\left(\frac{r_{o,2}}{r_i}\right)^2}{\left(\frac{r_{o,2}}{r_i}\right)^2 - 1}\left\{1 - \frac{1}{\left(\frac{r_{o,1}}{r_i}\right)^2}\right\}$$

$$\Delta P_3 = P_i - (\Delta P_1 + \Delta P_2)$$

$$\Delta P_2 = \frac{\sigma_{y,2}\left\{\left(\frac{r_{o,2}}{r_{o,1}}\right)^2 - 1\right\}}{\sqrt{3}\left(\frac{r_{o,2}}{r_{o,1}}\right)^2}$$

$$\Delta P_1 = \frac{\sigma_{y,1}\left\{\left(\frac{r_{o,1}}{r_i}\right)^2 - 1\right\}}{\sqrt{3}\left(\frac{r_{o,1}}{r_i}\right)^2}$$

Similarly, the pressure drop across the outer cylinder, ΔP_3, is given by

$$\Delta P_3 = \sigma_{r,3} + P_3' \qquad (4\text{-}21)$$

where

$$\sigma_{r,3} = \frac{P_i \left\{ \left(\frac{r_o}{r_{o,2}} \right)^2 - 1 \right\}}{(K^2 - 1)}$$

For P_i = 200,000 psi, Equation (4-21) gives a contact pressure, P_3' = 42,200 psi. Again, for P_i = 200,000 psi and P_3' = 42,200 psi, Equation (4-20) gives a contact pressure P_2' = 39,800 psi.

These calculated values for P_2' and P_3' are then inserted in Equation (4-18) and (4-19) to obtain the diametral interferences:

$$(\delta_r \times d)_2 = 0.0178 \text{ inches}$$

and

$$(\delta_r \times d)_3 = 0.033 \text{ inches}$$

The required temperature difference for shrink-fitting the inner and middle cylinders is

$$\Delta T = \frac{(0.0178 + 0.01)}{(7.5 \times 10^{-6})(4.16)} = 890°F$$

and the temperature difference for shrink-fitting the middle and outer cylinders is

$$\Delta T = \frac{(0.033 + 0.01)}{(7.5 \times 10^{-6})(8.64)} = 665°F$$

Since the maximum safe tempering temperature for the modified 4340 gun-steel is approximately 1275°F, the temperature requirements to shrink-fit the compression cylinder are compatible with the material used.

In the construction of the triplex vessel the inner and middle cylinders are assembled first. Then this unit and the outer cylinder are assembled. The outside diameter of the inner cylinder should be machined to 4.165 inches and the inside diameter of the middle cylinder should be machined to 4.147 inches. After shrink-fitting, the outside diameter of the assembly and the bore diameter of the outer shell should be machined to 8.644 and 8.611 inches, respectively. Thus, by cooling the inner units to -100°F and heating the outer cylinders to approximately 1000°F, the shrink-fit operation can be accomplished.

The maximum shear stress distribution for the compression cylinder operating at the design conditions is illustrated in Figure 5 and Table 3.

The closures selected for the compression cylinder were full Bridgman closures and the seal for the free piston was an O-ring seal.

Intensifier Design

The principal unit of the high pressure generation system was the intensifier which is shown in detail in Figure 6. The intensifier is of monoblock construction. It has a dual area piston with an area ratio of 10:1. The low pressure

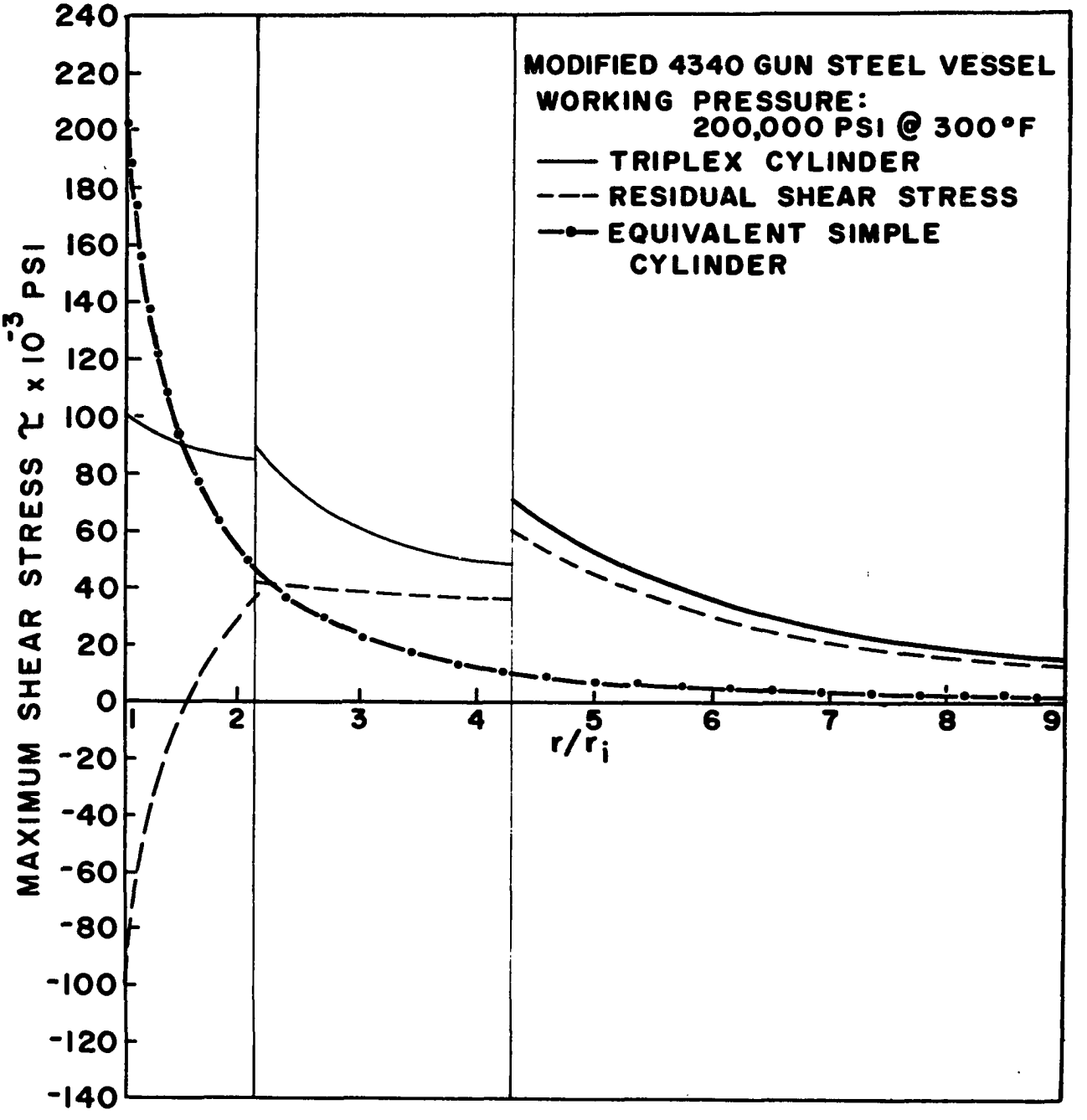

Figure 5. Shear Stress Distribution for Compression Cylinder

TABLE 3

SUMMARY OF DATA FOR FIGURE 5

r/r_i	$\tau \times 10^{-3}$	$\tau_e \times 10^{-3}$	$\tau_{R_n} \times 10^{-3}$
	Inner Cylinder		
1.00	100.2	202.5	-102.5
1.50	88.9	90.0	- 1.1
2.08	84.7	46.9	+ 37.8
	Middle Cylinder		
2.08	89.2	46.9	+ 42.3
3.00	61.2	22.5	+ 38.7
4.32	47.9	10.6	+ 37.3
	Outer Cylinder		
4.32	70.9	10.6	+ 60.3
6.00	36.9	5.6	+ 31.3
9.00	16.4	2.5	+ 13.9

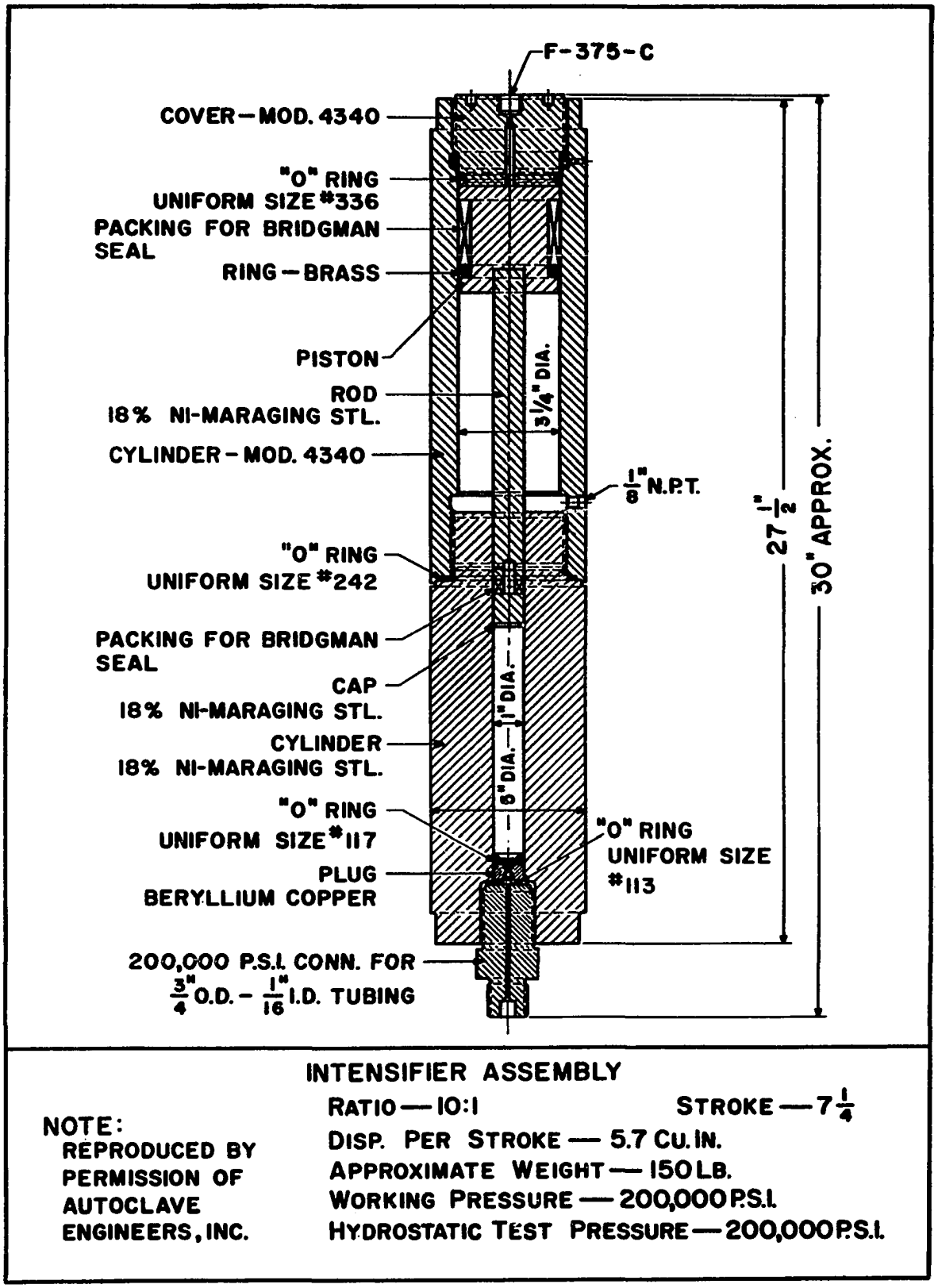

Figure 6. Details of Intensifier Assembly

end of the intensifier was fabricated from modified 4340 gun steel and the high pressure end was fabricated from Vascomax 250 CVM. O-rings were used to seal the closures on the intensifier, and a full Bridgman seal was used to seal the high pressure piston. The intensifier assembly was designed and built by Autoclave Engineers, Inc.

In order to generate 200,000 psi and to overcome frictional losses the low pressure cylinder of the intensifier must operate satisfactorily at a pressure which is slightly greater than 20,000 psi. For a diameter ratio of 1.538 and a minimum yield strength of 150,000 psi the elastic-breakdown pressure is

$$P_{max} = \frac{(150,000)(1.365)}{(\sqrt{3})(2.365)} = 50,000 \text{ psi.}$$

The elastic-breakdown pressure is considerably larger than the operating pressure of 20,000 psi on the low pressure side; therefore, the cylinder wall of the low pressure end of the intensifier will always remain in the region of elastic action.

In contrast to the low pressure side, the cylinder wall of the high pressure side of the intensifier does not remain in the region of elastic action throughout the wall since, from Equation (4-8) with K = 5, m = 1, and σ_y = 250,000 psi,

$$P_{max} = \frac{(2.5)(10^5)(24)}{(\sqrt{3})(25)} = 138,600 \text{ psi}$$

Thus, upon applying an internal pressure of 200,000 psi, the inner layers of the monoblock cylinder are deformed inelastically. After release of this internal pressure the wall will respond elastically as long as the applied pressure does not exceed 200,000 psi. The depth of the inelastic strains can be determined from Equation (4-17) to be:

$$r_e \approx 0.612 \text{ inches}$$

The maximum shear stress distribution for the high pressure cylinder of the intensifier is shown in Figure 7 and Table 4.

TABLE 4

SUMMARY OF DATA FOR FIGURE 7

r/r_i	$\tau \times 10^{-3}$	$\tau_e \times 10^{-3}$	$\tau_R \times 10^{-3}$
1.0	144.34	208.30	-63.96
1.1	144.34	172.15	-27.81
1.2	144.34	144.65	- 0.31
1.225	138.80	138.80	0
2.0	52.08	52.08	0
3.0	23.14	23.14	0
5.0	8.33	8.33	0

Auxiliary High Pressure Equipment

The tubing used in the high pressure system was obtained from Harwood Engineering Company, Inc. This

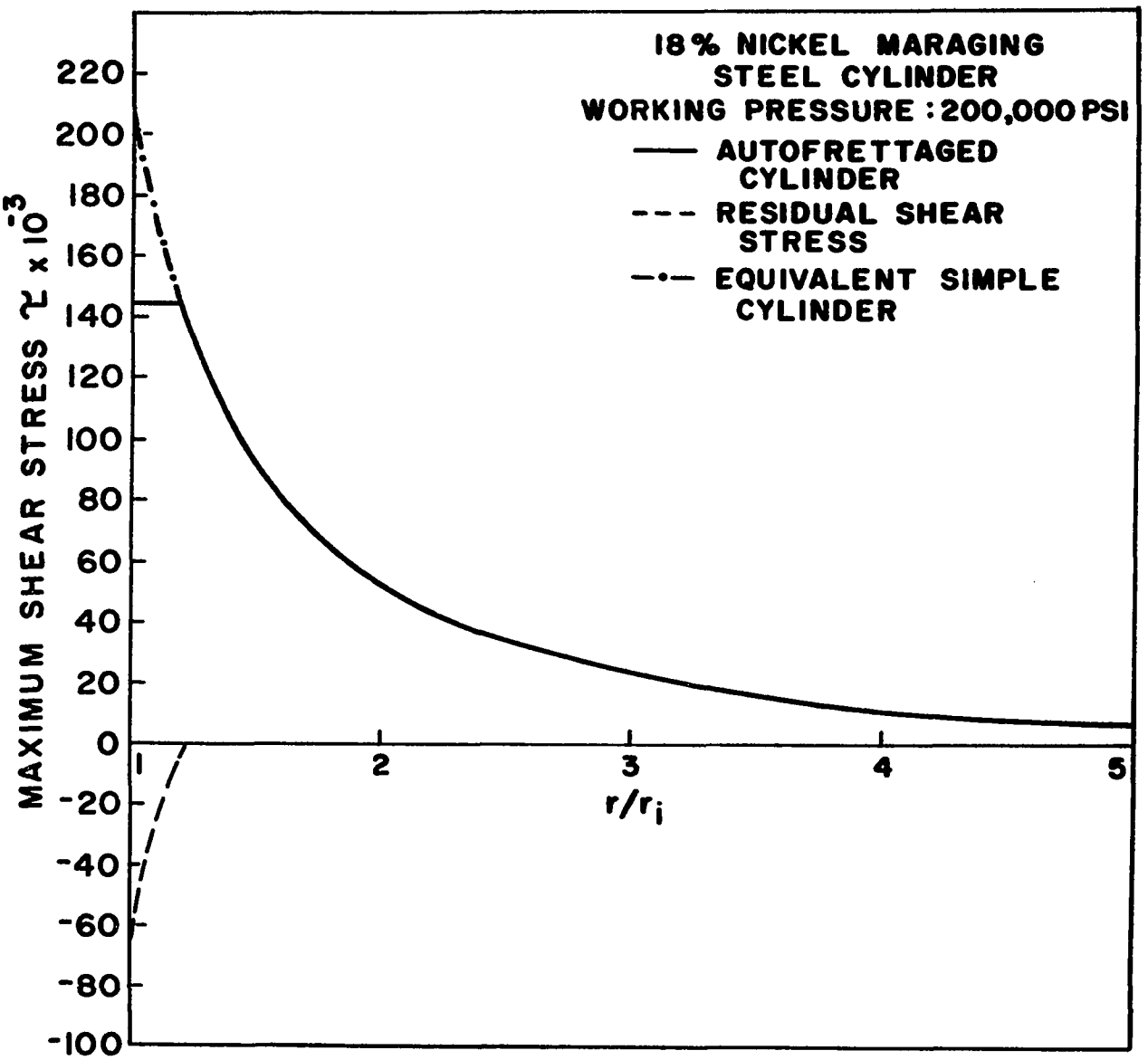

Figure 7. Shear Stress Distribution for Intensifier Assembly

standard composite (duplex) tubing, 3/4-inch o.d. by 1/16-inch i.d., had a strength rupture pressure rating exceeding 200,000 psi. The high pressure valves and fittings (tees, elbows, gland nuts, etc.) were designed and supplied by Autoclave Engineers, Inc. The pressure rating of these valves and fittings was 200,000 psi. All connections in the high pressure system were double cone connections.

The system pressure was measured with a manganin pressure cell obtained from Harwood Engineering Company, Inc., and recorded on a Foxboro Dynalog recorder. The pressure rating of the manganin pressure cell was 200,000 psi.

CHAPTER V

DESCRIPTION OF EXPERIMENTAL EQUIPMENT

The equipment used in this investigation was designed so that the partial oxidation or slow combustion of methane could be studied in a batch system at high pressures. Two reactors were used in this investigation. One reactor, loaned by Continental Oil Company, had a pressure rating of 25,000 psi at 1000°F. The other reactor, fabricated by Autoclave Engineers, Inc., had a pressure rating of 200,000 psi at 800°F. The reactor designed for 25,000 psi was made from 19-9DL alloy steel, whereas the reactor designed for 200,000 psi was made from 18 per cent nickel maraging steel.

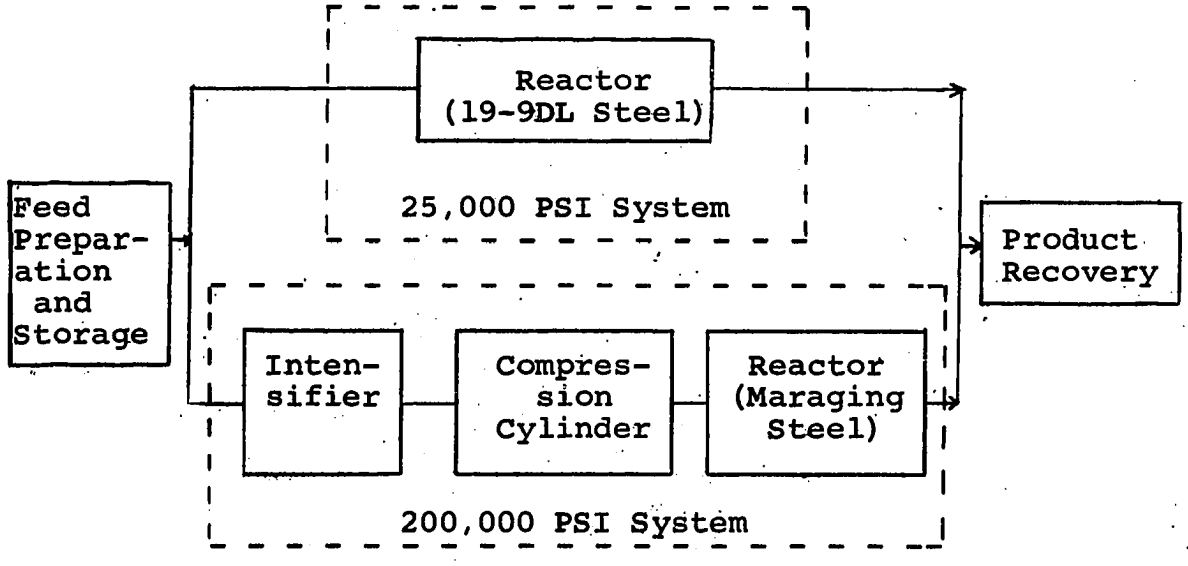

The 25,000 psi reactor was externally heated by an electric furnace. The 200,000 psi reactor was surrounded by a hot oil bath and contained an internal electrical heating element.

The process involves the preparation of the feed mixture at low pressures followed by compression and storage of the mixture at two pressure levels. This portion of the system was common for both reaction systems. In the 25,000 psi system the reactor was charged from the high pressure accumulator. At the completion of the run the reactor contents were expanded, cooled, and collected in a closed system. In the 200,000 psi system the reactor was charged by the high pressure generation unit. At the completion of the run, the reactor contents were expanded, cooled, and collected in a closed system. In the discussion which follows it is convenient to divide the process scheme into five sections: (1) feed preparation and intermediate pressure storage system, (2) 25,000 psi reaction system, (3) 200,000 psi reaction system, (4) product section, and (5) auxiliaries. The design of the 200,000 psi reaction system has been presented in the preceding chapter and the analytical equipment is discussed in Chapter VII.

Feed Preparation and Storage System

The principal components of the feed system were the low pressure gas-holder, the intensifier unit, the intermediate pressure accumulator, the pressure generation unit, and the high pressure accumulator. The feed system flow diagram is presented in Figure 8.

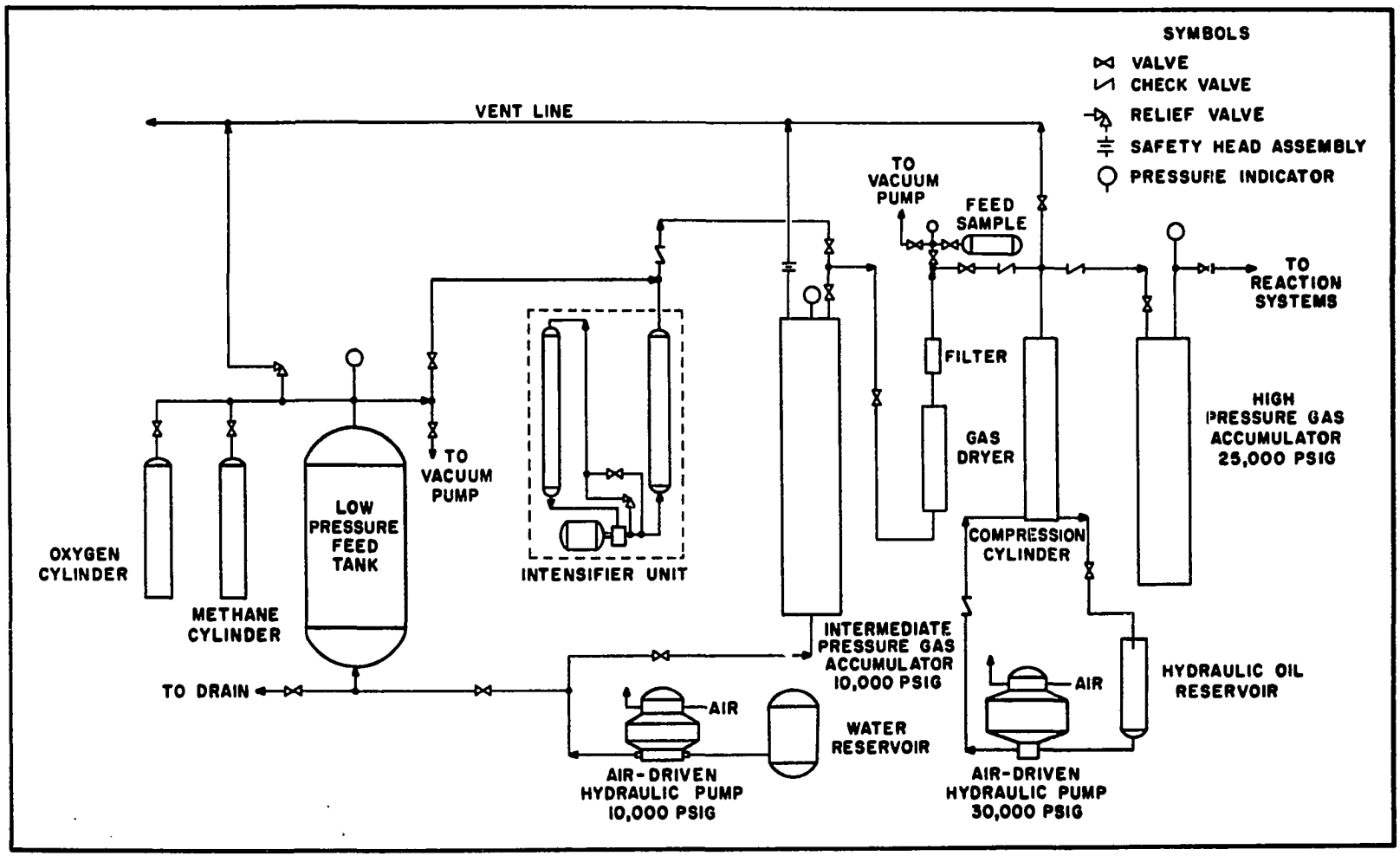

Figure 8. Process Flow Diagram of Feed System

The hazards involved in mixing oxygen and methane necessitated the low pressure preparation of the feed mixture. Mixing of the methane and oxygen was accomplished in a gas holder which had a volume of 18,000 cubic inches. This non-shatterable vessel, originally designed to contain breathing oxygen for the military, was 24 inches in diameter and 48 inches long (includes the hemispherical heads). The pressure rating of this gas holder was 400 psi. Two 1/4-inch openings, one in each head, were used for the feed gas input-output line and the input-output line to the Sprague, air-driven, hydraulic pump (also used for maintaining a constant pressure on the intermediate pressure accumulator). The bottom opening was connected to the discharge of the liquid pump by standard 1/4-inch o.d. by 1/8-inch i.d., 304 stainless steel tubing and to the drain line. The top opening was connected to the feed gas manifold, a pressure gauge, a relief valve, and the feed line to the intensifier unit. The relief valve was a 1/2-inch high capacity gas valve with a pressure setting of 350 psi.

The feed mixture was transferred to the intermediate pressure accumulator by the intensifier unit which was designed for a maximum pressure of 10,000 psi. The intensifier unit consisted of two oil reservoirs, two high pressure cylinders, and a Seco high pressure radial pump, Model No. 20LAH-3.

Storage of the feed mixture at an intermediate pressure (approximately 5500 psi) was provided by a gas

accumulator obtained from Autoclave Engineers, Inc. The accumulator, manufactured from 4340 alloy steel, was 12-inches o.d. by 8-inches i.d. by 52-inches internal length. This vessel was sealed with an O-ring self-sealing closure. The vessel had three openings in the top cover and two at the bottom; all connections were 3/8-inch AE cone connections. A pressure gauge, a rupture disc safety head assembly, and the feed gas input-output line were connected to the three openings in the top cover. One of the openings in the bottom of the accumulator was connected to the air-driven, hydraulic pump and the other bottom opening was connected to the drain line. The working pressure of this intermediate pressure accumulator was stated to be 15,000 psi at 72°F. The vessel was hydrostatically pressure tested at 22,500 psi at 72°F. The rupture disc was rated at 20,000 psi at 72°F.

The pressure in the accumulator was maintained at the desired storage pressure by pumping distilled water into the bottom of the accumulator with a Sprague, Model S-216-C-100, air-operated pump. The hydraulic fluid output pressure was 8800 psi for an input operating air pressure of 100 psi. The desired fluid discharge pressure could be regulated by properly adjusting the supply air pressure with a pressure regulating valve provided with the pump. Provisions were made to pump water to the accumulator or to the gas holder.

Since the feed mixture was stored over water, the gas was dried and filtered before being compressed to still

higher pressures. The dryer shell was a standard Autoclave Engineers Kuentzel Bomb, 1-inch i.d. by 8-inches internal depth. The vessel was manufactured from 316 stainless steel having a specified yield strength of 60,000 psi. Each end of the double-ended vessel had a confined copper, compression gasket-type closure. The maximum working pressure of this vessel was stated to be 10,000 psi at 650°F. Drierite was used as the desiccant. The filter was a standard Autoclave Engineers filter (No. 5C-A) with sintered metal discs.

After drying and filtering the feed mixture the pressure was increased to the desired storage pressure by the intermediate pressure generation unit which consisted of an air-driven hydraulic pump and the 25,000 psi compression cylinder. This compression cylinder, 3-inches o.d. by 1 5/16-inches i.d. by 16-inches internal depth, was originally used at the University of Michigan as an oil separator (37). This vessel was machined from heat-treated stainless steel, Series 400, and was fitted with an O-ring seal on the top closure. For the present application the bore was reamed and honed to a mirror finish. An aluminum piston, 2024-T351, was used to separate the hydraulic oil from the feed mixture to minimize contamination and loss of the feed gas. The seal between the piston and vessel bore was accomplished with a single Buna-N O-ring with two Teflon back-up rings. In the early part of this work the

piston was activated by pumping oil with a 40,000 psi, hand-operated hydraulic jack. Later an air-driven, hydraulic pump was used. Details of this assembly are presented in Figure 9.

The compressed gas was stored in the high pressure accumulator which was also obtained from the University of Michigan. This accumulator, which had a working pressure of 25,000 psi, was constructed from a surplus 75-mm gun barrel by welding end-plugs into the bore of the cylinder (37). Two, 1/4-inch high pressure connections were provided for the inlet and outlet lines and a 25,000 psi pressure gauge.

Photographs of the feed system are presented in Figures 10 and 11. In Figure 10 the low-pressure gas holder is shown in the center and the intermediate pressure accumulator is shown on the far left. In Figure 11 the high pressure compression cylinder is shown in the right center of the picture and the high pressure accumulator is shown on the far right.

25,000 psi Reaction System

A schematic diagram of the reaction system and associated equipment is shown in Figure 12. Continental Oil Company, Ponca City, Oklahoma, provided the reactor and electric furnace which are discussed in detail in this section.

The reactor, designed by P. A. Lobo of Continental Oil Company and C. M. Sliepcevich of the University of Oklahoma (15), was machined from 19-9DL alloy steel which was

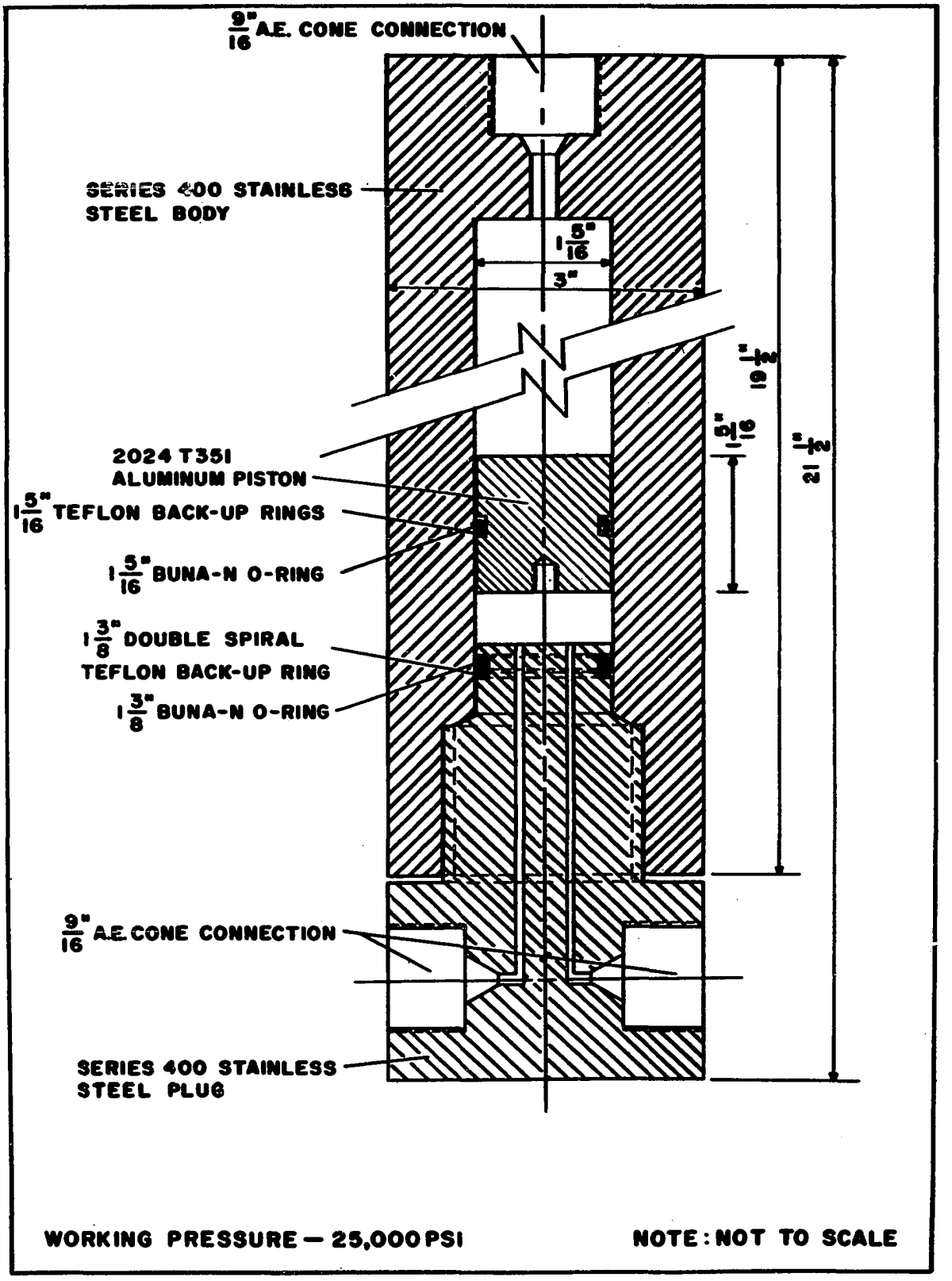

Figure 9. Details of 25,000 psi Compression Cylinder

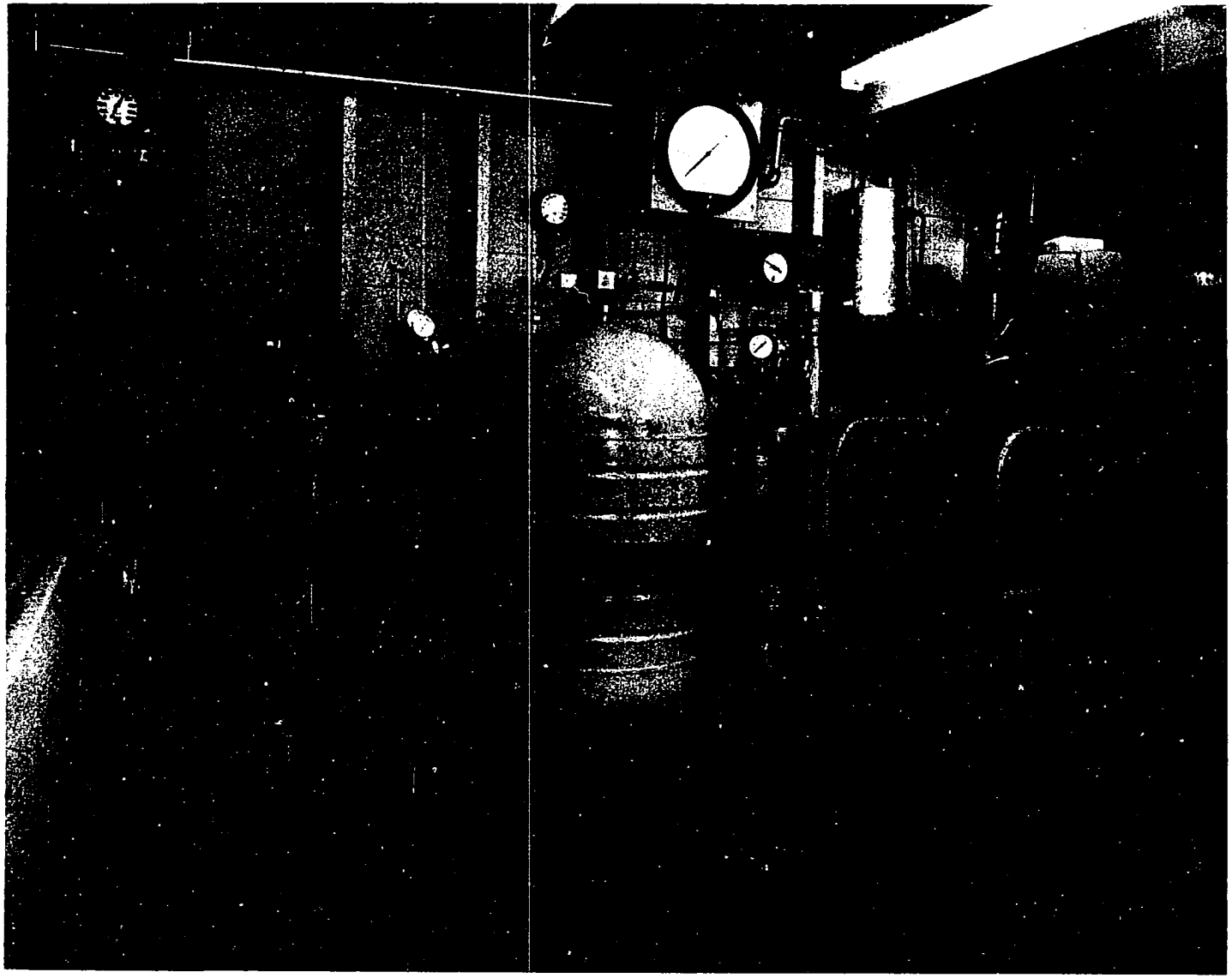

Figure 10. Equipment Inside the High Pressure Cell

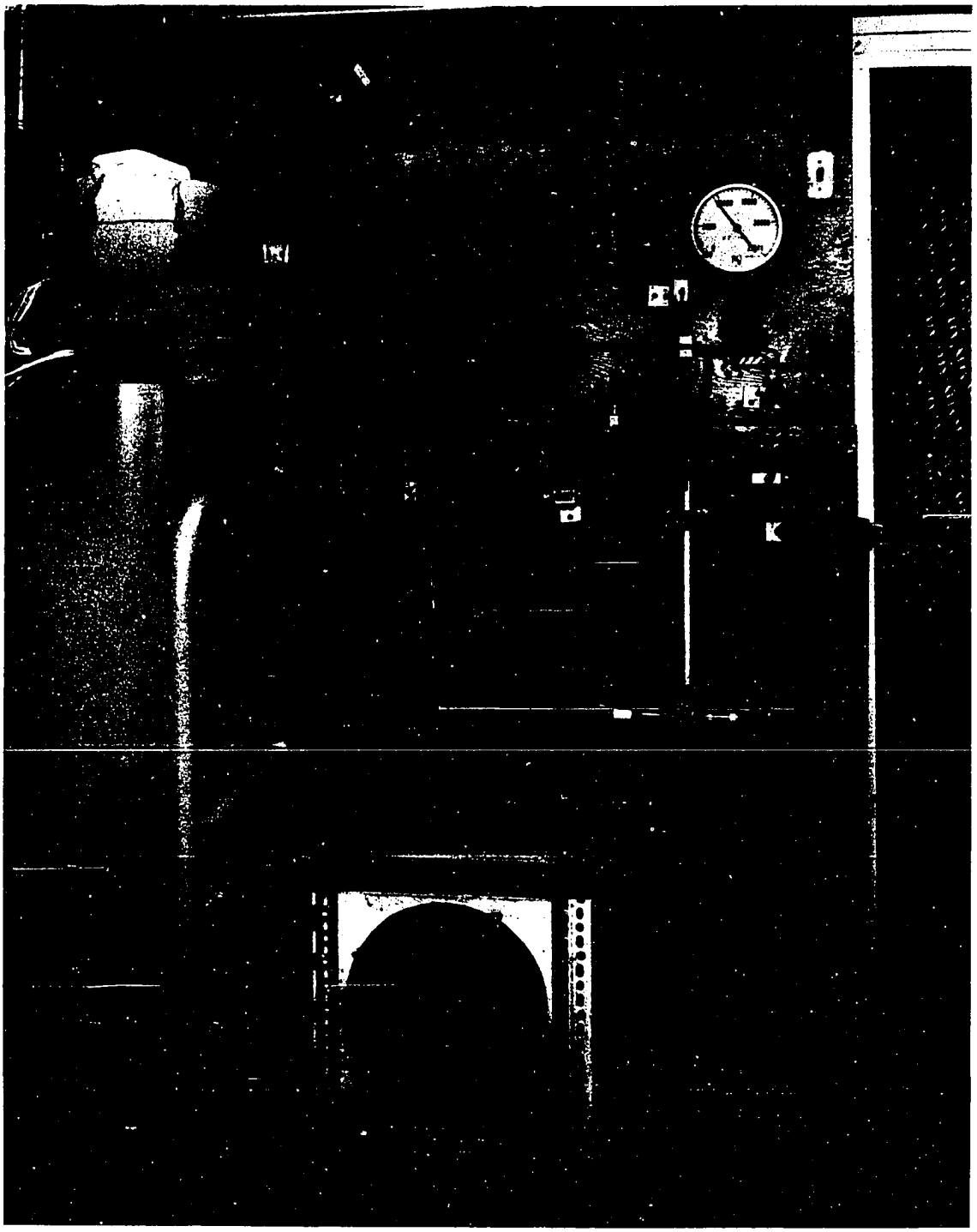

Figure 11. 25,000 psi Reaction System

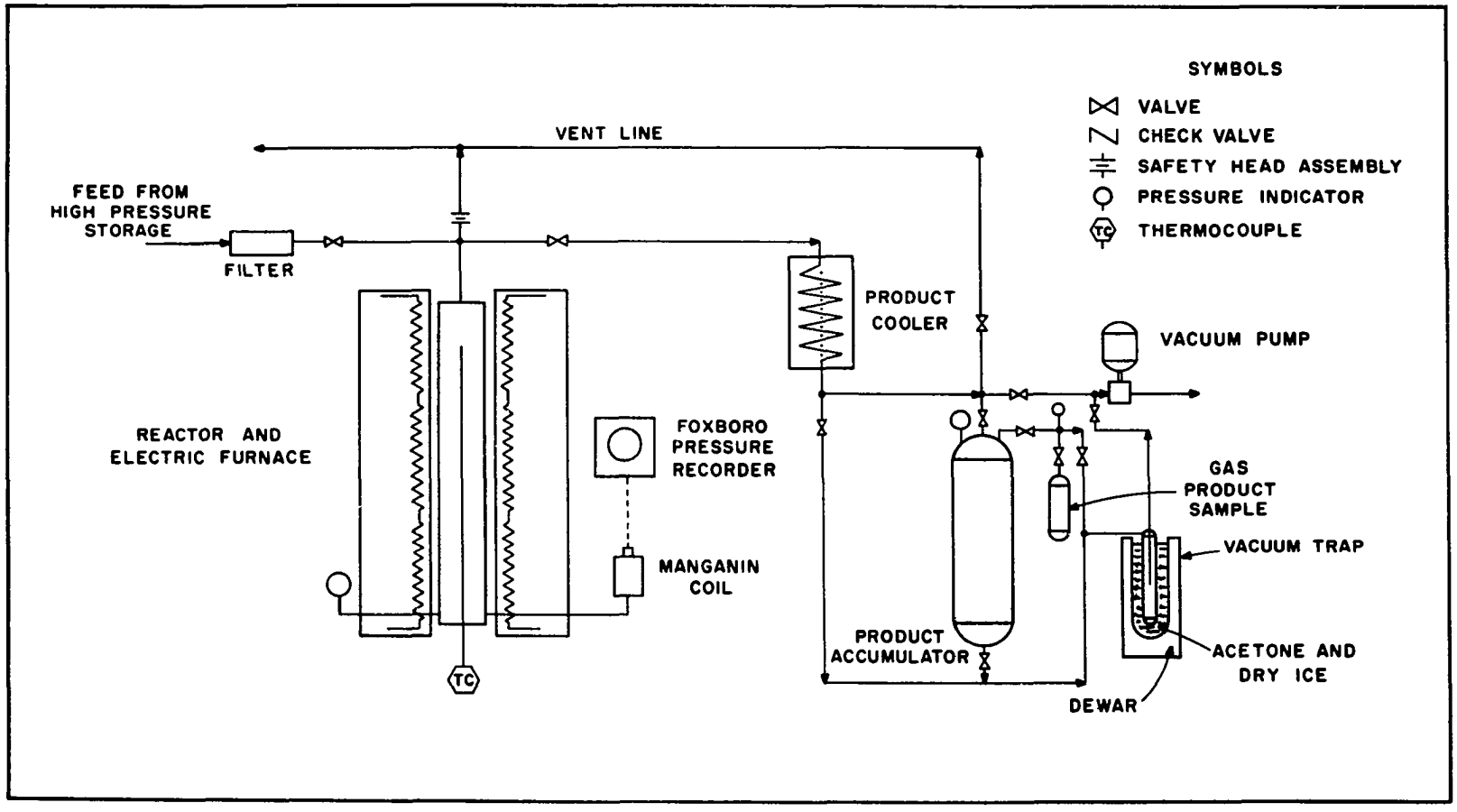

Figure 12. Process Flow Diagram of 25,000 psi Reaction System

heat-treated for 4 hours at 1650°F and air-cooled. The reactor, 4-inches o.d. by 1 1/4 inches i.d. by 30-inches internal depth, was designed for a working pressure of 25,000 psi at 1,000°F. The top closure was sealed with a full Bridgman self-sealing closure using Garlock #934 shredded metal packing (see Figure 13A). The end-plug, threaded and coned on one end, was connected to a top cross assembly (see Figure 13B). Two 1/4-inch connections, two 3/8-inch connections, and the connection for a safety head assembly had been provided by the top cross assembly, but in this investigation two of the connections were plugged. The rupture disc, which provided relief protection for the reactor, was rated at 30,000 psi at 72°F. Metal-metal 59° to 60° conical joints were used to seal all couplings. The reactor base closure assembly (see Figure 13C) provided three connections; the bottom connection was used for a thermowell and the two side connections were used for determining the system pressure. The thermowell, 3/8-inch o.d. by 1/8-inch i.d. by 40-inches long, 347 stainless steel tubing, which was welded over at one end, extended the internal length of the reactor body. Four iron-constantan thermocouples, one located at the top of the reactor, two located at the center of the reactor, and one located at the base of the reactor, measured the reactor temperature. Three of the temperatures, top, center, and bottom, were recorded on a Brown multi-point temperature recorder. The

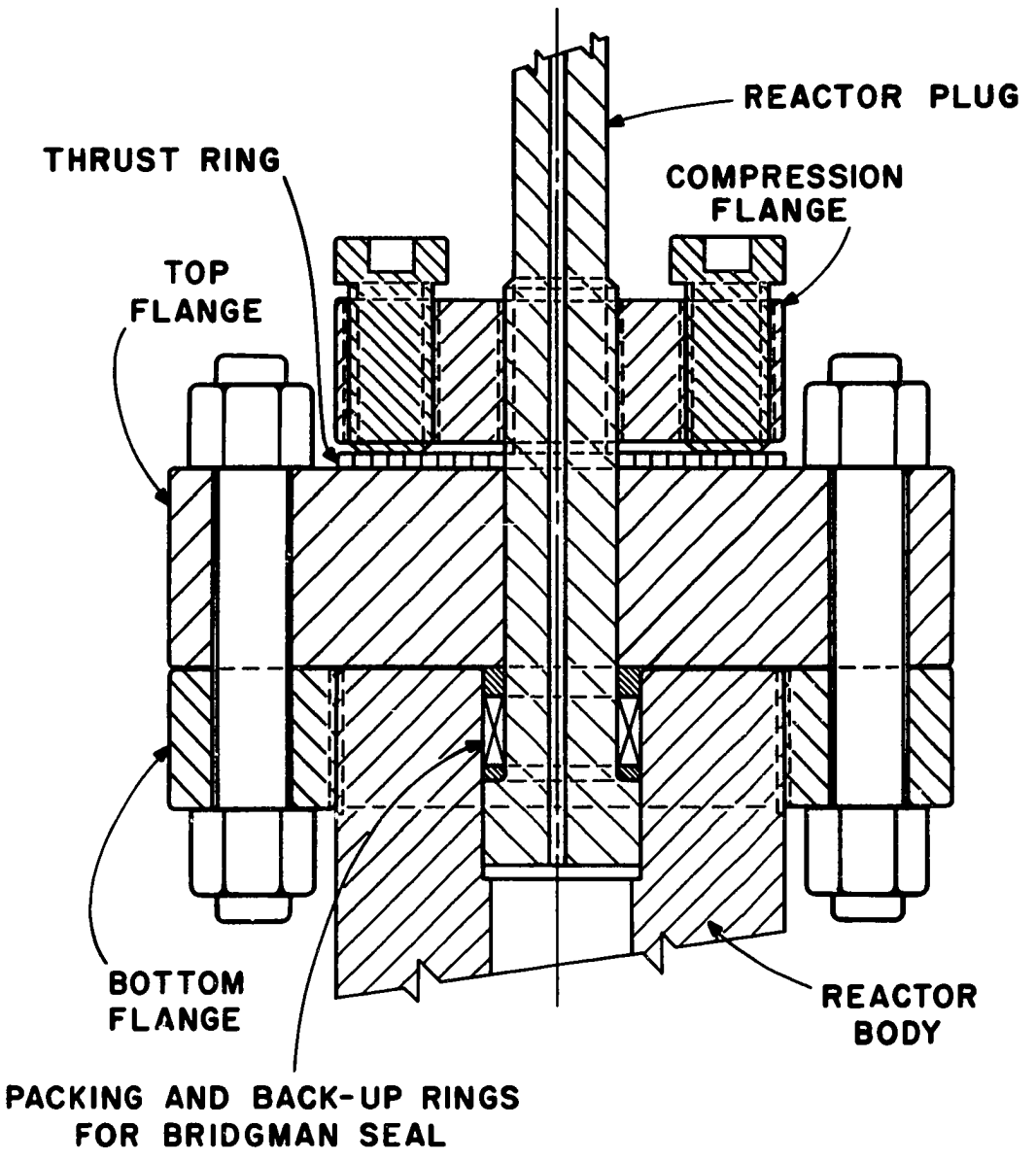

HIGH PRESSURE REACTOR
(TOP CLOSURE ASSEMBLY)

NOTE:
REPRODUCED BY PERMISSION OF
CONTINENTAL OIL COMPANY

Figure 13A. Details of 25,000 psi Reactor

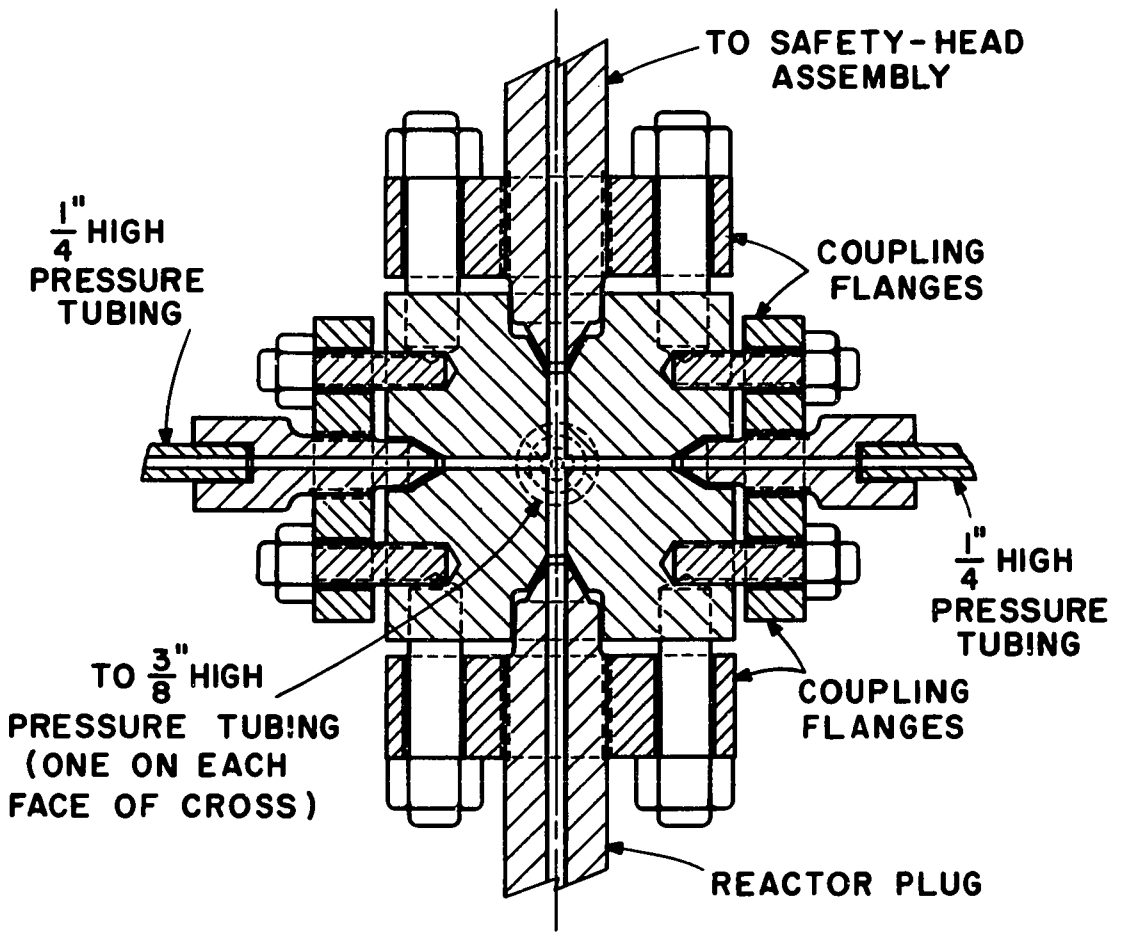

HIGH PRESSURE REACTOR
(TOP CROSS ASSEMBLY)

NOTE:
REPRODUCED BY PERMISSION OF
CONTINENTAL OIL COMPANY

Figure 13B. Details of 25,000 psi Reactor

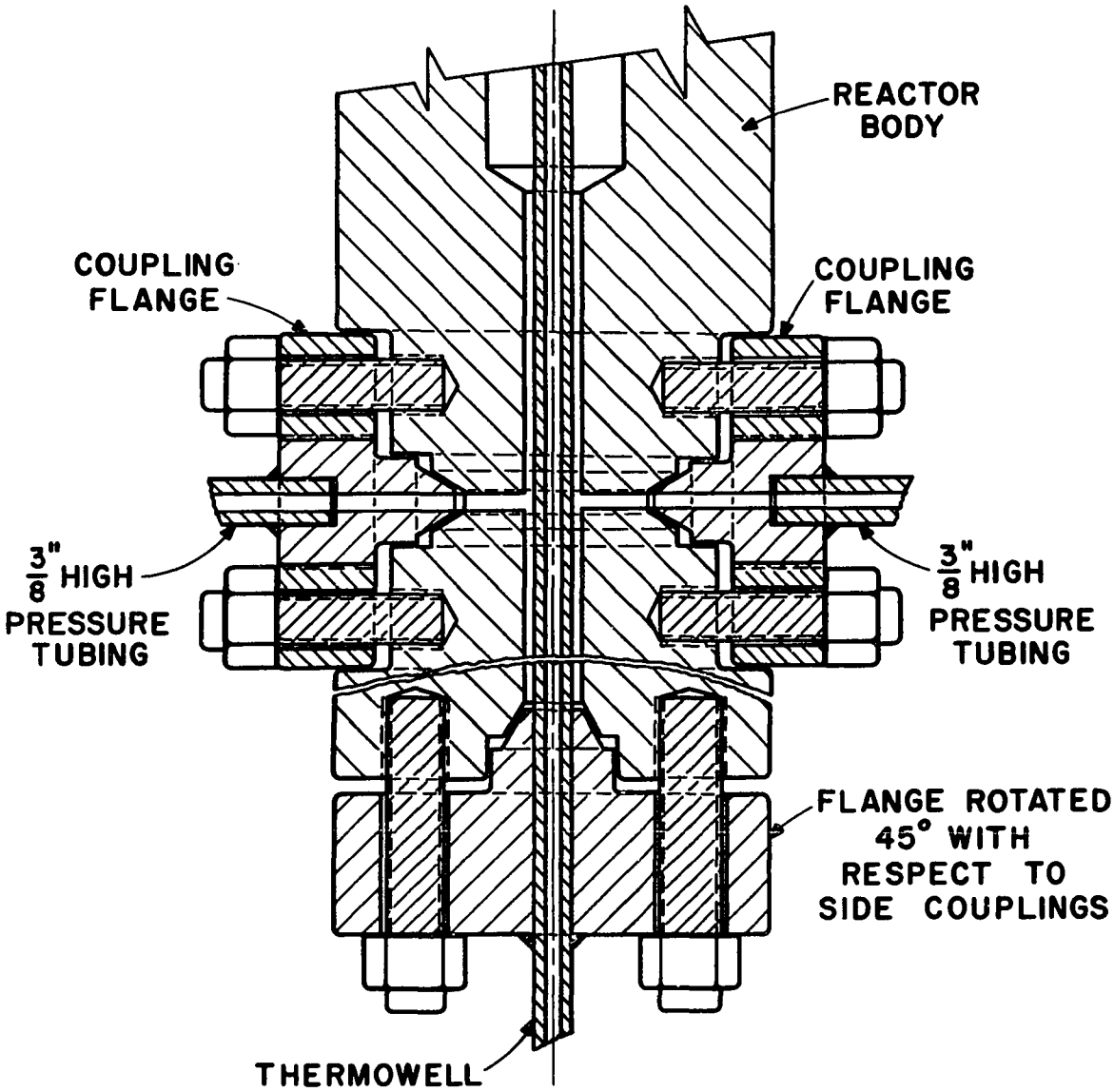

HIGH PRESSURE REACTOR
(BASE CLOSURE ASSEMBLY)

NOTE:
REPRODUCED BY PERMISSION OF
CONTINENTAL OIL COMPANY

Figure 13C. Details of 25,000 psi Reactor

remaining center temperature was recorded on a Bristol single-point recorder which had a chart speed of 2½ inches per minute.

The reactor pressure was measured by a Heise pressure gauge, 0-20,000 psi range with 20 psi scale divisions, and a manganin pressure cell. Pressure records were obtained by a Foxboro Dynalog recorder connected to the manganin pressure cell.

The reactor was supported inside an electric furnace by an adjustable semi-circular support which rested beneath the top flange of the reactor. The support was machined to accept the bottom part of the flange studs. Alignment of the reactor was accomplished by an adjustable brace located at the base of the reactor. The reactor and electric furnace were mounted in an angle iron and pipe framework. Removal of the reactor was accomplished by removing half of the cylindrical housing of the furnace.

The furnace was heated by 24 Chromalox heating elements, 200 watts each, arranged so that 8 elements connected in series constituted a set. Four elements of each set were mounted in the detachable half of the furnace housing. Power input to the three sets of heating elements was supplied by three Powerstat variable transformers. Insulation for the furnace (approximately 8 inches thick) was placed in the annular space of the housing.

The furnace and framework for the reactor are shown on the far right and left in Figures 10 and 11, respectively.

200,000 psi Reaction System

In Figure 14, the 200,000 psi reaction system is shown schematically. For runs above 15,000 psi, the previously described reaction system was replaced by a 200,000 psi system. It is convenient to divide this system into two sections: (1) the high pressure generation system and (2) the reactor.

High Pressure Generation System

The main items of the high pressure generation system were the air-driven, hydraulic pump, the intensifier, and the compression cylinder.

The generation of pressure was accomplished by charging the compression cylinder and reactor with the reaction mixture from the high pressure accumulator. Appropriate location of valves allowed the pressure to be increased to 23,000 psi. At this time the high pressure intensifier was activated and the reactor pressure was increased indirectly by the hydraulic pump. Provisions were made to recycle the intensifier and the free piston in the compression cylinder so many times as might be required to obtain the desired reactor pressure.

The SC air-driven, hydraulic pump, Model No. 10-600, was designed to deliver hydraulic fluid at 30,000 psi with an air supply of 100 psi. The fluid discharge pressure could be regulated by adjusting the pressure of the air supply with a pressure regulating valve. The hydraulic

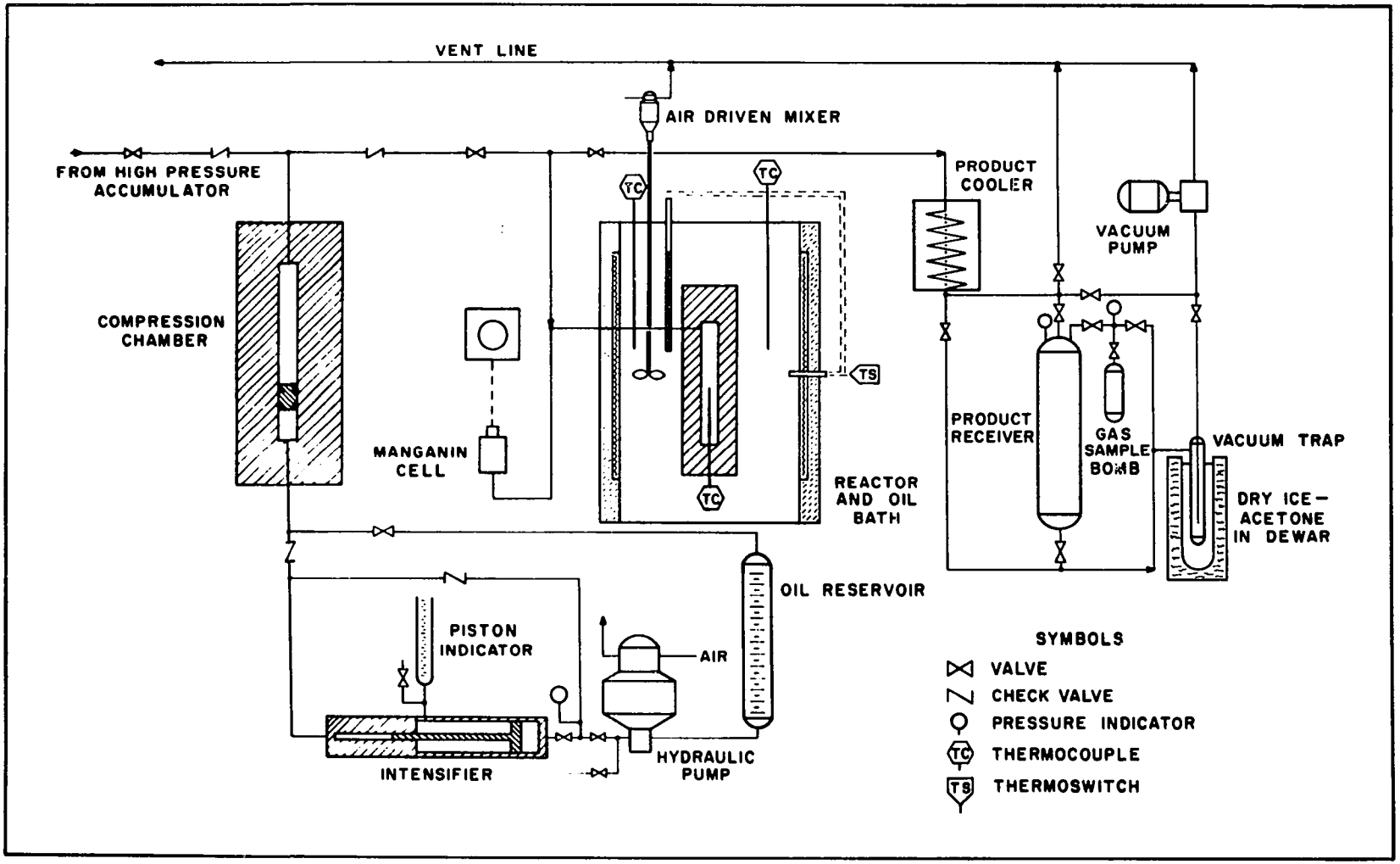

Figure 14. Process Flow Diagram of 200,000 psi Reaction System

fluid, Plexol 201, which was stored in a 2000 ml oil reservoir, was filtered before being admitted to the pump.

Although design of the intensifier was discussed in the preceding chapter, additional details are presented in this section. The intensifier, 1-inch i.d. on the high pressure end, 5-inches o.d., 30-inches overall length, and weighing 150 pounds, was mechanically operated with the 30,000 psi air-driven hydraulic pump. The low pressure end was fitted with a 3/8-inch AE cone connection for the pump discharge line and a 1/8-inch pipe connection to vent the cylinder cavity during the pressure stroke. Piston location was determined by the displacement of the oil which the cavity contained. The volume of displaced oil was measured in a 1000 ml graduated vessel connected to the 1/8-inch pipe connection. A standard 3/4-inch double cone connection was provided for the discharge opening of the high pressure cylinder. Block valves and check valves permitted the reversal of the intensifier by the 30,000 psi hydraulic pump without decreasing the pressure in the reaction system. All valves, fittings, and tubing (1/4-inch o.d. by 0.083-inch i.d., 304 stainless steel) used on the low pressure side of the intensifier had a minimum pressure rating of 30,000 psi.

The compression cylinder, shown in Figure 15, was a triplex vessel fabricated from 4340 gun steel. This vessel, 18-inches o.d. by 2-inches i.d., by 15-inches internal and

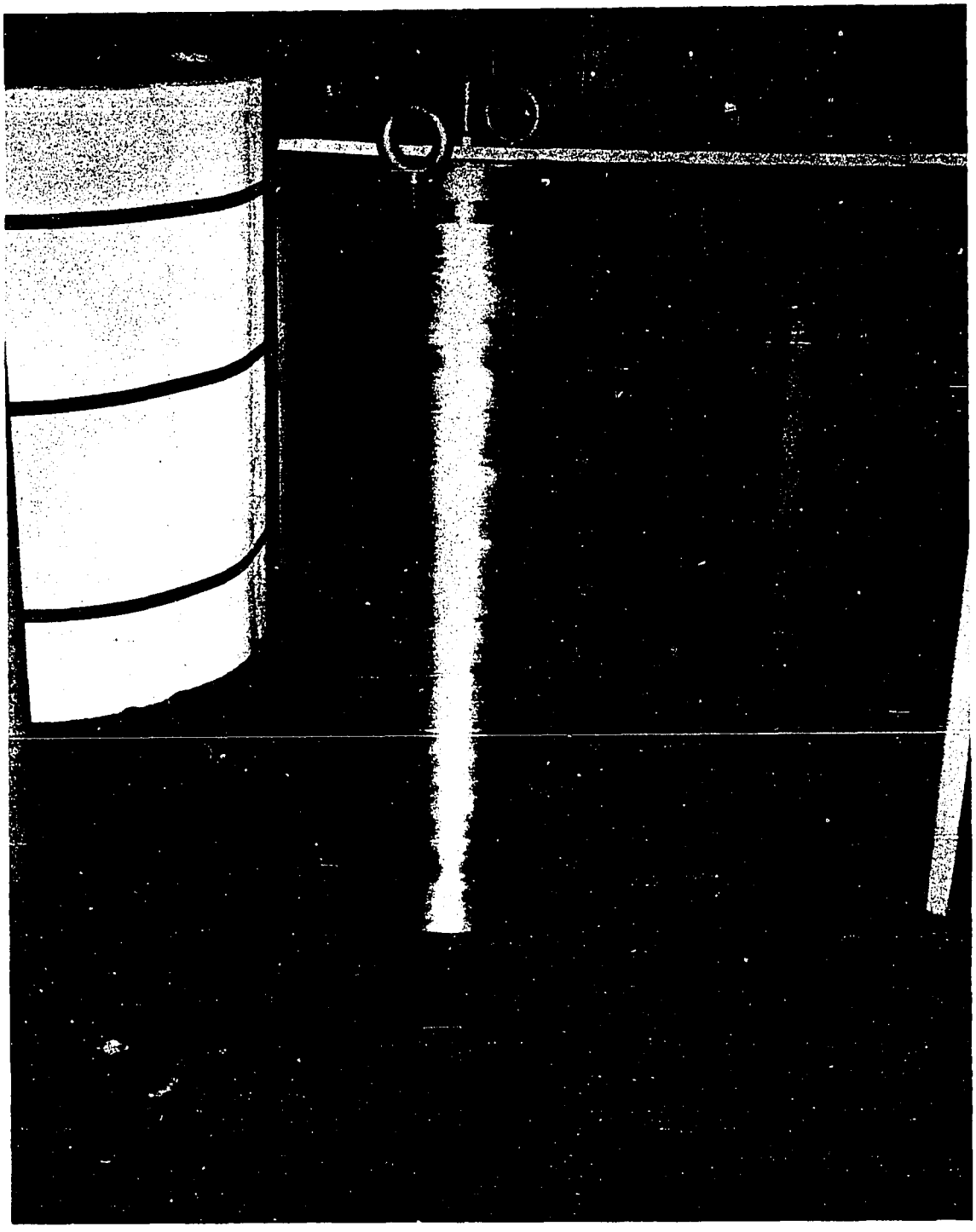

Figure 15. 200,000 psi Compression Cylinder

40-inches external length, and weighing 2400 pounds, had a free-piston to separate the hydraulic oil from the reaction mixture. The piston not only minimized contamination of the reaction mixture, but it also prevented loss of the gas in the hydraulic oil. One end of the compression cylinder was connected by 3/4-inch o.d. by 1/16-inch i.d. composite (duplex) tubing to the discharge of the high pressure cylinder of the intensifier and to the return line to the hydraulic oil reservoir. The other end of the compression cylinder was connected to the 200,000 psi reactor and high pressure accumulator with appropriate tubing and valves. The design details have been presented in Chapter IV.

The stand which supported the compressor cylinder consisted of two 3/8-inch thick steel plates separated by four equally spaced legs made from 2 inch pipe. The top plate of the stand was 20-inches o.d. with a 10-inch i.d. hole to permit the end-plug and gland nut to extend below the top plate. The four legs, 13 inches long, were welded to the top and base plates on a 7-inch radius. The base plate, which was also 20 inches in diameter, distributed the weight of the heavy vessel over a larger floor area.

Location of the equipment inside the high pressure cell is presented in Figure 16. The compression cylinder is shown in the center of the photograph. The intensifier with the air-driven hydraulic pump and associated equipment appears at the bottom.

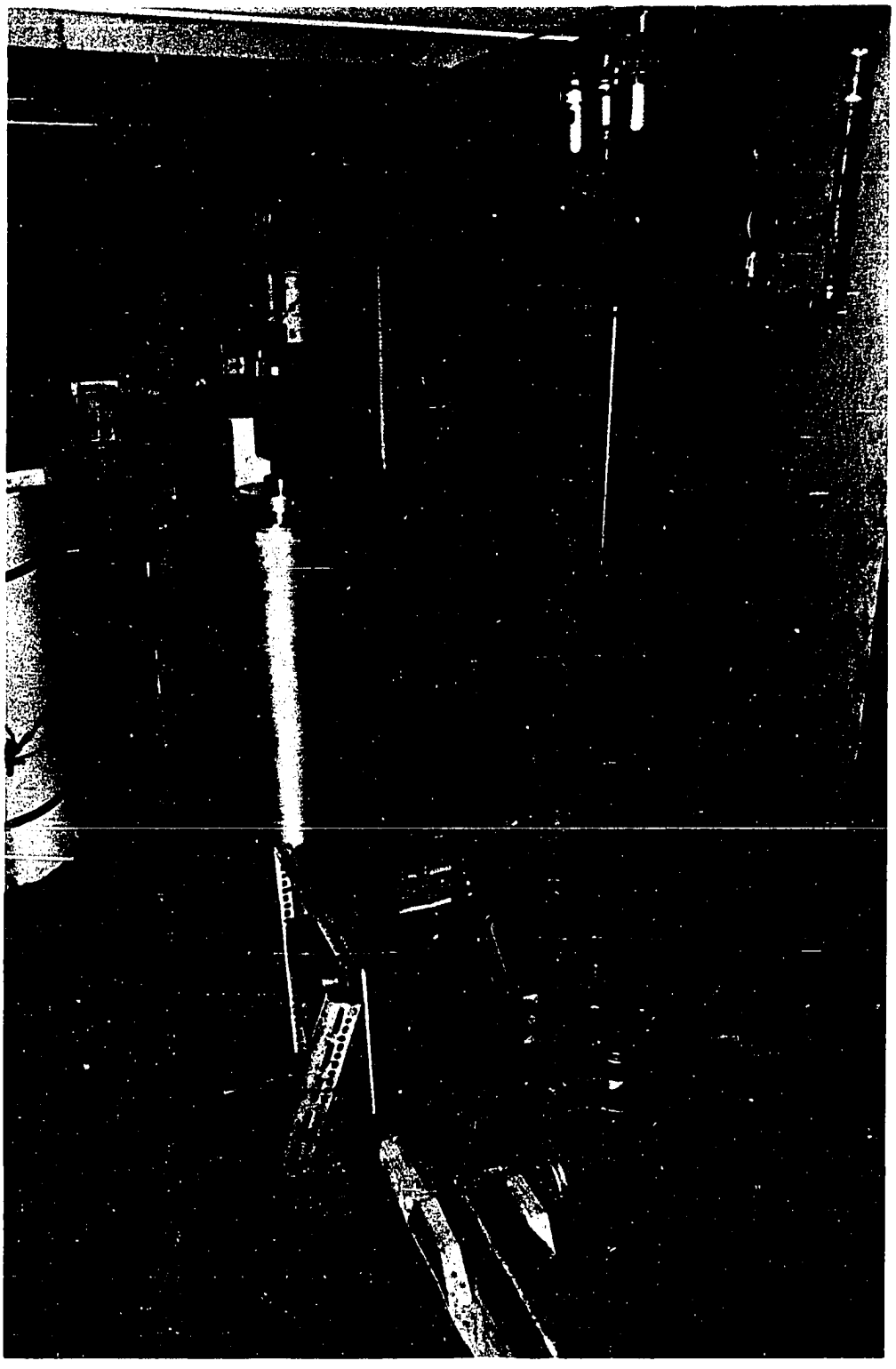

Figure 16. 200,000 psi Equipment Inside the High Pressure Cell

200,000 psi Reactor

Figure 17 is a photograph of the reactor. The design and construction of this duplex vessel was presented in Chapter IV.

The reactor was a compound vessel with an inside diameter of 2 inches, an outside diameter of 12 inches, and an internal length of 10 inches. The external length was 32 inches and the weight of the reactor was approximately 1000 pounds. Only one opening was provided, which was introduced through the wall of the vessel at one end. The reactor was internally heated with a 1000 watt resistance heater; the power input was manually controlled with a Powerstat variable transformer. The electrode for the heater (see Figure 3, Chapter IV) was introduced through the top closure of the reactor and sealed with an unsupported area type seal. The temperature inside the reactor was measured by a thermocouple (iron-constantan) located in the thermowell provided in the bottom closure of the reactor. Output from this thermocouple was measured with either a Leeds-Northrup Model 8662 or Model 8686 millivolt potentiometer and was recorded by a Bristol strip chart recorder.

The pressure in the reactor was determined with a Harwood manganin gauge and recorded on a Foxboro Dynalog recorder. The manganin gauge consisted of a manganin wire coil encased in a 200,000 psi pressure cell. The wire coil has a linear change of resistance with pressure.

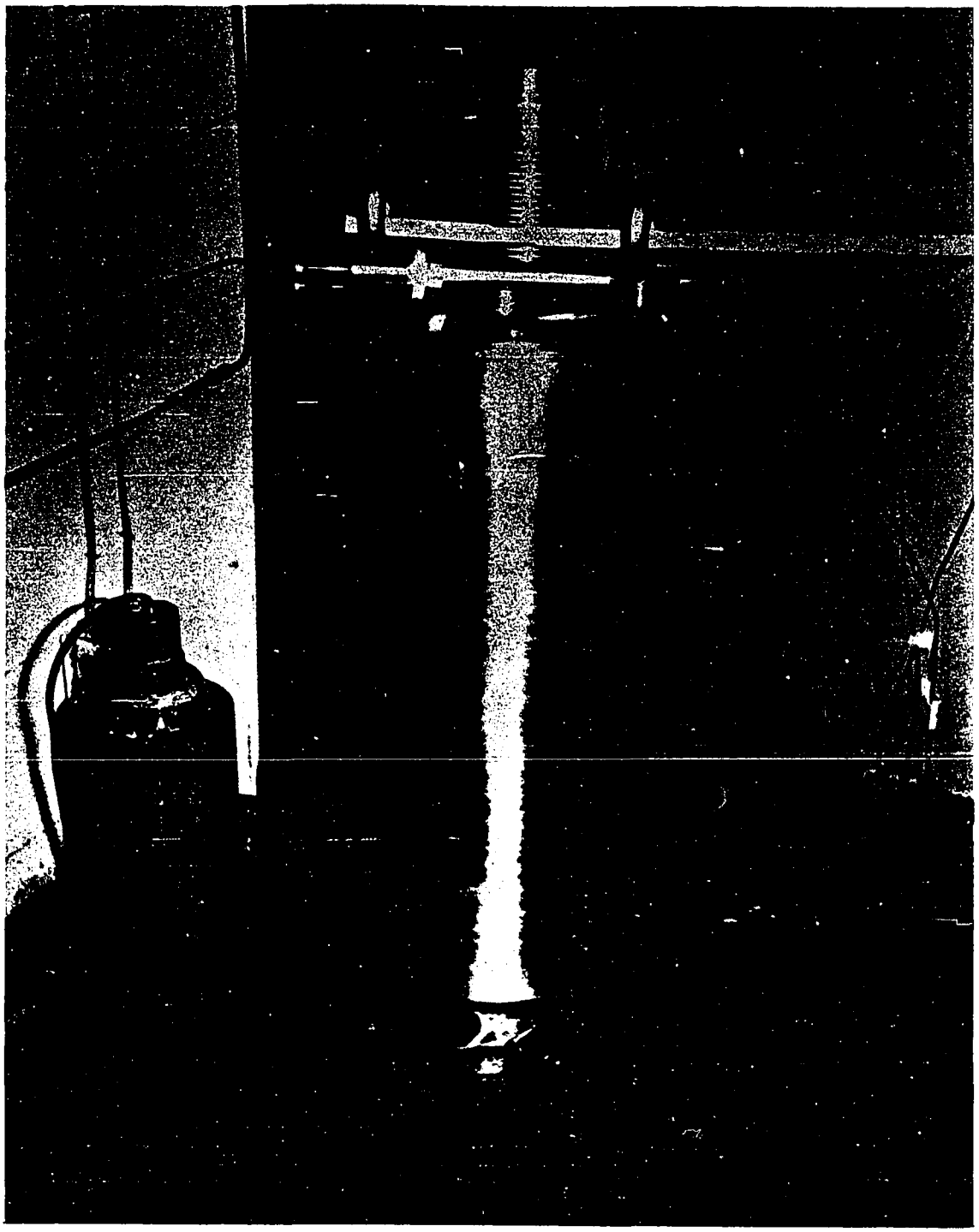

Figure 17. 200,000 psi Reactor

Internal heating of the reactor was accomplished with a 1000 watt resistance heater constructed from 30 feet of 18B and S gage Chromel A wire coiled around a piece of 30 mm Pyrex glass tubing, 8½ inches long. Spacing of the coil was accomplished by covering one-half of the bare resistance wire with ceramic beads, 0.17 inches o.d. by 0.068 inches i.d. This 15 feet of insulated wire was coiled around the Pyrex tubing, ending at the bottom of the support. The uninsulated portion of the wire, starting at the bottom of the Pyrex support, was coiled between the turns of the insulated wire. A high temperature adhesive, which was resistant to thermal shock, was used to cement the coiled wire to the Pyrex support. The internal heater with the end-plug of the reactor and other 200,000 psi fittings is shown in Figure 18.

The hot oil bath for the reactor was a vessel, 24 inches in diameter and 36 inches deep, filled with cottonseed oil. Since the end closure of the reactor prevented the reactor from resting directly on the bottom of the oil bath, a 3/8-inch thick steel ring, 12-inches o.d. by 6-inches i.d., and supported by four legs, was welded to the bottom of the oil bath to support the reactor. The cover for the tank was a 1/4-inch thick steel plate which rested on the outer edge of the vessel and was held in place by lugs welded to the inside of the vessel wall.

Six, 1000 watt chromalox strip heating elements were equally spaced around the outside of the oil tank.

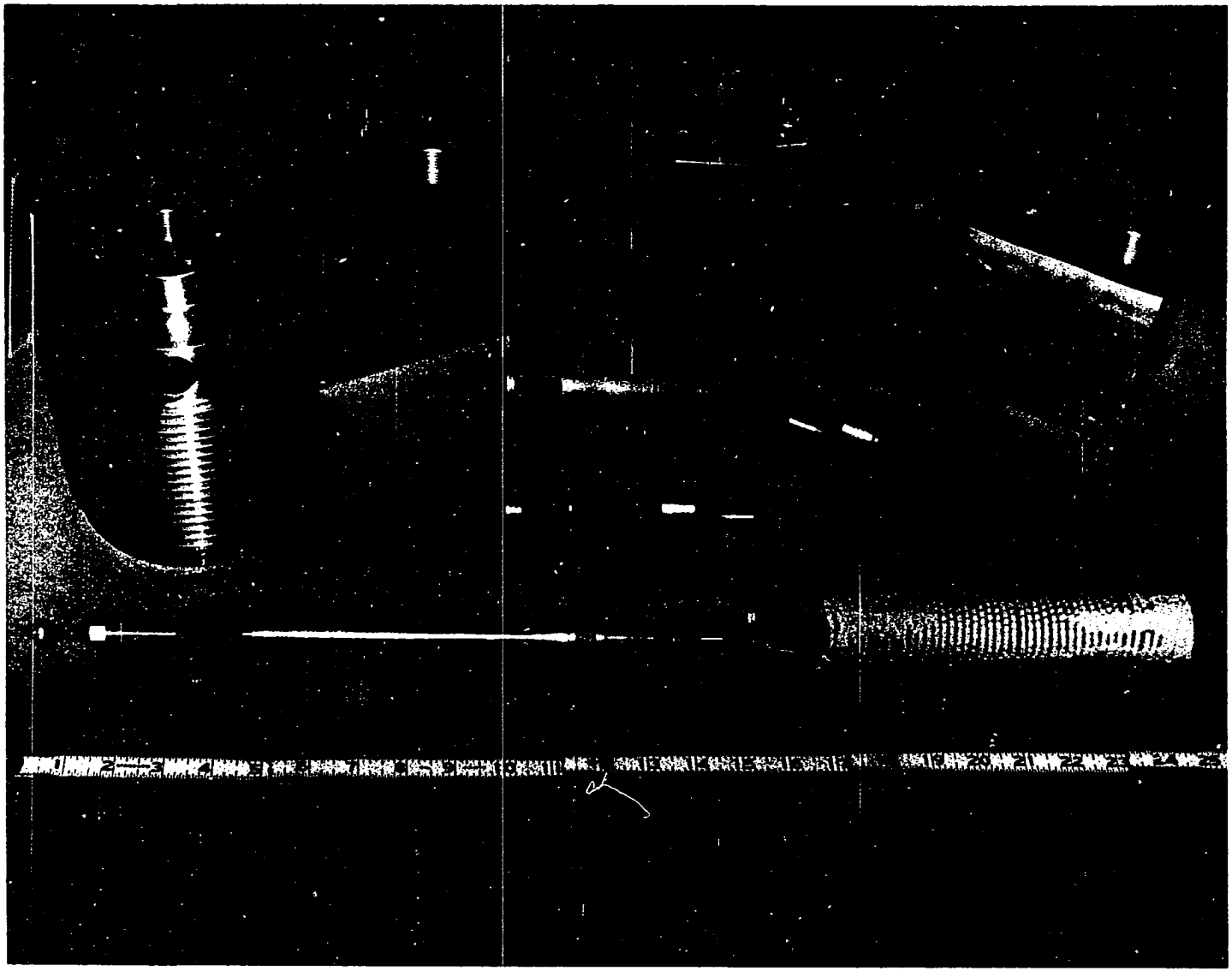

Figure 18. Internal Heater and High Pressure Fittings

Thermon "T-3" was used to increase the effective contact area between the heating elements and the wall of the vessel. The remaining area surrounding the embedded strip heaters was filled with asbestos cement. Kaylo high temperature pipe insulation, 2 inches thick, was then used to insulate the oil bath. The power input to the heaters, which were connected in parallel, was controlled by a Powerstat variable transformer supplied by a 240 volt circuit. A Chromalox heating cartridge(750 watts), placed in a heater well extending through the cover plate, was connected in series with a Fenwall Thermoswitch temperature controller located in the wall of the vessel. It provided a trim control for the oil bath.

Continuous agitation of the oil by an air-driven "Lightnin" mixer, (Model No. AR-25) improved the heat transfer coefficient and maintained a more constant temperature throughout the oil. The temperature of the oil bath was measured by two iron-constantan thermocouples placed in stainless steel thermowells which extended through the cover plate.

Product Section

The product section, common to both reaction systems previously described in this chapter, was a closed system designed to "freeze" the reaction and to collect the products of the reaction at a relatively low temperature and pressure. "Freezing" the reaction was accomplished by expanding and cooling the reactor contents.

The product cooler was constructed from a 17-inch length of 8-inch, schedule 40, carbon steel pipe and a 1/4-inch thick steel plate. The steel plate was drilled and fitted with a 1/4-inch Speedline coupling which was welded in place. Approximately 20 feet of 1/4-inch o.d. by 1/8-inch i.d., 304 stainless steel tubing was coiled on a 5-inch diameter and placed in the pipe shell. A thin film of polyester resin was applied to the inside of the water jacket to prevent rusting.

The product receiver, designed for a working pressure of 500 psi at 72°F, was constructed from a 24-inch length of 4-inch, schedule 40, pipe jacketed by a 6-inch, schedule 40, pipe which was 22½-inches in length. Standard 4-inch, schedule 40, pipe caps were used for the covers of the receiver. The jacket was sealed with 1/8-inch thick steel plate. Three, 1/4-inch pipe connections were located in the top cover of the receiver for installation of a pressure gauge, a gas sampling system, and the product inlet line. One, 1/4-inch pipe connection was installed in the bottom cover for the liquid sample and drain line.

Preliminary tests indicated that the volume of the product receiver was too small for the entire range of pressures to be covered in the investigation; therefore, a second receiver was added to the product system. This receiver was a 500 cu. in. stainless steel cylinder originally built to contain breathing oxygen.

Gas samples for analysis were collected in 1CC-3AA gas cylinders. Liquid samples were collected by freezing the condensable components at dry ice temperature.

Auxiliaries

All of the high pressure equipment used in this investigation, excluding the Sprague air-driven, hydraulic pump and the intermediate pressure intensifier unit, was located inside the high pressure cell. The original high pressure cell was 12-feet long by 12-feet wide by 8-feet high. The cell walls were constructed from a 1/4-inch thick cold-rolled steel plate backed by a 2-inch thick tongue and groove wood framing. The ceiling was made from 2-inch thick, tongue and groove wood, supported on 2-inch by 8-inch wood beams spaced 15 inches apart. The entrance to the barricaded cubicle was covered by a heavy Manila rope blasting mat.

In the early phase of this investigation when only a limited number of people occupied the first floor of the building where the high pressure facilities were located, the original barricades were adequate. However, before the studies at the extremely high pressure could be completed, it was necessary to incorporate additional safety precautions. A blow-out panel, 6 feet by 8 feet, was installed in the exterior wall of the high pressure cell. The exposed area behind the blow-out panels was protected by a Manila rope blasting mat installed approximately 3 feet from the outside of the blow-out panel. A 1/4-inch thick cold-rolled steel

plate backed by a wooden layer was also installed to provide a barricade on the west side of the cell which was not barricaded in the original facilities. To insure the safety of the personnel occupying the second floor of the building, the ceiling of the high pressure cell was covered with a 1/4-inch thick cold-rolled steel plate followed by a Manila rope blasting mat.

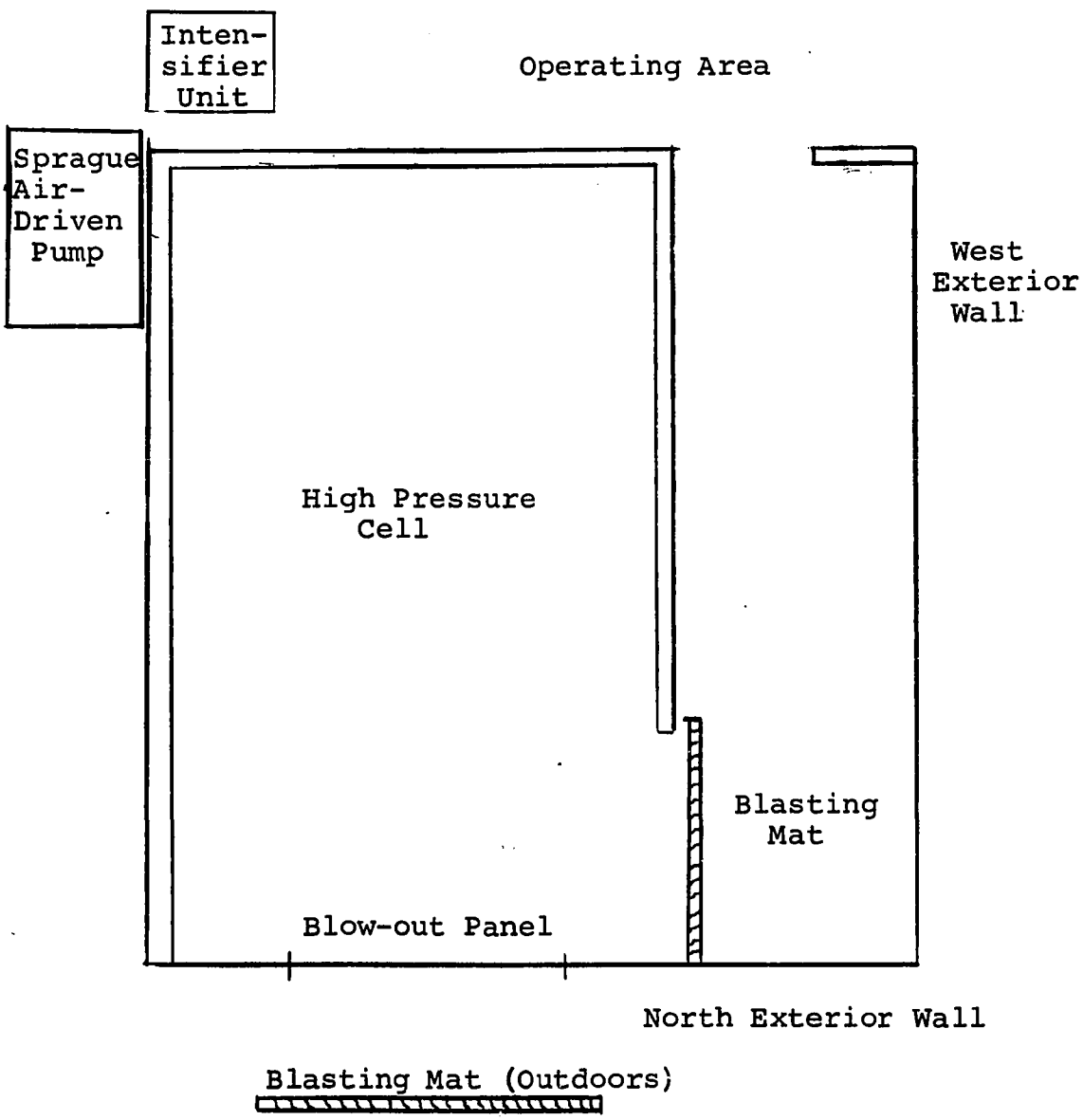

Additional safety features of the high pressure facilities included the installation of a 1725 rpm exhaust fan driven by a 1/4-hp explosion-proof motor. All relief valves, rupture discs, and vents were connected to a common vent line which extended outside the building. All valves had extensions through the cell wall so that all required operations at high pressures could be performed without going into the cell.

The size and weight of the high pressure equipment presented minor problems in the installation of the equipment inside the high pressure cell. An A-frame with a one-ton chain hoist was placed on top of the high pressure cell for installation and maintenance of the 200,000 psi reactor and compression cylinder. Further, the wooden floor of the high pressure cell was braced to accommodate the weight of the high pressure equipment.

CHAPTER VI

EXPERIMENTAL PROCEDURE

The discussion of the experimental procedure employed in this study on the partial oxidation of methane at high pressures is divided into three sections: preliminary procedures, run procedure, and difficulties encountered. Due to the variety of products formed in the oxidation process, a discussion of the analytical procedures is presented in a chapter devoted entirely to this subject.

Preliminary Procedures

The hazards associated with the mixing of methane and oxygen and the extremely high pressures involved in this study necessitated mixing the reacting gases at low pressure, followed by a two-or three-stage operation to increase the pressure to reaction pressures. In the preparation of the feed mixture, instrument grade methane, contained in a standard 1A gas cylinder fitted with a gas pressure reducing regulator, was connected to the gas holder. The gas holder was evacuated three times with alternate purges of methane before starting the mixing operation. Methane was then added to the gas holder until the pressure was approximately

90 psig. The methane cylinder was replaced with a 1A gas cylinder of pure oxygen which was fitted with a pressure reducing regulator designated for oxygen use only. The connection line to the gas holder was evacuated and purged with oxygen before admitting the oxygen gas to the methane in the gas holder. The discharge pressure of the oxygen pressure regulator was set at 100 psig before the block valve between the gas cylinder and gas holder was partially opened to add oxygen slowly to the system. Mixing the two gases in this way greatly reduced the explosion hazards since the methane-oxygen mixture was always above the upper explosion limit for this system at ambient temperature.

The intermediate pressure accumulator and intensifier, both previously evacuated, were filled with the gas mixture. The pressure of this portion of the system (gas holder, intensifier unit, and accumulator) was increased to approximately 250 psig by pumping water into the gas holder with the air-driven, water pump. The pressure of the gas holder was maintained at this pressure by continuously pumping water into the gas holder throughout the transfer of the remaining feed mixture to the intermediate pressure accumulator.

The intensifier unit, consisting of two hydraulic oil reservoirs connected through a high pressure liquid pump to two, high pressure cylinders, was put into operation to complete the transfer of the feed mixture. Briefly, the intensifier operation involved the filling of one high

pressure cylinder with the gas mixture from the gas holder followed by pumping hydraulic oil from the oil reservoirs into the high pressure cylinder which had been isolated from the gas system. The gas mixture, now at a pressure considerably greater than the pressure of the accumulator, was then transferred to the intermediate pressure accumulator. While the hydraulic oil in one high pressure cylinder was being moved back to the oil reservoir, the second high pressure cylinder was put into operation. This procedure was continued until the gas mixture in the gas holder was depleted. Depletion of the gas in the gas holder was determined by the quantity of water which had been pumped into the vessel.

After depletion of the gas mixture in the gas holder, the accumulator and intensifier were isolated from the system. The methane cylinder was connected to the gas holder and the water in the vessel was drained. A pressure of approximately 25 psig was maintained on the gas holder during the draining process. After draining the water in the gas holder, the entire procedure was repeated until sufficient feed gas for a series of experimental runs was available. Since a positive pressure of methane was always maintained on the gas holder, the evacuation and purging of the vessel could be omitted in subsequent preparations of the feed mixture.

After sufficient feed had been prepared and transferred to the intermediate pressure accumulator, the pressure in the isolated storage vessel was increased to approximately

5500 psi by pumping distilled water into the accumulator. With the appropriate air pressure supplied to the air-driven water pump, the pressure of the methane-oxygen mixture in the accumulator was always maintained at the desired value.

The feed mixture was then transferred through a dryer, filter, and the 25,000 psi compression cylinder to the high pressure accumulator. Initially the high pressure accumulator was evacuated and the pressure of the two accumulators was permitted to equalize at approximately 5500 psi. Additional transfer of the feed mixture was accomplished by activating the 25,000 psi compression cylinder. This operation involved the addition of feed mixture to the compression cylinder, isolation of the compression cylinder from the intermediate pressure accumulator, and activation of the free piston by pumping hydraulic oil into the compression cylinder. Before the acquisition of the air-driven liquid pump rated at 30,000 psi, the hydraulic oil was added to the compression cylinder with a manually-operated hydraulic jack rated at 40,000 psi. At the end of the compression stroke, which was determined by the volume of hydraulic oil added to the cylinder, the hydraulic oil vent valve was opened to reverse the piston of the compression cylinder. A check valve located between the compression cylinder and high pressure accumulator prevented the loss of pressure generated in the accumulator. This procedure was repeated until the desired storage pressure was obtained.

Before a run was made in the 25,000 psi reactor, the reactor temperature was adjusted to the desired temperature. Adjustment of the temperature was accomplished by manually adjusting the three Powerstat variable voltage transformers. In the 200,000 psi reaction system no preliminary temperature adjustments were required for each run since the oil bath in which the reactor was located was always maintained at 415°F by the on-off control provided by the Fenwall Thermoswitch temperature controller.

Run Procedure

In an attempt to retain a reproducible surface in the reactors, the reactors were always kept hot and at subatmospheric pressures between experimental runs. The latter condition was accomplished by isolating the evacuated reactors at the end of each run. Prior to each run, the product section and the reactor were evacuated for at least 15 minutes. After evacuation of the reactor the reactor discharge valve was closed and the product section isolated. This part of the run procedure was identical for both reaction systems.

The run procedure for the 25,000 psi reaction system is discussed first. After recording the pressure of the high pressure accumulator and starting the Bristol single-point recording potentiometer, the reactor inlet valve was slowly opened to admit the reactants from the high pressure accumulator. The apparent maximum rate of pressure increase during the filling process to avoid premature ignition was

approximately 1,500 psi per minute. This rate was determined experimentally in the early phases of this research when premature ignition of the feed mixture occurred during the charging operation. After filling the reactor to the desired pressure, the reactor inlet valve was closed and a stop watch was started. The time required to charge the reactor was recorded and the temperature and pressure recordings were marked. The course of the reaction was then followed by the temperature of the reactor until a maximum temperature was obtained. The time required to reach the maximum temperature after completion of the filling operation was recorded as the residence time. The reactor discharge valve was then opened to expand the gas into the product receivers.

The temperatures of the reactor and product receivers, and the pressures of the closed system and the high pressure accumulator, were recorded. A gas sample bomb and the vacuum trap situated in a dewar containing dry ice and acetone were connected to the product system. The product receivers were isolated from the product cooler and the reactor. The vacuum pump was then started and the contents of the reactor and product cooler were slowly passed through the vacuum trap to collect the condensable products. After the reactor and product cooler had been evacuated, the reactor discharge valve was closed.

Once the reactor had been evacuated and isolated, a gas sample was obtained in the gas bomb connected to the system. The gas bomb was evacuated and purged with the reaction

products at least three times before a gas sample was taken. All of the gas used for purging the sample bomb was passed through the vacuum trap. The sample bomb was then filled to a pressure of 30 psig and removed from the system.

Next, the contents of the product receiver were slowly passed through the vacuum trap. A needle valve was used to regulate the flow rate and to maintain a small positive pressure (2-4 psig) on the vacuum trap during the collection of condensable products. After the product receivers had been evacuated, the vacuum trap was removed from the system. The condensable products were weighed and were retained in sample bottles for analysis at a later time.

For the experimental runs made in the 200,000 psi reaction system, the reaction mixture was delivered to the 200,000 psi compression cylinder and to the reactor from the high pressure accumulator until the pressure was equalized in this system. This addition of feed gas was done slowly to avoid ignition of the reactants. The compression cylinder inlet valve was then closed and the discharge flow of the hydraulic pump (30,000 psi) was aligned to pump hydraulic oil directly to the 200,000 psi compression cylinder. The hydraulic pump was started and the reactor pressure was increased to 23,000 psi. At this time the inlet valve to the low-pressure cylinder of the intensifier was opened to switch the pump discharge flow to the low pressure cylinder of the intensifier. Observation of the piston indicator indicated

the position of the intensifier piston. At the end of the pressure stroke of the intensifier, the inlet valve to the low pressure cylinder of the intensifier was closed and the discharge valve was opened in order to pump hydraulic oil into the high pressure cylinder of the intensifier. After reversing the intensifier the operating procedure for the intensifier was repeated until the desired reactor pressure was obtained, or until the feed mixture in the compression cylinder had been displaced. In the latter case the depletion of feed mixture in the compression cylinder was determined by the volume of hydraulic oil added to the compression cylinder (approximately 550 ml.). Then the reactor block valve was closed and the compression cylinder vent valve was opened to reverse the free piston in order to return the hydraulic oil to the oil reservoir. After reversal of the piston in the compression cylinder, the compression cylinder inlet valve was opened to add more feed mixture from the high pressure accumulator. After equalization of the pressure in the two vessels, the compression cylinder inlet valve was closed. The pressure generation cycle was repeated until the pressure in the compression cylinder (determined by the pressure guage on the low pressure cylinder of the intensifier) exceeded the pressure in the reactor. The reactor inlet valve was then opened, and the pressure generation was continued until the desired reactor pressure was obtained.

In the above procedure it was not necessary to stop the hydraulic pump since the pump would stall-out when the

force on the large piston (air-driven) was equalized by the force on the small piston. The air pressure on the large piston was set for a maximum oil discharge pressure of 23,000 psi since this pressure was the maximum pressure recommended by Autoclave Engineers, Inc. to be applied to the low pressure cylinder of the intensifier to avoid deformation of the intensifier piston. To prevent the possibility of damaging the intensifier, the air pressure to the liquid pump was set to generate a maximum pressure of 23,000 psi and was not changed.

After the desired reactor pressure had been obtained, the reactor inlet valve was closed and the liquid pump was shutdown. The Bristol recording potentiometer was started, and the current to the internal furnace in the reactor was adjusted to approximately 7 amps. Once the reactor temperature reached the desired level, the current to the electric furnace was manually adjusted to maintain that temperature. As soon as a maximum temperature was observed, or after 120 minutes at the desired temperature, whichever came first, the reactor contents were expanded into the product receiver. The remaining portion of the procedure was identical to that presented for the lower pressure system.

Difficulties Encountered

In addition to the usual problems associated with high pressure studies, there were several problems encountered in this investigation which deserve some discussion.

The first difficulty encountered was the collection of the condensable products of the oxidation reaction. A crude liquid-vapor separator installed between the product cooler and product receiver was the first method attempted; however, only a small quantity of the liquid was collected in the separator. A system was then installed which would permit the collection of the condensable products by freezing. This system improved the situation considerably; however, several preliminary runs were required to develop the procedure presented in the preceding section. It was found that the final stages of the evacuation of the product receivers had to be conducted through the bottom of the product receivers.

Another problem encountered in the early phase of this study was that of determining a procedure to charge the 25,000 psi reactor. It was previously stated in this chapter that the maximum rate of pressure increase during the filling of the reactor was approximately 1,500 psi per minute to avoid ignition of the methane-oxygen mixture during charging. Several preliminary runs were required to establish this approximate rate. Inspection of the thermocouple wires revealed that the insulation of the thermocouple wires was discolored at the bottom of the reactor, which suggested that the ignition commenced at the bottom of the reactor during the compression of the feed mixture in the reactor.

The first major problem encountered in the 200,000 psi reaction system was the "shorting-out" of the electrode

introduced through the cover of the reactor when the reactor pressure was greater than 38,000 psi. By reducing the electrode seal area, and thus increasing the air gap between the electrode and the end-plug, this problem was remedied.

The original packing on the piston in the high pressure cylinder of the intensifier was found to be inadequate at pressures greater than 100,000 psi. Increasing the thickness of the leather packing* from 1/16-inch to 1/8-inch prevented further failure of this seal.

At pressures greater than 150,000 psi, it was observed that there was considerable disagreement between the reactor pressure as determined from the pressure gauge on the low pressure cylinder of the intensifier and that determined by the manganin pressure guage directly connected to the reactor. With a pressure of 22,000 psi on the low pressure cylinder of the intensifier the pressure in the reactor as obtained directly from the manganin gauge was approximately 170,000, rather than the 220,000 psi which would have been expected from a 10:1 intensifier ratio. This difference of 50,000 psi indicated an unexpected pressure drop in the system which could only be attributed to the viscosity of the hydraulic oil, Plexol 201, at pressures greater than 150,000 psi. For this reason the hydraulic oil was diluted with petroleum ether (boiling range--30° to 75°C). By using this mixture as the

---

*In this connection, army boot leather is superior to the usual commercial leathers (84).

pressure transmitting medium the pressure losses were decreased to approximately 5 per cent at 200,000 psi.

Another problem was the short life of the O-rings used to seal the free piston in the 200,000 psi compression cylinder. Inspection of the O-rings after failure indicated that the failure was caused by the extrusion of the O-ring. Installation of double spiral Teflon back-up rings would have been desirable; however, the width of the O-ring grooves in the piston would have had to be increased to accommodate these back-up rings. Installation of the single back-up rings extended the life of the O-rings. Inspection of the O-rings after completion of this study indicated that the single spiral back-up rings were only a partial solution; double rings would extend the life of the O-rings.

Although no difficulties were encountered with the valves during operation of the 200,000 psi system, another potential problem was discovered after dismantling the system for inspection at the conclusion of this investigation. It was observed that the stem of the reactor inlet valve was slightly distorted. A similar problem was encountered by Yoder (84). In the design of valves for future high pressure applications, modifications in the design or in the material used in the valve stem should be considered.

CHAPTER VII

ANALYTICAL PROCEDURE AND EQUIPMENT

The variety of reaction products from the partial oxidation of methane at high pressures increased the analytical problems tremendously. In addition to the reported products of carbon monoxide, carbon dioxide, water, formaldehyde, methanol, and formic acid, methyl formate and traces of an unidentified product were also detected in the reaction products. Quantitative analysis of the gas products by vapor phase chromatography gave satisfactory results; however, the analysis of the liquid products by gas chromatography failed to give satisfactory quantitative results for formaldehyde and formic acid. Quantitative determination of the formaldehyde and formic acid was accomplished by volumetric analyses.

Description of Chromatograph Equipment

The vapor phase chromatograph used in this research was built from the components of a unit previously described by Skinner (66). A photograph of the chromatograph apparatus as installed for the present investigation is shown in Figure 19. Since gas chromatography is a well-established analytical tool, the principles of chromatographic analysis are not

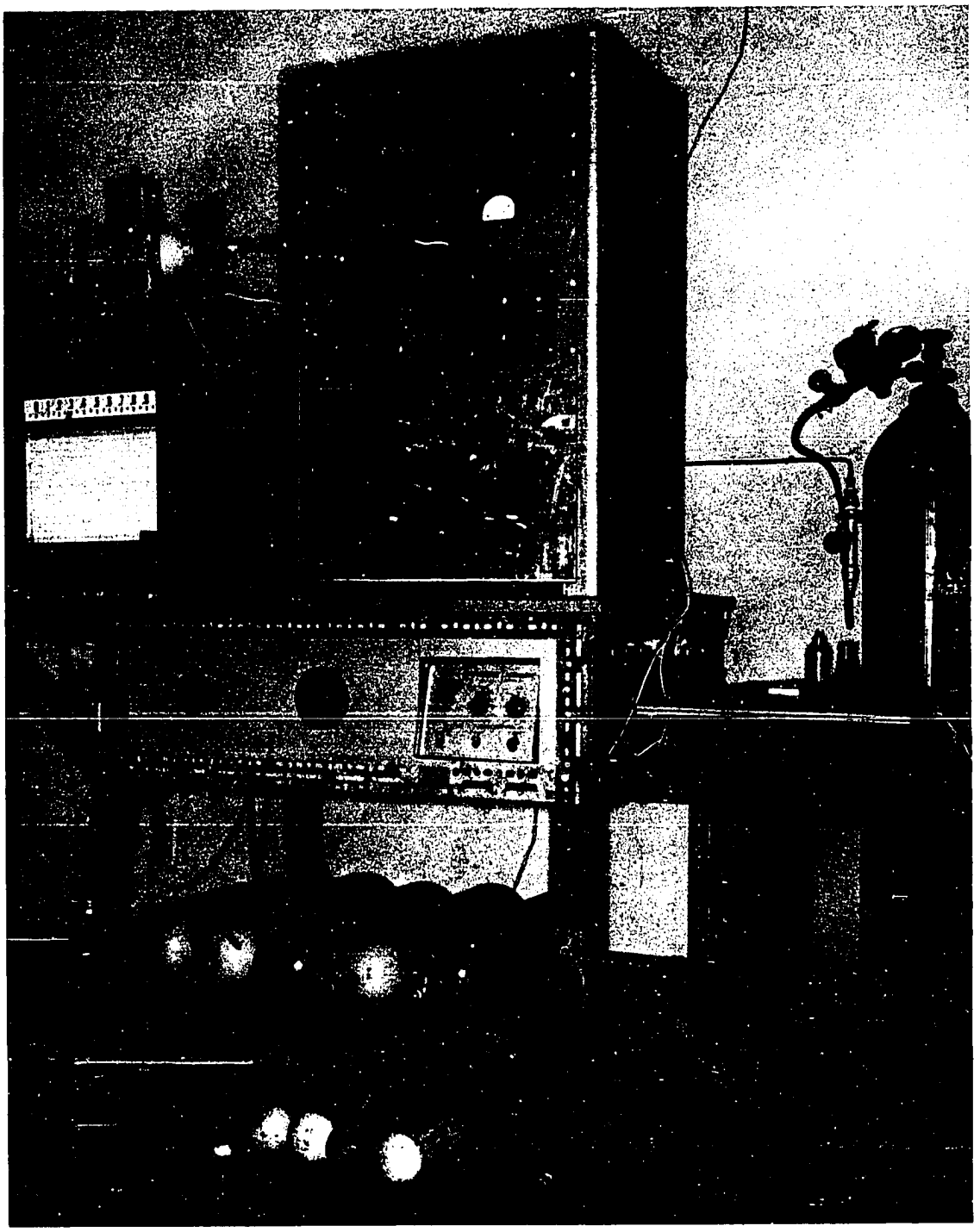

Figure 19. Chromatograph

presented and only a brief description of the equipment is presented. For additional information on gas chromatography the reader is referred to the works of Knox (32) and Purnell (60).

Instrument grade helium (99.99 per cent minimum purity), supplied in a standard 1A gas cylinder, was used as the carrier gas for the chromatograph analysis. A two-stage pressure regulator was used to maintain a constant upstream helium pressure at a Hoke, 20-turn, metering valve. A dryer using 5A molecular sieves (60/80 mesh) as the desiccant was installed just after the metering valve. The metering valve was used to regulate the helium flow rate which was measured by two methods: (1) a soap bubble flow meter and (2) a capillary differential flow meter. In the first method, the helium flow rate was determined by measuring the time required for a soap bubble or film to rise from the bottom to the top of a 50 ml burette. It is reported that an accuracy of 0.1 per cent can be obtained with a soap bubble flow meter (60). Although the capillary differential flow meter did not give an absolute flow rate, observation of the manometer indicated any changes in the flow rate.

Three columns packed with different materials were required to analyze the products of the oxidation reaction; two of these columns were required to analyze the gas products. The column used to separate hydrogen, oxygen, nitrogen, methane, and carbon monoxide was prepared by packing an 8-ft.

length of standard 1/4-inch copper tubing with 5A molecular sieves (60/80 mesh). The carbon dioxide content was determined with an 8-ft. length of standard 1/4-inch aluminum tubing packed with 180/200 mesh silica gel (4.2 grams per foot). Separation of the methanol, methyl formate, and water was accomplished with a column prepared by packing a 10-ft. length of standard 1/4-inch copper tubing with 30 per cent diglycerol on 80/100 mesh Chromosorb w.

The carrier gas preheater, packed column, and thermal conductivity cell were located in an air bath 12 inches high by 12 inches long by 7½ inches deep. To insure a minimum temperature gradient within the air bath, two, 2400 rpm fans were installed; one was located high on a side and the other was located low on an end. To minimize radiation effects from the electrical heaters, a 0.040-inch thick aluminum sheet was placed over the two electrical heaters. Approximately one-half of the output from the fan on the low end of the housing was directed beneath the aluminum sheet and across the heaters to decrease the lag time of the thermistor sensing probe. The air bath temperature was controlled by a Sargent Model T "Thermonitor" which provided power to a pair of heaters of 250 and 300 watt output. This on-off temperature controller uses a thermistor sensing element. A check on the temperature control of the air bath indicated that the air bath temperature could be controlled within ±0.4°F at 210°F, which approaches the capability of the temperature controller.

The chromatograph detector was a commercial Gow-Mac hot-wire thermal conductivity cell. This cell contained two pairs of matched tungsten filaments; one filament of each pair was mounted in the carrier gas and column effluent channels of a brass body. The potential unbalance in the Wheatstone bridge caused by the dilution of the helium carrier gas with the eluted components from the packed column was recorded by a Bristol Dynamaster d.c. millivolt instrument, Model 1PH560-51-T46-T88X. The recorder range was -0.05 to 1.00 millivolts; however, a shunt cell provided means of converting the output signal from the bridge of the detector into an acceptable input signal to the recorder.

Since oxygen and nitrogen were two of the constituents of the gas to be analyzed, the gas injection system was designed to eliminate contamination of the gas sample with air. This restriction immediately ruled out the use of a hypodermic syringe as the means of sample injection. The gas sampling system consisted of a sample tube, a carrier gas by-pass loop, and a vacuum pump connected by three, 3-way valves. With this arrangement the gas sample from the gas sample bomb could be injected into the stream of carrier gas with a minimum interruption of gas flow and without contaminating the sample with air.

Liquid injection was accomplished with a 10-microliter syringe with 0.1 microliter graduations. The liquid sample was injected into the helium carrier gas by inserting the

needle of the syringe through a rubber septum located in a standard 1/4-inch tubing tee. To insure instantaneous vaporization of the liquid sample, the carrier gas was heated to a temperature approximately 20°C hotter than the column temperature. This vaporizer was constructed from standard 1/4-inch copper tubing, 12 feet long, coiled around a cartridge heater well. The void spaces between the coil and heater well were filled with a heat transfer medium (Thermon "T-3") and the unit was then insulated with standard pipe insulation. The power input to the 375-watt Chromalox cartridge heater was manually controlled by a Variac variable transformer. Two iron-constantan thermocouples were embedded in the vaporizer, and a Leeds and Northrup potentiometer was used to measure the temperature of the vaporizer.

Operation and Calibration of the Chromatograph

For each of the three packed columns used to analyze the reactants and products of the oxidation reaction, operating conditions were established. The operating conditions for the three analyses were:

	Column Material		
	5A Mol. Sieves	Silica Gel	Diglycerol
Helium Flow Rate (ml/min)	90	60	110
Air Bath Temperature (°C)	33	80	120
Cell Current (milliamps)	150	150	150
Regulator Pressure (psig)	20	34	20

With the operating conditions established for the column packed with 5A molecular sieves, the average retention times for oxygen, nitrogen, methane, and carbon monoxide were 1.7, 2.7, 5.2, and 8.6 minutes, respectively. Ten minutes were required to complete the analysis. For the column packed with silica gel, the average retention times for methane (and other gases present) and carbon dioxide were 2.4 and 7.8 minutes, respectively. The time required for this analysis was also 10 minutes. For the column packed with 30 weight per cent diglycerol on Chromosorb w, the average retention times were 0.8, 1.5, and 5.75 minutes for the methyl formate, methyl alcohol, and water, respectively. However, the required time for an analysis was approximately 12 minutes because of the tailing tendency of water, i.e., the water peak had a sharp, leading edge and a long, drawn-out trailing edge.

Since different columns and operating conditions were required, several samples were accumulated before the chromatograph was put into operation. For the gas analyses the silica gel column was installed first in the air bath, and the system was allowed to reach steady-state conditions. A gas sample bomb was connected to the sampling system. The carrier gas flow was passed through the by-pass loop by switching the three valves. Evacuation and purging of the sample tube with gas sample was done at least three times to assure the elimination of air in the sampling system. The

valves were then switched to direct the helium carrier gas through the sample tube, which thus completed the injection of the gas sample. At least three analyses were made before another gas sample bomb was connected to the system for analysis, and the procedure was repeated. After analyzing the accumulated gas samples for carbon dioxide, the chromatograph was shut down. The column packed with silica gel was replaced by a column packed with 5A molecular sieves to analyze the gas samples for oxygen, nitrogen, methane, and carbon monoxide. The chromatograph was again allowed to reach steady-state conditions and the procedure was again repeated to complete the gas analysis.

Calibration of the chromatograph for gas analysis was accomplished by analyzing thirteen mixtures of known composition. The gas standards were prepared from Coleman grade carbon dioxide (99.99 per cent minimum purity), C. P. grade carbon monoxide (99.5 per cent minimum purity), extra dry grade oxygen (99.5 per cent minimum purity), and instrument grade methane (99.05 per cent minimum purity). Briefly, the procedure for preparing these standards was to evacuate and purge the 500 cu. in. stainless steel cylinder with methane at least four times before adding the desired quantity of methane, which was determined by a manometer connected to the system. The cylinder valve was then closed. The remaining portion of the system was evacuated and purged at least four times with the next constituent to be added.

The cylinder valve was then opened, and the next component was added to the mixture. This procedure was continued until all the components of the standard mixture were added. For safety reasons, oxygen was always the last constituent to be added to the mixture.

The calibration curves determined upon analysis of the gas standards are presented in Figures 49, 50, and 51 of Appendix A. Each gas standard was initially analyzed several times to establish the calibration curves, and then periodically thereafter, to check the calibration curve.

Calibration of the chromatograph for liquid analyses was also accomplished by analyzing mixtures of known composition. Reagent grade absolute methanol, practical grade methyl formate and distilled water were used to prepare the standard solutions. An analytical balance was used to determine the quantity of each of the components in the standard solutions. Each liquid standard was initially analyzed several times to establish the calibration curve. These standards were checked at least twice each time liquid analyses were made. The calibration curves for methyl alcohol and methyl formate are given in Figures 52 and 53 of Appendix A.

An attempt was made to analyze formaldehyde and formic acid on the chromatograph, but the results were poor. The temperature required to elute formaldehyde from the column packed with 30 weight per cent diglycerol on Chromosorb w

in a reasonable length of time caused the diglycerol to vaporize and subsequently to collect in the cavity of the thermal conductivity cell and on the tungsten filaments. At lower temperatures the time required to elute the formaldehyde was approximately 40 minutes. The peak was so poor that a good quantitative analysis could not be made. Analysis of formic acid by chromatography was also rejected on the basis that a good quantitative analysis could not be obtained.

Volumetric Analysis

Since a satisfactory quantitative analysis for formaldehyde and formic acid could not be obtained with the available chromatograph, volumetric analyses were used to determine their concentrations. Romijn's iodimetric method (62) was used to determine the formaldehyde concentration and neutralization with sodium hydroxide was used to determine the concentration of formic acid. The formaldehyde determination was found to be unaffected by the presence of methyl alcohol, methyl formate, and formic acid (see Appendix B). The procedures for these volumetric analyses are well established and are presented in Appendix B.

CHAPTER VIII

DISCUSSION OF RESULTS

In this chapter the experimental results obtained in the two reaction systems, previously described, are presented in the form of graphs and tables. For the 25,000 psi reaction system the data are sufficient to present the effect of pressure and temperature on the residence time* and the product distribution for the oxidation of methane at high pressures. Sufficient data at 50,000 psi in the 200,000 psi reaction system were also obtained to show the effect of residence time on the product distribution. However, since the remaining data between 50,000 and 200,000 psi are limited, they are presented only in tabular form.

Data on the effect of pressure and temperature on the residence time and product distribution were obtained in the 25,000 psi system for the following range of variables:

	Range
Pressure, psi	2,000 - 15,000
Temperature, °F	552 - 644
Residence Time, minutes	0.25 - 140
Methane-Oxygen Ratio	10:1

*Residence time is defined on page 143

The experimental results are presented in Appendix D. Approximately 45 experimental runs, which were made to determine operating procedures, have been omitted. Sample calculations are shown in Appendix E.

The limited data obtained in the 200,000 psi system covered the following range of variables:

	Range
Pressure, psi	15,000 - 200,000
Temperature, °F	476 - 517
Residence Time, minutes	0.25 - 138
Methane-Oxygen Ratio	11.6:1

All of the experimental data taken in the 200,000 psi reaction system are presented in Appendix D and Table 5.

Earlier investigations at elevated pressures have shown that the maximum methanol yield occurs at the maximum temperature reached during the course of the reaction (45). In this investigation it was necessary to define three different residence times depending on the method of loading the reactor and the reaction system used:

1. For the 25,000 psi system the reactor was first brought to the desired operating temperature. It was then loaded directly from the storage vessel which was maintained at ambient temperature. Because of the large mass of the reactor itself, as compared to the reactants, the temperature in the reactor at the end of the pressurizing operation was within a few degrees of the initial temperature of the

empty reactor. The instant at which the reactor was brought to the desired operating pressure was taken as zero residence time. As reaction proceeded, the temperature rose, and the elapsed time to reach the maximum temperature, at which point the reaction was frozen by dumping the contents of the reactor, was taken as the residence time.

2. For the 200,000 psi system the empty reactor was first brought to the oil bath temperature of approximately 400°F. The reactor was then loaded from the compression cylinder, maintained at ambient temperature, until a pressure somewhat below the desired operating pressure was reached. The internal heater was then turned-on and the temperature of the reactants was increased to the desired level with a corresponding pressure rise.

   a. Between pressures of 15,000 and 50,000 psi the residence time was taken as the elapsed time between the instant the reactants reached the desired temperature level and the maximum temperature attained due to reaction, at which point the reaction was frozen by dumping.

   b. Above 50,000 psi no maximum temperature due to reaction was observed. Therefore, for these runs the residence time was taken simply as the time the reactants remained in the reactor at the desired operating temperature prior to dumping. During the "residence period" there were essentially no changes in pressure or temperature.

Figure 20 is based on the results of the investigation conducted in the 25,000 psi system along with the results reported by Newitt and Haffner (45). Runs JLL-158, -160, -162, and -164, although at four different pressures (2190, 2040, 1900, and 1800 psi, respectively), are seen to agree with the results of Newitt and Haffner. Curves No. 1 and 2, for 7000 psi, are of particular interest. Curve No. 1 was established early in this investigation whereas Curve No. 2 was obtained at a later date. The results for one pressure level were not obtained during one time period, i.e., the pressure level was altered at random to check reproducibility. After observing this shift in the reaction rate, Run JLL-232 was made at 5400 psi and 586°F to check the reproducibility of the 5400 psi curve at the longer residence times. It is seen that the results of this test agree with the data obtained at an earlier date. It was pointed out in Chapter III that various authors reported different shapes for the kinetic curves and different values for the energy of activation for methane oxidation at low pressures, probably due to the condition or nature of the vessel wall. The shift in the curves at 7000 psi is thus attributed to a change in the nature of the reactor wall even though the cause for the change in the wall condition cannot be explained. It is interesting to observe that the two curves coincide at higher temperatures, which would indicate that the reaction rate at higher temperatures is not affected by the surface of the vessel.

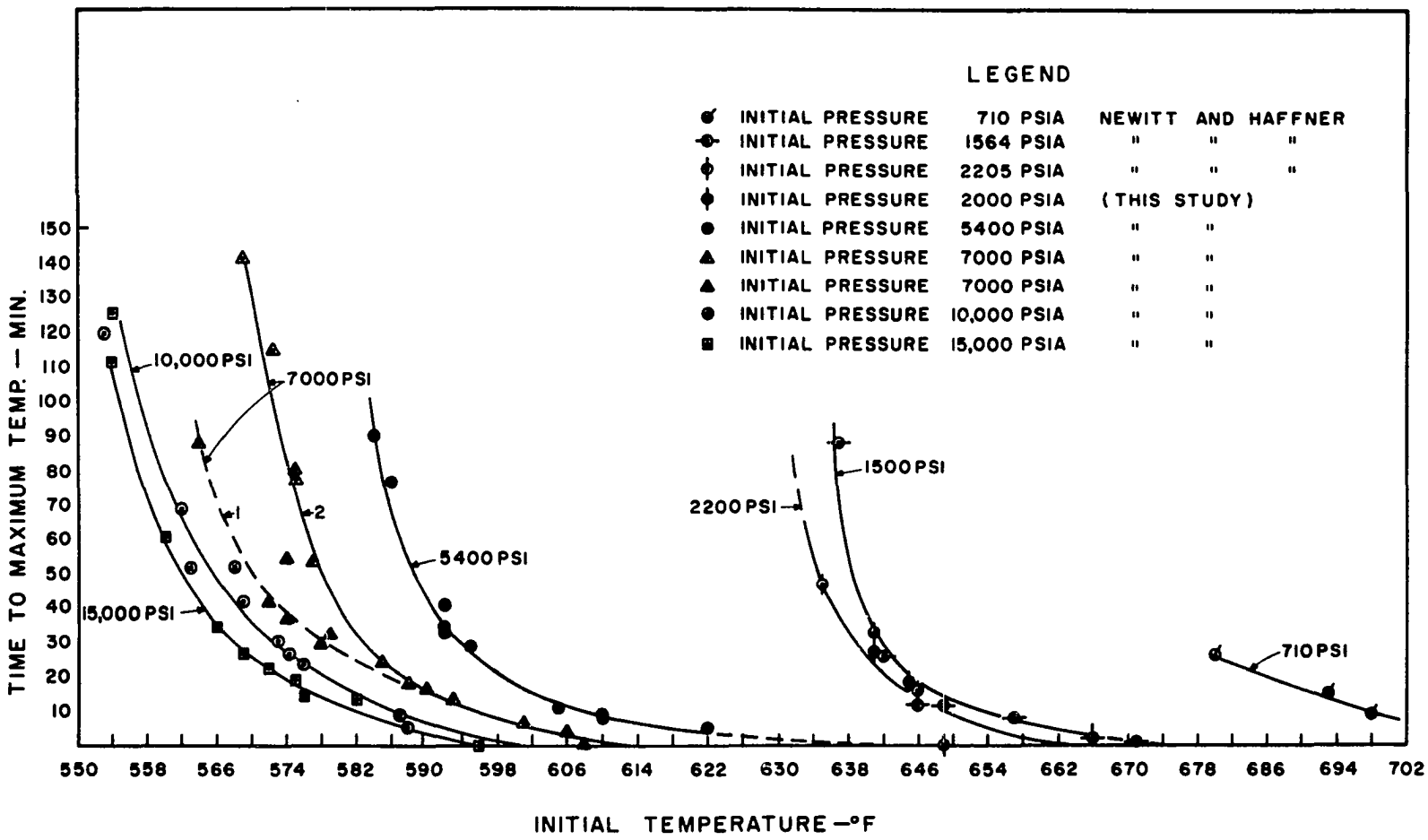

Figure 20. Effect of Temperature on Residence Time

It was possible to establish a temperature boundary between the slow oxidation and spontaneous ignition of methane by extrapolating the curves in Figure 20 to zero reaction time. Figure 21 is based on the results of this extrapolation.

The product distributions obtained for pressures of 5400, 7000, 10,000, 15,000, and 50,000 psi are presented in Figures 23 through 39. Figure 22 has been included to show the methanol distribution observed by Newitt and Haffner (45). At each pressure level investigated the product distribution has been presented in three ways: (1) the yield of the individual organic liquid products, (2) the total yield of organic liquid products, and (3) the carbon monoxide-carbon dioxide ratio. From these plots it is observed that the methanol and total organic liquid product yields apparently pass through a maximum at a temperature which gives a relatively short reaction time. Also an increase in pressure increases the yield of organic liquid products; however, the methyl alcohol yield increases slowly with an increase in pressure.

Newitt and Haffner (45) reported only traces of formic acid in the reaction products obtained at pressures up to 2200 psi, but the results of this investigation show that an increase in pressure above 2200 psi increases the yield of formic acid. Since both the alcohol and acid yields increase with pressure, it appears that the formic acid is formed by

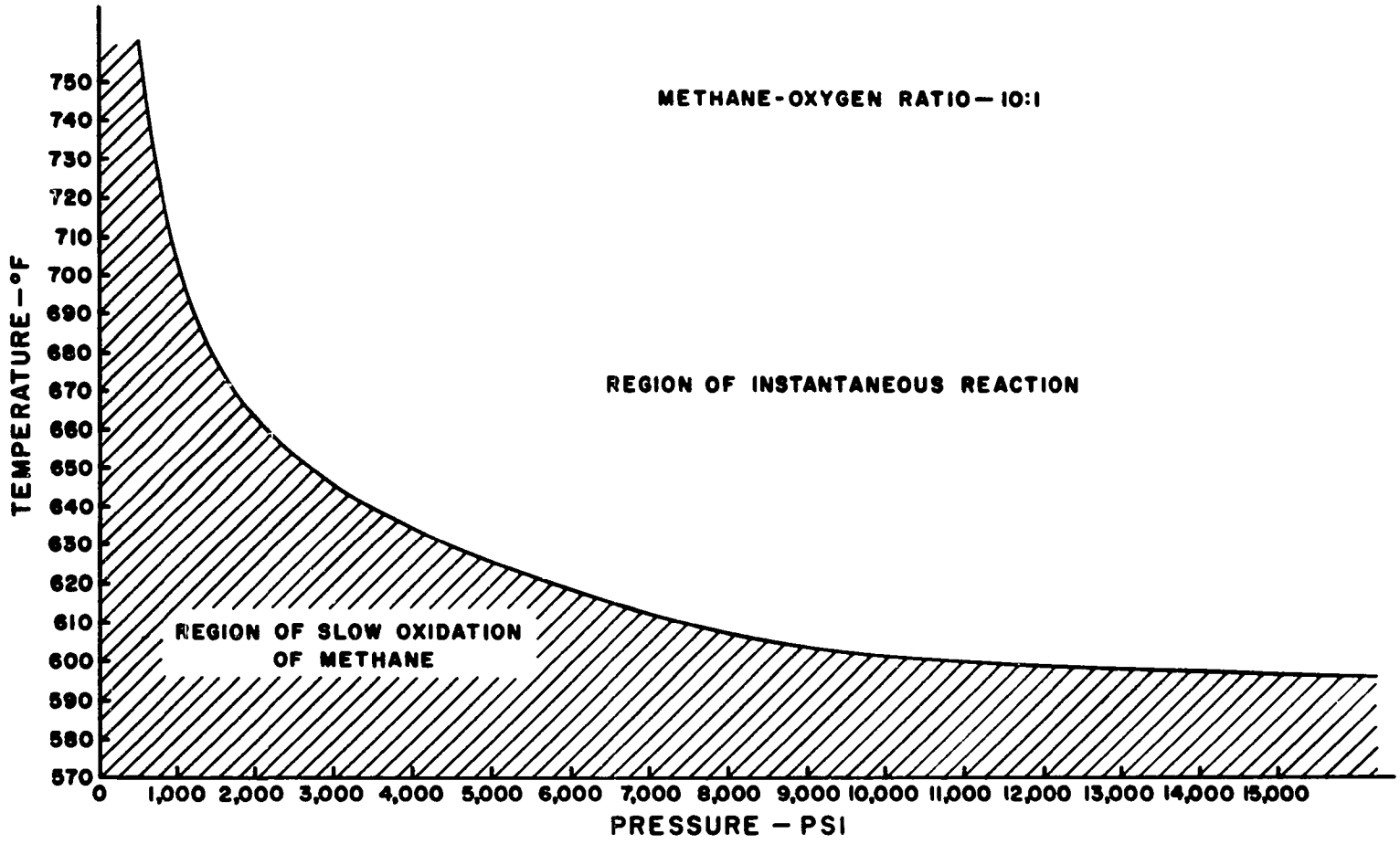

Figure 21. Observed Temperature Boundary Between Slow Oxidation Reactions and Instantaneous Reactions at High Pressures

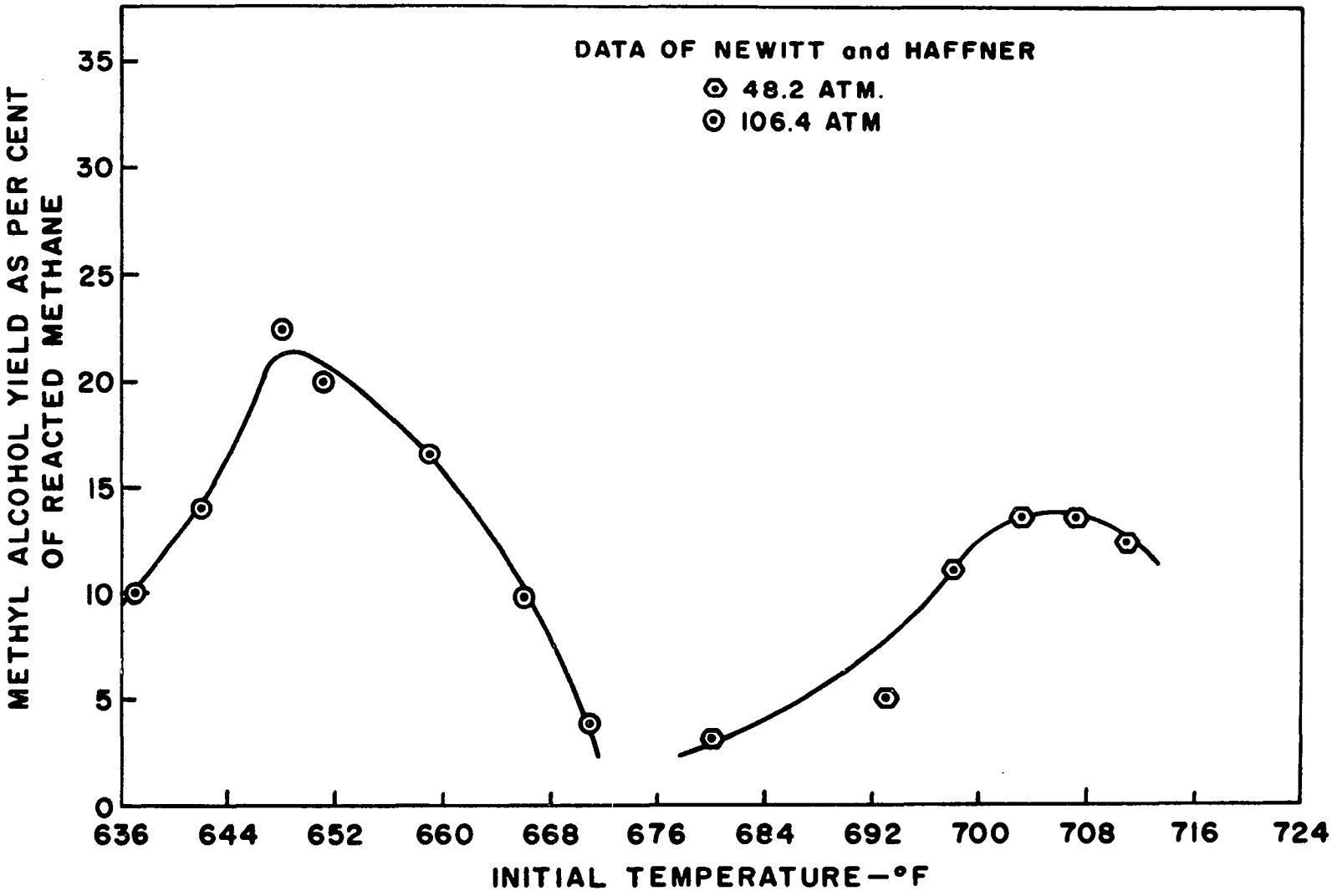

Figure 22. Effect of Temperature on Methanol Yield (Data of Newitt and Haffner)

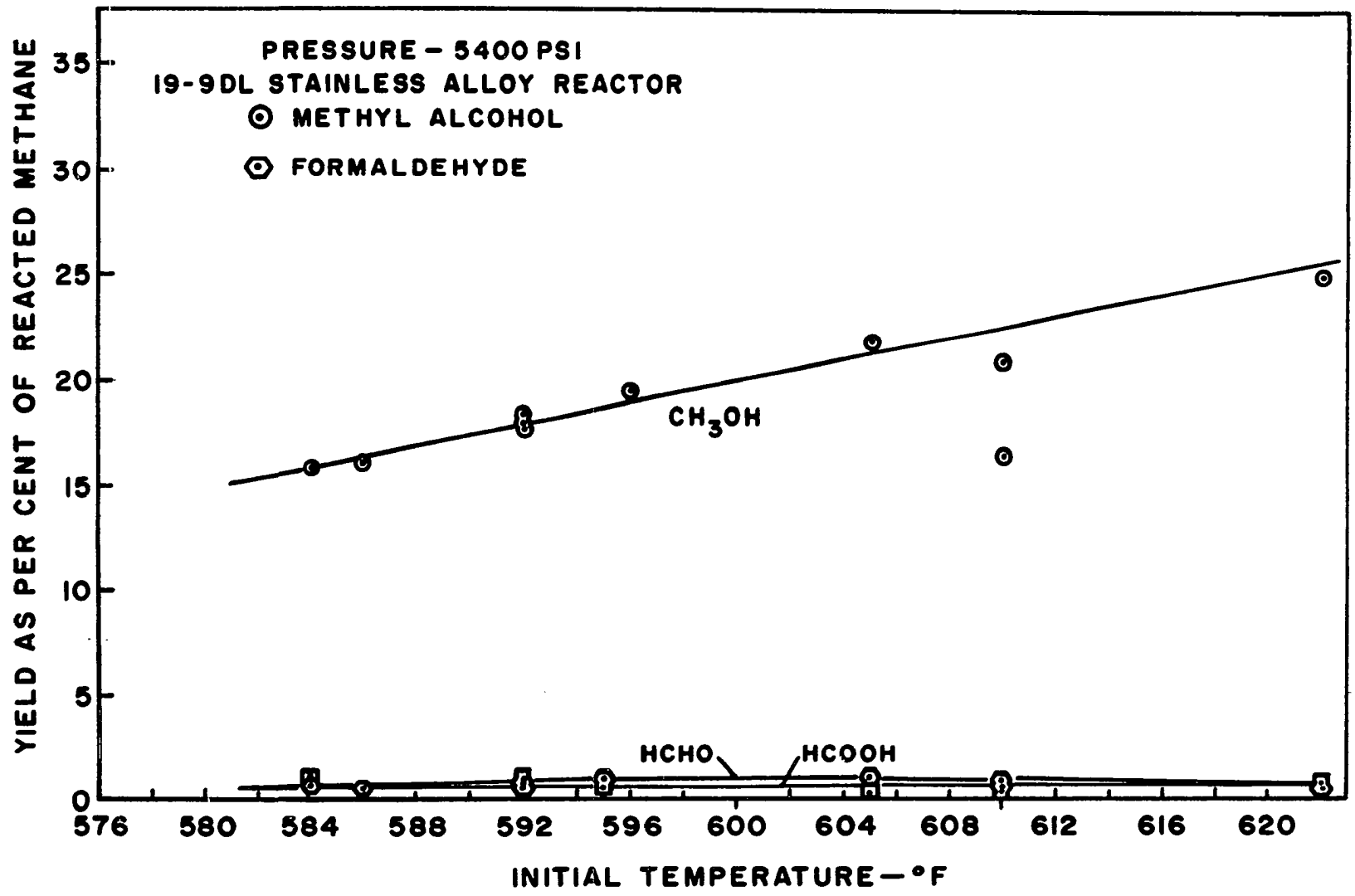

Figure 23. Effect of Temperature on Yield (5400 psi)

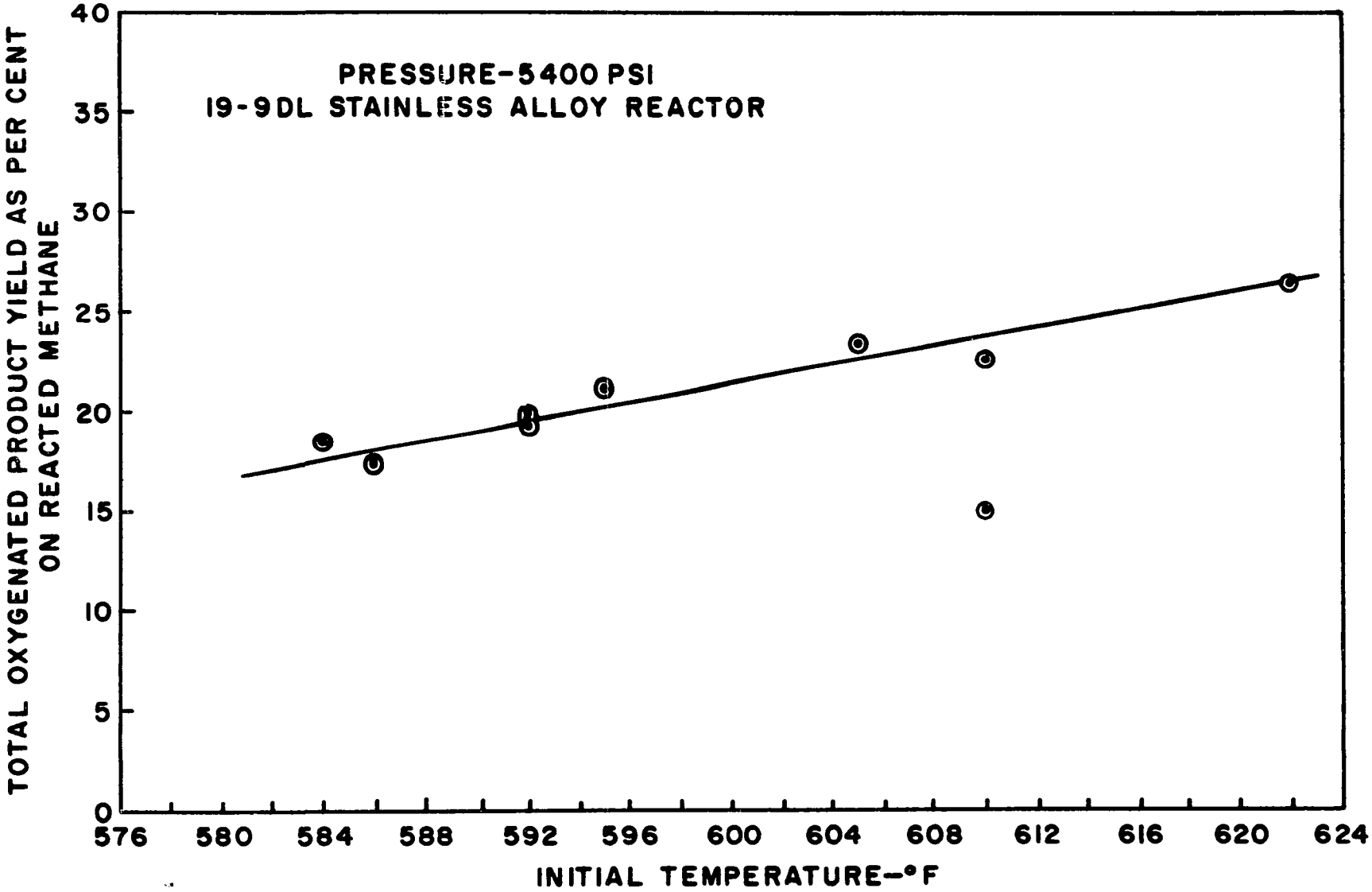

Figure 24. Effect of Temperature on Total Oxygenated Liquid Product Yield (5400 psi)

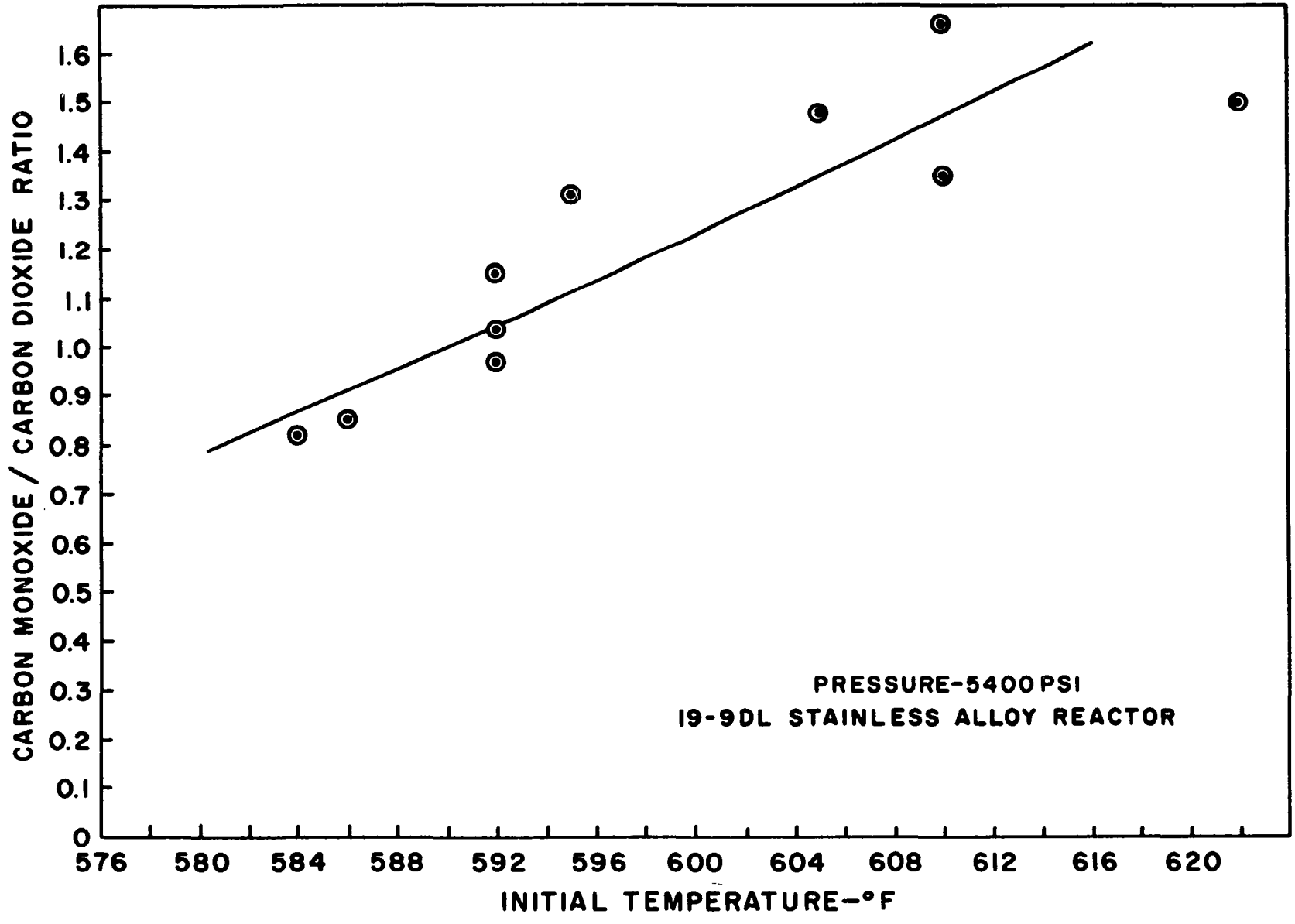

Figure 25. Effect of Temperature on Carbon Monoxide/Carbon Dioxide Ratio (5400 psi)

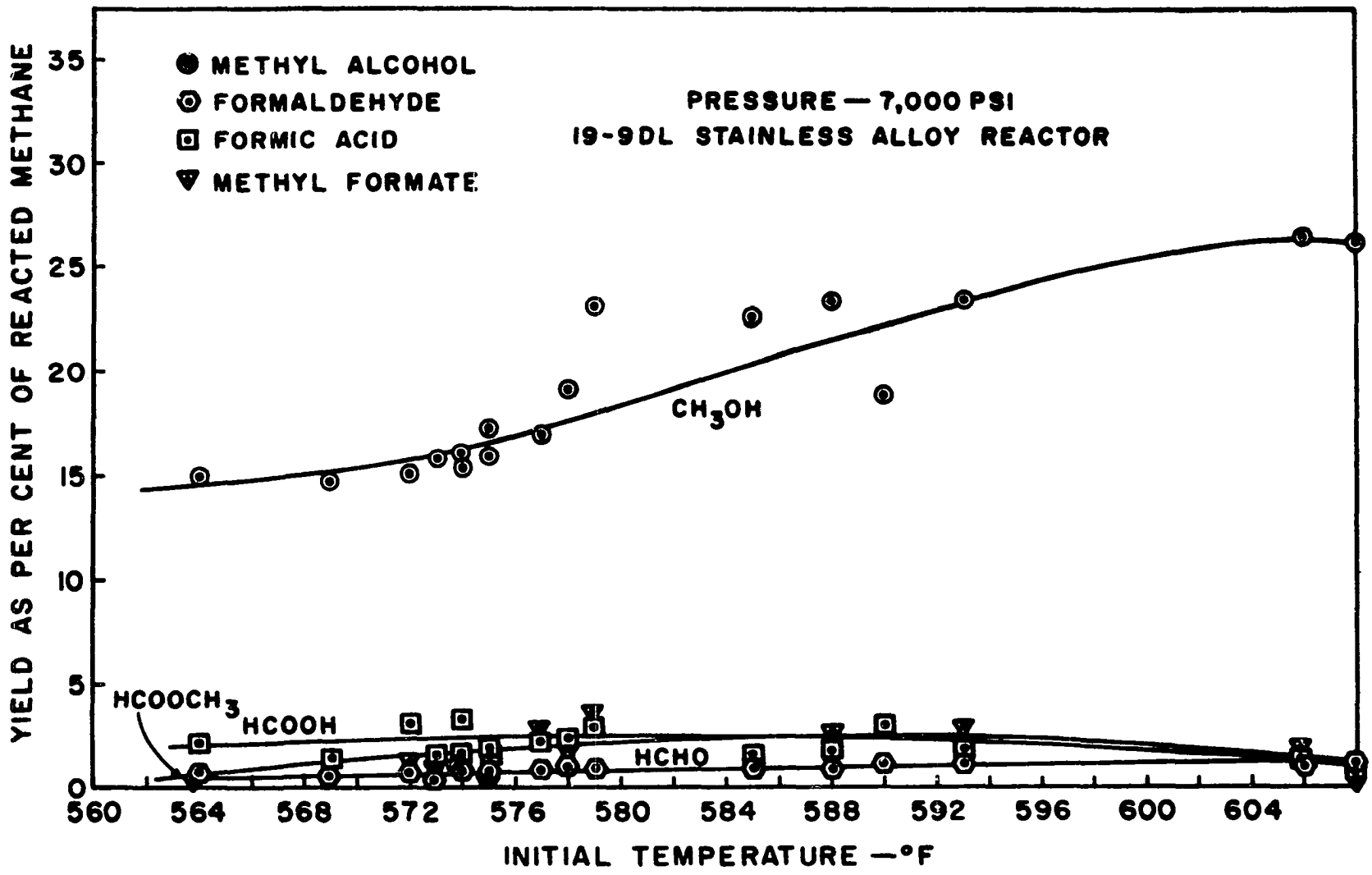

Figure 26. Effect of Temperature on Yield (7000 psi)

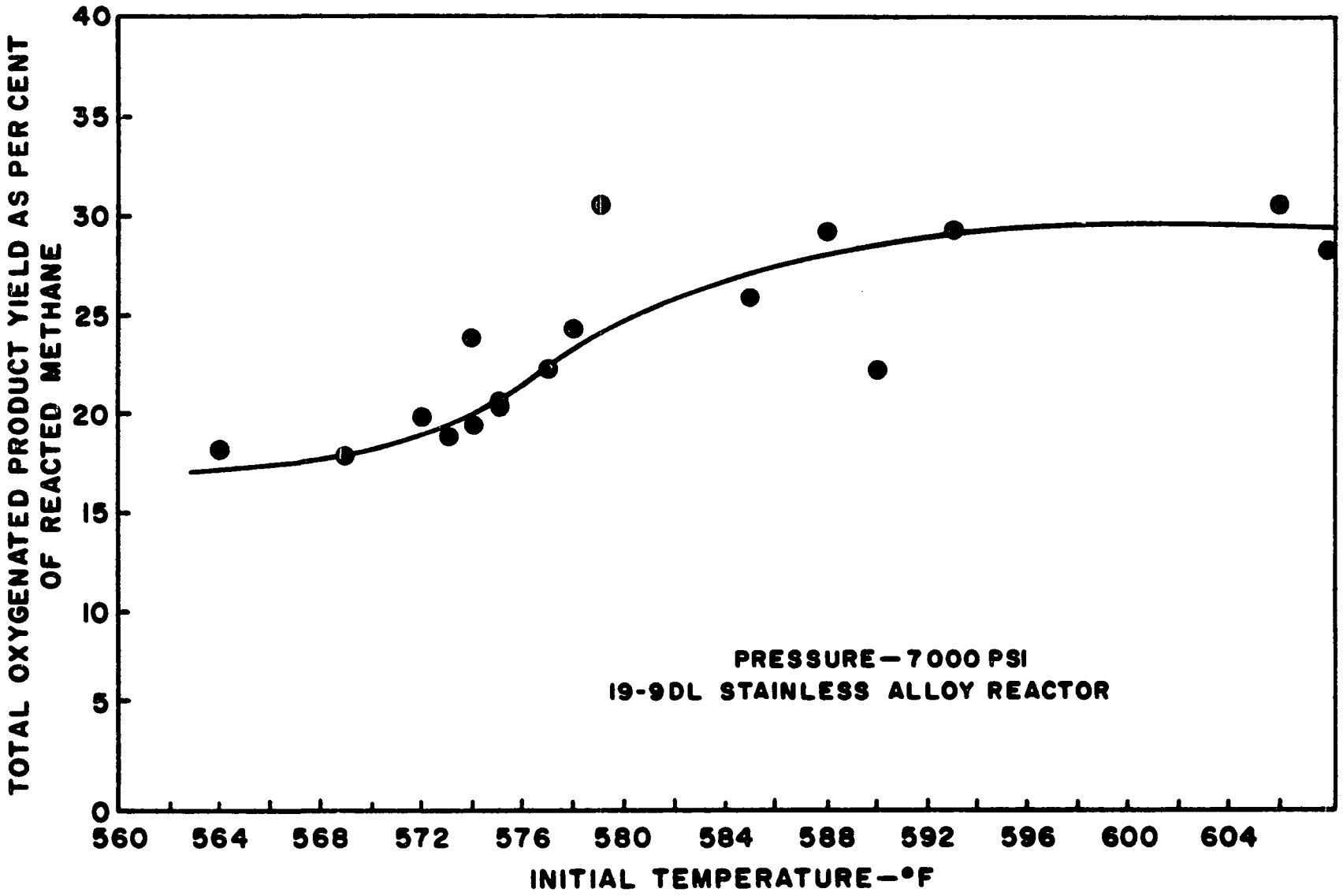

Figure 27. Effect of Temperature on Total Oxygenated Liquid Product Yield (7000 psi)

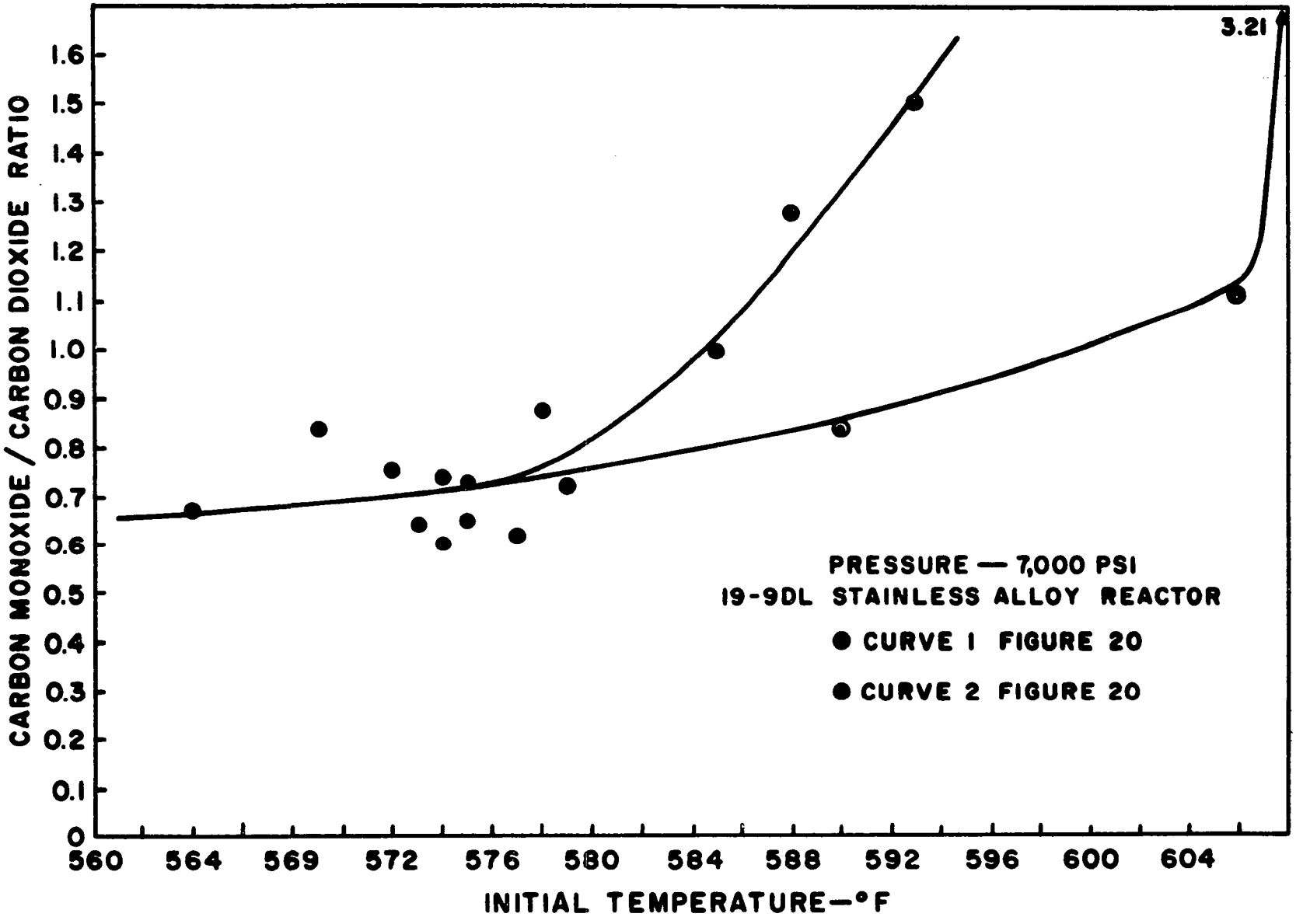

Figure 28. Effect of Temperature on Carbon Monoxide/Carbon Dioxide Ratio (7000 psi)

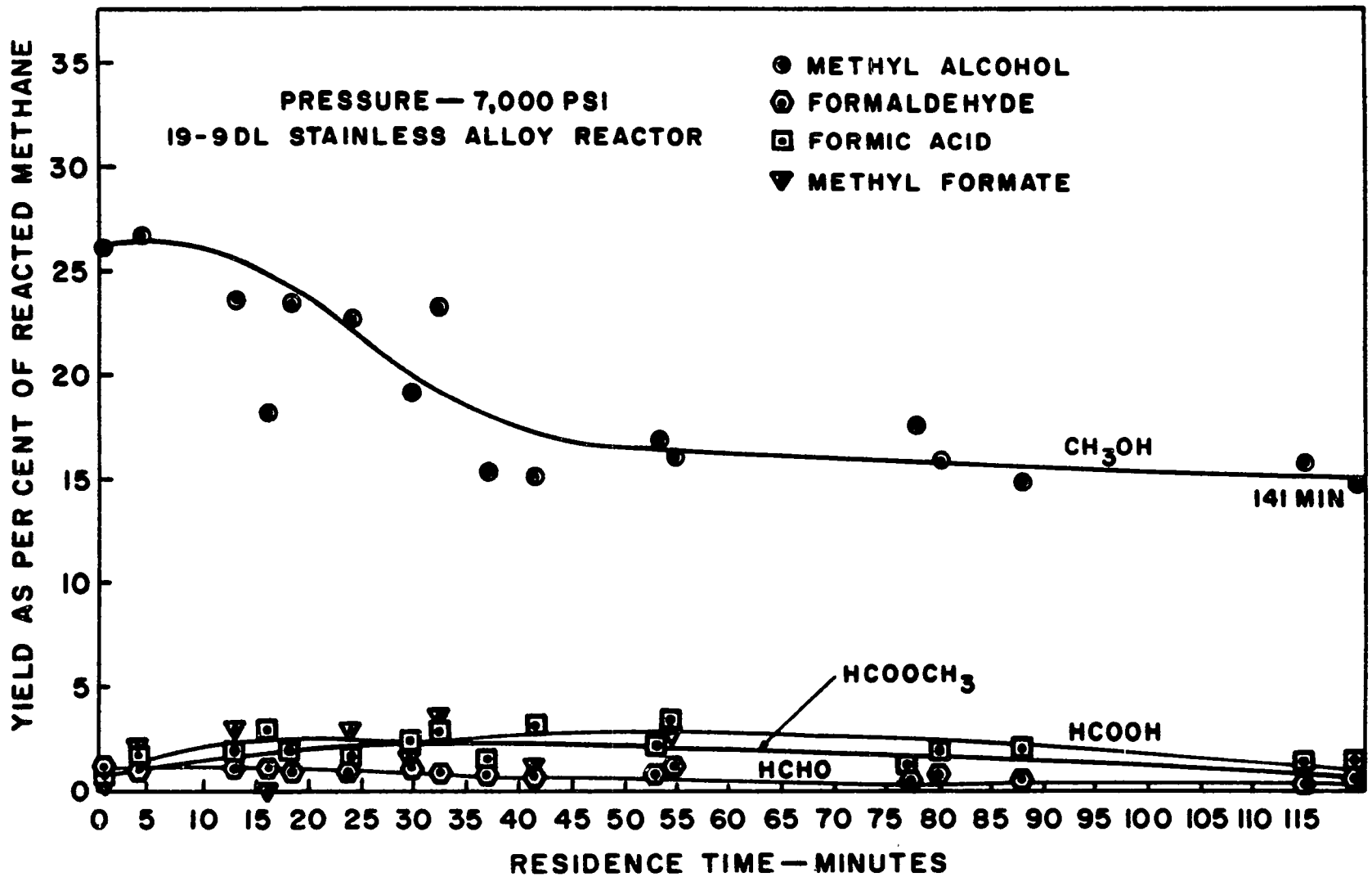

Figure 29. Effect of Residence Time on Methanol Yield (7000 psi)

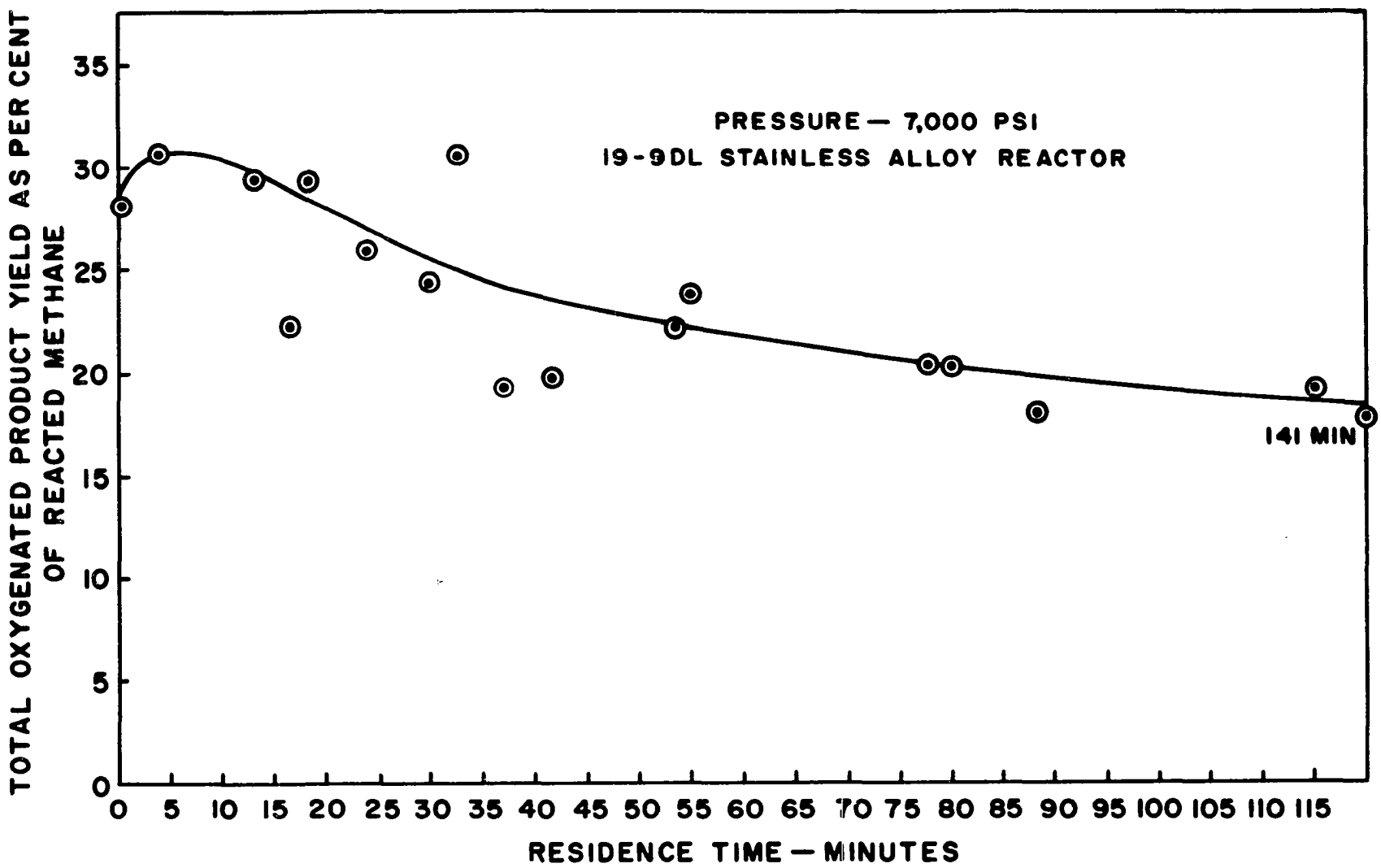

Figure 30. Effect of Residence Time on Total Oxygenated Liquid Product Yield (7000 psi)

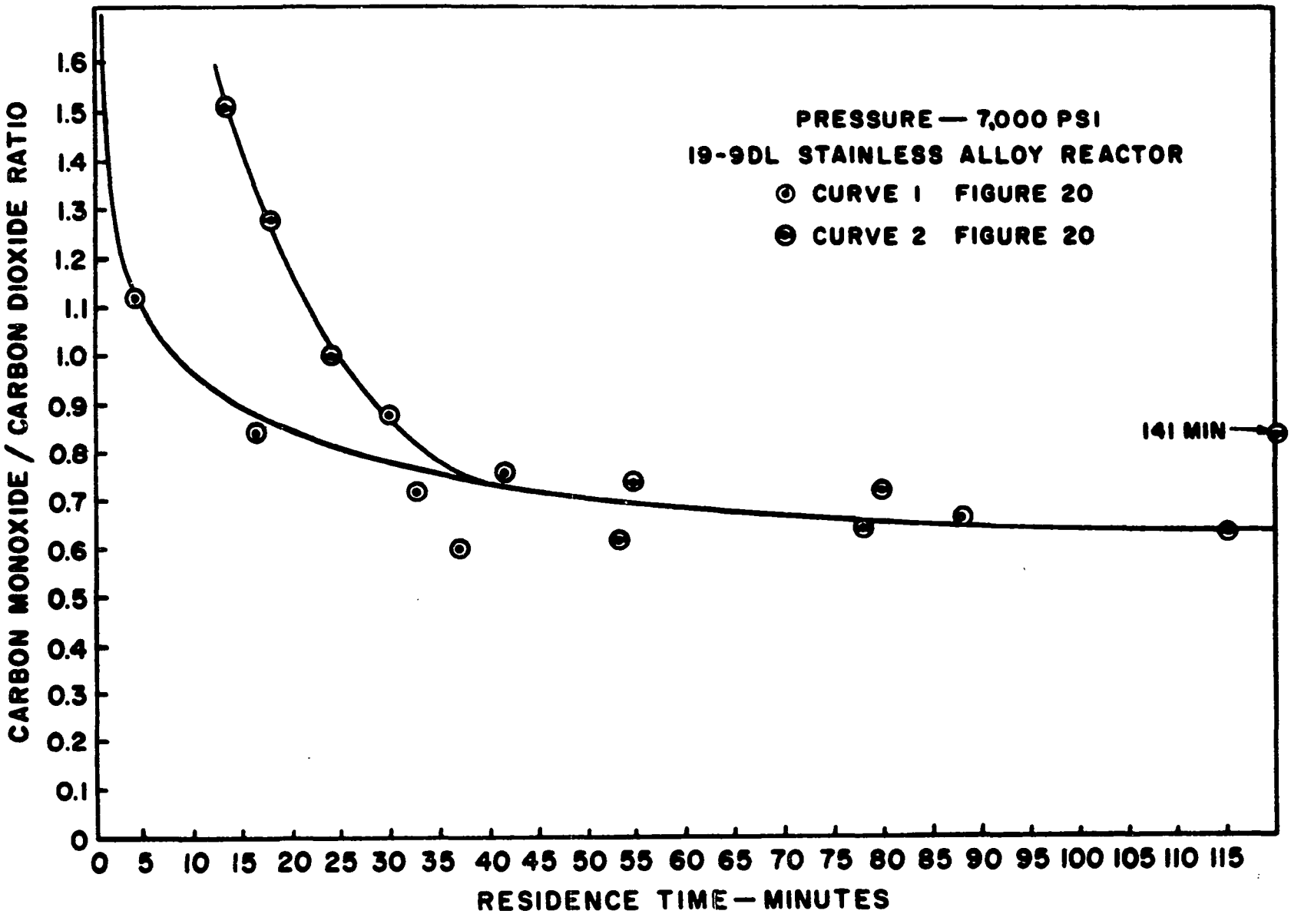

Figure 31. Effect of Residence Time on Carbon Monoxide/Carbon Dioxide Ratio (7000 psi)

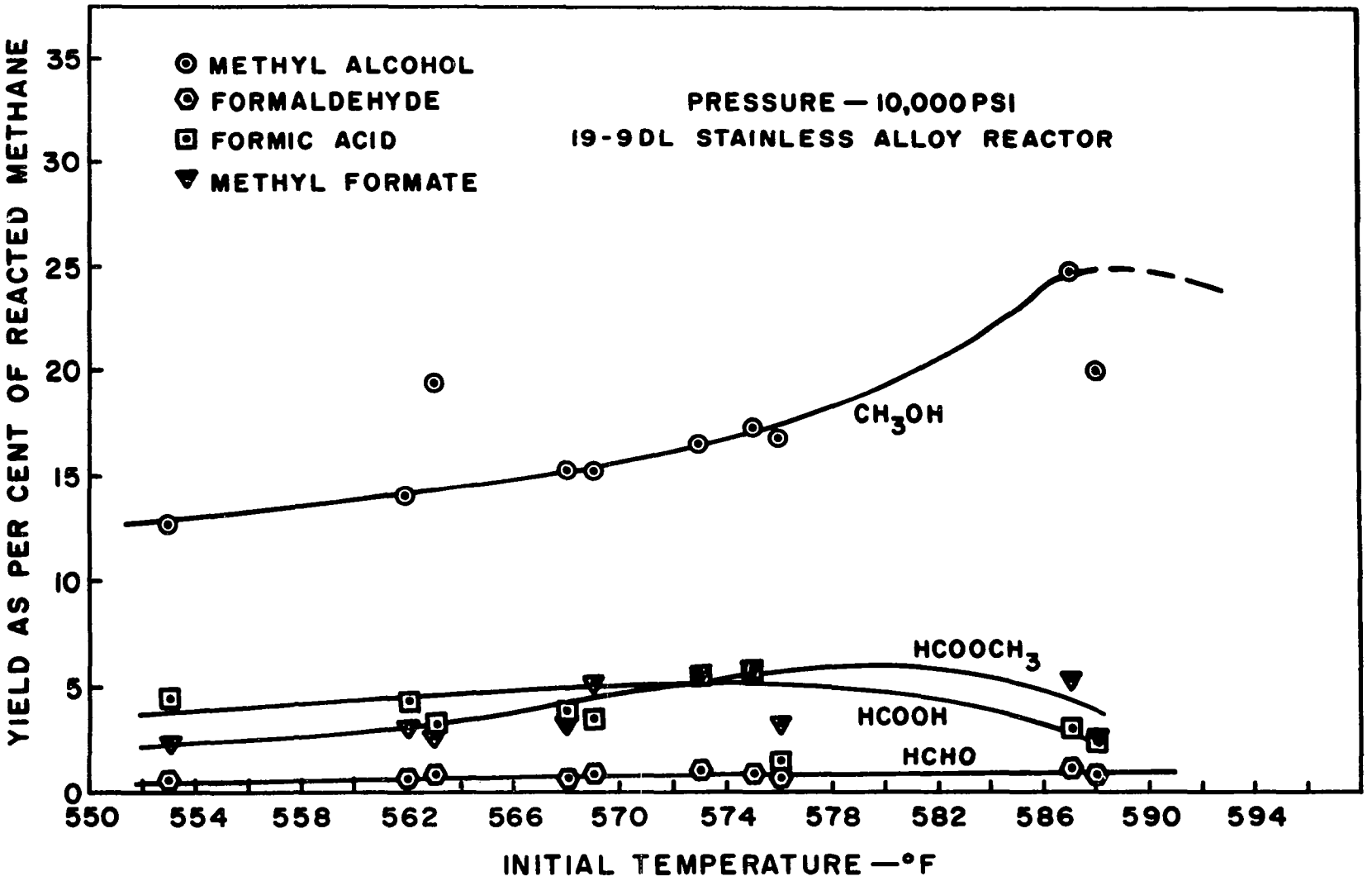

Figure 32. Effect of Temperature on Yield (10,000 psi)

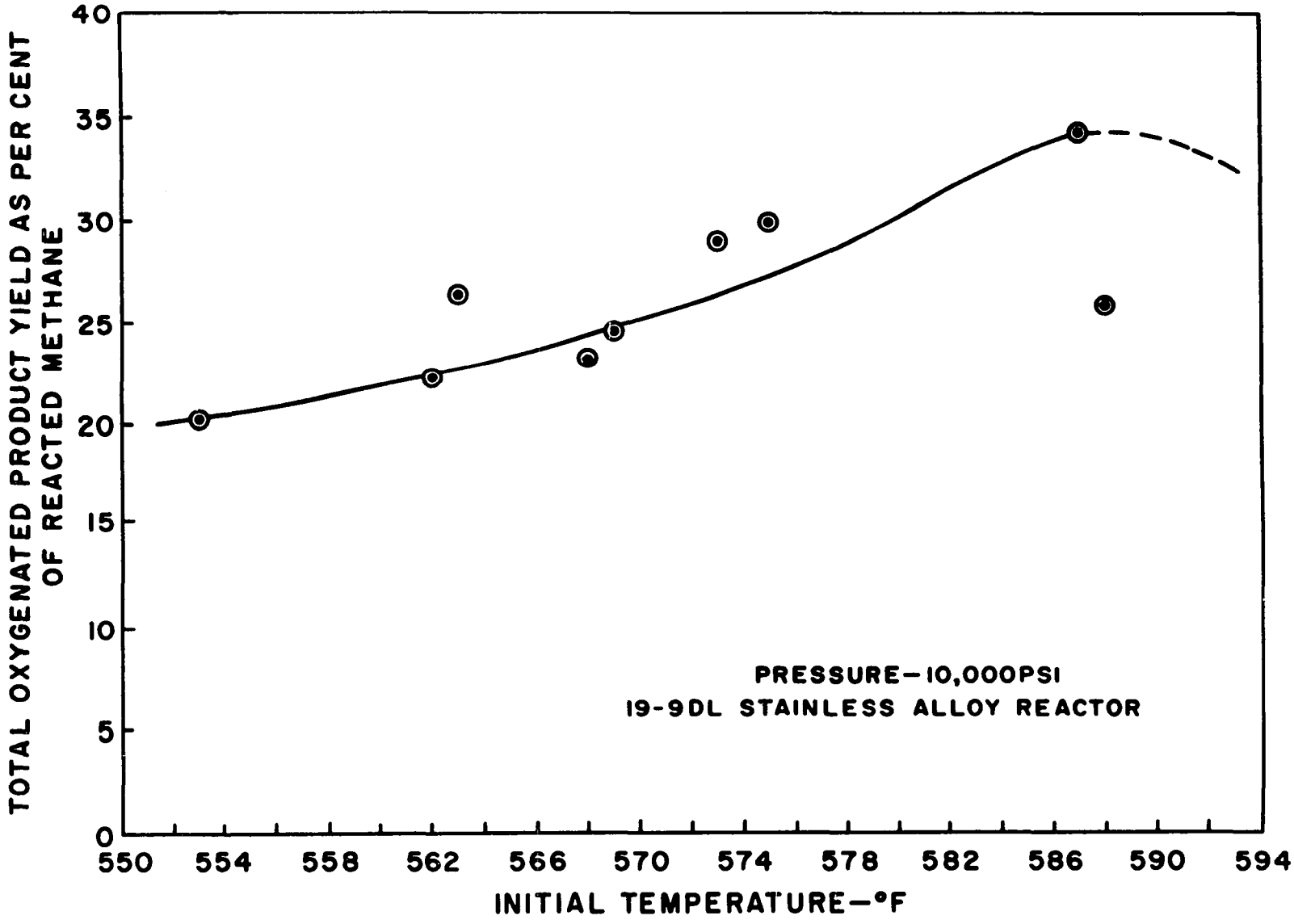

Figure 33. Effect of Temperature on Total Oxygenated Liquid Product Yield (10,000 psi)

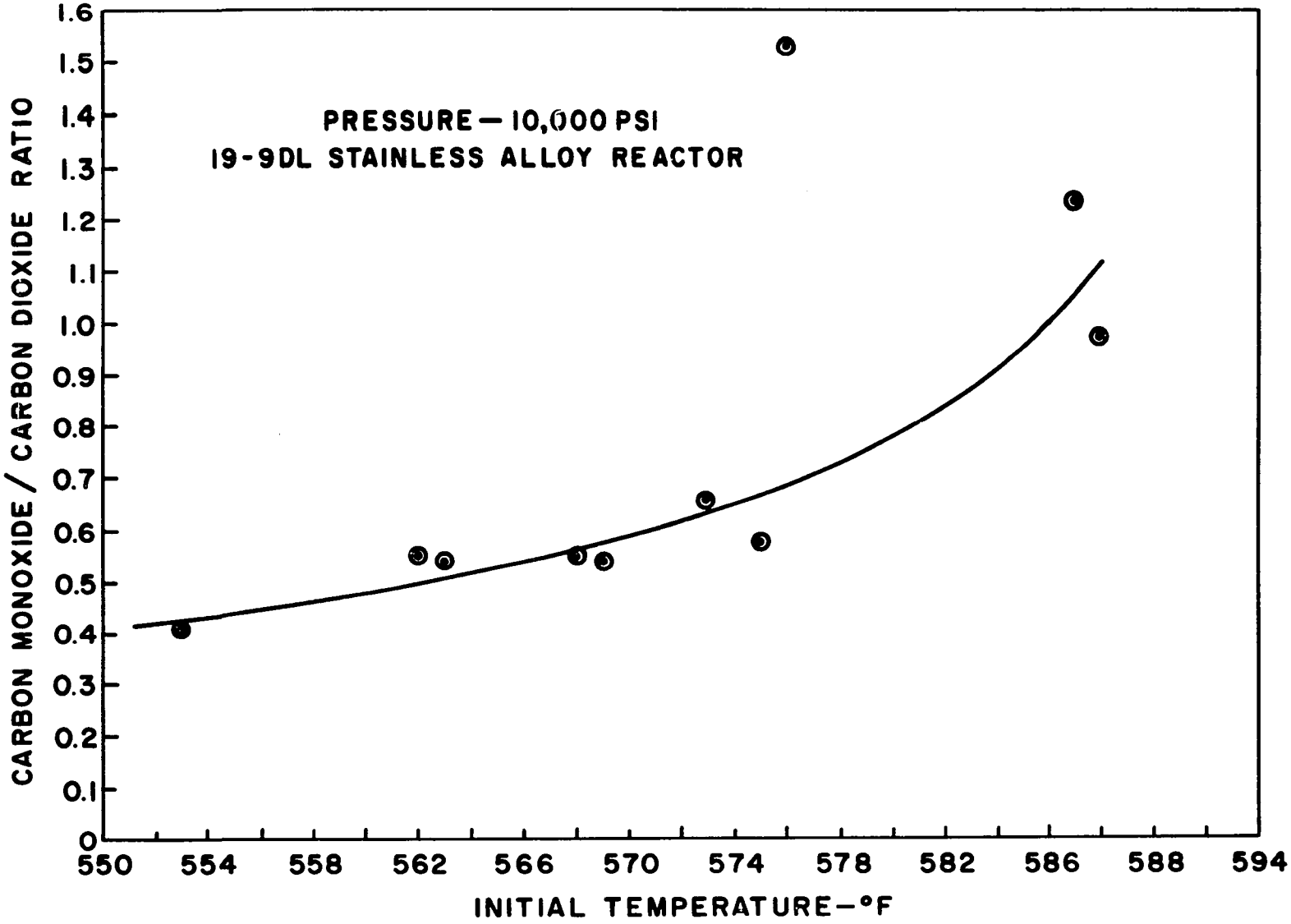

Figure 34. Effect of Temperature on Carbon Monoxide/Carbon Dioxide Ratio (10,000 psi)

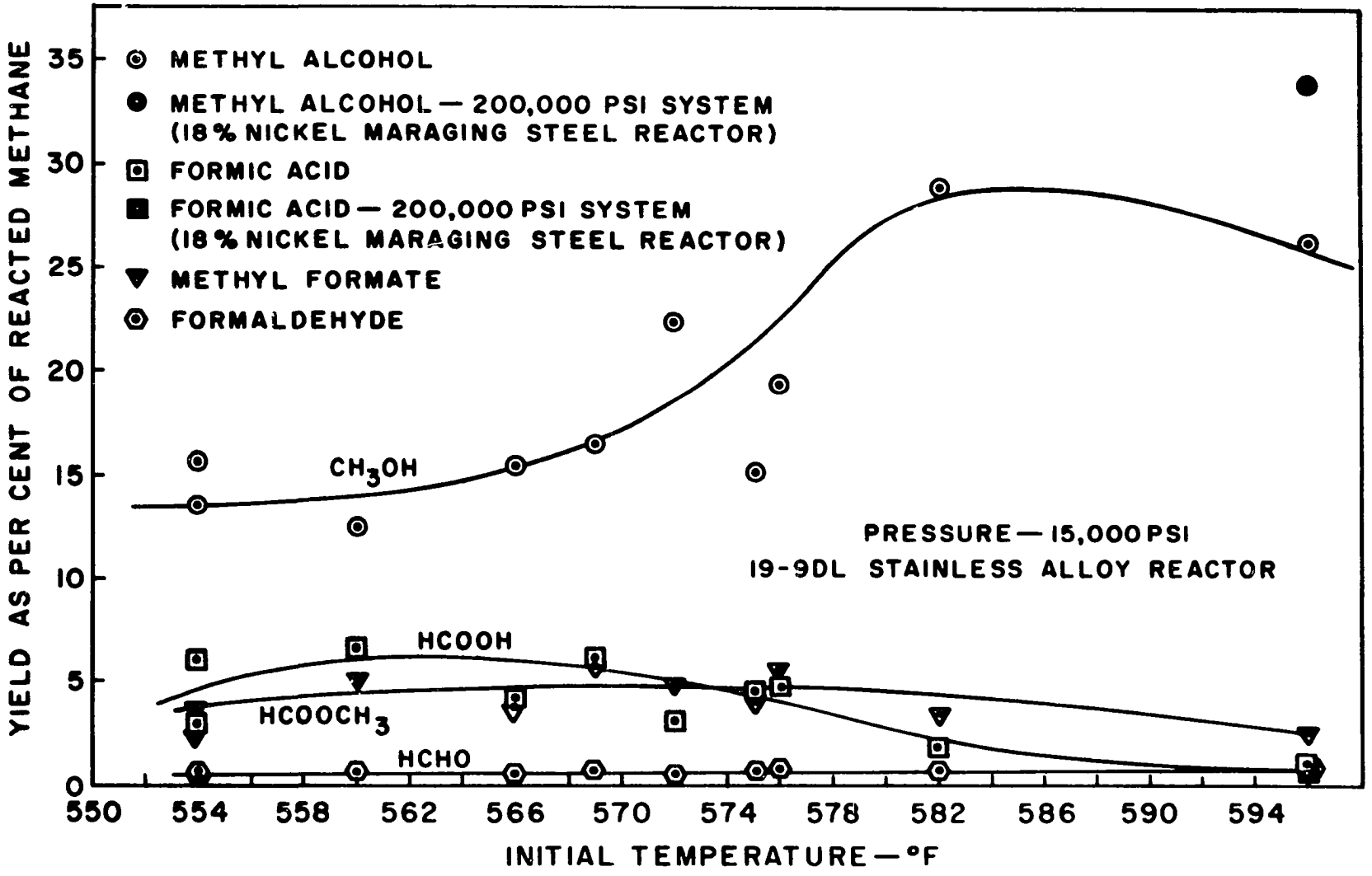

Figure 35. Effect of Temperature on Yield (15,000 psi)

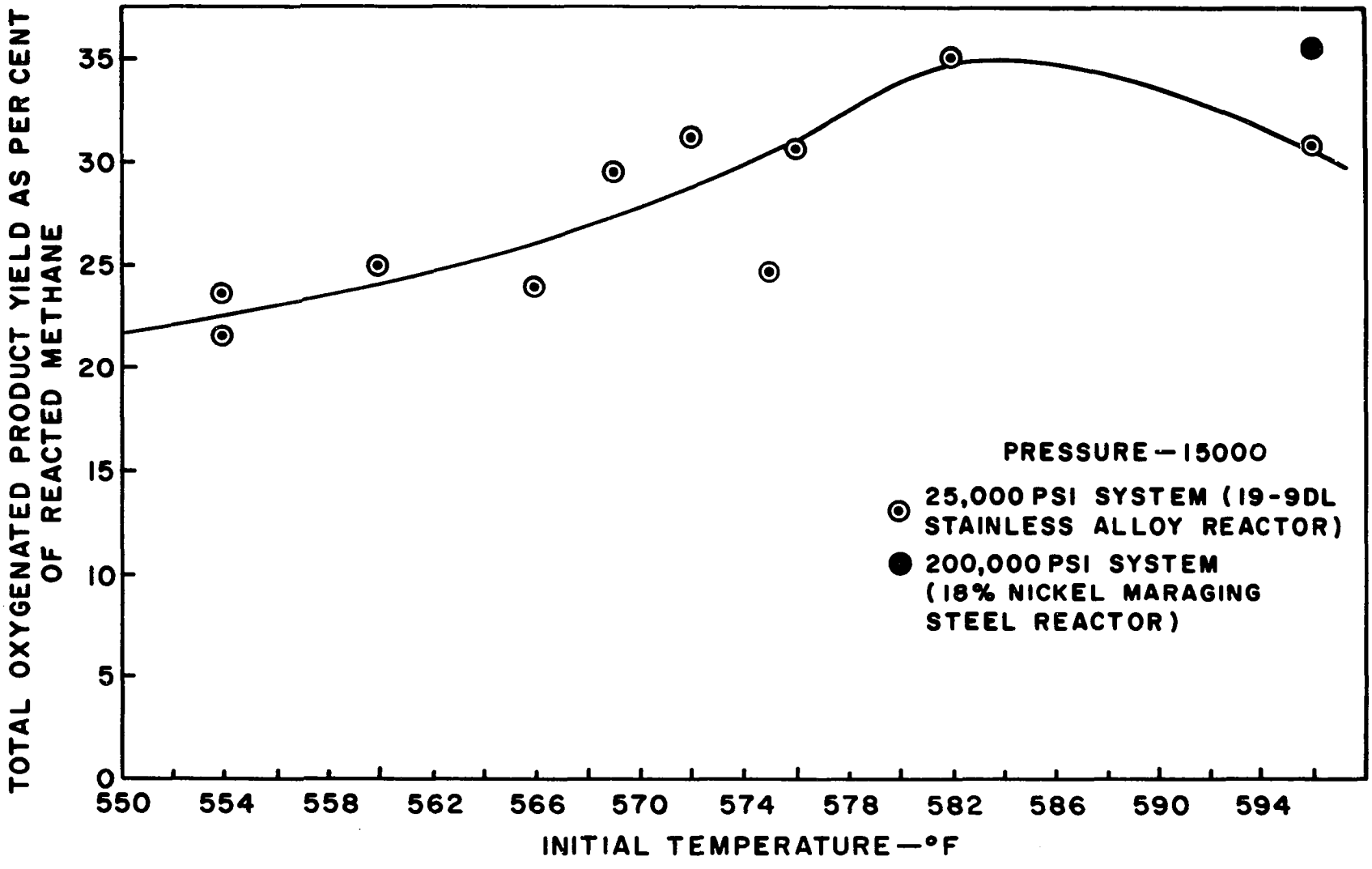

Figure 36. Effect of Temperature on Total Oxygenated Liquid Product Yield (15,000 psi)

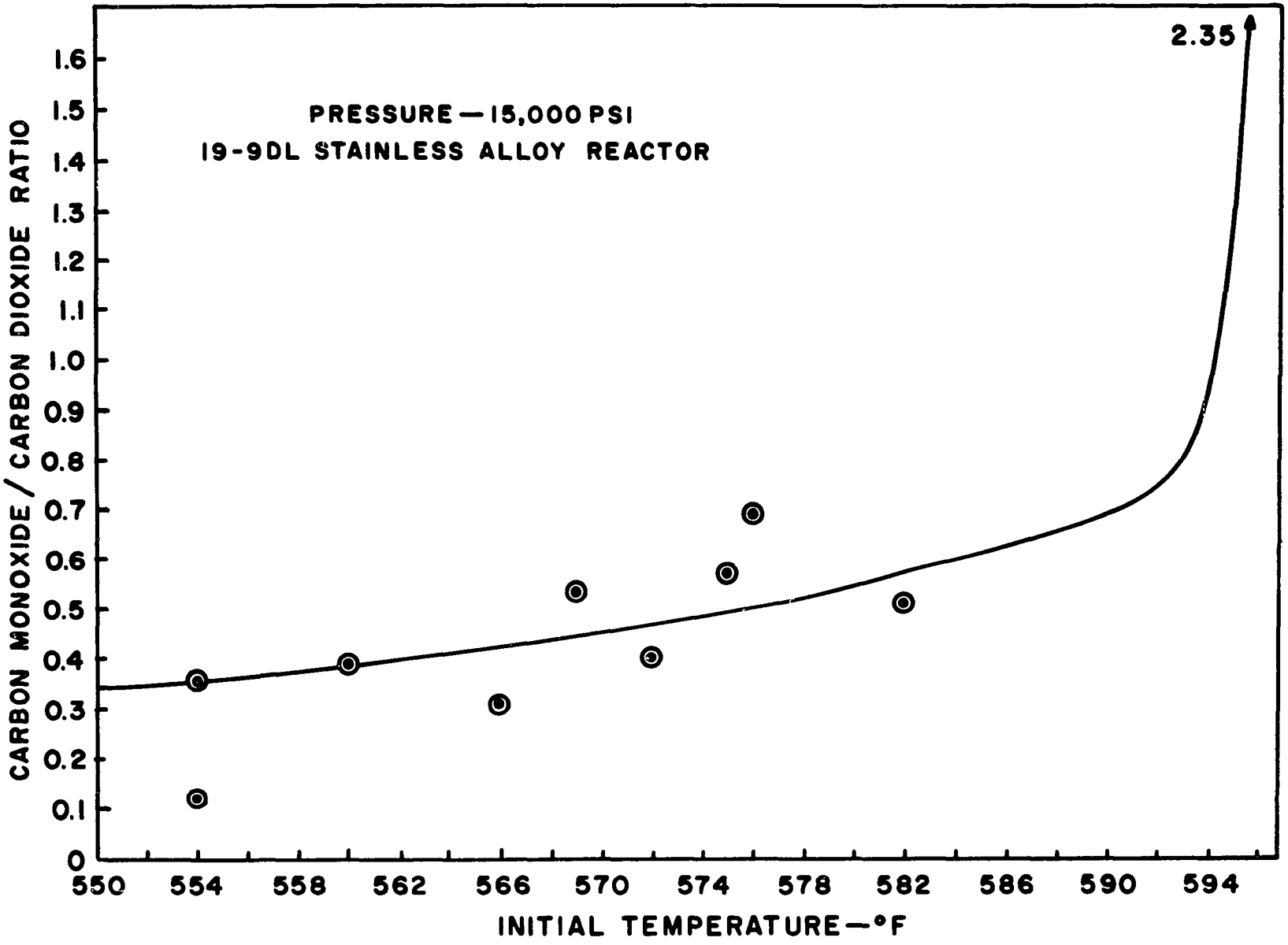

Figure 37. Effect of Temperature on Carbon Monoxide/Carbon Dioxide Ratio (15,000 psi)

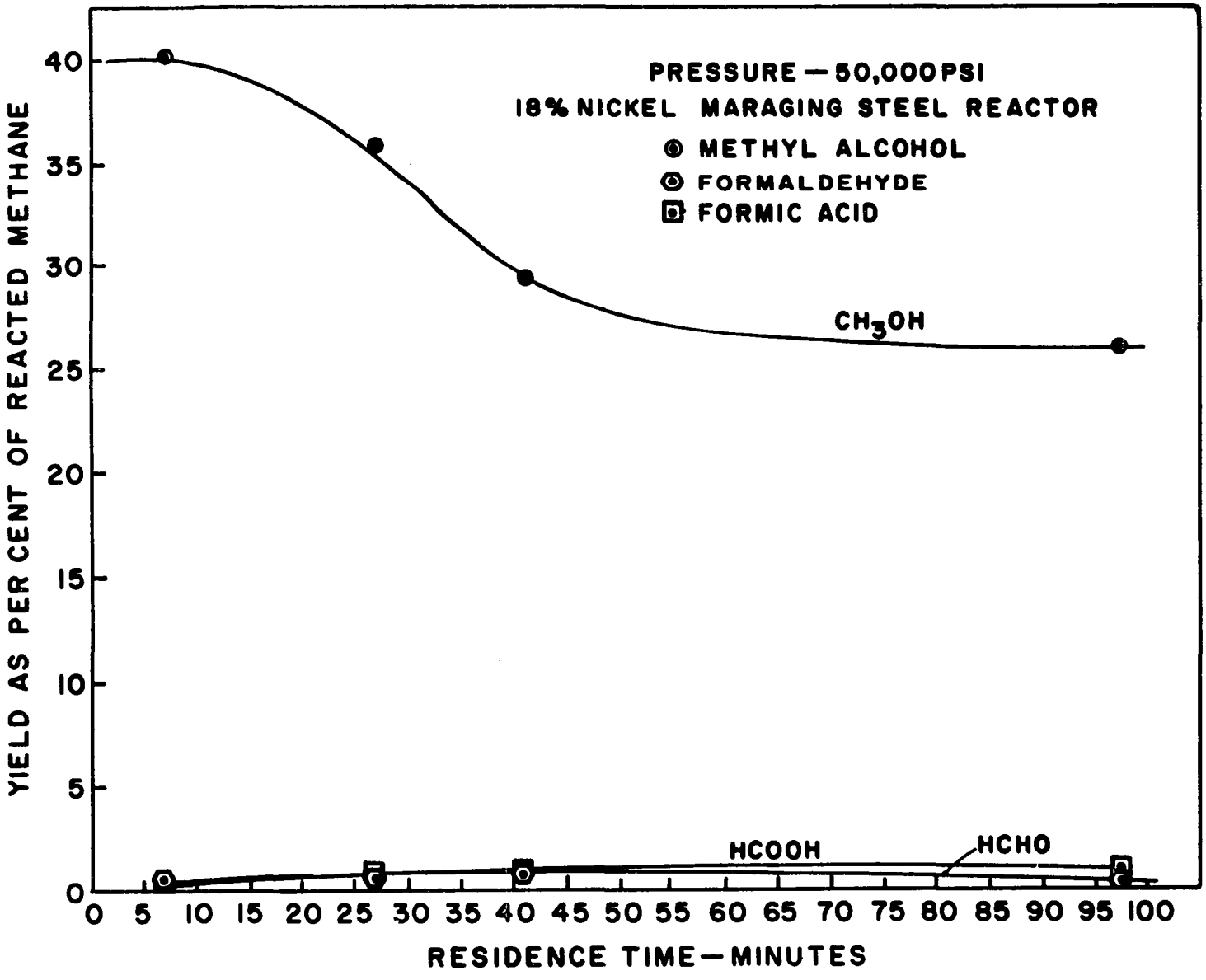

Figure 38. Effect of Residence Time on Yield (50,000 psi)

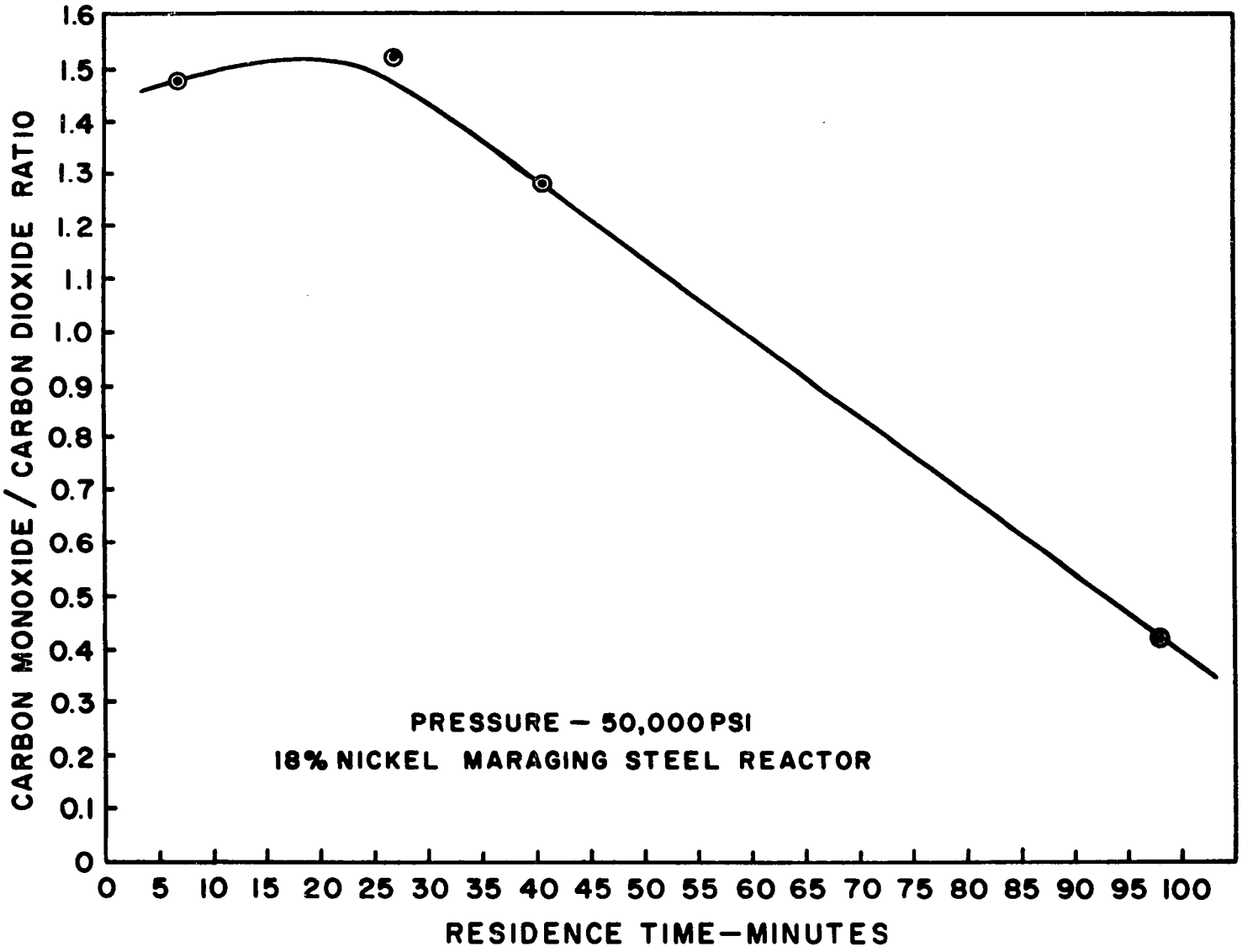

Figure 39. Effect of Residence Time on Carbon Monoxide/ Carbon Dioxide Ratio (50,000 psi)

the further oxidation of methyl alcohol. As the formic acid concentration becomes appreciable a secondary reaction between methyl alcohol and formic acid occurs to form methyl formate. At a pressure of 5400 psi methyl formate was not formed in quantities sufficient to analyze, but at the higher pressures both the formic acid and methyl formate yields increase.

This trend was observed up to 15,000 psi, which was the maximum pressure studied in the 25,000 psi system; at the high pressures (50,000 psi and above), there was a considerable drop in the yield of formic acid accompanied by the absence of any detectable methyl formate. Run JLL-290 was made to determine the pressure effect on the formic acid and methyl formate yields in the 200,000 psi system. The results of this run indicate that the change in yields was not a pressure effect. It is interesting to note (see Figures 35 and 36) that the methanol yield agrees quite well with the maximum yield of total organic liquid products. This agreement may be fortuitous; however, there arise the possibilities that the surface temperature and material of the reactor wall promote the heterogeneous oxidation of methyl alcohol, or that the Pyrex support for the internal furnace catalyzes the decomposition of formic acid. These possibilities will be discussed in turn.

The effect of the nature and condition of the vessel wall on the kinetics of methane oxidation at low pressures

has been discussed in Chapter III. In addition, due to the different means for heating the two reactors (see Chapter V for details) the cylinder wall in the 25,000 psi reactor (19-9DL stainless alloy) was at a temperature close to the reaction temperature whereas the wall of the 200,000 psi reactor (18% nickel maraging steel) was at a temperature considerably lower than the reaction temperature. In addition, the surface-volume ratio of the 25,000 psi reactor is approximately one and one-half times the surface-volume ratio of the 200,000 psi reactor. It is thus possible to visualize the heterogeneous oxidation of methyl alcohol occurring at the surface of the 25,000 psi reactor to a greater degree than in the 200,000 psi reactor.

If the decomposition of formic acid occurs, there are two possible reactions:

$$HCOOH \rightarrow H_2 + CO_2 \qquad (8\text{-}1)$$

or

$$HCOOH \rightarrow H_2O + CO \qquad (8\text{-}2)$$

Reaction (8-1) can be eliminated on the basis that hydrogen gas was not detected in the reaction products. It has been reported that glass does <u>not</u> promote the decomposition according to reaction (8-2) (69). The data of Perkins (54) indicate a higher decomposition rate for glass than previously reported; however, these data were obtained at sub-atmospheric

pressures. Assuming that the Pyrex glass does promote the decomposition of formic acid at high pressures, then the yield of methyl alcohol should be lower than found since the formic acid appears to be formed by the oxidation of methyl alcohol. On the other hand, inspection of the Pyrex glass structure at the end of the high pressure studies revealed that the surface of the glass had a frosted appearance and appeared to be pitted. This condition suggested that a reaction was occurring on the surface of the glass. Without additional information this decrease in formic acid yield cannot be explained further.

Returning now to the two curves obtained at 7000 psi in Figure 20, no apparent change in the liquid product distribution is observed for the shift in the kinetic curve at 7000 psi (see Figures 26, 27, 29, and 30). However, the CO/CO_2 ratio (see Figures 28 and 31) shows a marked change at the higher temperatures where the two curves of Figure 20 begin to merge. It is not surprising that the CO/CO_2 ratios at the lower temperatures (longer residence times) agree within experimental error since the oxidation of carbon monoxide would tend to minimize this ratio. Because there is no apparent change in the liquid product distribution and because the wall effect on the reaction rate at higher temperatures (shorter residence times) is apparently minimized or eliminated, the disagreement in the CO/CO_2 ratios cannot be explained.

The effect of pressure on the yields of methanol and total oxygenated liquid products based on the quantity of reacted methane is shown more clearly in Figures 40 through 44. Figures 40 and 41 show the yields as a function of temperature with pressure as a parameter. The data for a pressure of 50,000 psi have not been included in Figures 40 and 41 because reproducible residence times with respect to initial temperature were not obtained in the 200,000 psi reactor--sufficient experimental runs have not been made to establish a reproducible surface effect in the 18 per cent nickel maraging steel reactor. However, by plotting the yields as a function of residence time (see Figures 42 and 43) the effect of pressure on the yields is clearly indicated. Of particular interest is the reversal in methyl alcohol yield at 10,000 psi in Figure 42. This reversal can be attributed to the increase in yield of the formic acid and methyl formate with an increase in pressure. Inspection of Figure 43 shows that total yield of oxygenated liquid products increases with an increase in pressure; in this case the reversal at 10,000 psi is not observed.

The results of the high pressure runs (50,000 psi and higher) are presented in Table 5. In these runs there is no doubt that the reactor had not been "conditioned" by the oxidation process since Table 5 clearly indicates that an increase in temperature at a given pressure was required to obtain an appreciable reaction rate as more experimental

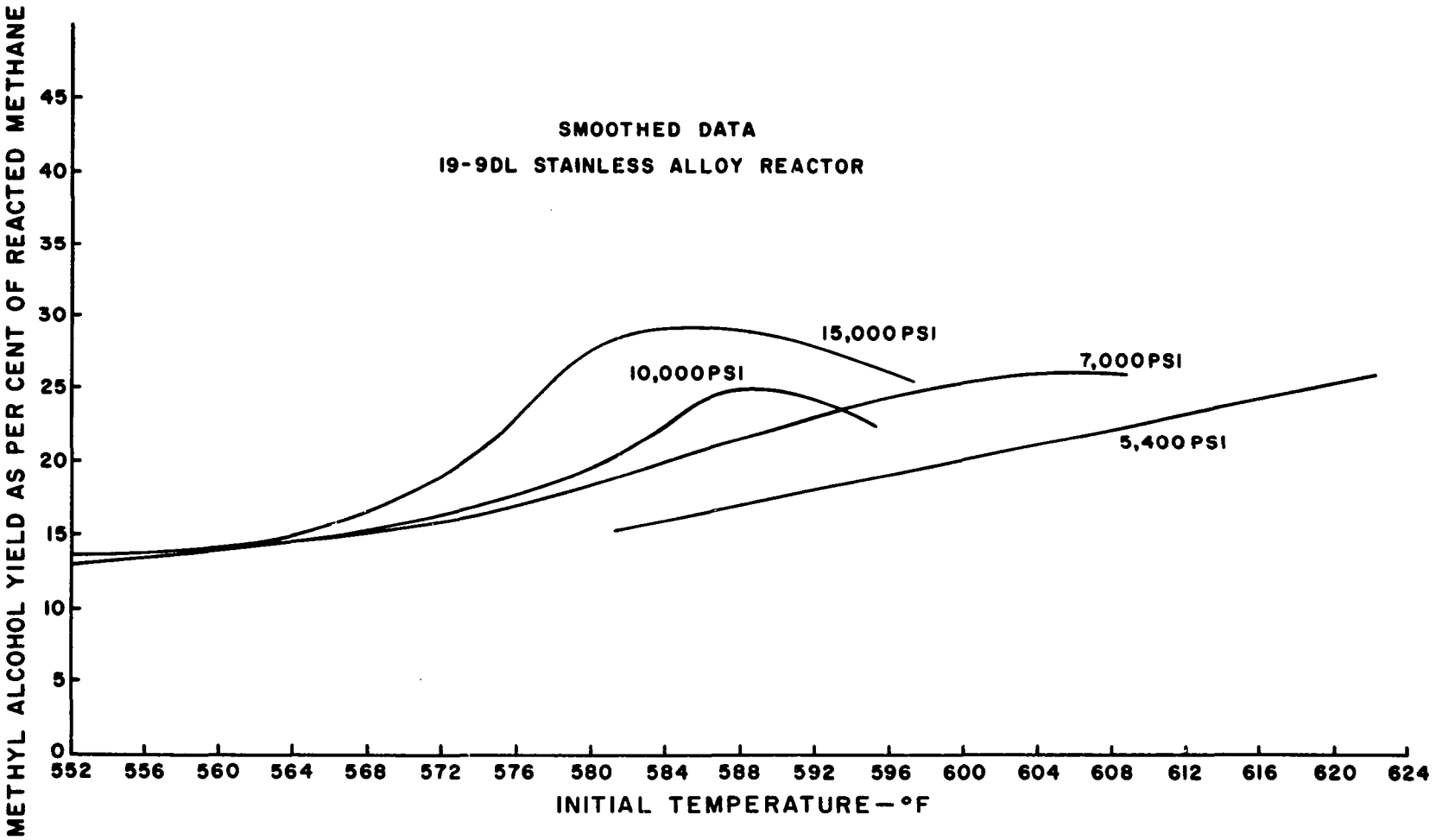

Figure 40. Methanol Yield Temperature Dependence at Various Pressures

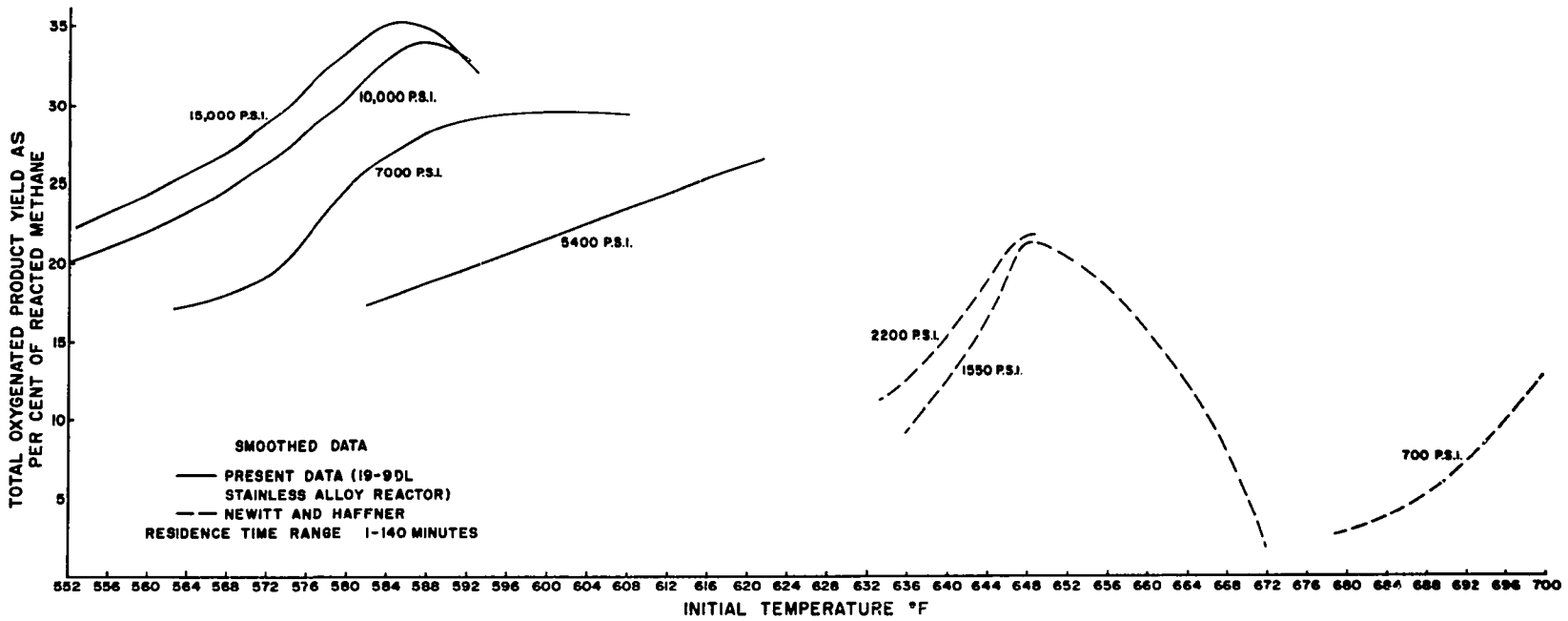

Figure 41. Total Oxygenated Liquid Product Yield Temperature Dependence at Various Pressures

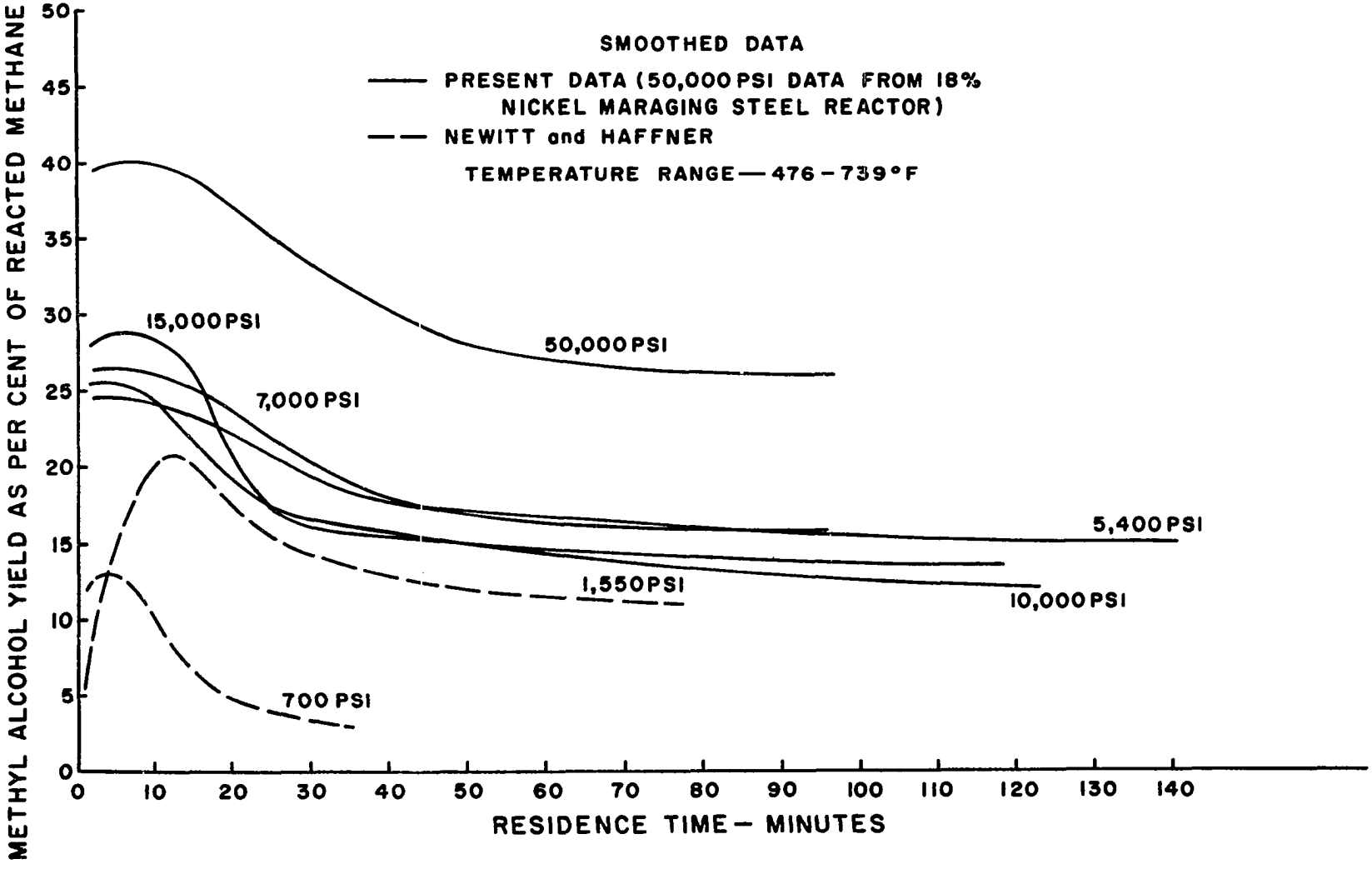

Figure 42. Effect of Residence Time on Methanol Yield at Various Pressures

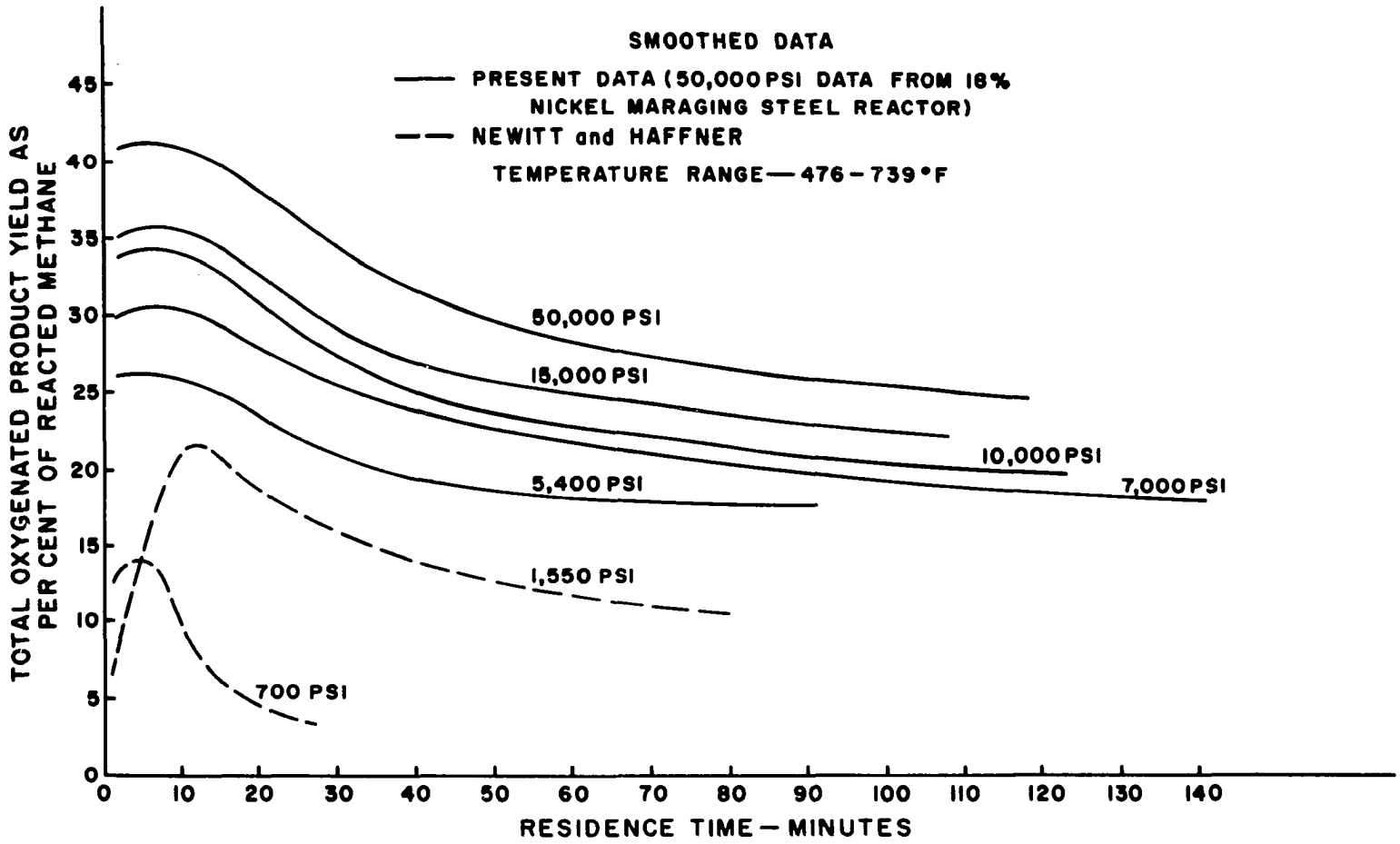

Figure 43. Effect of Residence Time on Total Oxygenated Liquid Product Yield at Various Pressures

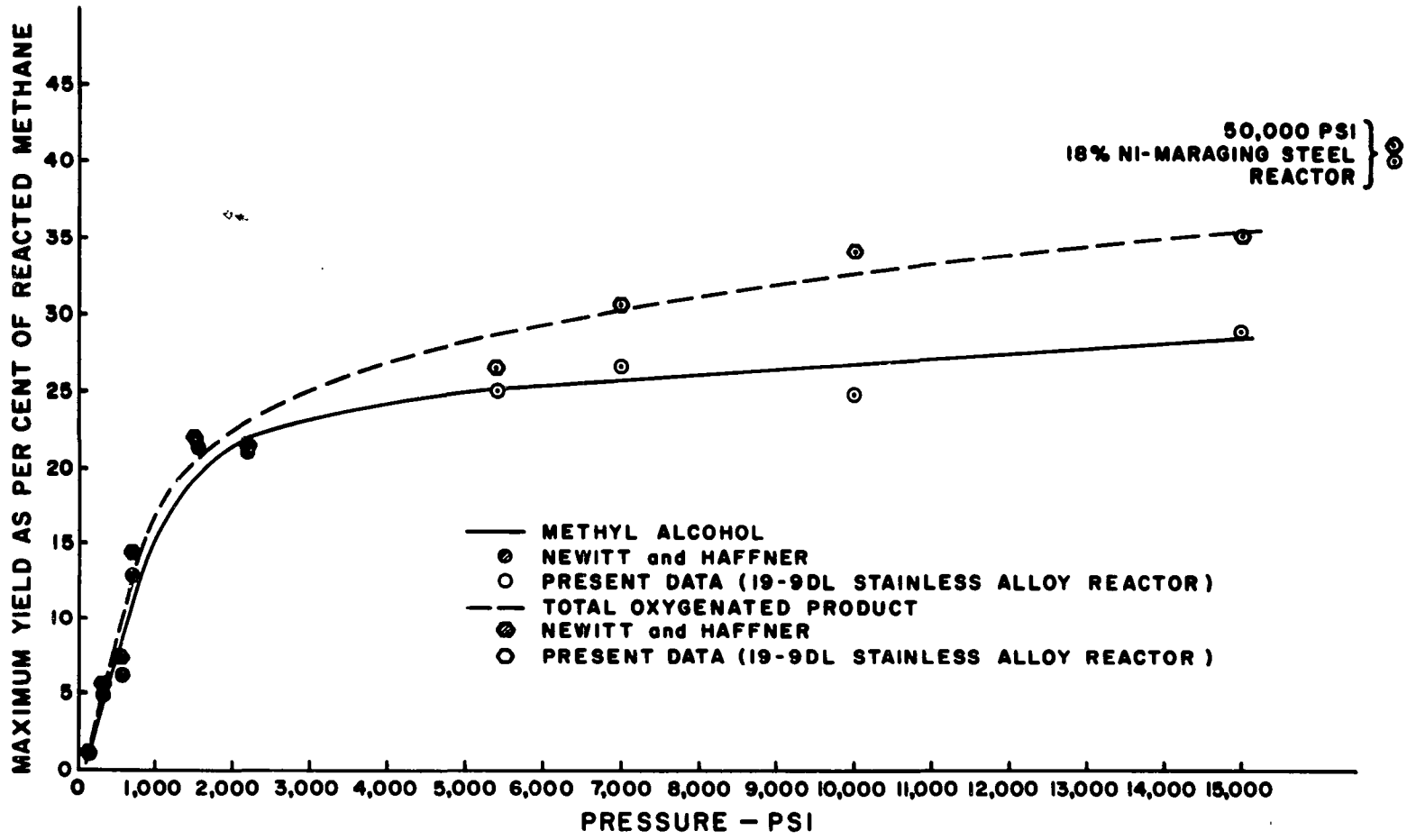

Figure 44. Effect of Pressure on the Maximum Oxygenated Liquid Product Yield

TABLE 5

SUMMARY OF EXPERIMENTAL RESULTS AT HIGH PRESSURES
METHANE-OXYGEN RATIO - 11.6
REACTOR 18% NICKEL MARAGING STEEL

Run No. JLL	Initial Temp. °F	Initial Pressure, PSI x 10^3	Residence Time Minutes	Per Cent of Reacted Methane Converted To					Methane Conversion %	Oxygen Conversion %	Remarks
				CH_3OH	HCHO	HCOOH	CO	CO_2			
238	476	50.0	98	26.14	0.57	1.01	26.80	64.73	4.06	92.26	
240	485	50.0	138	6.22	0.63	0.29	---	95.21	1.44	26.22	No temperature rise
242*	488	50.0	-	31.55	0.56	0.43	37.02	34.76	6.66	96.82	Instantaneous reaction
246	503	50.0	122	10.47	0.15	0.93	9.47	78.98	5.21	95.99	No temperature rise
254	504	47.5	41	29.36	0.83	1.03	39.72	30.95	4.66	87.93	
252	506	50.0	111	7.12	1.35	1.18	91.64	---	0.20	10.86	No temperature rise
258	508	50.0	7	40.10	0.64	0.45	58.13	39.28	6.29	95.16	
260	508	50.0	138	3.89	0.49	0.33	37.83	152.70	1.22	22.18	No temperature rise
248	509	50.0	-	33.29	0.73	0.45	42.31	26.79	6.42	95.72	Instantaneous reaction
262	512	50.0	120	4.11	0.58	0.44	26.98	98.17	1.45	22.31	No temperature rise
264	516	48.0	120	3.20	0.34	0.43	23.14	84.65	2.83	54.52	No temperature rise
256	517	50.0	27	35.93	0.77	0.89	39.93	26.60	5.32	95.97	
268	489	96.5	18	---	---	---	---	---	0.22	3.10	Thermocouple out
266	493	95.0	120	2.88	0.20	0.60	---	44.35	0.13	7.50	No temperature rise
270	498	100.0	90	---	0.90	1.06	13.15	85.28	0.66	15.24	No temperature rise
272	477	138.0	12	---	---	---	---	---	0	0	No temperature rise
280	491	136.0	120	5.11	0.13	0.61	---	65.22	0.52	12.76	Material held @100,000 psi and 415°F for 50 hours
282	491	181 - 140	120	3.72	0.28	1.20	---	94.23	0.80	18.11	Leak at discharge valve
284	491	165.0	120	5.53	0.36	2.09	---	127.20	0.77	16.41	No temperature rise
288	496	185.0	120	5.57	0.20	2.53	---	102.83	0.68	10.99	No temperature rise
292**	499	200.0	28	2.38	4.62	6.60	---	73.73	1.37	21.40	Initial feed contaminated with hydraulic fluid due to O-ring failure

* Reaction probably initiated by internal furnace during heat-up.
** $HCOOCH_3$ = 3.28%

runs were made. It should be remarked that approximately 45 tests were made in the 25,000 psi system (19-9DL stainless alloy reactor) before any of the data used in this work was taken. It has been shown in various investigations at low pressures that the nature and surface condition of the reaction vessel influenced the kinetics of the oxidation process, e.g., the oxidation rate in a "new" vessel is greater than the rate in an "aged" vessel.

At the higher pressures the time required to charge the reactor was extremely long (sometimes as long as 22 hours at pressures greater than 150,000 psi). The question thus arises as to whether or not any oxidation occurs during the charging process. Evidence that oxidation does not occur during the charging step is shown by Runs JLL-268 and 272. In Run JLL-268 the time required to charge the reactor to a pressure of 96,000 psi was 5 hours. The temperature of the reactor contents was approximately 415°F throughout the filling operation. The temperature was then increased to 490°F, and it was maintained at this temperature for 18 minutes before freezing the reaction by expanding and cooling the reactor contents. Analysis of the expanded gas (no liquid was obtained) indicated that a reaction had not occurred. Another illustration is Run JLL-280. In this case the reactor contents were held at 415°F and 100,000 psi for at least 50 hours. An additional 5 hours were required to increase the pressure to 136,000 psi by adding more feed. The

temperature was then increased to 490°F and maintained for 2 hours. The conversion of oxygen for Run JLL-280 was approximately 15 per cent. The chain nature of this reaction thus eliminates the possibility of any measurable reaction occurring while the reactor is being charged.

The unusual behavior exhibited by Run JLL-254 is worthy of a detailed discussion. This run was conducted at a pressure of 48,000 psi and an initial temperature of 504°F in the 18 per cent nickel maraging steel reactor. The temperature slowly increased from 504°F to 517°F over a period of 40 minutes. At this point the temperature increased rapidly to 528°F and then dropped to 517°F. A second temperature rise to 543°F followed shortly after the first. Both temperature rises were accompanied by a corresponding pressure rise. At low pressures a sharp rise and fall of the temperature and pressure followed by another such occurrence is known as the cool flame phenomenon. The cool flame phenomenon for methane at low pressures was first observed in 1955 by Vanpée (74). Prior to his observation it was believed that methane (and ethane) did not exhibit this characteristic observed in the oxidation of the heavier hydrocarbons. It is believed that the characteristics of the cool flame are fulfilled by Run JLL-254 and that the cool flame phenomenon also occurs at high pressures. The recorded pressure and temperature for this run are reproduced in Figures 45 and 46. In contrast to the cool flame, the hot flame can be illustrated by Figures 47 and 48 obtained in Run JLL-201.

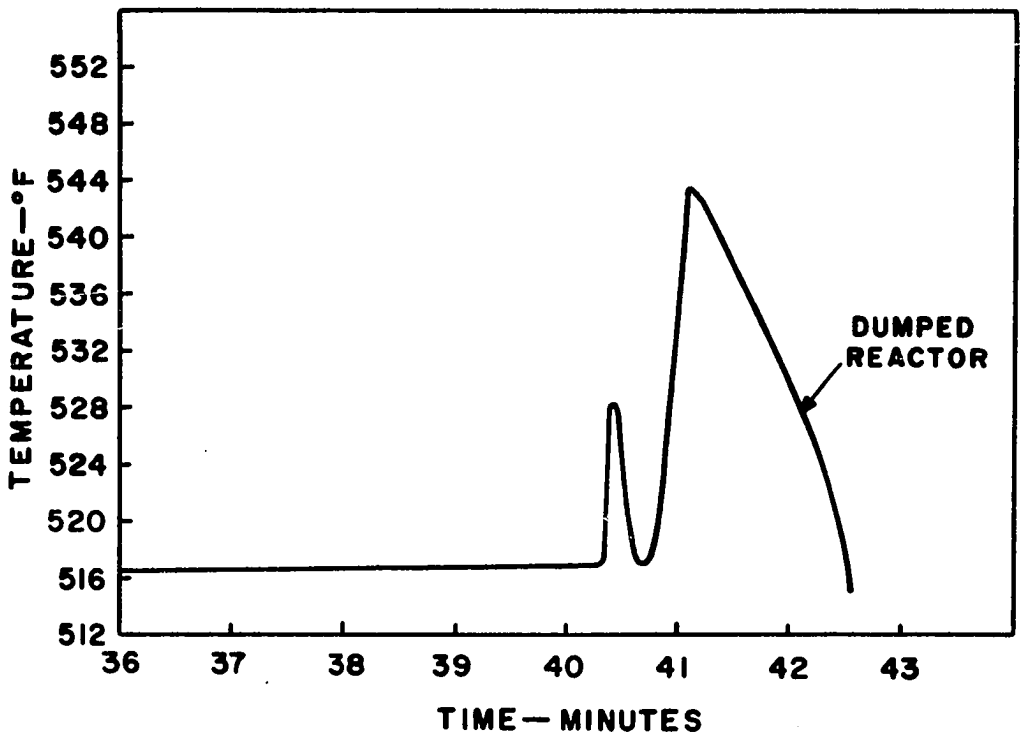

Figure 45. Cool Flame Phenomenon: Temperature-Time Curve (Run JLL-254)

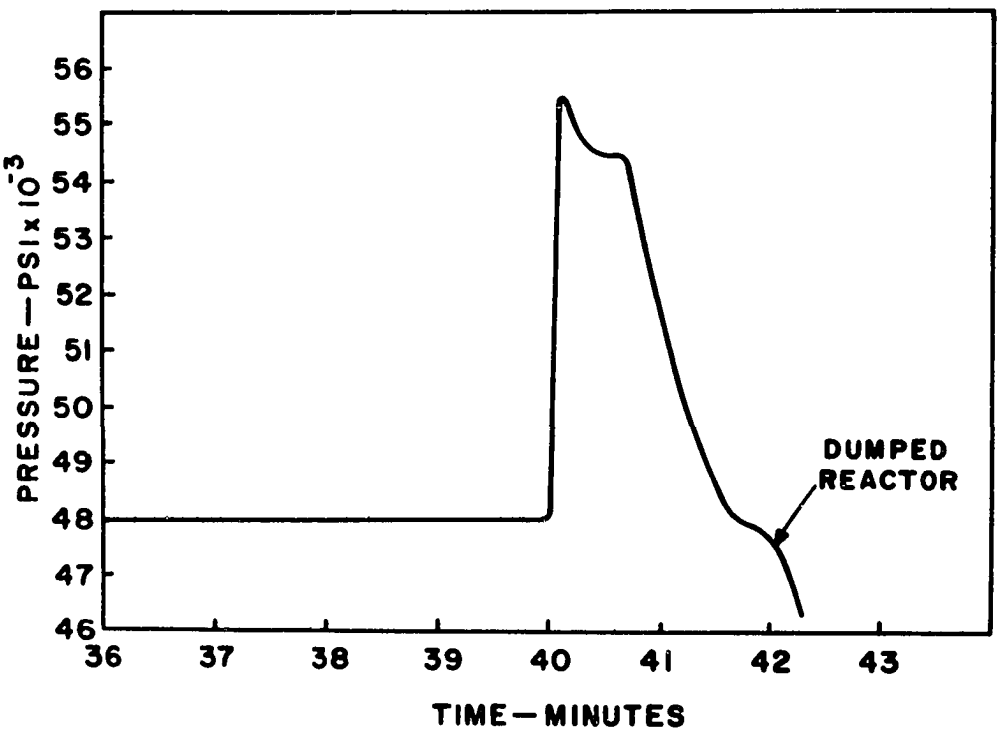

Figure 46. Cool Flame Phenomenon: Pressure-Time Curve (Run JLL-254)

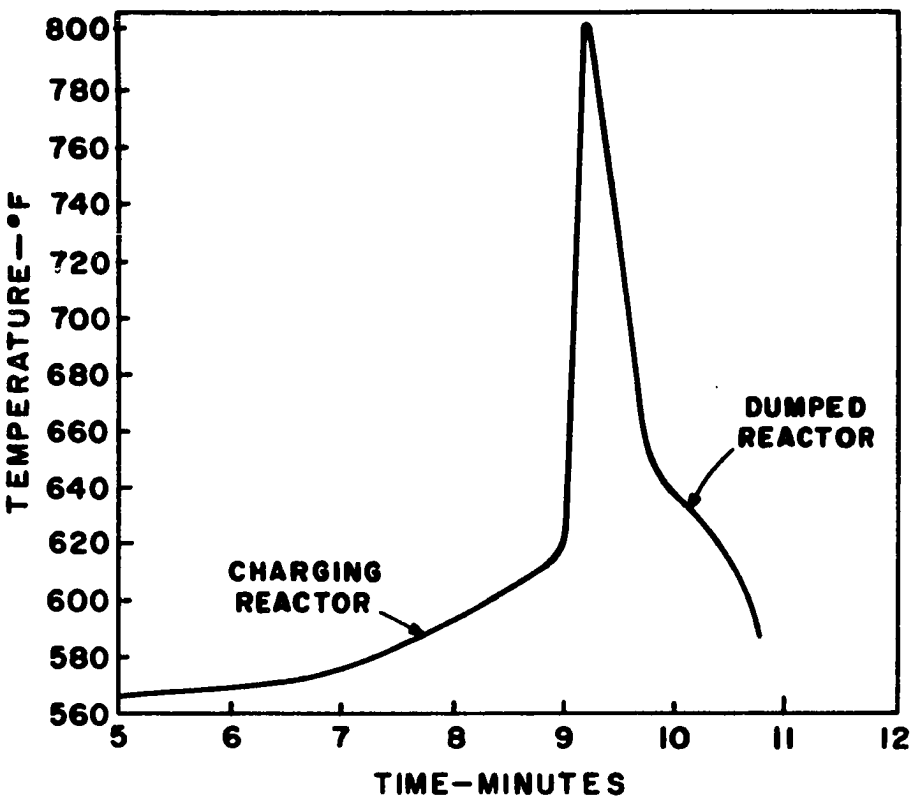

Figure 47. Hot Flame Temperature-Time Curve (Run JLL-201)

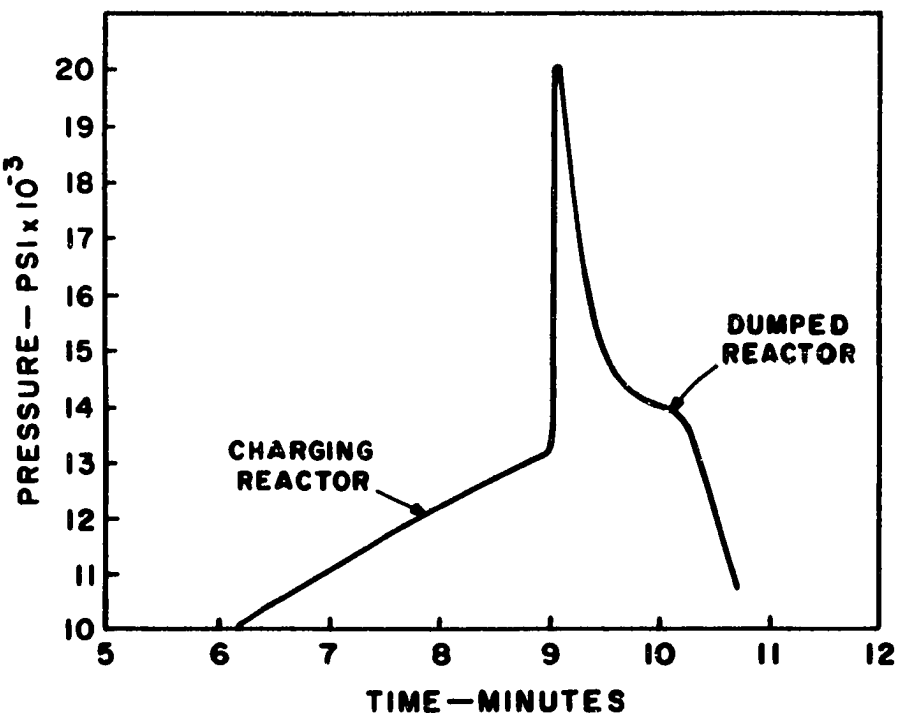

Figure 48. Hot Flame Pressure-Time Curve (Run JLL-201)

It is unfortunate that the run made at 200,000 psi was contaminated with the pressure transmitting fluid. The unusually high yields of aldehyde (reported as formaldehyde) and acid (reported as formic acid) are of special interest since the only alcohol detected was methyl alcohol. A titration of the hydraulic fluid indicated that the oil was neutral. It is also known from studies on the oxidation of heavier hydrocarbons that the corresponding alcohols, as well as methanol, are products of the oxidation. Since methanol was the only alcohol detected, and since the hydraulic fluid is neutral, it seems unlikely that the hydraulic oil could be totally responsible for the high yields of aldehyde and acid.

The following characteristics of a chain reaction with degenerate branching were observed in this investigation. First, the reaction exhibited a marked induction period. Second, the reaction was self-accelerating. Third, the condition of the reactor surface affected the reaction rate. Finally, the cool flame phenomenon was observed. Thus, the results of this investigation on the partial oxidation of methane at high pressures indicate that the reaction proceeds by a chain mechanism with degenerate branching, as first proposed by Semenov (see Chapter II). However, in his mechanism the isomerization and decomposition of the peroxide radical to form formaldehyde is very fast. On the other hand, for the extreme pressures used in the present investigation, it

is conceivable that the formation of formaldehyde is much slower and consequently could be the rate-controlling step. On this basis--and even though the results from this study are not adequate for positive, definite confirmation--the mechanism proposed by the writer in Equation (2-42) appears most plausible, at least under extreme pressures.

CHAPTER IX

CONCLUSIONS

In the oxidation of methane, pressure has a strong influence on the product distribution. In general an increase in pressure increases the yield of methyl alcohol and other oxygenated organic liquid products. At a given pressure the maximum yield of methyl alcohol occurs at an initial temperature corresponding to a relatively short residence time. The cool flame phenomenon was observed at high pressures for the first time; thus the phenomenon is not restricted to low pressures. The nature and surface condition of the vessel affects the kinetics of the oxidation process as well as the product distribution.

The most plausible mechanism for the partial oxidation of methane at high pressures is by a chain mechanism with degenerate branching. In this proposed mechanism the rate of formation of formaldehyde by the isomerization and decomposition of the peroxide radical must be considered since the speed at which it occurs is most likely commensurate with the rate-controlling step.

It has been demonstrated that high pressure equipment can be fabricated for studying chemical reactions in

fluid systems of at least 500 cubic centimeters at pressures up to 200,000 psi and temperatures up to 800°F. It is believed that this study is the first attempt to study chemical reactions at pressures greater than 120,000 psi.

Due to the complexity of the oxidation process at high pressures, there are numerous areas where further research on the oxidation of methane would be beneficial. Of these areas it is suggested that the first two studies should be: (1) The continuation of this work to determine the effect of pressure and the presence of glass on the product distribution over a pressure range of 50,000 to 200,000 psi, and (2) studies to determine the reaction mechanism at high pressures.

NOMENCLATURE

a = kinetic coefficient in general

= kinetic coefficient of chain propagation

b_n = outer radius of nth cylinder

d = diameter

E = modulus of elasticity

E_A = energy of activation

f = kinetic coefficient of chain branching

g = kinetic coefficient of chain termination

k = specific rate constant

K = diameter ratio

m = order of reaction with respect to methane concentration

= number of cylinders in compound vessel

n = concentration of active centers or free radicals

= cylinder number

= order of reaction with respect to oxygen concentration

n_i = concentration of active center i

P = pressure

P_i = internal pressure

P_o = external pressure

P_{os} = overstrain pressure

P_2^1 = residual contact pressure between inner and middle cylinder

p^1_3 = residual contact pressure between middle and outer cylinder

r = radius variable

r_e = radius at outer edge of region of inelastic strain

r_i = inside radius

r_o = outside radius

$r_{o,1}$ = outside radius of inner cylinder

$r_{o,2}$ = outside radius of middle cylinder

R = gas law constant

S = surface activity per unit area

t = time variable

= order of reaction with respect to pressure

T = temperature

T_i = inside wall temperature

T_o = outside wall temperature

W = rate of chain reaction

W_o = chain initiation reaction rate

Greek

α = ratio of the concentrations of formaldehyde and methane

β = probability of chain breaking

= temperature variable

γ = chain length

δ = probability of chain branching

δ_r = interference or shrinkage per unit of radial length

Δ = symbol for difference

ν = Poisson's ratio

σ = principal stress

σ_r = radial stress

σ_t = tangential stress

σ_y = yield strength in simple tension

σ_z = longitudinal stress

τ = dimensionless time variable

= shear stress

τ_e = shear stress of equivalent simple cylinder

τ_{R_n} = residual shear stress in n^{th} cylinder

φ = auto-acceleration parameter in chain theory

Subscripts

d = diametral

i = inside

= component i

n = n^{th} component

o = outside

os = overstrain

R_n = residual condition of nth cylinder

r = radial

t = tangential

y = yield point

z = longitudinal

0, 1, etc. = reactions 0, 1, etc.

= outside of component 1, etc.

[ ] = concentration

LITERATURE CITED

1. Aivazov, B. V., and M. B. Neiman, Zh. fiz. khim., 9, 231 (1937), (In reference 65).

2. Armstrong, H. E., Manual of Organic Chemistry, 216, 241, 275 (1874), (In reference 65).

3. Armstrong, H. E., J. Chem. Soc., 83, 1088 (1905).

4. Bach, A. N., Fh. russk. fiz-khim. obsheh., 29, 373 (1897), (In reference 65).

5. Bone, W. A., Nature, 481 (March 28, 1931).

6. Bone, W. A., and R. E. Allum, "The Slow Combustion of Methane," Proc. Roy. Soc., A134, 578 (1934).

7. Bone, W. A., and J. C. Cain, J. Chem. Soc., 71, 26 (1897).

8. Bone, W. A. and J. B. Gardner, "Studies on the Slow Combustion of Methane," Proc. Roy. Soc., A154, 297 (1936).

9. Bone, W. A., and B. Lean, J. Chem. Soc., 61, 873 (1892).

10. Bone, W. A., and R. V. Wheeler, "The Slow Oxidation of Methane at Low Temperatures," J. Chem. Soc., 81, 535 (1902).

11. Bone, W. A., and R. V. Wheeler, "The Slow Oxidation of Methane at Low Temperatures, Part II," J. Chem. Soc., 83, 1074 (1903).

12. Bone, W. A., and R. V. Wheeler, "The Slow Oxidation of Ethane at Low Temperatures," J. Chem. Soc., 85, 693 (1904).

13. Callender, H., Engineering, 123, 147, 182, 210 (1927).

14. Comings, E. W., "High Pressure Technology," McGraw-Hill, New York, (1955).

15. Continental Oil Company, "Design Notebook," (1956).

16. Egerton, A. C., G. J. Minkoff, and K. C. Salooja, "The Slow Oxidation of Methane, The Role of the Surface On the Course of the Oxidation of Methane," Combustion and Flames, 1, March, 25-52 (1957).

17. Engler, C., and E. Wild, Ber., 30, 1669 (1897), (In reference 65).

18. Fort, R., and C. N. Hinshelwood, Proc. Roy. Soc., A129, 284 (1930); A127, 218 (1930).

19. Furman, M. S., Khimicheskaya Promyshlennost, Nos. 1-2, 24 (1946), (In Gonikberg, M. G., "Chemical Equilibria and Reaction Rates at High Pressure," N.S.F. Publication, Translated from Russian, Washington, D. C., (1963).

20. Furman, M. S., A. D. Shestakova, and I. Sh. Radle-Desyatnik, Trudy GIAP, No. 1, 100 (1953), (In Gonikberg, M. G., "Chemical Equilibria and Reaction Rates at High Pressure," N.S.F. Publication, Translated from Russian, Washington, D. C., (1963).

21. Gray, P., Fifth Symposium on Combustion, New York, 535 (1955).

22. Hoare, D. E., "Reproducibility in the Slow Combustion of Methane," Trans. Farad. Soc., 49, 628 (1953).

23. Hoare, D. E. and A. D. Walsh, Fifth Symposium on Combustion, New York, 467 (1955).

24. Hoare, D. E. and A. D. Walsh, Fifth Symposium on Combustion, New York, 474 (1955).

25. Holy, G. R., and K. O. Kutschke, Canad. J. Chem., 33, 496 (1955).

26. Ingold, K. U., and W. A. Bryce, J. Chem. Phys., 24, 360 (1956).

27. Jost, W., Z. Elektrochem, 41, 232 (1935), (In reference 65).

28. Jost, W., L. Muffling, and W. Rohrmann, Z. Electrochem, 42, 488 (1936), (In reference 65).

29. Karmilova, L. V., N. S. Yenikolopyan, and A. B. Nalbandyan, Zh. fiz. khim., 31, 851 (1957); 34, 990 (1960), (In reference 65).

30. Karmilova, L. V., N. S. Yenikolopyan, and A. B. Nalbandyan, Zh. fiz. khim., 34, 1176 (1960), (In reference 65).

31. Kersten, J. prakt Chem., 84, 311-17 (1861), (In Marek, L. F., and D. A. Hahn, "The Catalytic Oxidation of Organic Compounds in the Vapor Phase," The Chemical Catalog Co., Inc., (1932).

32. Knox, J. H., "Gas Chromatography," Methuen and Co., Ltd., (London) (1962).

33. Knox, J. H., and R. G. W. Norrish, Trans. Farad. Soc., 50, 928 (1954).

34. Lame, G., "Lecons sur la Theorie Mathematique de L'Elasticite des Corps Solides," pp. 188-91, Bachelier, Paris (1852).

35. Lewis, B., J. Chem. Soc., 1555 (1927); 759 (1929); 58 (1930).

36. Lewis, B., and G. von Elbe, J. Am. Chem. Soc., 59, 970 (1937).

37. Lobo, P. A., C. M. Sliepcevich, and R. R. White, "Steel Catalyzed Hydrogenation of Carbon Monoxide and Dioxide," Ind. Eng. Chem. 48, 906 (1956).

38. Magee, E. M., "Kinetics of Methane Oxidation," Am. Chem. Soc. J., 81, 278-81 (1959).

39. Manning, W. R. D., "The Design of Compound Cylinders for High-Pressure Service," Engineering, 349-52 (1947), 464 (1950).

40. Mardles, E. W. J., Trans. Farad. Soc., 27, 681 (1931).

41. Mondain-Monval, P., and B. Quanquin, Compt. Rend., 191, 299 (1930); 189, 917, 1194 (1929), (In reference 65).

42. Mondain-Monval, P., and B. Quanquin, Ann. Chim. [10] 15, 309 (1931), (In reference 65).

43. Nalbandyan, A. B., and N. A. Kleimenov, Dolk. Akad. Nauk SSSR, 124, 119 (1959), (In reference 65).

44. Newitt, D. M., and J. B. Gardner, "Studies on the Slow Combustion of Methane," Proc. Roy. Soc., A154, 329 (1936).

45. Newitt, D. M., and A. E. Haffner, "The Formation of Methyl Alcohol and Formaldehyde in the Slow Combustion of Methane," Proc. Roy. Soc., A134, 591 (1932).

46. Newitt, D. M., and P. Szego, "Slow Oxidation at High Pressures," Proc. Roy. Soc., A147, 55 (1934).

47. Norrish, R. G. W., Cinetique et mecanisme de reactions d'inflammation et de combustion en phase gazeme, Paris, 16 (1948), (In reference 65).

48. Norrish, R. G. W., and S. G. Foord, "The Kinetics of the Combustion of Methane," Proc. Roy. Soc., A157, 503 (1936).

49. Norrish, R. G. W., and A. J. Harding, Disc. Farad. Soc., No. 10, 269 (1951).

50. Norrish, R. G. W., and D. Patnaik, Nature, 163, 883 (1949).

51. Norrish, R. G. W., and J. D. Reagh, Proc. Roy. Soc., A176, 429 (1940).

52. Paris, A., "Systematic Oxidation of Methane under Pressure," Chimie et Industrie, 411-20 (1934), (Chem. Abs. 5806^5, (1934)).

53. Patry, M., and P. Monceaux, "The Synthesis of Formaldehyde by the Controlled Oxidation of Methane at Atmospheric Pressure," Trans. Farad. Soc., Vol. 42, 341-45 (1946).

54. Perkins, T. D., Ph.D. Thesis, University of Oklahoma, (1963).

55. Pease, R. N., J. Am. Chem. Soc., 51, 1839 (1929).

56. Pease, R. N., J. Am. Chem. Soc., 56, 2034 (1934).

57. Pease, R. N., J. Am. Chem. Soc., 57, 2296 (1935).

58. Pease, R. N., and P. R. Cheseboro, Proc. Nat. Acad. Sci., 14, 472 (1928).

59. Pope, J. C., E. J. Dykata, and G. Edgar, J. Am. Chem. Soc., 51, 1875, 2203 (1929).

60. Purnell, H., "Gas Chromatography," John Wiley and Sons, Inc., (1962).

61. Rise, F. O., and A. L. Glasebrook, J. Am. Chem. Soc., 56, 409 (1934).

62. Romijn, G., Z. Anal. Chem., 36, 18 (1897); 39, 60 (1900), (In reference 70).

63. Semenov, N. N., "Chain Reactions," Oxford University Press (1935), (In reference 64).

64. Semenov, N. N., "Some Problems of Chemical Kinetics and Reactivity," Pergamon Press, London (1959) (Translated from Russian).

65. Shtern, V. Ya., "The Gas-Phase Oxidation of Hydrocarbons," Pergamon Press, Ltd., Oxford, England (1964) (Translated from Russian).

66. Skinner, J. L., "Kinetic Study of the Formation of Cyclohexene from Ethylene and Butadiene at Elevated Pressures and Temperatures," Ph.D. Thesis, University of Oklahoma, (1962).

67. Slotin, L., and D. W. G. Style, Trans. Farad. Soc., 35, 420 (1939).

68. Smithells and H. Ingle, Trans. Chem. Soc., 61, 216 (1892), (In reference 65).

69. Sosnovsky, H. M. C., J. Chem. Phys., 23, 1486 (1955).

70. Sutton, F., "A Systematic Handbook of Volumetric Analysis," J. and A. Churchill, Ltd., (London), 383-85 (1935).

71. Timoshenko, S., and J. N. Goodier, "Theory of Elasticity," Second Edition, McGraw-Hill, New York, (1951).

72. Ubbelohde, A. R., Proc. Roy. Soc., A152, 354 (1935).

73. Van Meersche, M., Ann. Min. Belg., 47, 1053 (1949), (In ref. 65).

74. Vanpée, M., Ann. Min. Belg., 47, 1053 (1948).

75. Vanpée, M., and F. Grard, "Formaldehyde and Oxidation of Methane," Fuel, V34, N4, Oct., A33-43 (1955).

76. Vartanyan, L. S., Z. K. Maizus, and N. M. Emanuel, Zhur. fiz. khim., 30, 856 (1956), (In reference 64).

77. "Vascomax 250 and 300, 18% Nickel Ultra High Strength Maraging Steels," Vanadium-Alloys Steel Company, Labrobe, Pennsylvania.

78. Walling, C. T., and J. Pellon, "Organic Reactions Under High Pressure, Part III, The Polymerization of Allyl Acetate," J. Am. Chem. Soc., 79, 4782-86 (1957).

79. Whalley, E., and S. Morris, "The Design of Pressure Vessels Subjected to Thermal Stress - IV." Int. J. Mech. Sci., 1, 369-78 (1960).

80. Wiezevich, P. J., and P. K. Frolich, "Direct Oxidation of Saturated Hydrocarbons at High Pressure," Ind. Eng. Chem., V26, N3, 267-276 (1934).

81. Wilson, F. W., "The Challenge of Higher Pressures," Chem Eng. (Oct., 1962).

82. Winnick, J., "Liquid-Liquid Phase Behavior of Binary Solutions at Elevated Pressures," Ph.D. Thesis, University of Oklahoma, (1963).

83. Yenikolopyan, N. S., Zh. fiz. khim., 33, 642 (1959), (In reference 65).

84. Yoder, H. S., Carnegie Institution, Geophysical Laboratory, Washington, D. C., Personal Communication, (1965).

APPENDIX A

CHROMATOGRAPH CALIBRATION

Although gas chromatography provides a convenient method of sample analysis, the individual components must be identified and the concentration of each component has to be determined in some manner. Identification of components can be accomplished by either corresponding retention times or independent analytical methods such as infrared and mass spectroscopy. Obviously the latter methods provide more positive identification; however identification of components by corresponding retention times is satisfactory when the components of an unknown sample can be predicted either from previous experimental results or from reactions which are known to occur. In this study identification of reactants and products was accomplished by comparing the retention time of a separated component to that of the pure compound.

Conversion of the resulting chromatograms of the separated components into quantitative information is generally accomplished by peak area measurements although peak height measurements are satisfactory for some applications. Approximation of the component areas can be carried out by

measurement of peak heights and half-band widths, by dividing the peaks into trapezoids, or by using a planimeter. According to Knox (32) these methods are accurate to about one per cent if extreme care is taken in making the measurements.

For the gas analysis in this work a combination of the first two methods was used. The areas of the oxygen, nitrogen, and methane peaks were determined by the first method since these peaks were relatively sharp and symmetrical when eluted from the column packed with 5A molecular sieves. However area approximations using triangles and trapezoids were used for the carbon monoxide eluted from the column packed with 5A molecular sieves and the carbon dioxide eluted from the column packed with silica gel. The total area of the remaining components (carbon monoxide, oxygen, nitrogen, and methane) was also approximated by the latter method since these components were not completely resolved on the silica gel column.

The chromatograph calibration data for gas analysis are presented in Tables 6 and 7. The calibration curves are shown in Figures 49, 50, and 51.

Calibration of the chromatograph for liquid analysis was accomplished by using peak height ratios rather than area approximations. An attempt to use areas resulted in less reproducible results than peak height ratios. Normally chromatograph analyses using component peak heights for

TABLE 6

CHROMATOGRAPH CALIBRATION DATA FOR
CARBON MONOXIDE, OXYGEN, AND METHANE

Standard	Component Mole Per Cent[a]			Component Area Per Cent		
	Methane	Oxygen	Carbon Monoxide	Methane	Oxygen	Carbon Monoxide
G-I	97.95	2.05	---	97.64	2.36	---
				98.00	2.00	---
				97.47	2.53	---
				97.51	2.49	---
				97.57	2.43	---
				97.54	2.46	---
				97.63	2.37	---
				97.59	2.41	---
				97.75	2.25	---
				97.72	2.28	---
				97.72	2.28	---
				97.72	2.28	---
				97.65	2.35	---
G-II	97.68	0.69	1.61	97.41	1.17	1.42
				97.08	1.09	1.83
				97.09	1.05	1.86
				97.04	1.12	1.84
				97.32	1.07	1.61
				97.34	1.05	1.61
				97.27	1.06	1.67
				97.34	1.16	1.50
G-III	97.49	2.51	---	97.17	2.83	---

TABLE 6 (CONTINUED)

Standard	Component Mole Per Cent[a]			Component Area Per Cent		
	Methane	Oxygen	Carbon Monoxide	Methane	Oxygen	Carbon Monoxide
G-IV	96.70	---	3.30	97.28	---	2.72
				97.34	---	2.66
				97.11	---	2.89
				97.13	---	2.87
				97.35	---	2.65
G-IV	96.70	---	3.30	97.44	---	2.56
				97.32	---	2.68
G-V	96.32	---	3.68	96.34	---	3.66
G-VI	95.16	---	4.84	95.29	---	4.71
				95.15	---	4.85
				95.53	---	4.47
				95.24	---	4.76
				95.16	---	4.84
				95.37	---	4.63
G-VII	94.99	---	5.01	95.28	---	4.72
				95.70	---	4.30
				95.36	---	4.64
				95.34	---	4.66
G-VIII	93.47	3.12	3.41	93.85	2.96	3.19
				93.77	3.01	3.22
				93.96	2.92	3.12
G-IX	93.34	6.66	---	93.50	6.50	---
				93.53	6.47	---
				93.28	6.72	---
				93.29	6.71	---
				93.21	6.79	---
				93.36	6.64	---

TABLE 6 (CONTINUED)

Standard	Component Mole Per Cent[a]			Component Area Per Cent		
	Methane	Oxygen	Carbon Monoxide	Methane	Oxygen	Carbon Monoxide
G-X	92.81	6.78	0.38	92.27	7.10	0.63
				92.78	6.62	0.60
				92.27	7.21	0.52
				92.69	6.68	0.63
				92.25	7.11	0.64
G-XI	92.34	---	7.66	92.28	---	7.72
G-XII	90.47	9.53	---	90.08	9.92	---
				90.19	9.81	---
				90.22	9.78	---
				90.05	9.95	---
				89.95	10.05	---
				89.84	10.16	---
				90.21	9.79	---
				90.13	9.87	---
				90.25	9.75	---
				90.02	9.98	---
				90.43	9.57	---
				90.33	9.67	---
G-XIII	88.64	3.82	7.52	89.17	3.48	7.35
				89.25	3.46	7.29
				89.33	3.52	7.15
				89.12	3.48	7.40

[a] Carbon Dioxide-Free Basis - Carbon Dioxide is irreversibly adsorbed on molecular sieves.

Column - 8 feet of 5A Molecular Sieves (60/80 Mesh)
Column Temperature 33°C — Helium Flow Rate 90 Ml/Min
Cell Current 150 ma — Regulator Pressure 20 psig

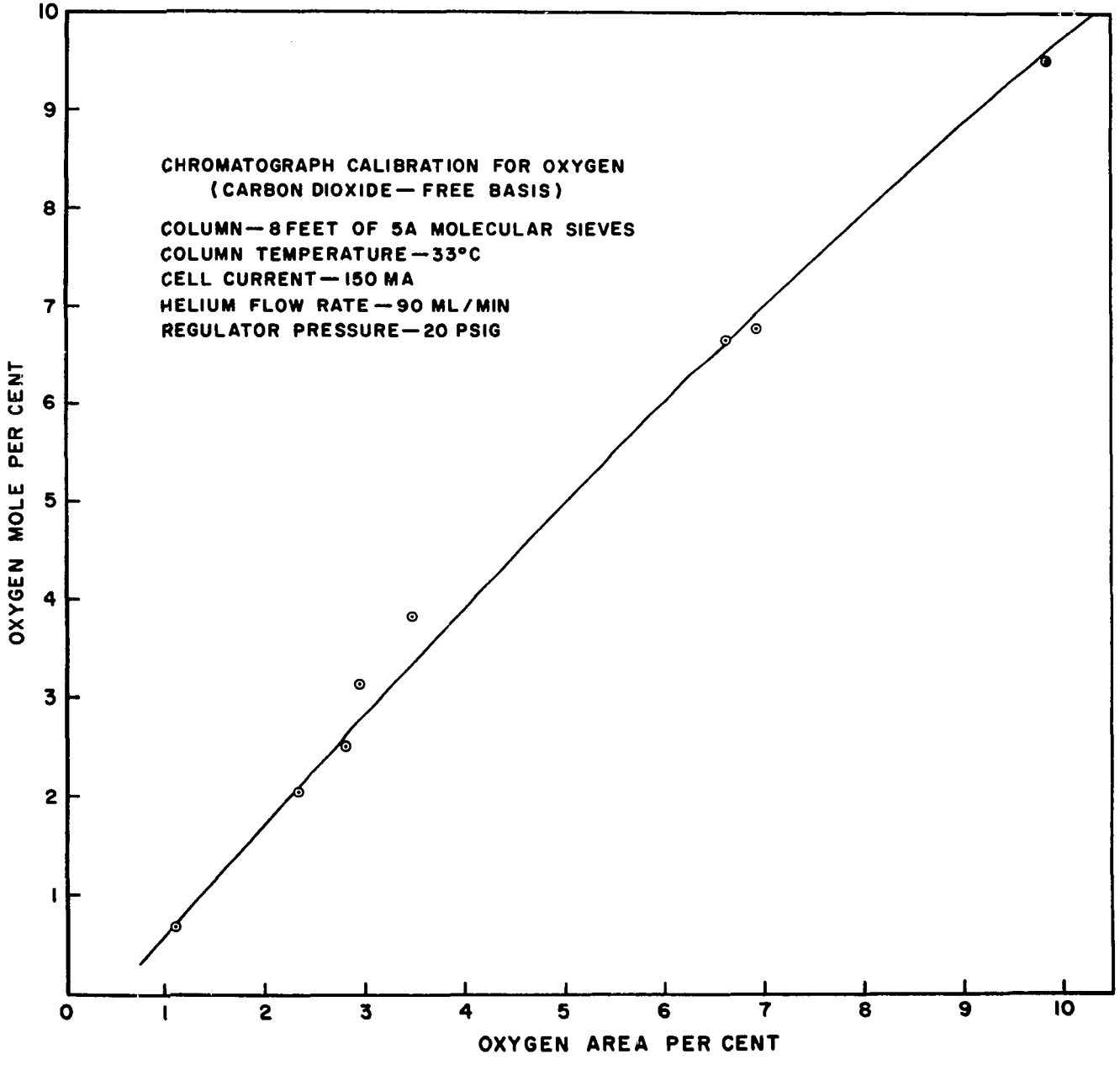

Figure 49. Chromatograph Calibration for Oxygen

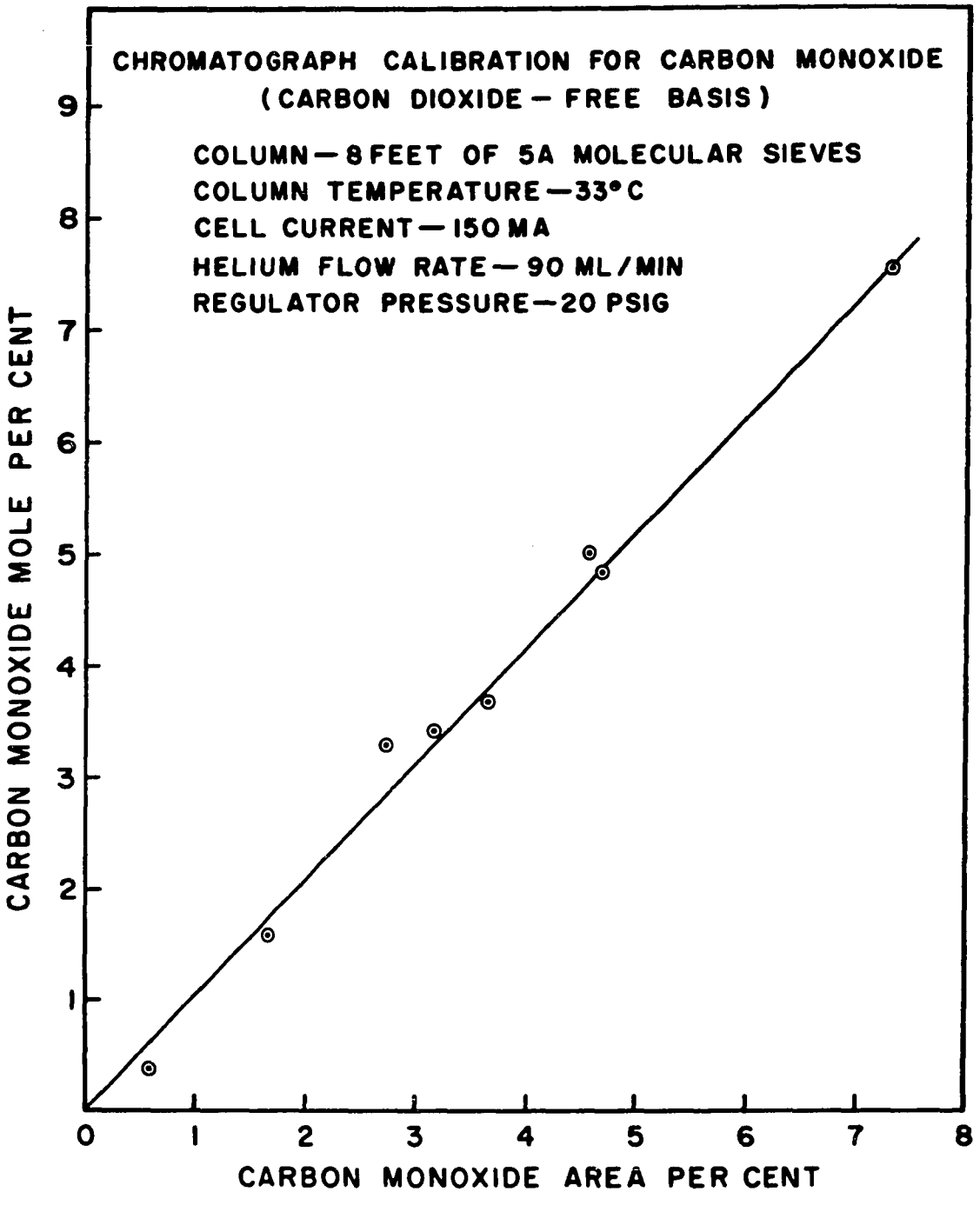

Figure 50. Chromatograph Calibration for Carbon Monoxide

TABLE 7

CHROMATOGRAPH CALIBRATION DATA
FOR CARBON DIOXIDE

Standard	Carbon Dioxide Mole Per Cent	Carbon Dioxide Area Per Cent
G-VI	1.47	1.14
		1.11
		1.26
		1.00
G-X	1.72	1.24
		1.12
		1.31
		1.15
G-VIII	2.44	2.67
		2.74
G-II	3.27	3.23
		3.25
		3.08
G-IV	3.62	3.47
		3.40
		3.16
		3.44
G-XIV	6.96	6.61
		6.71
		6.21
G-XIII	7.22	7.43
		7.49
		7.17
		7.29
G-XI	7.56	8.41
G-VII	8.40	8.53
		8.46
		8.29
		8.33
G-XV	8.46	9.12
		8.65
		8.68
		8.50

Column	8 Feet of Silica Gel (180/200 Mesh)
Column Temperature	80°C
Cell Current	150 ma
Helium Flow Rate	60 Ml/Min
Regulator Pressure	34 psig

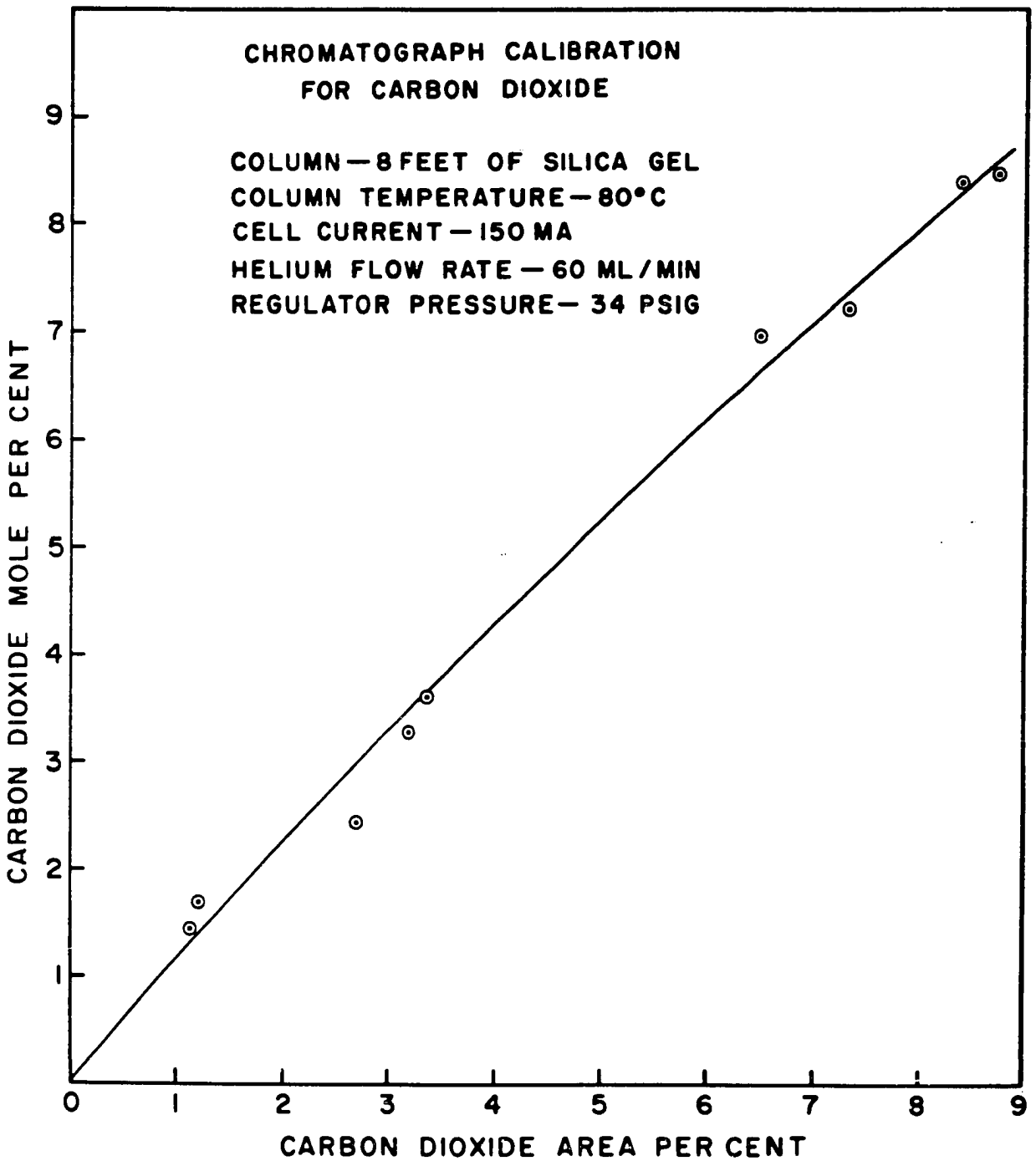

Figure 51. Chromatograph Calibration for Carbon Dioxide

quantitative analyses require sharp, symmetrical peaks. Methyl alcohol and methyl formate exhibited relatively sharp, symmetrical peaks with little or no tailing. On the other hand water exhibited a much stronger tailing tendency than the methyl alcohol and methyl formate. Although water does have this tailing, the use of peak height ratios provided a satisfactory means for the liquid analyses.

The chromatograph calibration data for liquid analyses are presented in Tables 8 and 9. Calibration curves are presented in Figures 52 and 53.

TABLE 8

CHROMATOGRAPH CALIBRATION DATA
FOR METHANOL

Standard	Methanol Weight Per Cent	Methanol-Water Peak Height Ratio
L-I	7.51	0.62
L-II	10.09	0.87
		0.87
L-III	11.11	1.00
		0.94
L-IV	12.19	1.16
		1.21
L-V	15.51	1.49
		1.53
		1.37
		1.37
		1.43
		1.36
		1.35
		1.32
		1.38
		1.44
		1.50
		1.59
		1.44
		1.39
		1.44
L-VI	20.85	2.18
		2.22
		2.00
		1.96
		2.28
		2.07
		1.96
		1.90
		1.94
		2.04
		2.06
		1.91
		1.93
		2.11
		2.04
		1.90
		1.94
		2.01
		2.05

TABLE 8 (CONTINUED)

Standard	Methanol Weight Per Cent	Methanol-Water Peak Height Ratio
L-	29.75	3.53
		3.54
		3.17
		3.10
		3.24
		3.17
		3.22
		3.16
		3.38
		3.44
L-VIII	39.62	4.49
		4.71
		4.60
		4.65
		4.82
L-IX	49.92	6.84

Column	8 Feet of 30% Diglycerol on Chromosorb W
Column Temperature	120°C
Cell Current	150 ma
Helium Flow Rate	110 Ml/min
Regulator Pressure	20 psig

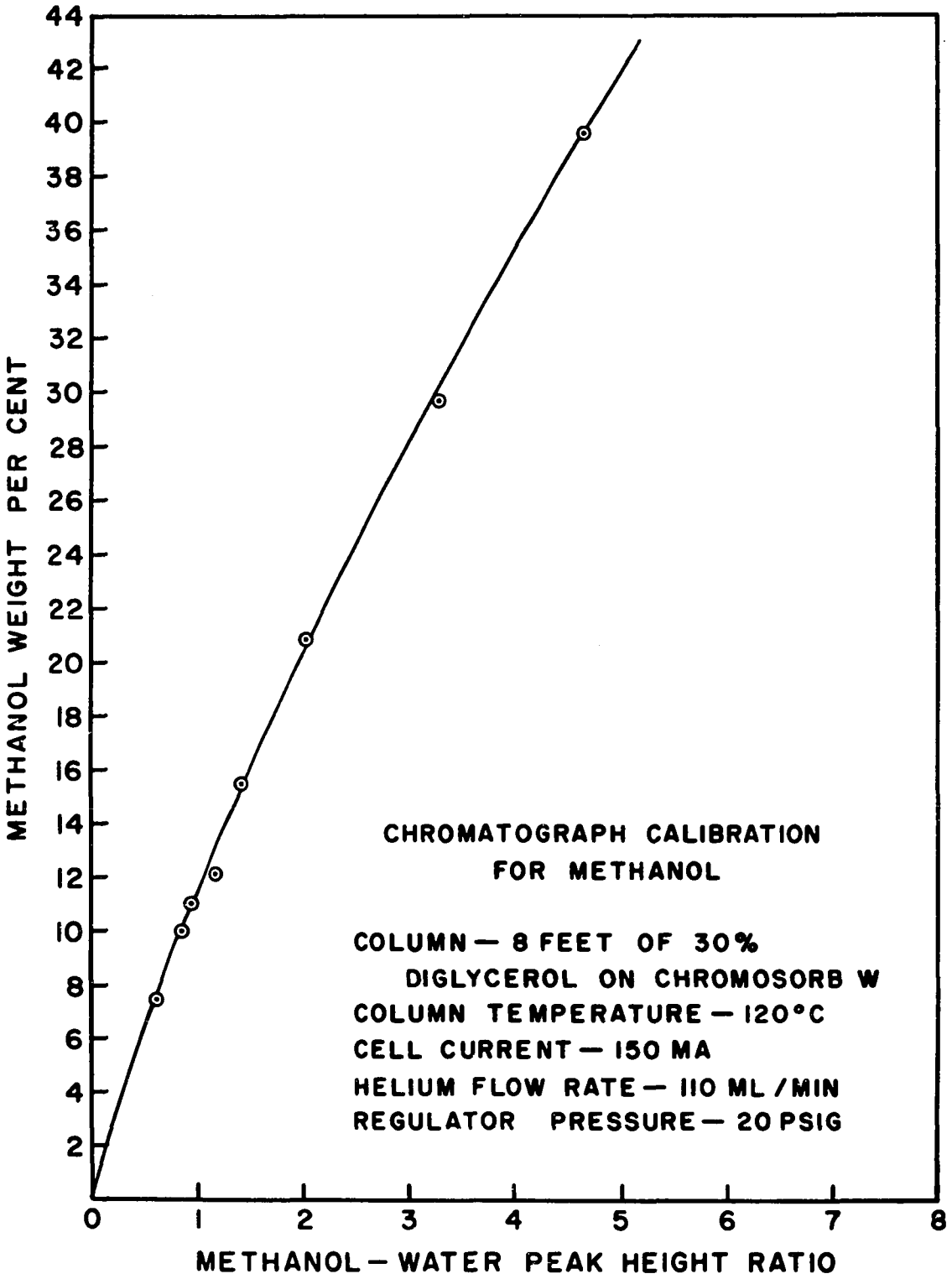

Figure 52. Chromatograph Calibration for Methanol

TABLE 9

CHROMATOGRAPH CALIBRATION DATA
FOR METHYL FORMATE

Standard	Methyl Formate Weight Per Cent	Methyl Formate-Water Peak Height Ratio
L-III	1.23	0.155
		0.138
L-II	2.45	0.372
		0.354
L-X	3.45	0.595
L-IV	4.85	0.881
		0.903

Column	8 Feet of 30% Diglycerol on Chromosorb W
Column Temperature	120°C
Cell Current	150 ma
Helium Flow Rate	110 Ml/Min
Regulator Pressure	20 psig

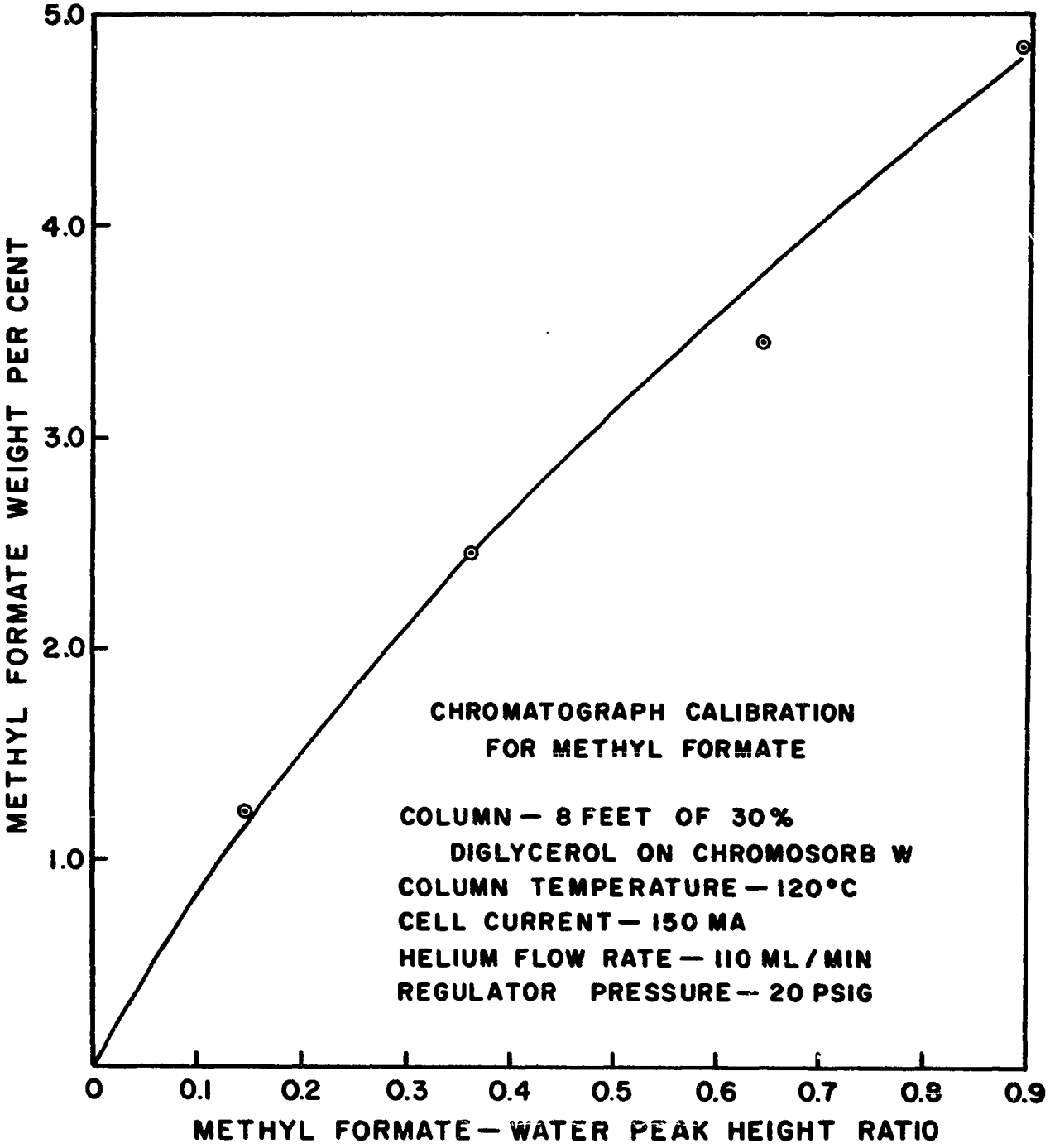

Figure 53. Chromatograph Calibration for Methyl Formate

APPENDIX B

VOLUMETRIC ANALYSIS

Since a satisfactory quantitative analysis for formaldehyde and formic acid could not be obtained with the available gas chromatograph, volumetric analyses were used for these reaction products. Although the volumetric analyses used are not specific for these compounds, qualitative analyses on the chromatograph indicated that formaldehyde and formic acid were the only members of the aldehyde compounds and acid compounds present.

Romijn's iodimetric method (62) was used to determine the formaldehyde concentration; however there are several other processes available for the determination of formaldehyde. The iodimetric method was selected because this method is very accurate and methyl alcohol, formic acid, and acetic acid do not alter the results (70). Analysis of the liquid products by gas chromatography indicated that methyl formate was also formed during the partial oxidation of methane at high pressures. It is logical to assume that methyl formate will not influence the formaldehyde determination either since it is a product of the reaction between formic acid and methyl alcohol. However to insure that methyl formate, as well as

methyl alcohol and formic acid, do not influence the results, known formaldehyde solutions containing the above compounds were analyzed. The results of these tests, presented in Table 10, indicated that formaldehyde solutions containing these compounds did not interfere with the formaldehyde determinations.

The procedure for the iodimetric analysis is briefly described below. The liquid sample, weighed to the nearest tenth of a milligram (approximately one milliliter of sample was used), was diluted with 25 milliliters of distilled water. The dilute solution was mixed with 25 milliloters of 0.1 N-iodine solution from a burette. A 4 N-sodium hydroxide solution was added dropwise until the liquid became a clear yellow. After approximately 10 minutes hydrochloric acid was added to liberate unreacted iodine. The liberated iodine was then titrated with a 0.1 N-sodium thiosulfate solution. Freshly prepared starch solution was used as the indicator. It was not added until the end-point was almost reached.

The formic acid concentration was determined by neutralization with sodium hydroxide since the ionization constant of formic acid (2.2×10^{-4}) is large enough to make this analysis feasible. Even though neutralization determines the total acid concentration, there are several reasons for reporting the results as formic acid. First, Newitt and Haffner (45) analyzed the products of the slow combustion of methane at intermediate pressures for total acids and, in

particular, for formic acid. The results of their analyses indicated that formic acid was the only acid present. Second, as mentioned above, a qualitative analysis by gas chromatography indicated that formic acid was the only acid present in the reaction products obtained in this study. Third, quantitative analysis by gas chromatography indicated that methyl alcohol was the only alcohol present in the reaction products, and methyl formate was the only ester present in the reaction products.

The reproducibility of the neutralization process is shown in Table 11. For the high concentrations of formic acid, the results were not as good as hoped; however these results were anticipated since extremely small samples were required to keep the consumption of sodium hydroxide solution below 50 milliliters. The results for low concentrations of formic acid were very good.

TABLE 10

INFLUENCE OF METHANOL, FORMIC ACID, AND METHYL FORMATE ON FORMALDEHYDE DETERMINATION

Sample No.	Sample Wt. Grams	CH_3OH Wt. Grams	HCOOH Wt. Grams	$HCOOCH_3$ Wt. Grams	HCHO Wt. Grams	
					Actual	Found
1	0.7869	0.0762	---	---	0.0183	0.0183
2	0.9882	0.0957	---	---	0.0230	0.0231
3	0.9965	0.0748	---	---	0.0212	0.0212
4	1.0809	0.0713	0.0874	---	0.0202	0.0203
5	1.0753	0.0637	0.1116	0.1011	0.0181	0.0180
6	1.0455	0.0704	---	0.1083	0.0200	0.0201

TABLE 11

REPRODUCIBILITY OF FORMIC ACID DETERMINATION BY NEUTRALIZATION

Sample No.	Sample Weight Grams	Formic Acid Weight Grams	
		Actual	Found
1	0.1031	0.0911	0.0854
2	0.1001	0.0885	0.0896
3	0.1041	0.0920	0.0839
4	0.9729	0.0197	0.0198
5	0.9709	0.0197	0.0198
6	0.9740	0.0198	0.0196

APPENDIX C

MANGANIN PRESSURE GAUGE CALIBRATION

The manganin pressure gauge and Foxboro recorder were calibrated by Jack Winnick (82). Another manganin coil which had previously been calibrated against the freezing points of mercury was used to calibrate the manganin pressure gauge and recorder simultaneously. The two manganin coils were connected to a common pressure apparatus. The recorder scale reading was calibrated against the resistance of the standard manganin coil which was measured on a Mueller bridge. According to Winnick the results indicated that the recorder reading was a linear function of the applied pressure. The results were reproducible on each of the 3 ranges of the recorder (50,000, 100,000, and 200,000 psi) to 0.25 per cent of the maximum scale reading. The results of this calibration are shown in Figure 54.

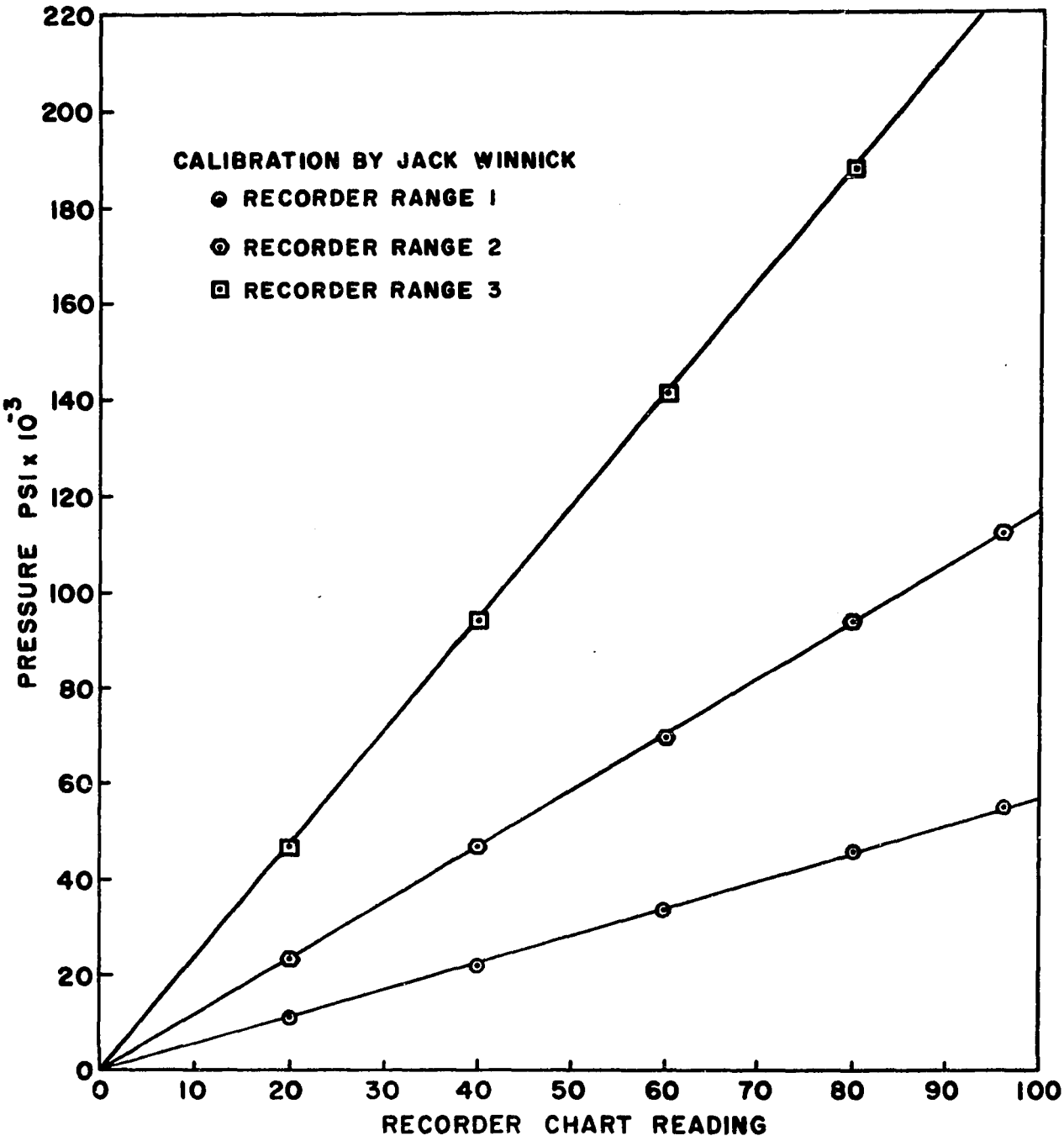

Figure 54. Calibration of Manganin Pressure Cell and Recorder

APPENDIX D

SUMMARY OF EXPERIMENTAL DATA

TABLE 12

SUMMARY OF EXPERIMENTAL RESULTS AT ELEVATED PRESSURES
METHANE-OXYGEN RATIO--10:1
REACTOR--19-9DL STAINLESS ALLOY

Run No. JLL	Initial Temp. °F	Initial Pressure psig	Residence Time[a] Minutes	Yield as Per Cent of Reacted Methane						Total Organic Liquid	Oxygen Conversion %	Methane Conversion %
				CH_3OH	HCHO	HCOOH	$HCOOCH_3$	CO	CO_2			
164	642	1800	23.0	22.64	0.84	---	---	41.99	27.69	23.48	68.28	5.05
162	641	1900	27.0	20.72	0.62	---	---	49.26	31.98	21.34	68.23	5.38
160	641	2040	33.0	20.83	0.62	---	---	46.50	25.93	21.45	63.72	5.05
158	645	2190	18.5	17.84	0.70	---	---	53.39	30.39	18.54	73.00	5.70
						5400 PSI						
232	584	5400	90.0	15.97	0.70	0.99	0.84	38.65	53.55	18.50	81.39	3.90
174	586	5380	76.5	16.02	0.61	0.63	---	40.26	45.78	17.26	72.75	4.58
175	592	5400	40.3	18.07	0.76	0.78	---	41.64	41.31	19.61	72.47	4.60
207	592	5420	34.5	18.52	0.86	0.60	---	44.30	47.21	19.98	73.14	4.81
177	592	5380	33.0	17.88	0.86	0.70	---	41.72	34.49	19.44	71.77	4.30
208	595	5150	29.5	19.56	0.99	0.64	---	44.85	42.01	21.19	71.65	4.82
206	605	5380	11.3	21.92	1.17	0.38	---	48.71	33.29	23.43	70.60	5.50
173	610	5500	9.5	21.05	0.91	0.70	---	49.84	34.24	22.66	62.72	4.15
205	610	5440	8.6	14.09	0.75	0.25	---	54.75	31.01	15.09	66.95	4.60
176	622	5380	5.3	25.04	0.71	0.80	---	47.80	29.55	26.55	65.47	4.50
						7000 PSI						
185	564	6940	88.0	14.92	0.68	2.09	0.44	32.83	46.16	18.13	82.40	5.20
230	569	6980	141.0	14.73	0.64	1.42	1.14	37.34	57.36	17.93	86.13	5.46
186	572	6960	41.5	15.08	0.75	3.03	1.09	34.76	51.02	19.95	78.58	4.97
223	573	6980	115.0	15.82	0.46	1.46	1.09	33.76	48.75	18.83	84.24	5.18
222	574	6970	54.7	16.11	1.06	3.28	3.40	33.09	51.74	23.85	77.30	5.18
184	574	6920	37.0	15.27	0.80	1.52	1.78	29.89	47.47	19.37	73.08	4.64
224	575	6970	77.8	17.27	0.64	1.39	1.37	34.52	48.96	20.67	79.78	5.78
226	575	6990	80.0	15.95	0.74	1.95	1.87	39.65	50.63	20.51	82.91	5.48
225	577	6970	53.2	16.82	0.86	2.25	2.28	32.82	48.82	22.21	80.90	5.30
181	578	6950	29.8	19.20	1.07	2.48	1.58	33.62	36.00	24.33	78.35	5.23
182	579	6950	32.5	23.16	0.93	2.88	3.66	30.55	40.09	30.63	72.85	5.20
231	585	6940	24.0	22.61	0.88	1.58	0.83	36.03	40.23	25.90	76.10	5.22
227	588	7000	18.3	23.40	0.98	1.88	2.87	43.76	38.01	29.13	67.02	4.96
178	590	6880	16.3	18.14	1.11	2.99	---	36.51	41.75	22.24	68.60	4.24
228	593	6980	13.0	23.51	1.08	1.86	2.96	49.46	35.40	29.41	73.52	5.53
229[b]	601	6990	6.8	---	---	---	---	---	---	---	---	---
183	606	6940	4.0	26.64	1.08	1.27	1.72	38.46	31.39	30.71	70.40	5.01
179	608	7000	---	26.08	1.17	0.97	---	62.26	16.62	28.22	69.55	5.70

TABLE 12 (CONTINUED)

Run No. JLL	Initial Temp. °F	Initial Pressure psig	Residence Time[a] Minutes	Yield as Per Cent of Reacted Methane						Total Organic Liquid	Oxygen Conversion %	Methane Conversion %
				CH_3OH	HCHO	HCOOH	$HCOOCH_3$	CO	CO_2			
10,000 PSI												
191	553	9900	119.5	12.70	0.54	4.54	2.32	22.82	53.00	20.10	89.98	5.22
194	562	9970	68.7	14.08	0.70	4.32	3.06	34.96	59.59	22.16	86.23	6.04
192	563	9990	51.5	19.47	0.90	3.44	2.61	34.03	58.03	26.42	84.10	6.61
203	568	9900	52.0	15.31	0.67	3.95	3.38	31.14	52.09	23.31	81.54	5.07
220	569	9990	41.5	15.31	0.81	3.55	5.03	23.16	52.46	24.70	76.50	4.90
218	573	9950	30.2	16.61	1.02	5.67	5.41	30.40	53.99	28.71	76.41	5.27
221	575	9970	26.7	17.35	0.84	5.90	5.76	24.28	50.03	29.85	78.83	5.31
204	576	9880	23.5	16.81	0.69	1.32	3.22	29.22	49.27	22.04	74.25	4.99
219	587	9960	8.9	24.81	1.07	3.05	5.30	39.13	32.19	34.23	70.84	5.35
193	588	9950	5.2	20.00	0.83	2.27	2.63	37.92	34.88	25.73	72.74	5.59
15,000 PSI												
198	554	14900	125.5	15.63	0.47	2.94	2.58	7.42	56.78	21.62	88.04	4.24
197	554	15000	112.0	13.57	0.57	6.01	3.62	21.76	56.77	23.77	90.39	5.33
214	560	14900	60.8	12.51	0.72	6.71	5.01	19.90	63.45	24.96	83.10	5.72
199	566	14950	34.8	15.51	0.58	4.18	3.72	21.02	63.96	23.99	84.86	4.80
215	569	14900	26.6	16.44	0.79	6.16	6.14	23.24	52.20	29.53	81.64	5.75
200	572	14950	22.8	22.42	0.68	3.13	4.97	25.72	46.12	31.20	75.30	4.95
213	575	14850	19.0	15.20	0.84	4.62	4.03	25.98	53.87	24.69	77.00	5.04
217	576	14750	14.9	19.32	0.85	4.83	5.69	25.94	44.11	30.69	77.53	5.45
202	582	14900	13.7	28.96	0.86	1.91	3.42	23.65	42.29	35.15	81.00	5.99
216	596	14450	---	26.20	1.04	1.12	2.57	48.68	21.53	30.93	79.33	6.59
290[c]	---	16000	---	33.90	0.96	0.74	---	57.54	25.08	35.60		

a. Defined as the elapsed time between completion of charge and the maximum temperature
b. Gas sample bomb leaked
c. Run made in 200,000 psi system -- 18% nickel maraging steel reactor

TABLE 13

SUMMARY OF ANALYTICAL RESULTS

Run No. JLL	Gas Product Composition Mole Per Cent[a]				Liquid Product Composition Weight Per Cent					Material Balances			Gram-Moles of Water Determined by			
	O_2	CO	CO_2	CH_4	CH_3OH	HCHO	HCOOH	$HCOOCH_3$	H_2O	O_2	H_2	C	O_2	H_2	Products	Analysis
164	3.42	2.25	1.70	92.63	21.44	0.75	---	---	77.81	0.981	1.003	0.986	0.1325	0.1168	0.1207	0.1260
162	3.42	2.55	1.84	92.19	20.23	0.57	---	---	79.20	0.986	0.996	1.001	0.1287	0.1351	0.1385	0.1236
160	3.89	2.25	1.47	92.39	19.39	0.55	---	---	80.06	0.979	0.999	0.997	0.1431	0.1388	0.1281	0.1348
158	2.92	2.84	1.84	92.40	16.70	0.62	---	---	82.68	0.984	0.996	0.999	0.1657	0.1730	0.1709	0.1593
							5400 PSI									
232	1.82	1.86	2.77	93.55	14.42	0.60	1.29	0.72	82.97	0.995	1.010	1.016	0.3497	0.2579	0.3950	0.3457
174	2.58	1.79	2.25	93.38	15.18	0.55	0.86	---	83.41	0.993	0.998	1.002	0.3153	0.3283	0.3414	0.3086
175	2.61	1.86	2.06	93.47	16.49	0.65	1.03	---	81.83	0.992	0.999	1.004	0.3209	0.3198	0.3291	0.3144
207	2.54	1.91	2.25	93.30	17.71	0.77	0.83	---	80.69	0.975	0.994	1.002	0.3132	0.3331	0.3434	0.2821
177	2.67	1.93	1.81	93.59	16.48	0.75	0.93	---	81.84	0.989	1.004	1.003	0.3327	0.3149	0.2922	0.3233
208	2.68	1.96	2.05	93.31	18.76	0.89	0.89	---	79.46	0.974	0.994	1.001	0.2871	0.3112	0.3161	0.2660
206	2.80	2.23	1.74	93.23	19.70	0.99	0.50	---	78.81	1.004	0.992	0.994	0.3071	0.3754	0.3287	0.3100
173	3.46	1.99	1.58	92.97	19.64	0.80	0.94	---	78.62	0.989	0.999	1.003	0.2735	0.2813	0.3053	0.2698
205	3.11	2.43	1.59	92.87	14.21	0.71	0.37	---	84.71	0.995	0.995	1.012	0.2953	0.3355	0.3322	0.2908
176	3.26	2.08	1.50	93.16	22.86	0.61	1.05	---	75.48	0.994	1.000	1.002	0.2869	0.2990	0.2841	0.2818
							7000 PSI									
185	1.67	1.68	2.58	94.07	13.35	0.57	2.69	0.37	83.02	1.002	0.999	0.998	0.4528	0.4594	0.4435	0.4543
230	1.39	1.89	3.10	93.62	13.28	0.54	1.84	0.97	83.37	0.994	0.996	1.003	0.4417	0.4732	0.5084	0.4346
186	2.05	1.61	2.58	93.76	13.38	0.63	3.87	0.91	81.21	0.995	1.020	1.000	0.4132	0.4392	0.4420	0.4083
223	1.57	1.72	2.68	94.03	13.50	0.37	1.79	0.88	83.46	0.990	1.002	1.000	0.4787	0.4850	0.4522	0.4680
222	2.25	1.57	2.65	93.53	14.15	0.88	4.14	2.80	78.03	0.966	1.000	1.008	0.4084	0.4426	0.4528	0.4037
184	2.56	1.35	2.36	93.73	13.64	0.67	1.95	1.49	82.25	0.955	1.005	1.010	0.3935	0.4016	0.3856	0.3980
224	2.01	1.73	2.65	93.61	15.67	0.55	1.81	1.17	80.80	0.991	0.993	0.996	0.4323	0.5019	0.4545	0.4229
226	1.70	2.00	2.75	93.55	14.24	0.62	2.50	1.57	81.07	0.995	0.996	1.005	0.4383	0.4735	0.4962	0.4333
225	1.90	1.67	2.68	93.75	14.94	0.72	2.87	1.90	79.57	0.992	0.998	1.000	0.4313	0.4427	0.4519	0.4273
181	2.08	1.73	2.07	94.12	16.48	0.86	3.06	1.27	78.33	0.952	1.008	1.004	0.4431	0.4331	0.3994	0.3888
182	2.60	1.45	2.12	93.83	19.57	0.74	3.50	1.71	74.48	1.014	0.999	0.996	0.3816	0.4100	0.3729	0.3987
231	2.37	1.84	2.25	93.54	20.46	0.75	2.06	0.71	76.02	0.995	1.000	1.001	0.4179	0.4176	0.4296	0.4122
227	3.24	1.93	1.87	92.96	20.81	0.82	2.41	2.40	73.56	0.971	0.999	1.007	0.3489	0.3915	0.4005	0.3484
178	2.97	1.50	1.93	93.60	15.36	0.88	3.64	---	80.12	0.996	1.002	1.000	0.3725	0.3486	0.3507	0.3678
228	2.62	2.41	1.92	93.05	20.98	0.91	2.39	2.48	73.24	0.997	0.994	1.002	0.3837	0.4599	0.4583	0.3812
229[b]	---	---	---	---	---	---	---	---	---	---	---	---	---	---	---	---
183	2.82	1.88	1.75	93.55	24.35	0.93	1.67	1.40	71.65	0.996	0.999	1.000	0.3678	0.3715	0.3745	0.3630
179	2.89	3.09	1.04	92.98	23.96	1.01	1.28	---	72.47	1.004	0.993	0.998	0.3815	0.4424	0.4286	0.3741

TABLE 13 (CONTINUED)

Run No. JLL	Gas Product Composition Mole Per Cent[a]				Liquid Product Composition Weight Per Cent					Material Balances			Gram-Moles of Water Determined by			
	O_2	CO	CO_2	CH_4	CH_3OH	HCHO	HCOOH	$HCOOCH_3$	H_2O	O_2	H_2	C	O_2	H_2	Products	Analysis
10,000 PSI																
191	0.97	1.18	2.96	94.89	10.28	0.41	5.28	1.76	82.27	1.000	1.004	0.998	0.6530	0.5956	0.5666	0.6449
194	1.33	1.69	3.10	93.88	11.87	0.56	5.23	2.42	79.92	1.013	0.990	0.997	0.5429	0.6991	0.6336	0.5595
192	1.54	1.66	3.05	93.75	16.27	0.71	4.13	2.05	76.84	1.024	0.985	0.992	0.5177	0.7498	0.6419	0.5499
203	1.79	1.55	2.81	93.85	14.04	0.58	5.20	2.91	77.27	1.026	0.994	1.000	0.5161	0.5491	0.5936	0.5105
220	2.33	1.11	2.71	93.85	13.29	0.66	4.43	4.09	77.53	0.997	1.000	1.000	0.5251	0.5238	0.5265	0.5312
218	2.34	1.41	2.71	93.54	14.18	0.82	6.95	4.33	73.72	0.999	0.994	1.001	0.4907	0.5614	0.5736	0.4875
221	2.11	1.22	2.71	93.96	14.77	0.67	7.22	4.60	72.74	0.998	0.998	1.000	0.5240	0.5513	0.5526	0.5218
204	2.45	1.42	2.61	93.52	16.81	0.65	1.90	3.02	77.62	0.993	0.994	1.000	0.4650	0.5368	0.5401	0.4600
219	2.89	1.95	1.80	93.36	21.72	0.88	3.84	4.35	69.21	1.000	0.997	1.000	0.4803	0.5145	0.5182	0.4796
193	2.60	2.07	2.12	93.21	21.39	0.83	3.50	2.64	71.64	1.083	0.980	0.982	0.4429	0.5761	0.5652	0.4454
15,000 PSI																
198	1.15	0.39	3.20	95.26	13.71	0.39	3.71	2.12	80.07	0.962	1.011	1.003	0.8160	0.5614	0.6203	0.7500
197	0.93	1.15	3.22	94.70	11.57	0.46	7.36	2.89	77.72	0.990	1.000	1.001	0.7760	0.7619	0.7826	0.7593
214	1.69	0.97	3.29	94.05	10.49	0.57	8.10	3.94	76.90	1.002	0.992	0.996	0.6803	0.8129	0.7499	0.6836
199	1.45	0.99	3.23	94.33	13.66	0.48	5.29	3.07	77.50	0.973	0.999	1.004	0.6926	0.7618	0.7358	0.6459
215	1.84	1.23	2.96	93.97	14.11	0.64	7.60	4.94	72.71	1.029	0.995	1.000	0.6632	0.7680	0.7451	0.6849
200	2.36	1.06	2.67	93.91	20.72	0.59	4.16	4.31	70.22	0.989	0.997	1.002	0.5938	0.6230	0.6547	0.5756
213	2.28	1.28	2.85	93.59	13.92	0.72	6.08	3.46	75.82	1.002	0.997	1.002	0.6209	0.6773	0.7157	0.6236
217	2.24	1.39	2.56	93.81	17.53	0.72	6.30	4.84	70.61	0.999	0.997	1.000	0.6412	0.6931	0.6999	0.6400
202	1.84	1.32	2.58	94.26	25.72	0.72	2.44	2.85	68.27	1.002	0.997	0.997	0.6668	0.7304	0.6774	0.6700
216	2.07	3.17	1.60	93.16	26.49	0.99	1.63	2.44	68.45	1.001	0.993	1.001	0.6586	0.7425	0.7951	0.6600
290	0.68	3.36	1.70	94.26	31.41	0.84	0.99	---	66.76	1.031	0.983	0.995	0.4564	0.7101	0.6298	0.4915
50,000 PSI																
238	0.69	1.07	2.80	95.44	18.53	0.38	1.03	---	80.06	0.966	1.011	1.010	0.9178	0.7627	0.7414	0.8071
240	6.22	---	1.30	92.48	4.86	0.46	0.33	---	94.35	1.048	1.000	1.000	0.2325	0.2744	0.2383	0.2678
242	0.29	2.48	2.55	94.68	30.36	0.51	0.59	---	68.54	1.035	0.998	1.005	0.8320	0.9133	0.9703	0.8511
246	0.36	0.49	4.30	94.85	10.44	0.14	1.34	---	88.08	1.034	0.995	1.002	0.8141	0.9431	0.9432	0.8329
254	0.89	1.84	0.53	95.74	26.45	0.70	1.33	---	71.52	0.998	1.000	1.002	0.6701	0.6636	0.6573	0.6487
252	6.15	0.17	---	93.68	1.98	0.35	0.48	---	97.19	0.989	1.004	1.000	0.1309	0.0400	0.3447	0.1161
258	0.36	2.77	1.97	94.90	36.48	0.55	0.59	---	62.38	1.024	0.985	1.004	0.5701	0.8822	0.9409	0.5862
260	5.73	0.23	1.15	92.89	3.47	0.41	0.44	---	95.68	1.027	0.991	0.999	0.1210	0.1135	0.2414	0.1212
248	0.39	2.73	1.95	94.93	29.55	0.61	0.57	---	69.27	1.045	1.002	1.004	0.9148	0.8674	0.9141	0.9110
262	5.75	0.23	0.93	93.09	3.66	0.49	0.57	---	95.28	1.031	0.994	0.998	0.1440	0.1368	0.2290	0.1739
264	3.45	0.51	1.96	94.08	2.85	0.29	0.55	---	96.31	1.034	0.995	0.998	0.4044	0.5420	0.4903	0.4370
256	0.30	2.21	1.57	95.92	33.95	0.68	1.21	---	64.16	0.992	1.000	1.005	0.7021	0.6636	0.7477	0.6708

TABLE 13 (CONTINUED)

Run No. JLL	Gas Product Composition Mole Per Cent[a]				Liquid Product Composition Weight Per Cent					Material Balances			Gram-Moles of Water Determined by			
	O_2	CO	CO_2	CH_4	CH_3OH	HCHO	HCOOH	$HCOOCH_3$	H_2O	O_2	H_2	C	O_2	H_2	Products	Analysis
96,000 - 200,000 PSI																
268	7.06	---	0.20	92.74	---	---	---	---	---	0.998	0.999	1.001	---	---	---	---
266	6.75	---	0.26	92.99	3.02	0.20	0.90	---	95.88	1.003	1.001	1.000	0.0974	0.0228	0.0450	0.0820
270	6.22	0.08	0.61	93.09	---	0.01	1.35	---	98.64	1.019	1.000	1.001	0.1452	0.1590	0.1594	0.1581
272	7.42	---	0.15	92.43	---	---	---	---	---	---	---	---	---	---	---	---
280	6.40	---	0.44	93.16	4.56	0.11	0.78	---	94.55	0.994	1.003	1.002	0.1724	0.0598	0.1103	0.1589
282	6.03	---	0.72	93.25	3.29	0.24	1.53	---	94.94	0.997	1.002	1.002	0.1989	0.1334	0.1901	0.1913
284	6.20	---	0.82	92.98	4.99	0.31	2.71	---	91.99	0.998	1.000	1.002	0.1553	0.1565	0.2142	0.1513
288	6.73	---	0.01	93.26	5.11	0.17	3.34	---	91.38	0.997	1.001	1.002	0.1427	0.1008	0.1593	0.1360
292[c]	6.09	---	1.15	92.76	3.38	6.15	13.44	4.37	77.03	1.001	0.998	1.003	0.0820	0.2210	0.2941	0.1657

a. Nitrogen free basis
b. Gas sample bomb leaked
c. Contaminated with hydraulic fluid

APPENDIX E

SAMPLE CALCULATIONS

Run No. JLL-220 Date: 9/2/64

Overall Material Balance

Reactants:

Reactor Pressure: 680 atm Reactor Volume: 683 c.c.

Reactor Temperature: 572°K Compressibility Factor: 1.327 (From API Project 44)

$$\text{Moles Reactsnts} = \frac{(680 \text{ atm})(683 \text{ c.c})}{(1.327)(82.06 \text{ atm-cc/gm-mole - °K})(572°K)}$$

$$= 7.4544 \text{ gm-moles}$$

Components		Moles	Grams
Oxygen:	(7.4544 gm-moles)(0.0913)	0.6798	21.7536
Methane:	(7.4544 gm-moles)(0.8999)	6.7082	107.3312
CO_2:	(7.4544 gm-moles)(0.0018)	0.0134	0.5896
Nitrogen:	(7.4544 gm-moles)(0.0071)	0.0529	1.4812
Total:		7.4543	131.1556

Products:

Product Receiver:

Pressure: 11.1 atm Volume: 14200 c.c.

Temperature: 293°K Compressibility Factor: 0.981 (From API Project 44)

$$\text{Moles Gas Product} = \frac{(11.1 \text{ atm})(14200 \text{ c.c.})}{(0.981)(82.06 \text{ atm-cc/gm-moles-°K})(293°K)}$$

$$= 6.6780 \text{ gm-moles}$$

Reactor:

Pressure: 11.1 atm Volume: 683 c.c.

Temperature: 573°K Compressibility Factor: 1.002 (From API Project 44)

$$\text{Moles Gas Product} = \frac{(11.1 \text{ atm})(683 \text{ cc})}{(1.002)(82.06 \text{ atm-cc/gm-moles-°K})(573°K)}$$

Total Moles of Gas Product = 6.6780+0.1608 = 6.8388 gm-moles

Components		Grams	Wt.%
Oxygen:	(6.8388 gm-moles)(0.0233)(32)	5.0990	4.29
CO:	(6.8388 gm-moles)(0.0111)(28)	2.1255	1.79
CO_2:	(6.8388 gm-moles)(0.0271)(44)	8.1546	6.87
Methane:	(6.8388 gm-moles)(0.9305)(16)	101.8151	85.76
Nitrogen:	(6.8388 gm-moles)(0.0080)(28)	1.5319	1.29
Total:		118.7271	100.00

Liquid Products:

Gross Weight	53.8915
Tare Weight	43.1174
Net Weight	10.7741 grams.

Components		Gram-Moles
Formaldehyde:	(10.7741 gm)(0.0066)/30.03	0.00237
Methyl Alcohol:	(10.7741 gm)(0.1329)/32.04	0.04469
Formic Acid:	(10.7741 gm)(0.0443)/46.03	0.01037

Components (cont'd)		Gram-Moles
Methyl Formate:	(10.7741 gm)(0.0409)/60.06	0.00733
Water:	(10.7741 gm)(0.7753)/18	0.46406

Total Product Weight = 118.7271 + 10.7741 = 129.5012 grams

Overall Material Balance = 129.5012/131.1556 - 0.9874.

The overall material balance is good; however, the uncertainty of the actual charge weight determined by the compressibility factor is such that it is more convenient to base the remaining calculations on the charge weight determined by the sum of the weights of liquid and gas products. Thus

Charge Weight = 118.7271 + 10.7741 = 129.5012 grams.

Components		Grams
Oxygen:	(129.5012 gm)(0.16586)	21.4791
Methane:	(129.5012 gm)(0.81833)	105.9747
CO_2:	(129.5012 gm)(0.00450)	0.5828
Nitrogen:	(129.5012 gm)(0.01129)	1.4624

Oxygen Balance

Oxygen In = 21.4791 + 0.5828 (0.7273) = 21.9038 grams

Oxygen Out = 118.7271 {0.0429 + 0.0179(0.5714) + 0.0687(0.7273)}
+ 10.7741 {0.1329(0.5) + 0.0475(0.5333)
+ 0.0443(0.6957) + 0.7753(0.8889)}
= 20.9857 grams.

Oxygen Out/Oxygen In = 20.9857/21.9038 = 0.9581

Carbon Balance

Carbon In = 0.75(105.9747) + 0.5828(0.2727) = 79.6399 grams

Carbon Out = 118.7271 {0.8576(0.75) + 0.0179(0.4286)
+ 0.0687(0.2727)} + 10.7741 {0.1329(0.375)
+ 0.0475(0.4) + 0.0443 (0.2605)}
= 80.3669 grams

Carbon Out/Carbon In = 80.3669/79.6399 = 1.0091

Hydrogen Balance

Hydrogen In = 0.25(105.9747) - 26.4937 grams

Hydrogen Out = 118.7271(0.8576)(0.25) + 10.7741 {0.1329(0.125)
+ 0.0475(0.0667) + 0.0443(0.0435)
+ 0.7753(0.1111)}
= 26.6858 grams

Hydrogen Out/Hydrogen In = 26.6858/26.4937 = 1.0072

Water Balance

The water balance is calculated by three methods and is based on the following reactions:

$$2CH_4 + O_2 \rightarrow 2CH_3OH$$

$$CH_4 + O_2 \rightarrow HCHO + H_2O$$

$$2CH_4 + 3O_2 \rightarrow 2HCOOH + 2H_2O$$

$$HCOOH + CH_3OH \rightarrow HCOOCH_3 + H_2O$$

$$2CH_4 + 3O_2 \rightarrow 2CO + 4H_2O$$

$$CH_4 + 2O_2 \rightarrow CO_2 + 2H_2O$$

Method #1:

Product	Gram-Moles	Equivalent Water, Gm-Moles
Formaldehyde	0.00237	0.00237
Formic Acid	0.01037	0.01037
Methyl Formate	0.00733	0.01466
Carbon Monoxide	0.07591	0.15182
Carbon Dioxide	0.17209	0.34418
Total Water		0.52340

Method #2:

Hydrogen Consumption = (26.4937 - 25.4551)/2

= 0.51930 gm-moles

Product	Gram-Moles	Equivalent Hydrogen, Gm-Moles
Methyl Alcohol	0.04469	0.08938
Formaldehyde	0.00237	0.00237
Formic Acid	0.01037	0.01037
Methyl Formate	0.00733	0.01466
Total		0.11678

Equivalent Water = 0.51930 - 0.11678 = 0.40252 gm-moles

Method #3:

Oxygen Consumption = (21.4791 - 5.0990)/32

= 0.51187 gm-moles

Product	Gram-Moles	Equivalent Oxygen, Gm-Moles
Methyl Alcohol	0.04469	0.02235
Formaldehyde	0.00237	0.00118
Formic Acid	0.01037	0.01037
Methyl Formate	0.00733	0.00733

Product	Gram-Moles	Equivalent Oxygen, Gm-Moles
Carbon Monoxide	0.07591	0.03795
Carbon Dioxide	0.17209	0.17209
Total		0.25127

Equivalent Water = 2(0.51187 - 0.25127) = 0.52120 gm-moles

Water by Analysis = 0.46406 gm-moles.

A correction to the liquid weight is now made in an attempt to balance the water. Method #3 has been selected to calculate the liquid product which would correspond to the gas product weight. This correction is made to smooth the data since only a small error in the determination of the weight of the gas products will alter the preceding material balances.

Corrected Liquid Weight = (0.5212)(18)/0.7753

= 12.1006 grams

Component		Gram-Moles
Formaldehyde	(12.1006 gm)(0.0066)/30.03	0.00265
Methyl Alcohol	(12.1006 gm)(0.1329)/32.04	0.05019
Formic Acid	(12.1006 gm)(0.0443)/46.03	0.01164
Methyl Formate	(12.1006 gm)(0.0409)/60.06	0.00824
Water	(12.1006 gm)(0.7753)/18	0.52120

Corrected Charge Weight = 118.7271 + 12.1006 = 130.8277 grams

Component		Grams	Moles
Oxygen	(130.8277 gm)(0.16586)	21.6991	0.67809
Methane	(130.8277 gm)(0.81833)	107.0602	6.69126

Component		Grams	Moles
CO_2	(130.8277 gm)(0.00450)	0.5887	0.01338
Nitrogen	(130.8277 gm)(0.01129)	1.4770	0.05275

Oxygen Balance

Oxygen In = 21.6991 + 0.5887 (0.7273) = 22.1273 grams

Oxygen Out = 12.2396 + 12.1006 (0.8118) = 22.0625 grams

Oxygen Out/Oxygen In = 22.0625/22.1273 = 0.9971

Carbon Balance

Carbon In = 0.75(107.0602) + 0.5887(0.2727) = 80.4557 grams

Carbon Out = 79.5009 + 12.1006(0.0804) = 80.4737 grams

Carbon Out/Carbon In = 80.4737/80.4557 = 1.0002

Hydrogen Balance

Hydrogen In = 0.25(107.0602) = 26.7651 grams

Hydrogen Out = 25.4551 + 12.1006 (0.1078) = 26.7600 grams

Hydrogen Out/Hydrogen In = 26.7600/26.7651 = 0.9998

Water Balance

Method #1:

Product	Gram-Moles	Equivalent Water, Gm-Moles
Formaldehyde	0.00265	0.00265
Formic Acid	0.01164	0.01164
Methyl Formate	0.00824	0.01648
Carbon Monoxide	0.07591	0.15182
Carbon Dioxide	0.17195	0.34390
Total Water		0.52649

Method #2:

Hydrogen Consumption = (26.7651 - 25.4551)/2

= 0.65500 gm-moles

Product	Gram-Moles	Equivalent Hydrogen, Gm-Moles
Methyl Alcohol	0.05019	0.10038
Formaldehyde	0.00265	0.00256
Formic Acid	0.01164	0.01164
Methyl Formate	0.00824	0.01648
Total		0.13115

Equivalent Water = (0.65500 - 0.13115) = 0.52385 gm-moles

Method #3:

Oxygen Consumption = (21.6991 - 5.0990)/32

= 0.51875 gm-moles

Product	Gram-Moles	Equivalent Oxygen, Gm-Moles
Methyl Alcohol	0.05019	0.02509
Formaldehyde	0.00265	0.00132
Formic Acid	0.01164	0.01164
Methyl Formate	0.00824	0.00824
Carbon Monoxide	0.07591	0.03795
Carbon Dioxide	0.17195	0.17195
Total		0.25619

Equivalent Water = 2(0.51875 - 0.25619) = 0.52512 gm-moles

Oxygen Conversion = 0.51875/0.67809 = 0.7650

Methane Conversion = (107.0602 - 101.8161)/107.0602

= 0.0490

Per Cent of Reacted Methane Converted to

Methyl Alcohol	= (0.05019/0.32775)(100)	= 15.31
Formaldehyde	= (0.00265/0.32775)(100)	= 0.81
Formic Acid	= (0.01164/0.32775)(100)	= 3.55
Methyl Formate	= (0.01648/0.32775)(100)	= 5.03
Carbon Monoxide	= (0.07591/0.32775)(100)	= 23.16
Carbon Dioxide	= (0.17195/0.32775)(100)	= 52.46
		100.32

Per Cent of Reacted Oxygen Converted to

Methyl Alcohol	= (0.02509/0.51875)(100)	= 4.84
Formaldehyde	= (0.00265/0.51875)(100)	= 0.51
Formic Acid	= (0.01746/0.51875)(100)	= 3.36
Methyl Formate	= (0.01648/0.51875)(100)	= 3.18
Carbon Monoxide	= (0.11386/0.51875)(100)	= 21.95
Carbon Dioxide	= (0.34390/0.51875)(100)	= 66.29
		100.13